The structure of Guadeloupe, Maderas and Mt Cameroon volcanoes and the impact of strike-slip movements

Lucie Mathieu

Université Blaise-Pascal, Clermont-Ferrand, France - Trinity College Dublin, Ireland

Ecole doctorale ED 178 "Sciences Fondamentales"
Département de Géologie
Laboratoire de Magmas et Volcans

The structure of Guadeloupe, Maderas and Mt Cameroon volcanoes and the impact of strike-slip movements

Lucie Mathieu

Disciplines: Géologie, Volcanologie, Tectonique

Thèse de doctorat

Directeur de recherche en France: Benjamin van Wyk de Vries
Directeur de recherche en Irlande: Valentin R. Troll

Date de soutenance: 3 Juillet 2010

Jury: John Walsh, University College Dublin, Ireland

Dave Chew, Trinity College Dublin, Ireland

John Graham, Trinity College Dublin, Ireland

Jean-Christophe Komorowski, Institut de Physique du Globe de Paris

Alfredo Mahar Francisco Lagmay, University of the Philippines

Contents

Résumé

Il y a trois catégories de failles décrochantes: les failles purement décrochantes, transtensives et les failles transpressives. Ces failles ont été décrites dans bien des environnements géodynamiques et sont le type de faille le plus communément associé avec les volcans, qui se situent souvent au-dessus ou prés d'une faille décrochante. L'impact que ces mouvements régionaux ont sur la morphologie de volcans coniques a été étudié à plusieurs reprises ces dernières années. Ce travail de thèse s'intéresse à un grand nombre de catégorie de failles et de géométrie volcaniques à travers trois exemples naturels: les volcans de Guadeloupe dans les Petites Antilles, le Mt Cameroun d'Afrique de l'ouest et le volcan de Maderas, au Nicaragua. Ce projet a permis d'établir des cartes structurales de ces trois volcans peu étudiés, grâce à des études de terrain détaillées et à des observations satellites. Les cartes ont ensuite été comparées avec les structures obtenues expérimentalement, en déformant un cône analogue à un volcan avec des mouvements décrochants, transtensifs et transpressifs. L'étude des volcans Guadeloupéen a conduit à une nouvelle interprétation de leurs phases de construction. Une faille régional senestre, transtensive et orientée NW-SE est responsable de l'alignement des volcans Guadeloupéens, de l'orientation de leur dykes et de l'effondrement d'une partie de leurs flancs. En ce qui concerne le Mt Cameroun, la zone de rift et la morphologie allongée du volcan sont contrôlées par un faille décrochante inactive de la croute continentale, au-dessus de laquelle le volcan c'est développé. Cette étude montre également que le Mt Cameroun s'est étalé sur sont les sédiments peu compétents de son substratum. Les structures du volcan de Maderas, c'est-à-dire sont graben sommital, sont alignement d'édifices monogénétiques, les demi grabens de ses flancs inférieurs et ses linéaments sommitaux sont liés à des mouvements régionaux et à l'étalement gravitaire du volcan. L'orientation de ces structures indique que Maderas c'est construit au-dessus d'une faille dextre, transtensive et orientée NW-SE. Le modèle théorique de l'interaction entre failles décrochantes et cônes volcaniques établi grâce aux expériences analogiques peu être appliqué aux volcans étudiés durant se projet ainsi qu'à d'autre volcans, dans le but de déterminer la position, l'orientation, la quantité et le sens du mouvement des failles cachées par une couverture de dépôt éruptifs récent et par une érosion intense.

Mots clefs: volcans, structure, failles, travail de terrain, modèles analogiques, images satellite, modèles numérique de terrain, Guadeloupe, Nicaragua, Cameroun

Summary

There are three kinds of strike-slip faults: pure strike-slip, transtensional and transpressional. They have been recognized in all geodynamic environments and are the most common fault type associated with volcanic activity. Many volcanic edifices are built in the vicinity of a fault with strike-slip motion. The impact of strike-slip fault movements on a volcanic cone has been addressed by several studies over the last decade. This study considers a broad range of fault and volcano geometries through three natural examples: the Guadeloupe volcanoes in the Lesser Antilles, Mt Cameroon in West Africa and Maderas volcano in Nicaragua. Detailed field and remote sensing studies are used to establish structural maps of these three little studied volcanoes. These maps are then compared with experimental structures that have developed in analogue cones deformed by strike-slip, transtensional and transpressional faults. The study of the Guadeloupe volcanoes leads to a new interpretation of their constructional phases. A regional NW-SE striking sinistral transtensional fault on which the Guadeloupe volcanoes have been built is responsible for their alignment, for the dyke trends and for the major collapse events. On Mt Cameroon, the rift zone and elongated morphology are controlled by an inactive strike-slip fault on which the volcano has been built. This study also reveals that Mt Cameroon volcano has spread over its weak sedimentary substratum. On Maderas volcano, the summit graben, vent alignment, lower flank half-grabens and summit lineaments are related to gravitational spreading and to regional tectonic movements. The orientation of these structures indicates that the Maderas volcano was built above a NW-SE striking dextral transtensional fault. The theoretical model of strike-slip motion and volcanic cone interaction established with the analogue models can be applied to these and to other volcanoes to determine the location, slip, kinematics and strike of structures hidden by recent eruptions and intense erosion.

Keywords: volcanoes, structures, faults, field work, analogue models, remote sensing, digital elevation models, Guadeloupe, Nicaragua, Cameroon

Chapter 1

-

Introduction

Chapter 1: Introduction

1. Basic purpose

Many volcanoes are associated with faults that facilitate the transport of magma in the crust. Active faults interact with the volcano as it grows or/and as it becomes eroded.

There are three types of strike-slip faults: pure strike-slip, transtensional and transpressional. They are found in every geodynamic context and are the most common fault type associated with volcanic activity.

This thesis focuses on three volcanic edifices interacting with active transtensional and inactive strike-slip faults. These volcanoes are the Basse Terre Island of Guadeloupe in the Lesser Antilles, Mt Cameroon volcano in western Africa and Maderas volcano in Nicaragua. Completing our knowledge of the structure and geology of these poorly understood volcanoes is one of the objectives of this thesis.

A volcanic environnement is not ideal for structural studies mostly because fault planes are rapidly covered by new volcanic output. Also, a part of the fractures and faults observed at the surface of a volcano are related to the movements of magma in the edifice, to the cooling of lava or to the instability generated by the accumulations of loose pyroclasts (cf. Appendix A). The structures related to tectonic movements are easy to mistake for the fractures and faults formed by the volcanic activity. For this reason, the field measurements have been compared to analogue models in which the bulk of faults observed are formed by the strike-slip deformations imposed to the model.

2. Aim of the study

Faults with a strike-slip component originate from small angular differences between plate motions and plate boundaries. They are the major type of structure associated with volcanic

edifices and there is probably a close relationship between regional strike-slip faults and magmatic feeder systems. When associated with an extensional or a compressional component of movement, strike-slip faults are named transtensional and transpressional faults, respectively.

Volcanoes are also deformed by local processes such as gravitational spreading, which has been observed worldwide (van Bemmelen, 1953; Merle and Borgia, 1996; Borgia et al., 2000). The gravitational spreading is a slow and continuous deformation of a steep and heavy relief. The spreading of a volcanic cone occurs when the edifice forms over a weak sedimentary substratum, which is made, for example, of marine sediments (cf. Oceanic Island volcanoes) or of clay and salts horizons contained in a sedimentary basin.

This thesis examines the structure of stable and spreading conical volcanic edifices interacting with faults which have a strike-slip component of movement. The aim of this study is to produce a general model of the interaction between volcanic edifices and regional strike-slip, transtensional and transpressional fault zones.

In order to produce as general a model as possible, three volcanoes with highly contrasting morphologies, geodynamic location and substratum composition have been selected. These volcanoes have a large (Mt Cameroon, Guadeloupe) or small volume (Maderas). They are rounded (Maderas, individual Guadeloupe volcanoes) or elongated (Mt Cameroon, Guadeloupe Island). They are made of low viscosity magma (Mt Cameroon) or of a more viscous magma (Maderas, Guadeloupe). They sit upon inactive (Mt Cameroon) or active transtensional faults (Maderas, Guadeloupe). They sit on either continental (Mt Cameroon), thin continental or ophiolitic (Maderas) or thick oceanic (Guadeloupe) crust. They are underlain by either a thin (Guadeloupe) or thick layer of weak sediments (Mt Cameroon, Maderas), which promotes gravitational spreading in the last two cases. The volcanoes are terrestrial (Cameroon), oceanic (Guadeloupe) or are located within a lake (Maderas).

This study aims also to comprehend the structure of the little studied Mt Cameroon and Maderas volcanoes. Guadeloupe volcanoes have received more structural attention but the studies are contradictory and their structure has not been fully mapped.

Our understanding of these volcanoes is limited because they are covered with dense rain forests. Besides, strike-slip faults have an average slip of 1 mm to 1 cm per year (Dusquenoy et al., 1994; Bourne et al., 1998; Groppelli and Tibaldi, 1999; Corpuz et al., 2004) and fault planes are rapidly hidden by volcanic output and fast erosion of the accumulated volcanic

deposits. The faults formed in a volcanic area are often un-accessible to surface field geology. For this reason, the field studies were confronted to analogue models, which enable the preservation and easy measurement of structures.

3. Location and Morphology of the studied volcanoes

3.1. Location and geodynamic context of the Guadeloupe, Mt Cameroon and Maderas volcanoes

The three studied volcanoes have formed in very distinct geodynamic contexts. The Basse Terre Island volcanoes form the western and most recent part of the Guadeloupe archipelago. This Quaternary volcanic island is still active and is the highest summit (1467 m) of the Lesser Antilles (figure 1-a). It is a large oceanic volcano that is about 2500-3000 m high when its sub-marine base is taken into consideration. Mt Cameroon (4090 m) is one of the largest continental volcanoes worldwide and the most active volcano in West Africa (figure 1-b). In contrast, Maderas volcano is a small (1345 m high) and dormant continental volcano. It forms the southern half of Ometepe Island, Lake Nicaragua, located in southern Nicaragua (figure 1-c).

Guadeloupe and Maderas are arc volcanoes, which have formed following the subduction of, respectively, the Atlantic and Cocos oceanic lithosphere beneath the Caribbean plate. The Caribbean plate is made of thick oceanic lithosphere in the vicinity of Guadeloupe and continental or ophiolitic crust beneath Maderas. At the surface, the magma has dominantly an andesite composition in both cases. The origin of Mt Cameroon magma is still debated (e.g. Déruelle et al. 1991). This basalt dominated volcano is made of a much less viscous magma than the other two.

All three volcanoes have been built above regional strike-slip faults. In the case of Mt Cameroon, the regional fault is an inactive Pan-African structure. Guadeloupe and Maderas volcanoes sit upon active transtensional faults, both of which originate from oblique

subduction. The regional fault zone in Guadeloupe strikes NW-SE and has a sinistral motion. The strike and kinematics of the Maderas fault zone are hidden by Lake Nicaragua sediments.
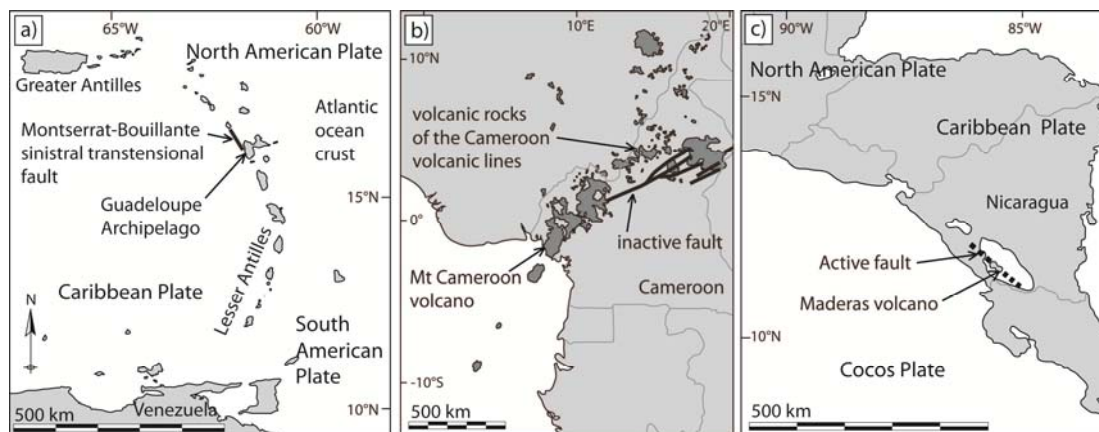
Figure 1: Geographical location of the Guadeloupe Archipelago (a), Mt Cameroon volcano (b) and Maderas volcano (c).

3.2. Morphology of the Guadeloupe, Mt Cameroon and Maderas volcanoes

The three studied volcanoes have contrasting morphologies. Basse Terre Island is a 50 km long alignment of three main central volcanoes. The largest edifice forms the northern part of the island and is elongated NNW-SSE. The southern part of the island is made of several edifices roughly aligned NW-SE, parallel to the regional transtensional fault. The alignment of volcanoes and eruption age data indicate that the magmatic activity has progressively migrated form north to south (Samper 2007). Mt Cameroon is a 35x50 km elongated edifice. It is an unusually steep lava-dominated volcano that possesses a flat summit plateau, sharp breaks-in-slope, a rift zone, a deep valley in the northern flank and topographic steps at its base (Gèze 1953, Déruelle et al. 1987). Maderas is a rounded edifice with a diameter of 11 km. Both Maderas and Mt Cameroon volcanoes sit on a thick succession of weak sediments and are undergoing gravitational spreading. The structure of Maderas is a combination of gravitational spreading and regional stress-related structures (van Wyk de Vries and Merle 1996). It possesses a NW-SE elongated graben, a summit crater and several small vents at its base.

The structure of these volcanoes is poorly known. Structural studies in Guadeloupe have focused on its recent dome, geothermal systems and offshore regional faults (Julien and Bonneton 1984, Gadalia et al. 1988, Feuillet 2000). Mt Cameroon and Maderas structures are mostly known from remote sensing data. There are several reasons for this. Mt Cameroon is located in a remote area. Maderas is small, inactive and quite remote. The volcanoes are also covered with dense rain forest that renders field (including mapping and geophysical studies) and remote sensing analysis difficult. Geochemical (including age determination) and petrological studies are often prevented by the intense weathering of rocks.

4. Methods

4.1. Field study

Fieldwork is a major component of this project. Fieldwork alone could provide the detailed data needed to understand the structure of the studied volcanoes as all three are densely forested. The field work was mostly carried out in river beds. A river is often the only path available to penetrate dense forest established on steep areas. The main inconvenience of rivers is the water, which may rise quickly to a dangerous level (e.g. frequent tropical storms create flash floods), especially in canyon areas, which are impossible to escape from rapidly. Also there are many waterfalls (up to 100 m high in Guadeloupe) that are logistical barriers. On the other hand, the rivers cut into fresh rocks and thus provide good clean outcrops. Forested volcanoes involve danger and discomfort but are attractive because of their hidden treasure of data. Many rivers where explored on foot and some were visited with canyoning techniques. Other outcrops were found along the shore line of Guadeloupe or at the denuded summit of Mt Cameroon. This latter map area necessitated the organisation of a week duration expedition with collaborators from Ghent (Belgium) and Buea (Cameroon) Universities and about 30 local porters. Field work in Guadeloupe was done with local canyoning guides and Master assistants (Elodie Lebas, Claire Mannessiez, Nelly Mazzoni, Cécile Savry). On Maderas, fieldwork was conducted together with local geologist Martin Pilato.

4.2. Remote sensing data

Remote sensing data are used to study the shape of the volcanoes. I have mostly used Digital Elevation Models (DEM), which are 3D topographic maps of an area. A DEM may be visualized as contour levels, slope maps, hill shade maps and aspect maps. I mostly used the SRTM dataset (Shuttle Radar Topographic Mission), which was computed in 2000 and is accessible for free from the USGS-a website. Several other DEM with a better resolution were also computed for the purpose of this study. Apart from DEM data, I have used aerial photography images, which are available for Maderas volcano, and ASTER images (Advanced Spaceborne Thermal Emission and Reflection Radiometer, GLCF and USGS-b websites) to establish the summit map of Mt Cameroon. The bathymetry of Guadeloupe would have been useful to grasp the full morphology of this oceanic volcano, but I have unfortunately been denied access to these data.

4.3. Analogue modelling

Analogue modelling is used to quantify the location, strike, kinematics and slip of faults that develop in a cone sheared by strike-slip, transtensional or transpressional fault. The models were carried out in the Laboratoire de Magmas et Volcans, Blaise-Pascal University, Clermont-Ferrand, France. They are used to establish a general model of the interaction between volcanic cones and strike-slip faults, which is then compared with the three natural examples.

5. Presentation of the manuscript

The PhD thesis is structured according to the field areas and the methods used. The first three chapters present the field and remote sensing analysis of Guadeloupe (chapter 2), Cameroon (chapter 3) and Nicaragua (chapter 4). These chapters propose a structural map for each studied volcano. The fifth chapter presents the analogue models and compares them to the natural examples described in the previous chapters. The last chapter is the final discussion and conclusion which briefly summarises the main results of this study.

Chapter 2

-

The geology and structure of Basse Terre Island volcanoes, Guadeloupe Archipelago, Lesser Antilles
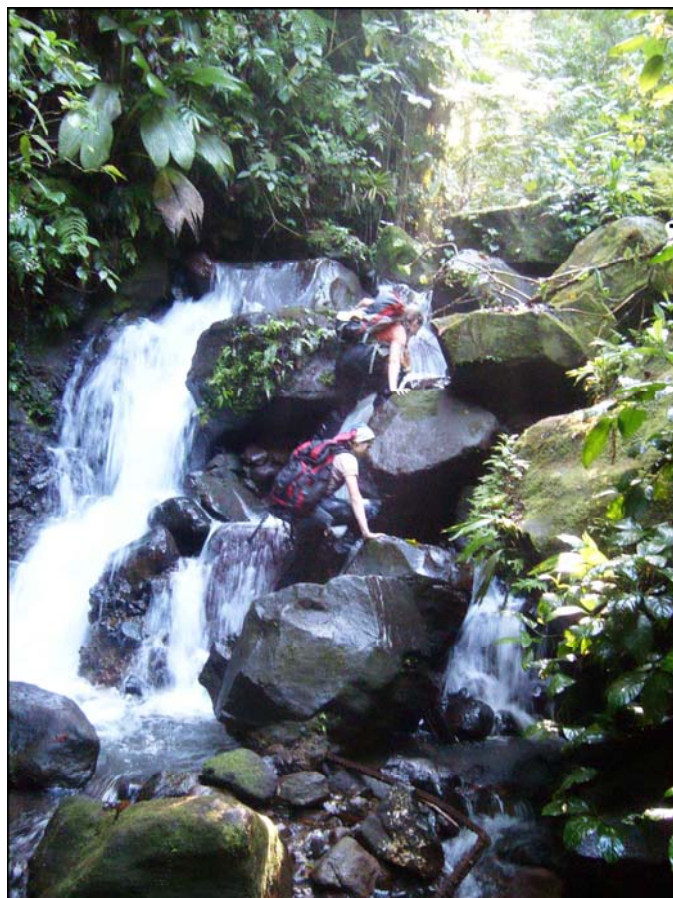
Chapter 2: the geology and structure of Basse Terre Island volcanoes, Guadeloupe Archipelago, Lesser Antilles

1. Introduction

Basse Terre Island forms the western part of Guadeloupe Archipelago, Lesser Antilles. It is comprise of late Tertiary to Quaternary volcanoes. This 50 km long island is the highest mountain of the Lesser Antilles Volcanic Arc with its 1467 m-high summit (La Soufrière dome).

The structure of the Basse Terre volcanoes is poorly known. The island is surrounded by two offshore grabens and a regional sinistral transtensional fault, according to Feuillet (2000). Its crest is elongated NNW-SSE to NW-SE and it corresponds to the volcanic axis of the edifice. The stress field of Basse Terre Island has been deduced from the fractures of the recent La Soufrière dome (1440 AD) and those of the Galion waterfall lava flows (Julien and Bonneton 1984). The Bouillante geothermal field has also received structural attention, mostly by authors from the BRGM (Bureau de Recherche Géologique et Miniére; e.g. Gadalia et al. 1988 for example).

The aim of this study is to describe and interpret the structure of Basse Terre volcanoes by paying attention to the whole island rather than focusing only on its recent dome, its active geothermal system, its mountain crest or coastal outcrops. The Guadeloupean volcanoes are studied because they form a large edifice located in a complex tectonic situation, over a regional transtensional fault. They are used to comprehend the interaction between volcanic cones and regional transtensional fault movement.

The northern extremity of the island is made of intensely weathered horizons. The southern extremity, on the other hand, is covered with recent volcanic products, which obscure other structures. Exploratory fieldwork has revealed that Mt Caraïbe structures are linked to the accumulation of unstable pyroclastic and not to tectonic movements (southern extremity of the island). For this reason this study will focus on the central part of the island, which is made of the Northern Chain, the Axial Chain and the Bouillante Chain volcanoes. Outcrops are not abundant in the rain forest and the mapping was done along the western shore line and in the river beds, where exposure if often good.

First, the geological setting of Basse Terre Island is presented. The next section analyses the general morphology of the volcanoes, using a Digital Elevation Model (DEM) and then, the field data are presented.

2. Geological setting

2.1. Lesser Antilles Arc

Guadeloupe is a volcanic archipelago of the Lesser Antilles Arc, which is located on the eastern extremity of the Caribbean Plate. The northern half of the arc is bordered by two convergent margins and by a fracture zone. The northern border is a transpressional sinistral fault associated with the Greater Antilles volcanism. The southern border of the northern arc is the 15.20 fracture zone of the Atlantic oceanic crust, which separates the North and South American plates (figure 01). There is a curved subduction zone with the 6 km-thick, Jurassic to lower Cretaceous Atlantic oceanic lithosphere subducting beneath the Caribbean Plate (Bouysse et al. 1990). The slab plunges slowly (2 ± 0.2 cm/y) with an angle of 50°-60° in the northern Lesser Antilles and is cut along the 15.20 fracture zone (Jordan 1975, La Mouel et al. 1979, Roest and Collette 1986, Bouysse et al. 1990).

The Caribbean plate drifts toward the east (090 $\pm$ 2°; e.g. GPS studies by DeMets et al. 2000 and Weber 2001) and its convergence direction with the Atlantic oceanic crust is either 102 (Bouysse and Westercamp 1990) or 120 $\pm$ 10° (Chabellard et al. 1986).

Present-day magma activity is restricted to the central part of the Lesser Antilles arc (Bouysse et al. 1990). The active arc is bordered by inactive volcanic islands (from Anguilla to the Grenada islands) and seamounts.
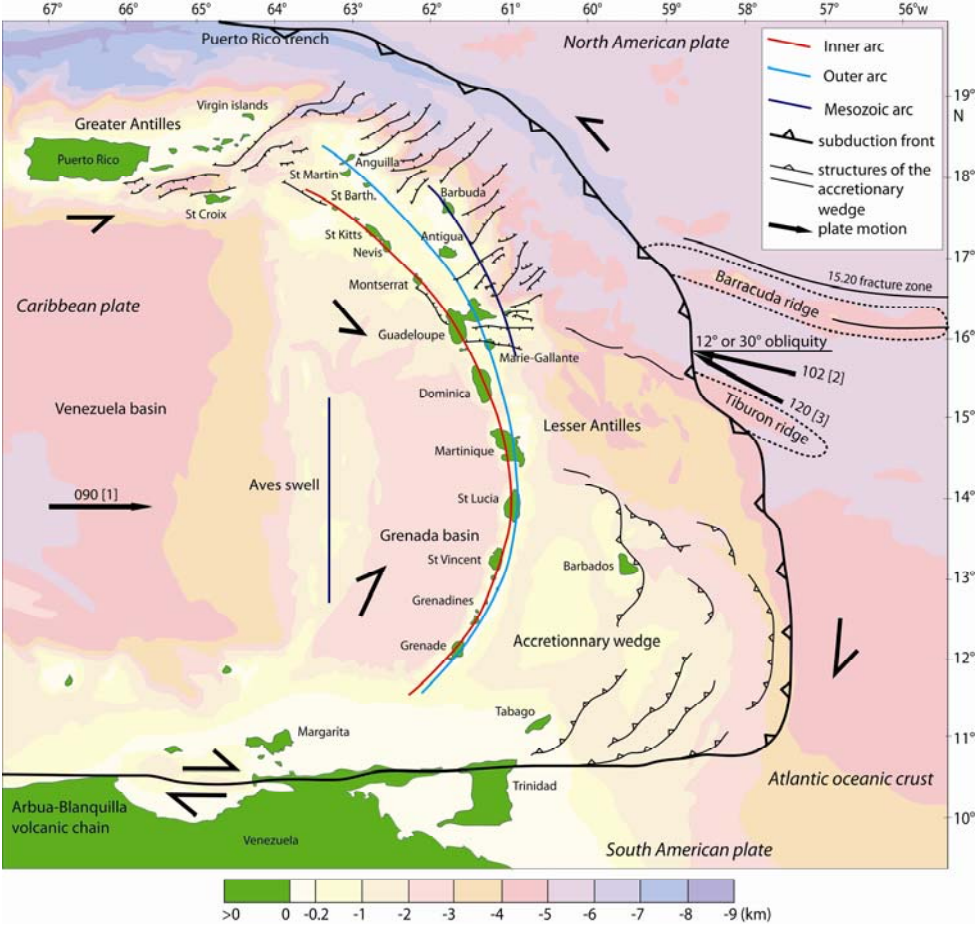
Figure 01: This map presents the islands of the Lesser Antilles volcanic arc. The bathymetry is from Bouysse et al. (1990) and the regional tectonic framework is after Feuillet (2000). The plate motion is from [1] DeMets et al. (2000) and Weber (2001), [2] Bouysse and Westercamp (1990) and [3] Chabellard et al. (1986).

The sedimentary load is limited in the north (some 100s of meters thick) possibly because the steep angle of subduction does not favour much scraping off of oceanic sediments. The absence of an accretionary wedge enables good exposure of structures. The WNW convergence along a NNW striking subduction front results in an oblique angle subduction (figure 01). As a consequence, strike-slip motion is associated with compressive motion. These movements are partitioned: the subduction front accommodates the shortening and the

volcanic front accommodates the strike-slip movements (Fitch 1972, Dickinson and Seely 1979, Jarrad 1986). In the north, the strike-slip movement is accommodated by sinistral transtensional strike-slip faults located west of the volcanic arc and by NE-SW to E-W striking grabens (figure 01; Feuillet et al. 2002). The whole NE part of the Caribbean plate is internally deformed by large-scale strike-slip movements (Lopez et al. 2010). The Atlantic ocean crust contains several gravimetrically uncompensated ridges (transform faults) and buoyant ridges (mid-oceanic ridges) that have fully entered the subduction zone. The Tiburon and Barracuda uncompensated ridges, for example, reached the subduction front 10 Ma ago (Bouysse and Westercamp 1990). The collision of ridges with the subduction front is responsible for uplift (Bouysse et al. 1990), subduction locking and jumps of the volcanic front toward the west. As a consequence, the Lesser Antilles are made up of three successive volcanic arcs: the Mesozoic, the Outer and the Inner arcs (figure 01).

The Mesozoic arc forms the substratum of northern Lesser Antilles volcanoes as well as the Aves swell, the Greater Antilles and the Arbua-Blanquilla Chain (Venezuela). The Outer arc was active between about 50 and 30 Ma (Bouysse and Westercamp 1990, Chabellard et al. 1986). The active Inner Arc has formed following a 10 Ma gap in the volcanic activity caused by the breaking of the slab following the subduction of a buoyant ridge (Bouysse and Westercamp 1990, Bouysse et al. 1990).

2.2. The Guadeloupe Archipelago: Geology and local tectonics

2.2.1. Geology of the archipelago

The Guadeloupe archipelago is made of magmatic rocks from the Mesozoic arc (La Desirade, Petite Terre), the Outer arc (Grande Terre, Marie-Gallante) and the Inner arc (Basse Terre, Les Saintes archipelago). The Mesozoic and Outer Arc islands are flat-topped eroded volcanoes covered with recifal limestone. The active Inner Arc volcano of Basse Terre Island is an elongated mountain.

The analysis of aerial photography as well as a detailed study of the faults of the La Soufrière dome (latest magmatic eruption of Guadeloupe), indicate that the maximum and minimum

horizontal stresses are oriented 120 and 030 in Guadeloupe (Chabellard et al. 1986, Julien and Bonneton 1984).

2.2.2. Offshore grabens

Two grabens have been identified offshore and onshore of the Guadeloupe area (figure 02). Grande Terre Island is located on the southern edge of the NE-SW striking Bertrand-Flamouth graben that formed 2 Ma ago (Feuillet et al. 2002). This graben is similar in strike and depth to the grabens of the northern Lesser Antilles arc (Feuillet 2000; figure 01).

The Marie-Gallante graben is shallower (possibly younger), strikes E-W and has formed since 0.5 Ma (Feuillet et al. 2002). It may extend to Basse Terre Island and may underlie the active volcano (Feuillet 2000, Feuillet et al. 2002).

The Bertrand-Flamouth and Marie-Gallante grabens are contemporaneous and intersect in Grande Terre Island (Feuillet 2000). Their formation has been attributed to the deformations generated by the forced subduction of the Tiburon ridge (Bouysse and Westercamp 1990). The Tiburon ridge is however a small structure which can not have generated all the deformations observed in the NE Caribbean plate. The NE-SW striking grabens more likely accommodate the deformation generated by the oblique subduction (Feuillet et al. 2002). The Marie-Gallante graben is parallel to the plate motion and may have developed parallel to the main regional horizontal stress. This E-W striking graben is located at the transition between the northern and southern Lesser Antilles Arcs, which are characterised by two different slab plunging angle and velocity (La Mouel et al. 1979, Bouysse et al. 1990). The Marie-Gallante graben may accommodate strike-slip movements at the transition between the two parts of the arc.

2.2.3. The Montserrat-Bouillante sinistral transtensional fault

The Montserrat-Bouillante fault is located west of Basse Terre Island (figure 02). It is a sinistral transtensional fault, which strikes NW-SE and extends offshore between Montserrat and Basse Terre Islands. This structure is made up of en-échelon normal faults. It intersects Basse Terre Island in the Bouillante bay area according to Feuillet (2000). The fault is thought to extend onshore through the E-W striking Bouillante-Capesterre normal fault (Feuillet et al. 2001), which is supposed to be part of the Marie-Gallante graben. The Capesterre fault strikes

120 and dips toward the NE in eastern Basse Terre (Baubron 1990). The Montserrat-Bouillante fault is also thought to be deflected around Basse Terre Island (e.g. bathymetry data obtained west of the island) with a 160 strike, and to connect with the Les Saintes fault system (Thinon et al. 2004, Thinon et al. 2010; figure 02).
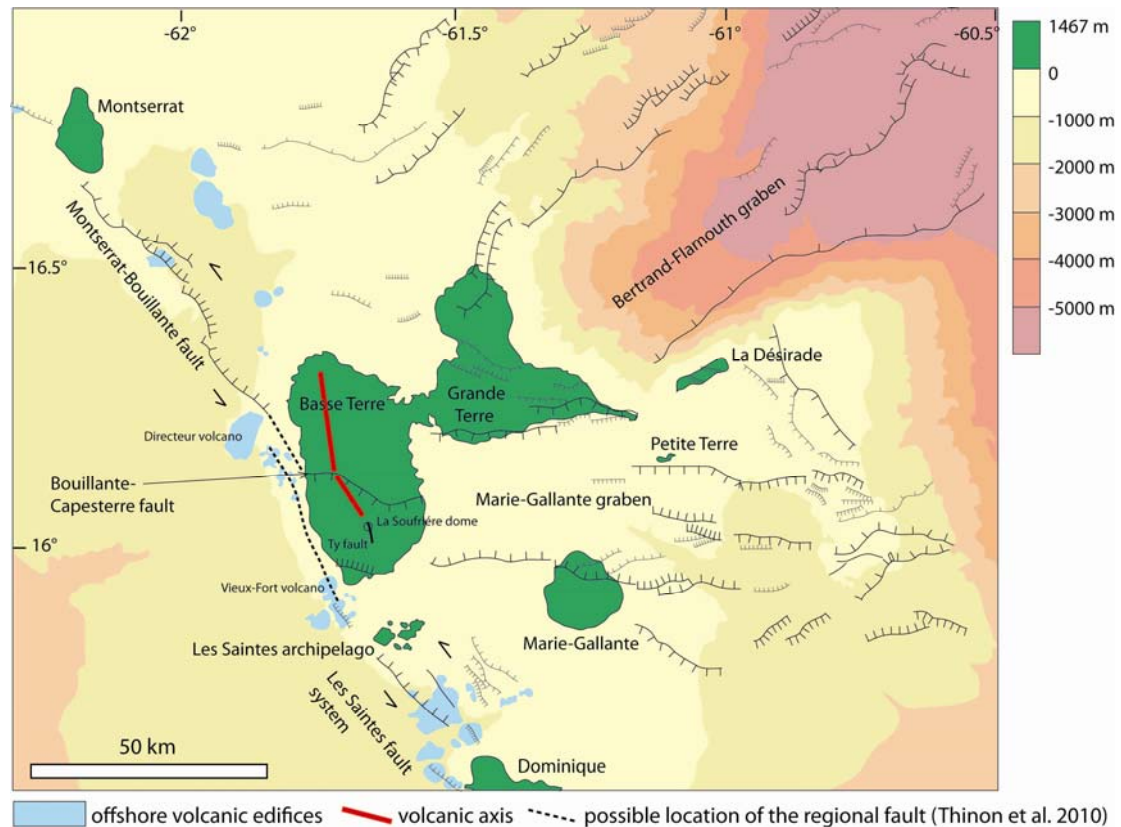
Figure 02: Map showing the 3 main structures of the Guadeloupe archipelago: the Monsterrat-Bouillante sinistral transtensional fault, the Bertrand-Flamouth graben and the Marie-Gallante graben. The faults, contour levels and seamounts are from Feuillet (2000).

The Bouillante Bay area possesses an exploited geothermal field that occurs at the intersection between the regional transtensional fault and E-W structures (Traineau et al. 1997). The Montserrat-Bouillante fault underlies an alignment of small-scaled seamount NW of the Bouillante Bay and is intersecting the island in this bay (Feuillet 2000).

Drilling (Sanjuan et al. 2004, Lachassagne et al. 2009, Genter and Traineau 2004) indicates that the substratum of the Bouillante Bay is made of N-S striking lava flows and

hyaloclastites dipping toward the west. These units pass upward into aerial rocks between 200 to 400 m below the surface, indicating that the area has subsided. This movement is accommodated by several onshore and offshore 100-120 striking and steeply dipping (70°-90°) normal faults associated with a limited amount of slip according to field measurement (Traineau et al. 1997, e.g. figure 03). The 300 fractures, veins and small scale normal faults measured in the vicinity of the Bouillante town reveal that the main structural directions are, in order of importance: 110-120, 080-090 and 010 (Traineau et al. 1997).

The Montserrat-Bouillante fault is poorly documented onshore, where 140 striking fault planes have not been identified, while its offshore outline is well documented (Feuillet 2000). This fault accommodates the deformation of the NE Caribbean plate generated by the oblique subduction (Feuillet et al. 2002). It has developed parallel to the volcanic front, possibly because this structure a thermally activated weak zone of the lithosphere (Viruete et al. 2006). In turn, the regional fault has facilitated the transport of magma in the crust, as evidenced by the many seamounts that have formed along the fault plane.
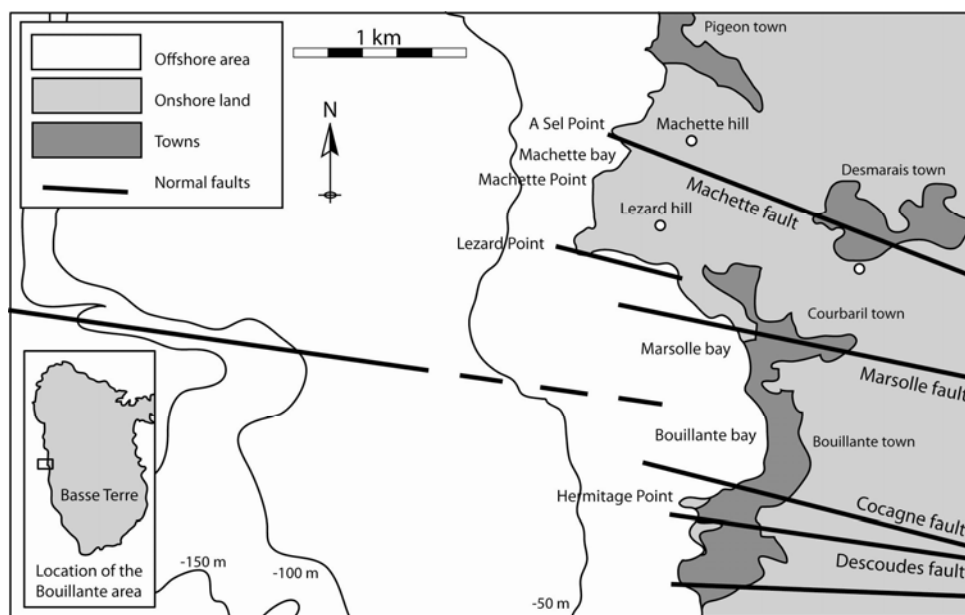
Figure 03: Map of the onshore and offshore parts of the Bouillante area. The normal faults are drawn after Traineau et al. (1997) and Guisseau et al. (2007).

2.3. Basse Terre Island

2.3.1. Alignment and age migration of volcanoes

Basse Terre Island is made up of a NNW-SSE to NW-SE alignment of volcanoes, which are progressively younger from north to south (figure 04). Several volcanic edifices and seamounts are however located away from the general alignment of edifices and others do not enter in the progressive southward migration of the volcanic activity. This migration is either attributed to the subducted Tiburon ridge, which approached the volcanic front 2 Ma ago (Bouysse and Westercamp 1990) or to repeated sector collapses (Boudon et al. 1992). The velocity of this migration (1.8 cm/y 2.8 Ma ago and 2.5 cm/y for 1.8 Ma) is similar to the regional convergence velocity of plates according to Samper (2007) and may correspond to the northward movement of the NE Caribbean plate upon a fixed magma source. The random distribution of some of the volcanic edifices is attributed to the melting of independent sediment pockets around the subducted Tiburon ridge (Bouysse and Westercamp 1990). It is however unlikely that a patchy distribution of partial melting at 150 km depth may be expressed with such detail at the surface. The location of volcanic centres is more likely controlled by regional (e.g. the Montserrat-Bouillante fault) and local (e.g. collapse scar) tectonics.

The oldest part of Basse Terre is a NNW-SSE elongated relief or volcanic crest, the orientation of which is linked to the propagation of the Bertrand-Flamouth graben in northern Basse Terre 3 Ma ago, according to Samper (2007). South of Les Mamelles domes (figure 04), the NW-SE volcanic axis is possibly located on top of the Montserrat-Bouillante fault that has, according to this theory, propagated into Basse Terre 1 Ma ago. The Directeur Seamount and the Bouillante Chain (western Basse Terre) would be located on top of a different en-echelon system parallel to the Monsterrat-Bouillante fault (Samper 2007). Structures transverse to the NW-SE volcanic axis were also postulated to explain the eccentric location of these volcanoes (Bouysse et al. 1985). Other alignments of vents in southern Basse Terre are either parallel to the NE-SW striking least compressive stress according to Julien and Bonneton (1984) or have formed along the Marie-Gallante graben border faults according to Feuillet et al. (2002).
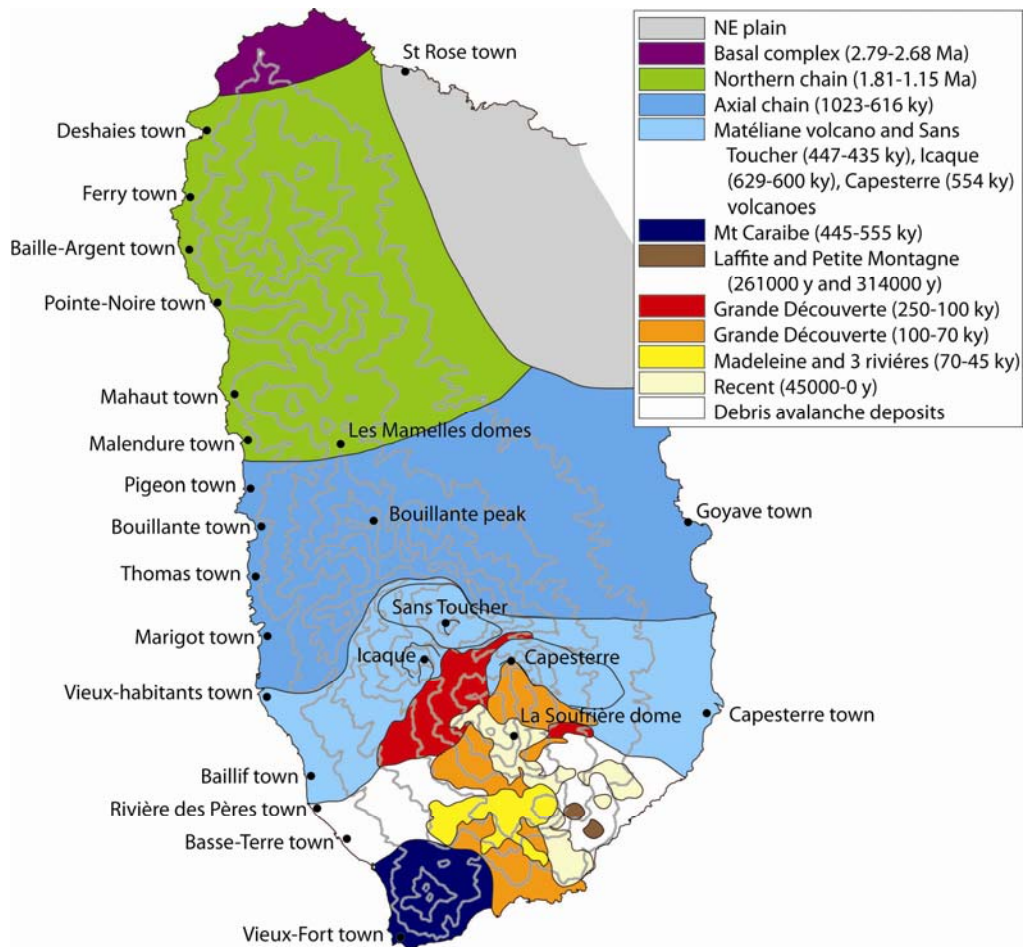
Figure 04: The geology of Basse Terre Island according to the age dating study of Samper (2007); "ky" stands for kilo-years. The contour lines (every 200 m) are from the SRTM (Shuttle Radar Topographic Mission).

2.3.2. The volcanic Chains

Basse Terre is made up of composite volcanoes built by pulses of volcanic activity (Davidson and De Silva 2000). Each edifice, or Chain, is geographically, petrologically and chronologically different from the others (figure 04, 05).

We have limited access to the initial stages of Basse Terre formation, which consisted of pillow lava flows interbedded with pelagic sediments. Shallower activity formed hyalotuff deposits (see Appendix A) interbedded with reef limestone. The hyalotuffs are covered by thick lava flows, domes and scoria cones. The lava flows cover a third of Basse Terre Island (Samper 2007). The late activity of each Chain is marked by the emission of more acidic

17

products through violent Plinian eruptions and by a large amount of sector collapses (12 collapse events less than 50,000 yr old have been recognised in Basse Terre Island; Komorowski et al. 2002, 2005).

Oldest rocks – The oldest exposed area of Basse Terre Island is possibly the NE plain. This intensely weathered area does not possess recognisable volcanic structure and is undated. The Directeur (3.7 to 3.4 Ma; Bouysse et al. 1985) and the Vieux-Fort (2.5-2 Ma; Bouysse et al. 1985) seamounts are located west of the northern and southern extremities of Basse Terre, respectively (e.g. figure 02 for location). The Basal Complex (northern Basse Terre; figure 04, 05) is made of sub-aerial lava flows, eroded volcanic edifices and coastal domes (e.g. Piton St Rose; figure 05). This weathered area is 6 to 4 Ma old (Bouysse et al. 1985, Maury et al. 1990) or 2.79 to 2.68 Ma old according to the recent study of Samper (2007).

Northern Chain - The Northern Chain (figure 04, 05) is a central volcano which has formed south of the Basal complex between 1.81 and 1.15 Ma (Samper 2007). The orientation of the highest crest is interpreted to be a NNW-SSE trending cluster of eruptive fissures called a volcanic axis, although dyke outcrops are lacking. Several eruptive vents formed successively (Westercamp 1980, Westercamp and Tazieff 1980, Dagain 1981): 1) formation of the Morne Goton dome, which is associated with quartz-dacite pyroclastic flows; 2) emission of viscous products such as the Piton Baille-Argent dome, the thick Mahaut ridge lava flow and the Gros Morne vent; 3) the volcanic activity ended with the undated Les Mamelles dacite domes that were emplaced on a 1.5 Ma old lava flow and are associated with the Malendure pyroclastic deposits (e.g. at Malendure town, figure 05). According to Boudon et al. (1992), the Malendure deposit corresponds to two sector collapses, and a third similar event produced the Deshaies deposit. The Deshaies and Malendure deposits have also been attributed to the Baille-Argent dome by Dagain (1981) and to the Bouillante Chain by Gadalia et al. (1988), respectively.

Axial Chain - The Axial Chain formed between 1-1.25 Ma and 0.445 Ma (Blanc 1983, Bouysse et al. 1985, Komorowski et al. 2005, Carlut et al. 2000, Samper 2007). Its lava flows do not overlie with the Northern Chain products and were probably erupted from WNW-ESE

fissures parallel to the Montserrat-Bouillante strike-slip fault system (Komorowski et al. 2005, Samper 2007).

The oldest north-western part of the Chain contains the Piton Bouillante peak (figure 05) and the Beaugendre valley. The origin of this valley has been attributed to: 1) the formation of a caldera (Westercamp and Tazieff 1980, Dagain 1981), 2) to a 8 km^3 sector collapse, which occurred 0.75 Ma ago (Boudon 1987), 3) to a hydrothermally altered area affected by the slow sliding movement of a pile of lava flows on top of argilised hyaloclastites (based on a geophysical anomaly; Gadalia et al. 1988) and 4) to erosion because it contains the oldest dated rock of the Axial Chain (e.g. Morne Soldat; Samper 2007). There are neither large pyroclastic deposits nor debris avalanche deposits associated with the valley, although such deposits may have been eroded and/or carried to the Grenade basin by submarine channels.

The Mateliane volcano was built south of the Beaugendre valley and is cut by the Vieux-Habitants valley. This valley is either: 1) a caldera that has produced the Danois rhyolitic pumice deposit (0.244 Ma ± 0.018 Ma; Westercamp 1980, Dagain 1981, Boudon 1987 and dated by Blanc 1983) or, 2) a 3 km^3 sector collapse 0.659-0.629 Ma old (Samper 2007) which has occurred along the Bouillante-Capesterre fault (Feuillet 2000). There are therefore several proposed origins for the Beaugendre and Vieux-Habitants structures, which are the largest valleys on Basse Terre.

The Vieux-Habitants valley is filled with volcanic products from the Icaque (0.629 to 0.6 Ma), Capesterre (about 0.544 Ma) and Sans Toucher (0.447 to 0.435 Ma; figure 05) volcanoes, which have built south of the Mateliane volcano (Blanc 1983, Samper 2007).

Mt Caraibe - This volcano forms the southern extremity of Basse Terre Island and is 0.6-0.4 Ma old (Bouysse et al. 1985, Blanc 1983). It was built by Surtseyan eruptions, which ended with the formation of the Houëlmont and Boucanier domes (figure 05).

Bouillante Chain - This Chain is a NW-SE to NNW-SSE alignment of sub-marine and sub-aerial monogenetic hydrovolcanic vents (e.g. table 1) with a wide range of magma compositions (basalt to rhyolite) located on the western flank of the Axial Chain (figure 05). It formed between 0.5 Ma or 0.8 Ma and 0.25 or 0.15 Ma (Westercamp and Tazieff 1980, Blanc 1983, Bouysse et al. 1985, Gadalia et al. 1988, Poussineau 2005, Samper 2007).
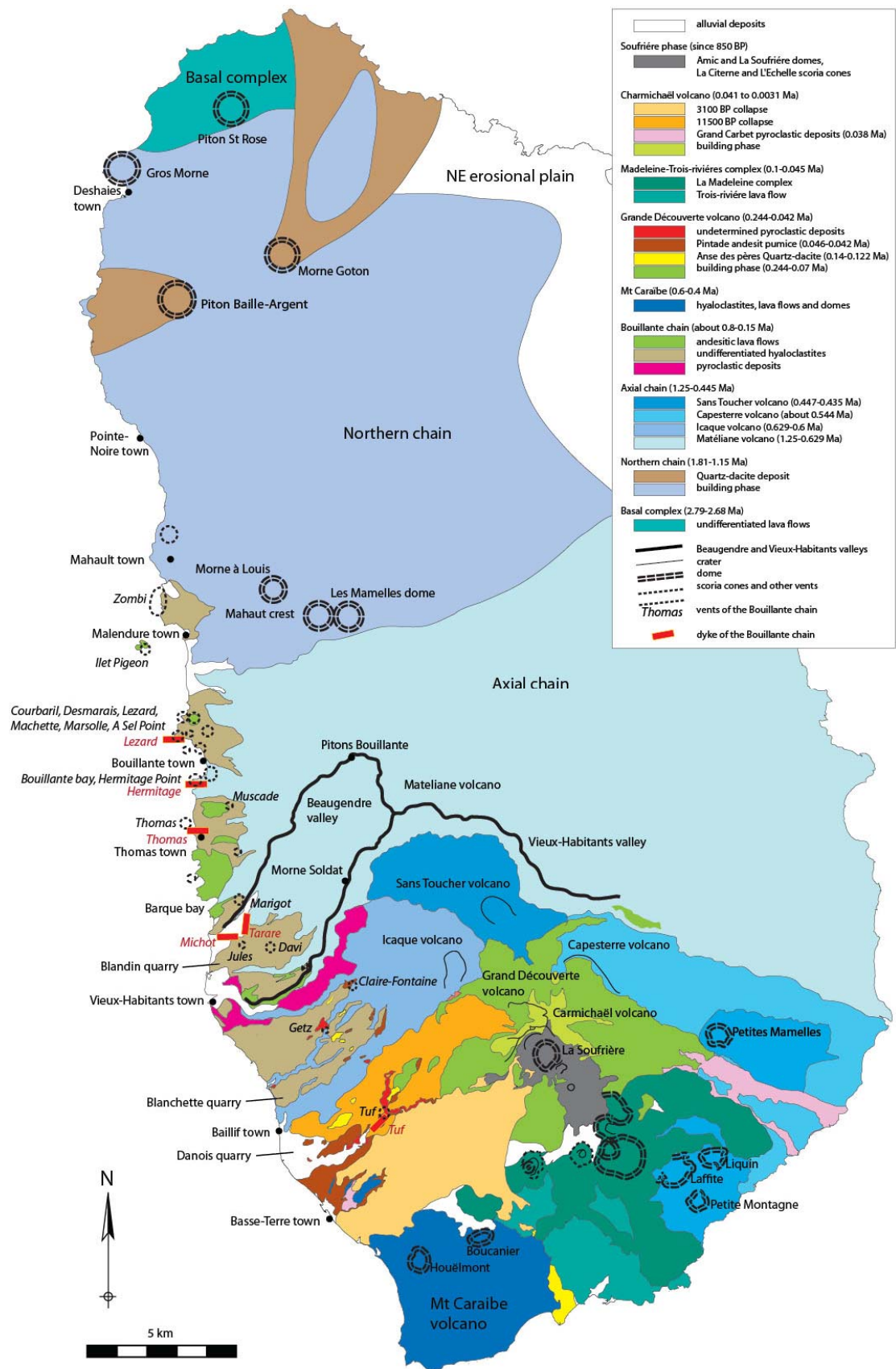
Figure 05: Geological map of the Basse Terre Island (after Boudon et al. 1988, Dagain 1981, Gadalia et al. 1988, Samper 2007).

Table 1: The eruptive vents of the Bouillante Chain (after Gadalia et al. 1988, Fabriol 2001, Sanjuan et al. 2008, Bouchot et al. 2010 and Blanc 1983); *see figure 05 for location

Name of vents	Age (Ma)	Description of deposits	Type of vent
Zombi *	0.57-0.35	coarse breccia and pyroclastic deposits	maar
Ilet Pigeon	n/a	hyalotuffs and lava flows	maar
A Sel Point	0.84	red and welded scoria, lava flow	scoria cone
Bouillante area	0.32 to 1.12	Hyalotuffs and lava flows from the Courbaril, Desmarais, Lezard Hill, Machette Hill, Bouillante bay, Marsolle Point and Hermitage Point vents	maars
Muscade-Thomas	0.48 0.6 1.3	hyalotuffs and other pyroclastic deposits, lava flows and the 090 striking dyke of Thomas bay.	from maar to scoria cone
Marigot	0.91	Hyalotuffs, pumice and 080 Michot dyke	maar
Getz, Davi and Claire-Fontaine	0.27 or 0.83	fallout and pyroclastic flows (e.g. Blandin quarry) associated with the 000 trending Tarare dyke.	contemporaneous vents
Jules	n/a	Debris flow with a pumice-rich matrix	maar and dome
Blanchette	n/a	Blanchette quarry pyroclastic deposits	uncertain
Tuf	0.32	rhyolitic pyroclastic deposits and 045 obsidian dyke	maar
Bouvier	0.24	Pintade Qz-dacite of Danois quarry	uncertain

Unnamed edifice - There is a gap of 0.4 to 0.3 Ma in the dates between the Axial Chain and The Grande-Découverte edifice formation, which may correspond to the formation of an unamed edifice that is today covered by the Grande-Découverte lava flows. This edifice may have produced the Petites Mamelles vent and the Petite Montagne (0.314 Ma; Samper 2007), Morne Laffite (0.261 Ma; Samper 2007) and Morne Liquin domes (figure 05), which are generally attributed either to the Mt Caraïbe volcano or to the Bouillante Chain (Boudon et al. 1988).

Southern Basse Terre - The southern and active part of Basse Terre Island has been studied in detail (e.g. geological map of Boudon et al. 1988). The Grande Découverte phase (0.244 to 0.042 Ma; Blanc 1983, Samper 2007) initiated with a large pyroclastic eruption, which has

formed a deposit (e.g. Danois rhyolitic pumice) used as a reference horizon to separate the more recent activity from the Axial Chain deposits. The Grande Découverte volcano effusive eruptions were interrupted by two large explosive events (Anse des Pères and Montval quartz-dacite, 0.14 and 0.108 Ma) and at least one sector collapse (Boudon et al. 1992). It ended with the formation of the Grande Découverte caldera (e.g. Pintade andesite pumice; Bouysse et al. 1985).

The monogenetic vents of the Madeleine-Trois-Rivières Complex (0.1 to 0.045 Ma; Samper 2007) had a feeding system independent from the Grande Découverte sub-volcanic complex (Boudon et al. 1992). It is a group of hydromagmatic and effusive vents that have produced lava flows, flow-domes, domes and rare scoria cones. These vents are aligned along the E-W border faults of the Marie-Gallante graben according to Feuillet (2001), however the E-W alignment is not clearly established, nor is the continuation of the grben faults into Basse Terre.

The Charmichaël volcano grew in the Grande Découverte caldera between 0.041 Ma and 0.0115 Ma (Samper 2007). Its effusive eruptions were punctuated by at least 3 explosive events and by several sector collapses. The largest of these collapses may have occurred along regional faults (trending 000, 020, 080, 150) and has produced extensive Debris Avalanche Deposits in the western part of the volcano (e.g. 11,500 BP and 3,100 BP events; Komorowski et al. 2005, Bouysse et al. 1985).

The Soufrière phase started 850 BP in the 3,100 BP collapse scar (Samper 2007). This phase formed several scoria cones and domes among which is the Soufrière dome, which results from the most recent magma eruption of Guadeloupe (1440 AD).

3. Contribution to the geological map of Guadeloupe

3.1. Remote sensing data

3.1.1. Presentation of data

The best way to study the morphology and the characteristics of a volcano or any mountainous area is with Digital Elevation Model (DEM) which is a 3D map of an area. A DEM is a grid made of X columns and Y rows and each node (e.g. the intersection between a row and a column) is associated with three numbers: X, Y and Z. The X and Y numbers refer to the location of the node in a geographical system. The Z number is a modelled elevation of the Earth surface at each of these locations.

In 2000, a DEM of the world was computed from radar data. It is called SRTM (Shuttle Radar Topographic Mission) and is accessible for free from the USGS-a website (e.g. bibliography). Its resolution is 3 arc seconds, which means that the size of its square pixel is 90 m by 90 m. The main advantage of the SRTM is to represent the whole Earth with a resolution sufficient for regional analysis at the scale of continents or countries. But this resolution is insufficient for an island the size of Guadeloupe, which is represented by less than 500 pixels along a N-S striking line. For example, it is hard to distinguish the La Soufrière dome (figure 06-a) with such a poor resolution.

Fortunately, I had access to another DEM that has been computed by the IGN (Institut Géographique National). It has a resolution of 25 m but has been computed for the southern part of Basse Terre Island only (south of Les Mamelles domes). I call it the IGN-25m-DEM (figure 06-b).

Having these two DEMs, I tried to improve their resolution, especially in the northern part of the island. In a first attempt I tried to extract a DEM with a resolution of 10 m by digitizing the contour lines of the IGN 1:25000 map of Guadeloupe. This method is however too time-consuming. I then try to extract a DEM from ASTER images (Advanced Spaceborne Thermal Emission and Reflection Radiometer). This second tentative also failed and the resulting

DEM was meaningless for several reasons: 1) all the available ASTER images have clouds which hide the crests; 2) the steep and complex slopes of the volcano generate shadows which hide extensive areas; 3) the small contrast offered by the rain forest renders the DEM computation almost impossible.
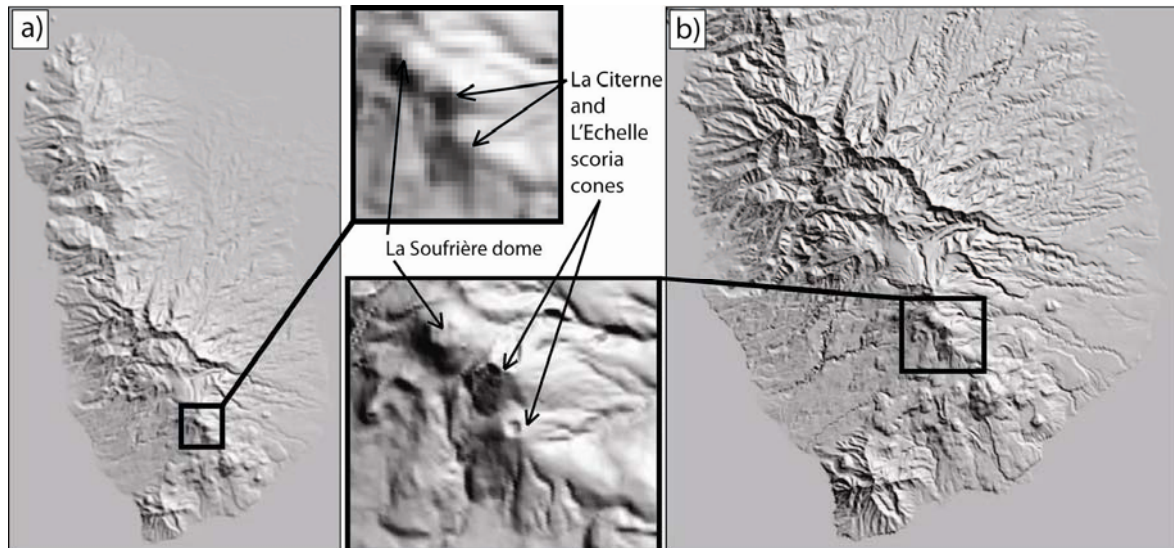
Figure 06: a) SRTM of Guadeloupe Island presented as an hill shade image (sun elevation = 45°, azimuth = 45°). The resolution is 90 m; a) IGN-25m-DEM presented as an hill shade image (sun elevation = 45°, azimuth = 45°). The resolution is 25 m.

3.1.2. Bathymetric data

3.1.2.1. Presentation and description of the bathymetric map

An offshore DEM for the Guadeloupe area was computed in 1998-1999 following the AGUADOMAR bathymetric campaign. I have been denied access to these data. However, the bathymetry DEM was published in 2001 by N. Feuillet whose thesis contains reproductions of it. I have used these pictures to better grasp the tectonic environnement of Guadeloupe. The aim of this section is not to list the strike, kinematics and slip of faults located in the vicinity

of Guadeloupe Island because this work was done with great detail and accuracy by N. Feuillet (2000) who had access to seismic profiles and bathymetry data. The aim of this section is to synopsize the regional tectonics of the area.

There are several valleys, such as the Pointe Noire and Basse Terre valleys on the west side of Basse Terre Island (e.g. figure 07). These valleys transport sediment from the volcanic activity and erosion of the island and prevent their deposition at the base of the volcanic edifice. For this reason, the debris avalanche deposits observed onshore (e.g. 11,500 BP and 3,100 BP events) do not have offshore equivalents, as already pointed out by A. Le Friant (2001).

Several NE-SW structures such as the Bertrand-Flamouth graben and some N-S striking lineaments are located east of the Guadeloupean archipelago (figure 07). These structures are located tens of kilometres NW of Basse Terre Island and are likely to have a limited effect on its structure. The island is surrounded by 090 and 140-160 striking lineaments. The majority of the 140-160 structures belong to the Montserrat-Bouillante and Les Saintes sinistral transtensional fault systems, which are located west of Basse Terre Island. The 140-160 striking structures occupy a wider area and define a corridor or fault zone whose eastern margin is possibly bordered by the NW-SE structures which develop on the middle of Grande Terre Island. This fault zone is about 50 km wide (e.g. figure 07). It contains and is surrounded by 090 extensional structures, including the Marie-Gallante graben. Most of the recent volcanic edifices, including Basse Terre volcanoes, Montserrat and Dominique Islands, Les Saintes archipelago and most seamounts, are located within the sinistral transtensional fault zone.

3.1.2.2. Interpretation of the bathymetric data

The bathymetric data indicate that the Monsterrat-Bouillante fault zone is a wide fault zone which overprints the volcanic front (figure 07). The volcanic front is a dyke swarm that enables the transportation of magma in the lithosphere. Its location and orientation correspond to the projection, at the surface, of the partially melted mantle. The melt is generated along the slab as it reaches a depth of about 150 km, which correspond to the depth of the Benioff zone beneath Basse Terre Island (Bouysse et al. 1990). The volcanic front is a major lithosphere discontinuity and the Monsterrat-Bouillante fault has overprinted it for this reason. Thus, the

strike of the fault is constrained by the location of the partially melted mantle and not by the tectonic movements generated by the oblique subduction that the fault accommodates.

The Marie-Gallante graben has formed parallel to the plate motion and to the main regional horizontal stress. This graben may accommodate the tensional movements of the Monsterrat-Bouillante fault, even if it is located more than 30° from the fault plane.
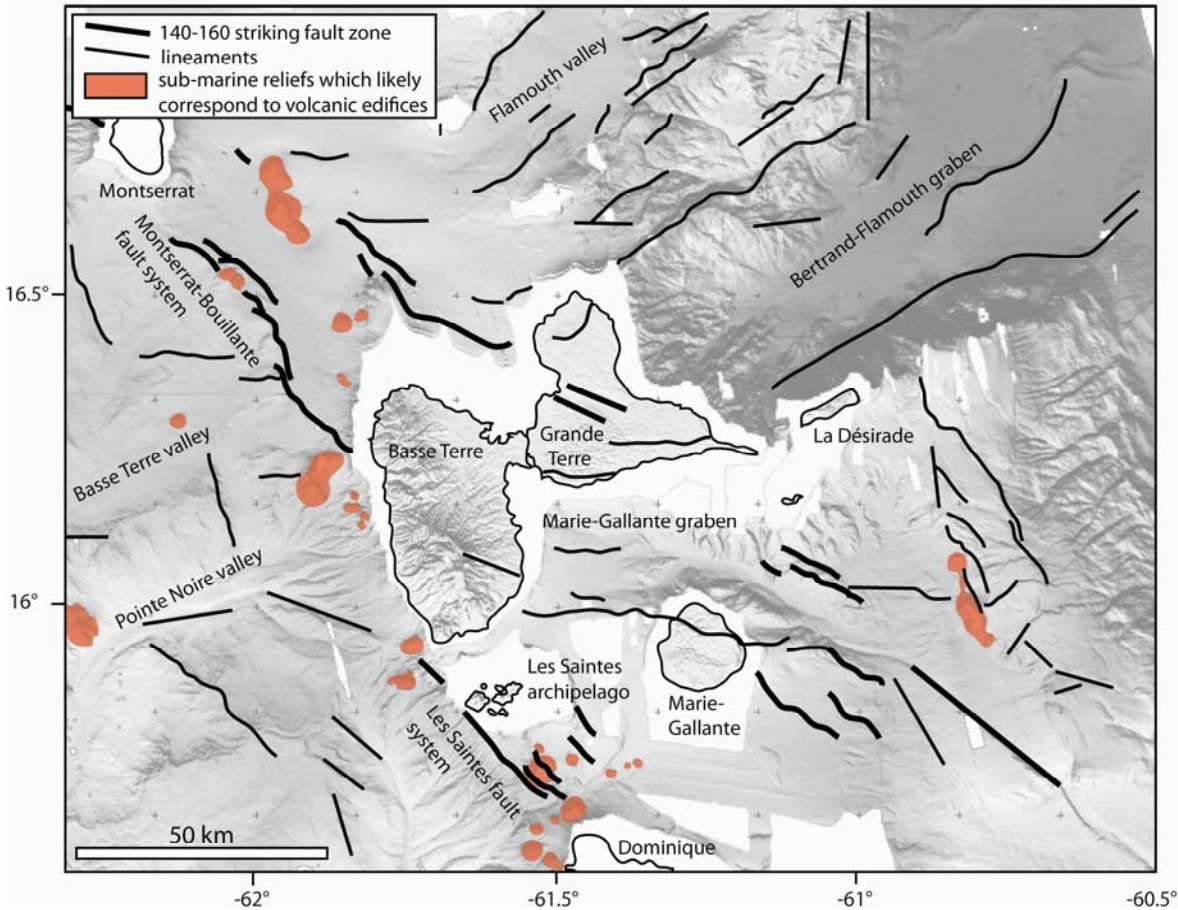
Figure 07: Onshore (IGN data, resolution= 50 m) and offshore (bathymetric data from the AGUADOMAR 98-99 campaign) DEM of the Guadeloupe area extracted from the thesis of N. Feuillet (2001). The sub-marine edifices and the main lineaments are shown (modified after Feuillet 2000).

3.1.3. Analysis of Digital Elevation Models

There are 4 main ways to present and analyse a DEM. It may be turned into 1) a slope map for which a specific colour is attributed to each slope value (figure 08); 2) a hill shade map, which is a relief map with an artificial and oriented lighting (figure 09-a); 3) a contour map, which corresponds to contour lines extracted from a DEM; 4) and an aspect map for which a colour is attributed to each flank depending on the geographical direction that they are facing.
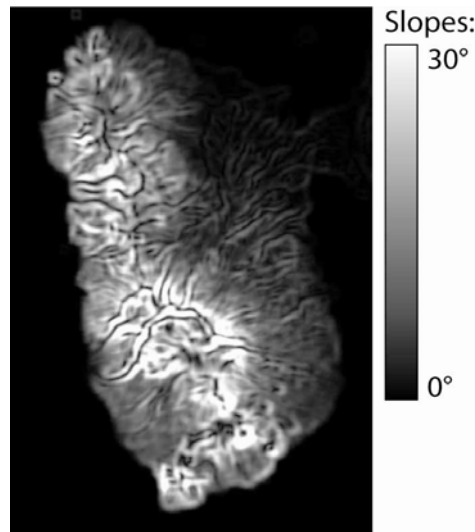
Figure 08: simplified slope map extracted from the SRTM.

A simplified slope map (figure 08) provides large scale information on Basse Terre Island. Based on this map, the island may be divided in two parts, which are located north and south of Les Mamelles domes. In the northern half, the steepest slopes are located in the Petite and Grande Plaine valleys (e.g. figure 09-b) and steep slopes are distributed at half-height around the volcanic edifice. Steep slopes are more frequent in the southern part of the island because it is made up of more recent (less eroded) volcanic products. There, the steepest slopes (25°-30°) make up the summit of the Axial Chain and Grande Découverte volcano and are organised along a NW-SE striking line (e.g. volcanic axis). The shallowest slopes (< 5°) are encountered in the NE plain. The most abundant slope encountered in Basse Terre Island is 15° (value computed with the statistical tool of ENVI software).

Basse Terre Island may be subdivided in three units according to the aspect map (figure 09-b). The first unit contains the northern half of the island (north of Les Mamelles domes) that has well developed W and E facing flanks. It is a NNW-SSE elongated edifice and its mountain

crest has been interpreted as a volcano-tectonic axis by Feuillet (2001). The SW part of the edifice is cut by the Grande and Petite Plaine valleys. These large valleys contrast with the smaller erosion valleys that dissect the rest of the Northern Chain. They are "drop-shaped": they are large in their upper part and become narrower at lower elevations. They may originate from catastrophic events such as collapses or caldera formation.
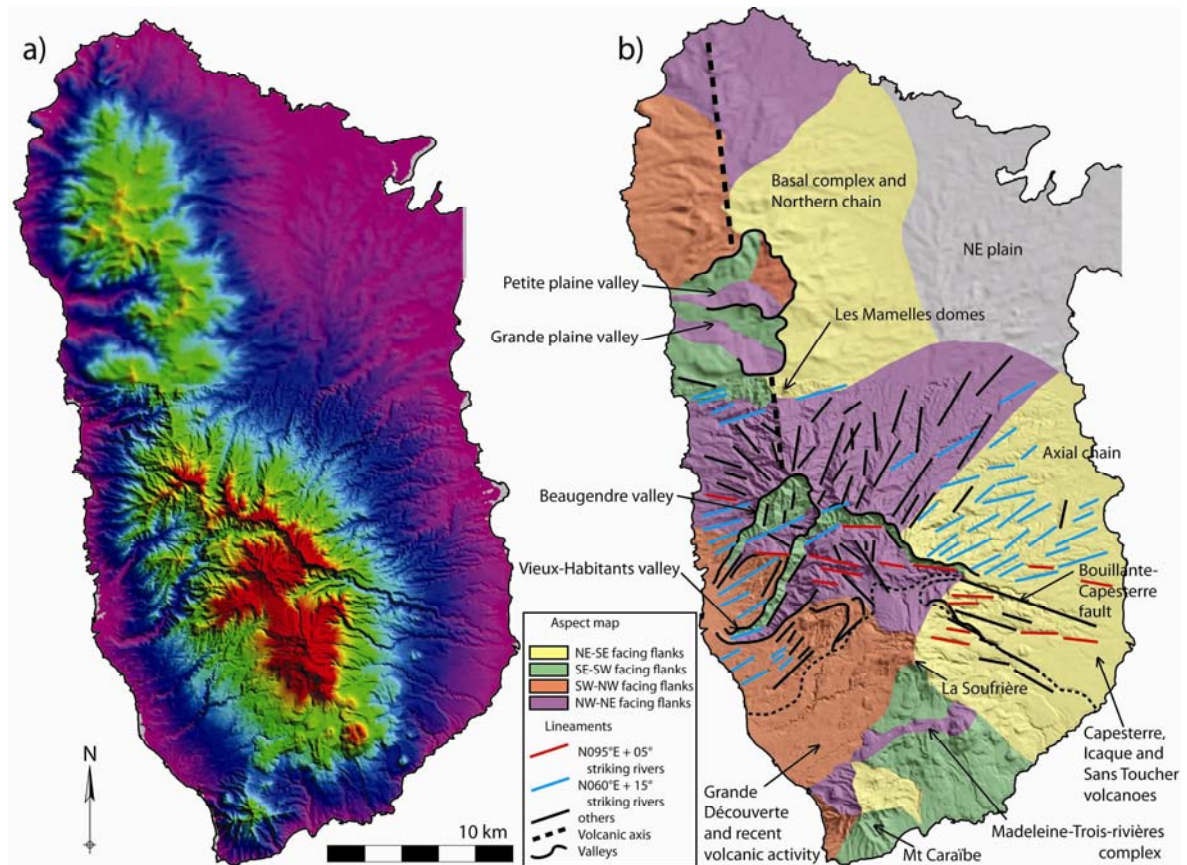
Figure 09: a) Basse Terre DEM presented as a hill shade map (sun elevation = 45°, azimuth = 045), resolution = 25 m; b) Basse Terre DEM presented as a hill shade map (sun elevation = 45°, azimuth = 045), resolution = 25 m, on top of which a simplified aspect map is presented as well as the main lineaments (rivers, valleys and mountain crest orientations).

The Axial Chain and the recent volcanoes are roughly rounded edifices, which form the second unit and the southern half of the island. The northern part of this area contains the Beaugendre and Vieux-Habitants valleys, which are both large and were possibly formed by

catastrophic events such as lateral collapse(s). The role played by erosion in the enlargement of these valleys after their initial rapid formation can not be quantified here. After 0.6 Ma (age of Icaque volcano, Samper 2007) the volcanic activity shifted toward the SE and formed several volcanic edifices inside the Vieux-Habitants valley. The largest of these edifices is the Grande Découverte volcano. It is a rounded edifice located south of the Vieux-Habitants valley, which culminates at the La Soufrière dome. The Madeleine-Trois-Rivières complex forms a roughly E-W striking crest on the southern flank of this edifice. The Mt Caraïbe is the third unit and forms an independent edifice, rounded in plan view, and located at the southern extremity of Basse-Terre Island.

A slope map is more reliable than hill shade maps to spot structures because lineaments are neither hidden nor emphasized by shadows. Initially, the general strike of rivers and valleys has been traced on several hill shade maps with different lighting azimuth. The strikes were then compared to those traced on a slope map of the IGN-25m-DEM that has a sufficient resolution for such analysis. The results are presented on figure 09-b. The rivers have a rough radial distribution on the flanks of the rounded Axial Chain volcano. There are, however, an excess of rivers striking 060 ± 15° and 095 ± 05° (figure 09-b). Beaugendre valley for example is oriented 065. The upper part of Vieux-Habitants valley strikes 090 and the central part of this valley is occupied by several rivers with similar trends. The 060 direction may correspond to a tectonic structure. The 095 ± 05° striking valleys are roughly parallel and possibly related to the 110-120 striking Bouillante-Capesterre normal fault along which the Vieux-Habitants valleys is thought to have developed (Feuillet 2000) and which is buried beneath the Capesterre River (figure 09-b) according to geochemical studies (Boudron 1990).

3.2. Field study

3.2.1. Method

3.2.1.1. Field area:

Basse Terre Island volcanoes are covered with a dense rain forest in which outcrops are rare and weathered. The most extensive, fresh and continuous outcrops were found along the western shore of the island, which receives less rainfall than the eastern one. Apart from this

area, the outcrops were found in river beds. Rivers have the double advantage of exposing continuous outcrops and tend to be easier to walk on than the surrounding forest, which is generally established over steep sloping areas. It has the disadvantage of containing waterfalls, steep banks and cliffs area (e.g. canyons) and to have a water level which raises fast during major rainfall. Some rivers were studied with canyoning techniques and all were visited during the dry season.

3.2.1.2. Lava flow cooling joints:

An important part of the field study consisted of measuring the orientation of lava flows. This was done directly when the base or top of a flow was exposed. However such outcrops are rare and most lava flow orientations were determined by the strike of their cooling joints. Most of these joints consist of closely spaced parallel fractures, which are parallel to the lava flow margins. The sub-horizontal to 30° dipping joints are parallel to the base of the flow and their orientations correspond roughly to these of the lava flows (figure 10). The sub-vertical joints are generally parallel to the margin of the flow, to levées (e.g. Appendix A) and to the flow direction. The first are referred to when a value for the orientation of flows is given in the text, the second are referred to as flow direction. Cooling joint orientations give a rough local measurement of the lava flow orientation and flow direction within a 10°-20° error.

Note that the bulk of plans measured on the field are characterized, in this thesis, by their strike, their amount of dip and their dip direction.

3.2.2. Geology of Basse Terre Island

This section described the geology of the Northern Chain (between Deshaies and Malendure towns), the Axial Chain (Bouillante, Vieux-Habitants towns) and the Grande Découverte volcano (La Soufrière dome area). The reader is referred to Appendix B to J for a detailed description of the outcrops studied on the field and for an access to the maps established during this study.
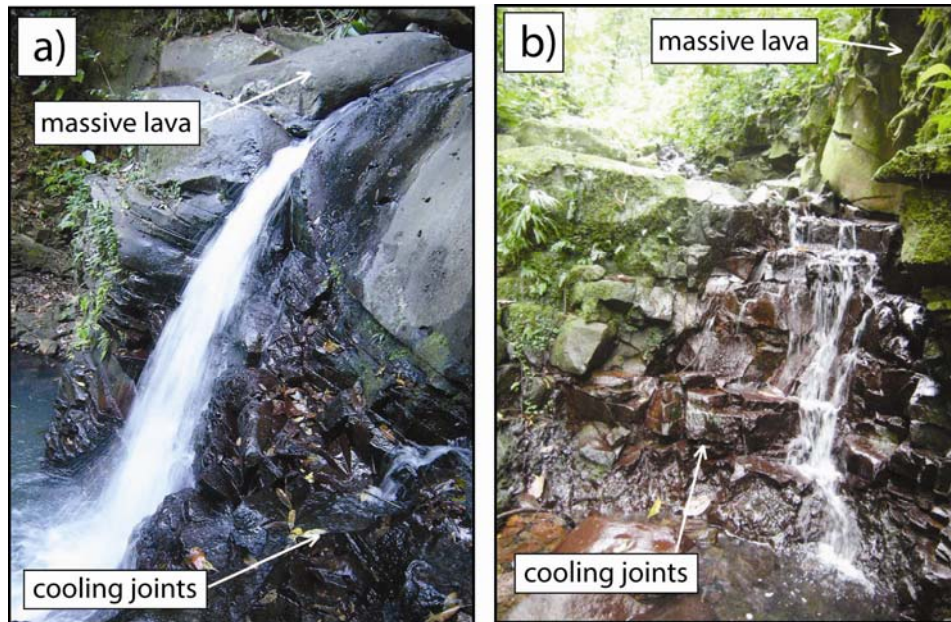
Figure 10: a-b) Pictures of massive lava flows with sub-horizontal cooling joints; the waterfalls are 5 m height.

3.2.2.1. The rocks found in the rivers of western Basse Terre

Most of the rocks found in rivers are fresh or weathered lava flows. The weathered flows are white clay rocks and are often observed upstream where the river is not large enough to deeply incise the weathered substratum to expose fresh rocks. The other rock type found in rivers are debris flows and river sediments (thin sand), which usually topped the lava pile.

However, several outcrops of weathered lava (Deshaies and Petite Plaine valley rivers, western Northern Chain; Appendix B-C) and river sand (Esperance, Losteau, Bouillante, Beaugendre, Vieux-Habitants and Plessis rivers; Appendix E and G) are interbedded with fresh lava flows. These clay and sand horizons correspond to phases of erosion between two lava flows eruptions. The debris flow deposits interbedded with lava flows in the Bourceau and Losteau rivers area (NW Axial Chain, figure 11; Appendix E) indicate that the formation of the Axial Chain lava flows were contemporaneous with the intense erosion of a nearby relief. Also, the unconsolidated horizons (clay, alluvium and debris flows) located in the lava pile are potentially low strength layers that may be exploited by landslide scare.
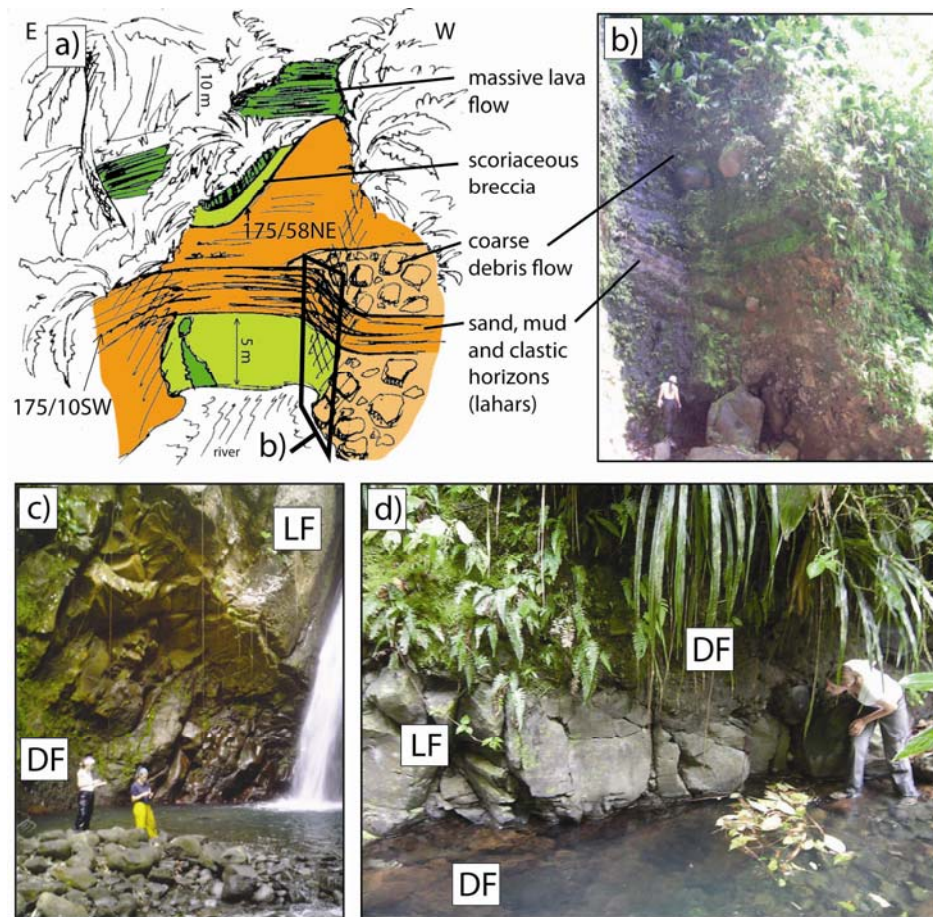
Figure 11: a-b) Sketch and picture of the 60 m high waterfall located upstream of Esperance River and exhibiting an imbrication of lava flows and palaeovalleys filled with debris flows and lahars; c) Lava flow located on top of lahars (Bourceau River); d) alternation of debris flows and thin lava flows (Bourceau River). DF stands for debris flow and lahar deposits; LF stands for lava flows (e.g. Appendix E for a location of these outcrops).

The debris flows deposits which topped the lava pile are thin and small extent block-rich deposits. Most of them correspond to small volume landslides formed by the destabilisation of the valley walls. In the Losteau River area (NW Axial Chain, Appendix E), a debris flow contains varicoloured clay blocks and originates from the destabilisation of the nearby Les Mamelles domes. The rivers of the Grande Découverte volcano contain few outcrops of fresh lava flows topped by many alluvial deposits, debris flows and debris avalanche deposits derived from the products of the recent activity and fast erosion of the Grande Découverte, Charmichaël and La Soufrière volcanoes (figure 12). Lahars and debris flows containing

pumice blocks and/or lenses of layered pumice-rich deposits are found downstream Bouillante and Beaugendre rivers and along the road south of Vieux-Habitants and Plessis Rivers (Appendix E and G).

The Vieux-Habitants River crosses the Axial Chain from E to W and was fully explored in order to determine if the topographic crest of Basse Terre corresponds or not to a dyke swarm. This river contains mostly massive lava outcrops as well as a limited extend accumulation of lava blocks which may correspond to a scoria cone (Appendix G). It contains only 4 exposed dykes (cf. section 3.3). Several dyke outcrops may however be hidden by the lava flows of the Sans-Toucher volcano, which have filled the Vieux-habitants valley (figure 05).
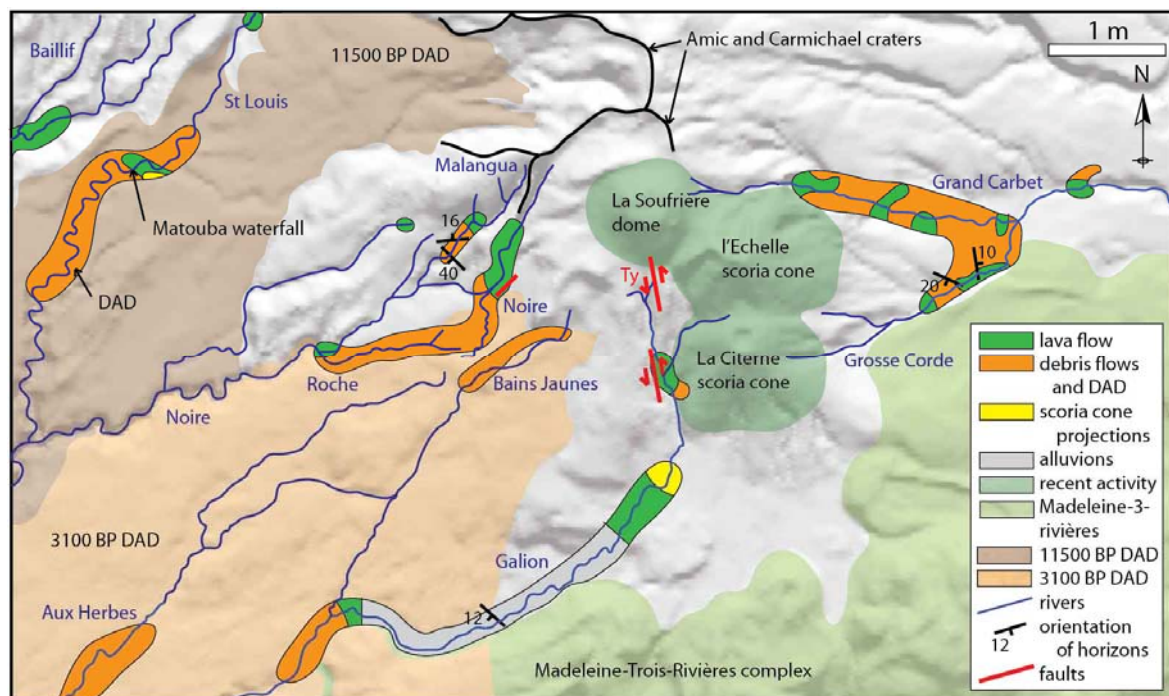
Figure 12: Map of the summit area of Basse Terre Island and geology of the area visited in the field (mostly rivers). The topography is a hill shade map of the IGN-25m-DEM. The Ty fault is drawn after Julien and Bonneton (1984). DAD stands for Debris Avalanche Deposit. The extent of the 11,500 BP and 3,100 BP DAD and their associated collapse scars (e.g. Amic and Charmichaël craters) are drawn after Boudon et al. (1988).

An important goal of this work was also to study the Bouillante Chain, which is described as an alignment of monogenetic hydrovolcanic vents rooted on the regional strike-slip fault.

However, none of the outcrops visited correspond to hydrovolcanic deposits. Also, the rhyolitic pyroclastic deposits of the Claire-Fontaine vent, which occur as road and river outcrops (e.g. Plessis River area) according to Gadalia et al. (1988), were not observed. Finally, the Tarare outcrop, which has been interpreted as a dyke, is actually a lava flow.

3.2.2.2. The western shore of Basse Terre Island

The western shore of the island provides good quality outcrops of debris flows, lahars, pyroclastic deposits and lava flows.

a) Western Northern Chain outcrops:

The lava flows of the western Northern Chain sandwich 5 to 15 m thick lahars and fallout deposits (Mahaut town area; Appendix D) and are topped by thick lahars and debris flow deposits. These deposits rework pyroclastic deposits (Deshaies town) and hydrothermally altered rocks (Ferry town area; Appendix B). The deposits of the Ferry town area are located over the quartz-dacite deposit identified by Dagain (1981) and attributed by this author to the Baille-Argent dome formation (Appendix B). The deposits mapped during this study correspond to the erosion of the hydrothermally altered Baille-Argent dome and its associated pyroclastic deposits and not to a primary volcanic deposit.

b) The Malendure and Pigeon deposits:

In the Malendure town area (Appendix D), extensive debris flows alternated with pyroclastic deposits topped the Northern Chain lava flows. The pyroclastic deposits are fallouts (figure 13-a), pyroclastic flows and block and ash flows (figure 13-b). I have named this assemblage of pyroclastic and debris flow deposits the Malendure deposit.

In the Bouillante town area (Appendix F), the Axial Chain lava flows and eruptive vents (A Sel point vent) are covered with a thick accumulation of debris flows, pumice-rich lahars, surges, pyroclastic flows and fallouts. I have named these rocks the Pigeon deposit. This deposit is thick in valleys, thin to absent over summit area, contains abundant horizons of ash and pumice with, locally, a curved base. According to these characteristics, I interpret the Pigeon deposit to be a pyroclastic flow deposit. I disagree with the hydrovolcanic origin usually attributed to these rocks (Gadalia et al. 1988).

The Malendure and Pigeon deposits are both a thick accumulation of pyroclastic and debris flows and may have a similar and contemporaneous origin.
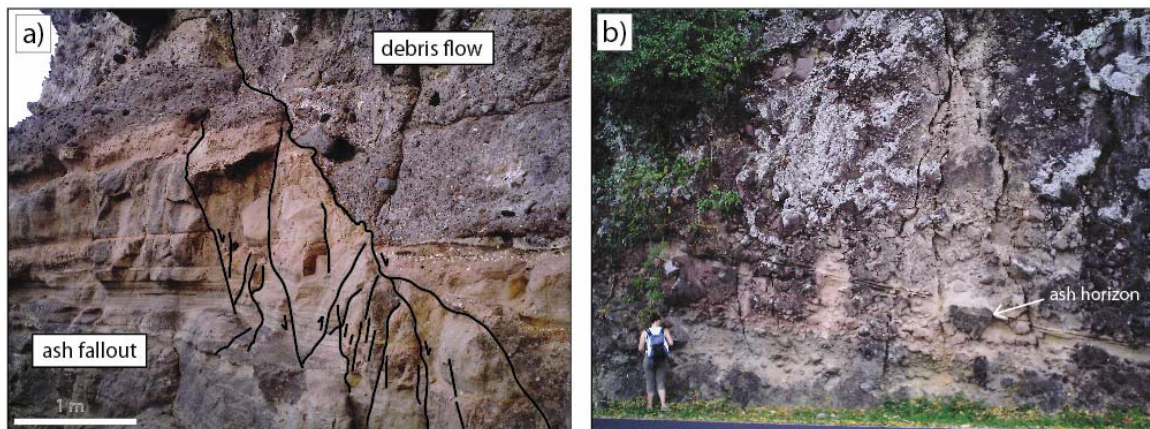
Figure 13: a) Normal fault (000/65E) with a slip of 1m. The fault offset the contact between debris flow and ash fallout (Malendure Point); b) block and ash deposit (Malendure town).

c) Western Axial Chain outcrops:

Between Bouillante and Vieux-Habitants towns (western Axial Chain, Appendix G), an accumulation of < 2 m thick fallout deposits and pumice-rich to poor lahars is topped by at least one lava flow. In the Vieux-Habitants town area, ash with accretionary lapilli, pumice-rich pyroclastic deposits and lahars are observed. South of Vieux-Habitants town, the Axial Chain lava flows are topped by < 5m thick pyroclastic deposits. These deposits are topped by up to 50 m thick lahars and debris flows that have reworked several pyroclastic deposits containing andesite and rhyolithic pumice (figure 14-b, c).

3.2.3. Orientation, thickness and petrology of lava flows

This section is based on field observations of lava flow thicknesses. It includes field estimates of the thickness of lava flows and of the size and relative abundance of feldspar, pyroxene and olivine phenocrysts.

The orientation of lava flows is presented by figure 15 and Appendix I. In the Northern Chain area, most of the lava flows strike N-S and dip 20° toward the west (figure 15-a). The flows located east of the volcanic axis (topographic crest) have a similar orientation. At the SW base of the Northern Chain volcano (Losteau River), several horizontal flows are measured. In the northern Axial Chain, the lava flows have a radial distribution around the Piton Bouillante Peak. In the southern Axial Chain, a limited amount of data indicates that lava flows strike N-S and dip toward the west.
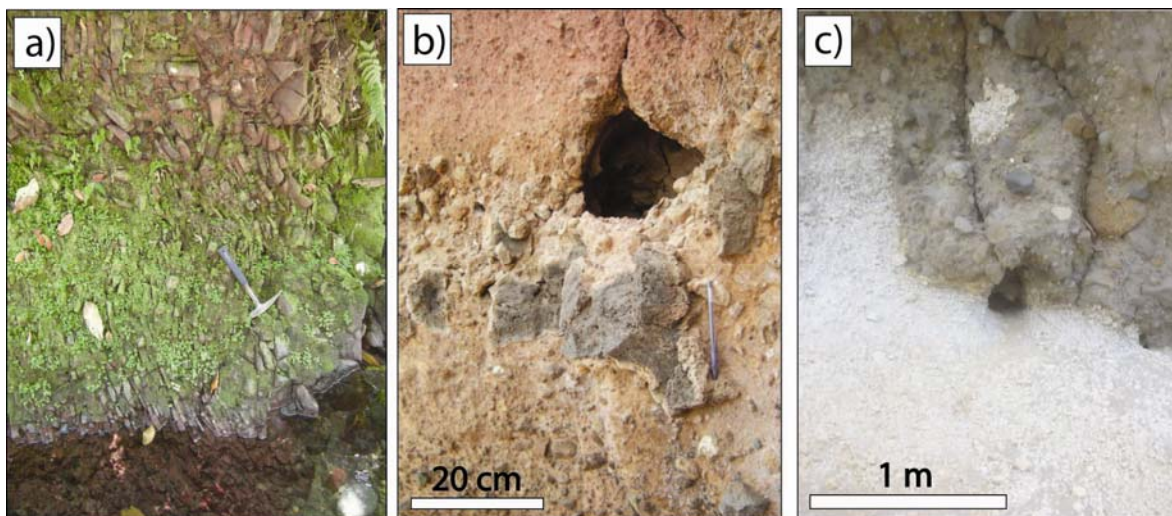
Figure 14: a) picture of a 145 striking fault zone, Beaugendre River (the hammer gives the scale); b) picture of big andesite pumice (dm sized) embedded in a lahar deposit (Rocroy beach); c) picture of rhyolitic pumice capped by a lahar deposit (north of Rocroy beach). The reader is referred to Appendix G for a location of these pictures.

In the Northern Chain area (from Deshaies to Losteau rivers) the lava flows are about 10-20 m thick. Thinner lava flows are observed in Zombi Point (2-5 m thick flows) and close to P^t687 eruptive vent (5-8 m thick flows). These flows contain less then 5 mm long (usually less than 1 mm long) phenocrysts of feldspar (about 50% of the volume of phenocrysts) and pyroxene (~ 50%). About 20% of the lava outcrops observed contains 10-20% of olivine phenocrysts. The olivine is observed in all the rivers, in Zombi Point lava flows and in the Losteau River dykes.
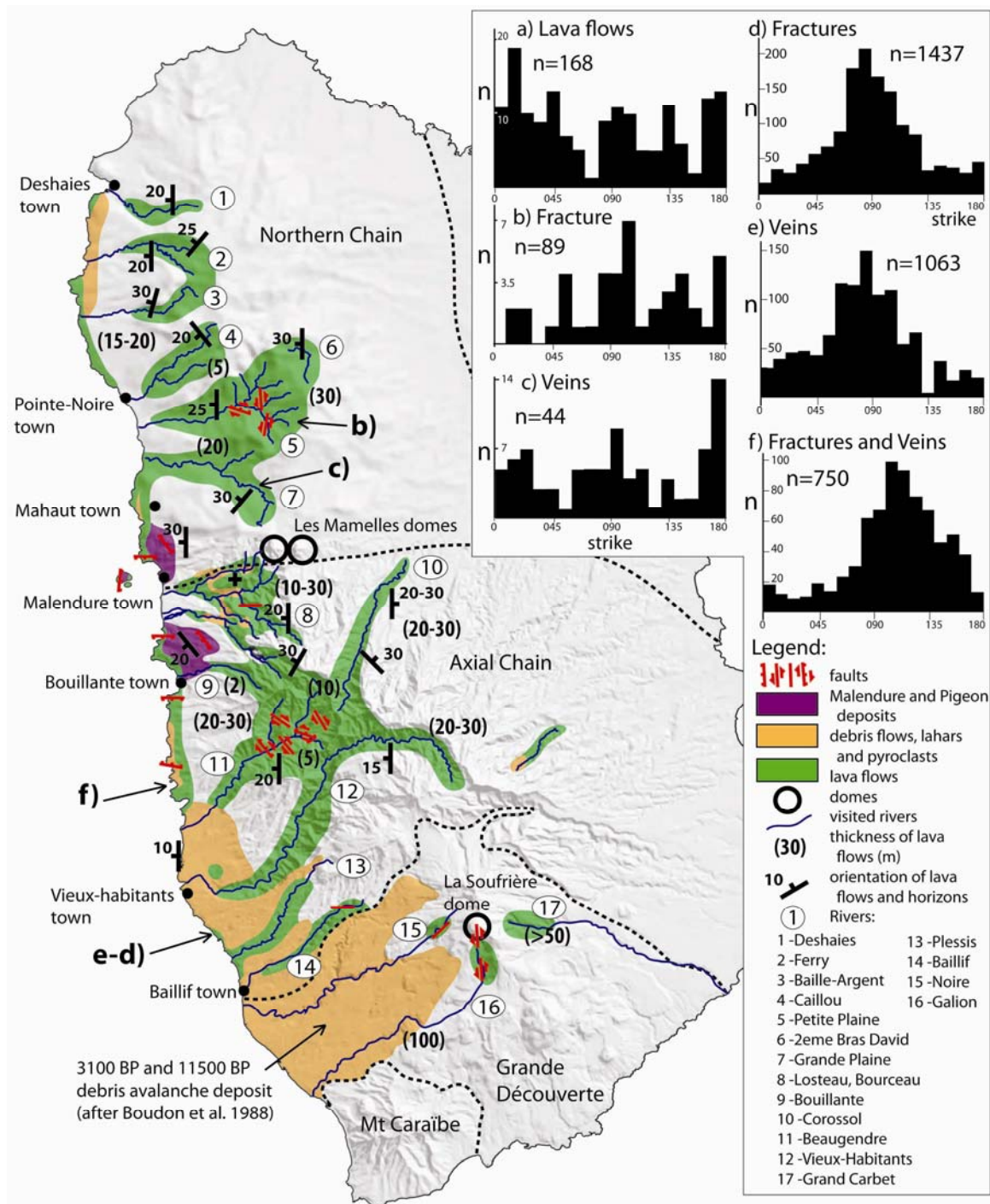
Figure 15: Simplified geological map of Basse Terre Island. The small-volume landslide originating from the erosion of valley walls are not represented; a-f) Histograms of the strike of structures measured in Basse Terre Island, a) lava flow orientation and flowing directions (Northern Chain); b) fractures (Petite Plaine valley); c) veins (Grande Plaine valley); d-f) fractures and veins measured south (d-e) and north (f) of Vieux-Habitants town.

In the Axial Chain area (from Bourceau to Baillif rivers) the lava flows are 5-20 m thick. The flows are thicker around Piton Bouillante Peak (~ 30-50 m thick flows) and south of it (over 30 m thick flows). Along the shore and in Racoon River (eastern flank of Piton Bouillante volcano), the phenocrysts of feldspar (~ 70%) and pyroxene (~ 30%) are over 5 mm long. In the northern Axial Chain (Bourceau Rivers) the lavas are aphyric or contain less than 2 mm long phenocrysts of feldspar (~ 50%) and pyroxene (~ 50%). South of this area, the phenocrysts are less than 5 mm long (~ 2 mm long) and there is usually more feldspar (~ 50-70%) than pyroxenes (~ 50-30%). The dykes of Beaugendre River have a similar composition.

Further south, the lava flows of the Grande Découverte volcano tend to be thick. The flows of the Madeleine-Trois-Rivières complex (figure 05), for example, which are well preserved in the topography, are 100 m thick.

3.2.4. Structures measured in the rivers of Basse Terre Island

This section presents the structures measured in the rivers of Basse Terre Island (Appendix J-table J-01). These structures are faults, vertical fractures and mineralised fractures (veins). Only 10 faults have been documented in the rivers by over 5 months of fieldwork. I have also measured many fractures and veins to better grasp the pattern of the tectonic movements which affect Basse Terre Island.

A fracture is either formed by tectonic movements or by local processes such as the cooling of a lava flow (cooling joints), by the flowing and deposition of pyroclasts or blocks and by the erosion and destabilisation of deposits (landslides, sea cliff erosion). For instance, the fractures and veins parallel and orthogonal to the flow direction of a deposit are possibly related to the flowing, deposition (debris flows) and cooling (lava flows) of the rocks. For example, the E-W and N-S striking fractures measured in lava flows (Appendix J-table J-01; figure 15-b, c), which have dominantly flown from east to west (see previous section), are interpreted to be cooling joints.

However, the dominant strike of fractures measured in the bulk of rivers (Axial and Northern chains) is 000 ± 15° (29% of the 647 data available). The N-S striking structures are especially well represented in the northern half of Basse Terre Island and have either a

tectonic origin or correspond to the natural fracturing of rocks located over a N-S striking slope.

The 050 ± 05° striking structures measured in the 11,500 BP and 3,100 BP Debris Avalanche Deposits (DAD) located west of La Soufrière dome are parallel to the deposit flow direction and are likely related to the generation and emplacement of the DAD. The 170 ± 05° striking structures measured in this deposit (Appendix J-table J-01) may have a tectonic origin.

Other structures may form in a lava flow as it emplaces and cool. For example, its levées (Appendix A) may be deformed by the flowing rocks that it channels. This mechanism has possibly formed the 120/62SW striking strike-slip fault measured in the Grande Plaine valley and the 080-100/90° and 120-130/40N-S oriented fractures measured in the well exposed margin of a lava flow downstream Bois Malaisé River (Appendix J-table J-01).

The 170-010 sinistral striking strike-slip faults measured in the Northern Chain and Grande Découverte volcano may have a tectonic origin (figure 15). The 170 striking fault located in the upper reaches of the 170 striking Galion River may correspond to the prolongation of the Ty fault, which is a 170 striking strike-slip fault documented in the La Soufrière dome by Julien and Bonneton (1984).

The Beaugendre River contains four 140 and one 110 striking normal and strike-slip faults (figure 14-a, 15; Appendix J-table J-01). Most of these faults have a well developed fault zone and their slip could not be quantified due to the absence of a suitable reference horizon in the lava pile. These structures may have a tectonic origin.

3.2.5. Structures measured along the western shore of Basse Terre Island

3.2.5.1. Structures measured along the western shore of the Northern Chain:

Along the western shore of the Northern Chain, the largest amount of structures has been measured in the Malendure deposit. North of this deposit, the fractures and veins measured in lava flows are cooling joints, which strike 160-015 (e.g. parallel to lava flow orientation) and

085-110 and 130-150 (e.g. parallel to lava flows direction, Appendix J-table J-02). The structures contained in the debris flows that capped these lava flows have a similar strike.

The horizons of the Malendure deposit are oriented 170/08-50W (n=19) and 035 ± 10°/20E-W and 100 ± 10°/20N-S when they are found by channel borders (n=21; figure 16). The Malendure deposit has flown from east to west and has been channelised by NE-SW and E-W striking valleys. It contains a large amount of veins, fractures and faults which have the following characteristics.

The veins, fractures and normal faults (figure 17-b) of the Malendure deposit are mostly striking 140 and, to a lesser extent, 100-110 and 000 (Appendix J-table J-02). A normal fault located at the Malendure point strikes 120/70NE and has the largest slip (10 m) documented in this area (figure 18; Appendix J-table J-02). It is associated with another E-W striking and south dipping normal fault located in the unmapped area and observed from afar (e.g. figure 17-a). These faults border a subsiding area (figure 17-a). Eventually, the 010/65SE oriented normal faults (dip < 1m) measured in the fallout deposit of Ilet Pigeon Islands are parallel to the N-S striking depression in which the pyroclasts have accumulated.
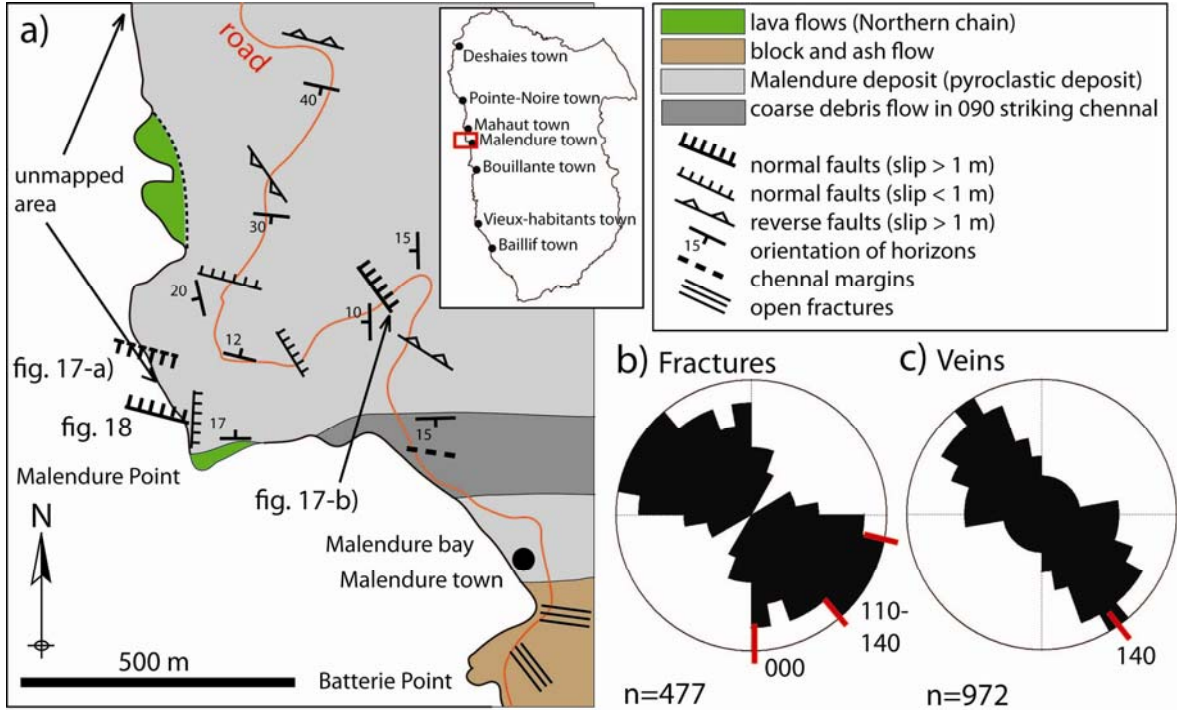
Figure 16: The Malendure deposit; a) Structural sketch; b) Rose diagram made with the 477 fractures measured in the Malendure deposit; c) Rose diagram made with the 972 veins measured in the Malendure deposit.
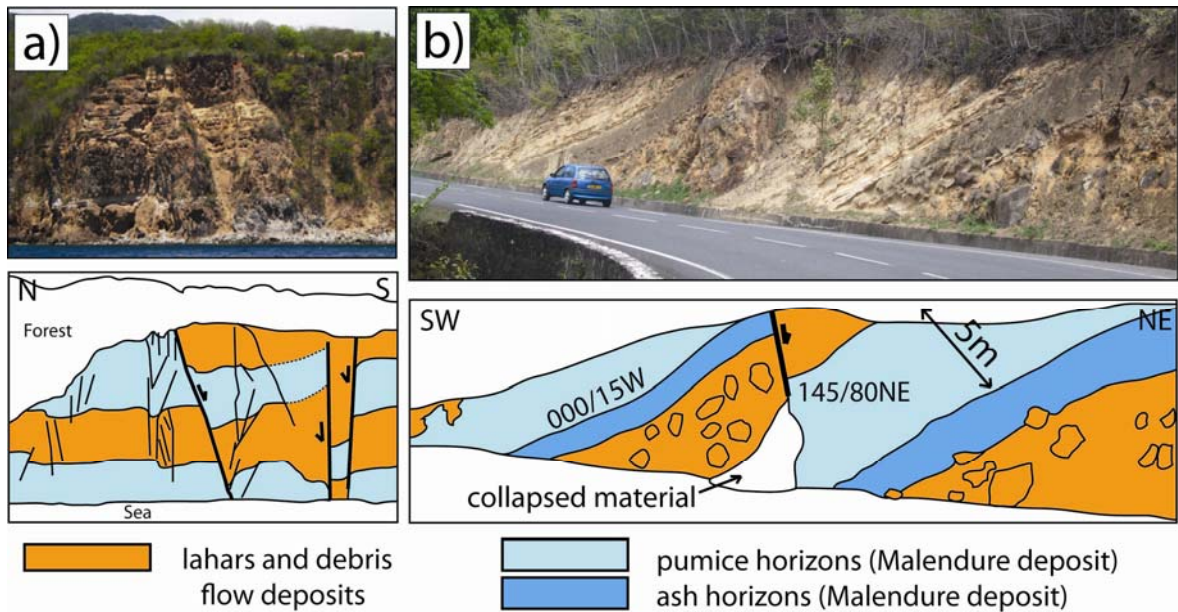
Figure 17: a) Pictures of E-W striking normal faults of the Malendure deposit observed from afar (unmapped area), the cliff is 50 m high (Malendure point). The southern fault is accessible from the shore (figure 18); b) Road outcrop of a 145 striking normal fault (cf. figure 16 for location).
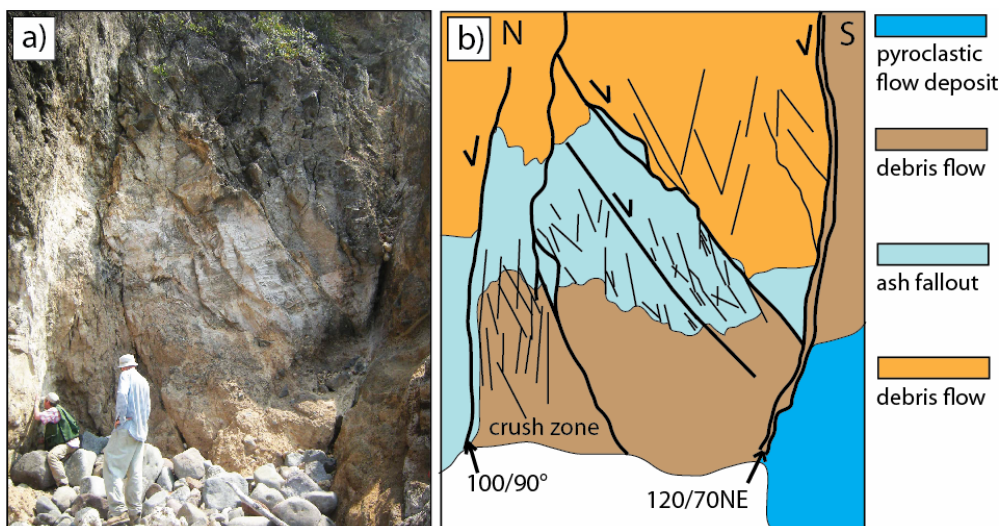
Figure 18: a-b) Picture and sketch of a 120 striking steeply dipping normal fault located a few meters north of Malendure point (cf. figure 16 for location). The fault zone is 4 m thick, the dip-slip of the fault is 10 m and the strike-slip component of movement, if any, has not been quantified. The outcrop is observed from the west.

The structures contained in the Malendure deposit are parallel or normal to the flow direction of the material, and parallel to the substratum topography (valleys walls). These structures have either a tectonic origin or originate from the destabilisation of loose pyroclasts and blocks deposited over steep valleys walls. Both mechanisms may have formed the brittle structures measured in the Malendure deposit.

3.2.5.2. Structures measured along the western shore of the Axial Chain:

a) The Bouillante geothermal field area

In the Bouillante area, the Axial Chain substratum is made of a scoria cone (A Sel point vent) and a pile of lava flows eroded by E-W striking valleys (cf. figure 09-DEM analysis section). This substratum has been hydrothermally altered by the Bouillante geothermal field (Appendix F). The dominant strike of veins and fractures measured in these rocks is 080-120 (Appendix J-table J-03) and may correspond to lava flow cooling joints exploited by hydrothermal fluid circulation or may have a tectonic origin.

The Hermitage point (Appendix F) lava flows contain a cluster of 110, 110/60NE and 110/60SW striking fractures and veins, which may have been formed by normal faulting (Appendix F and J-table J-03).

The Axial Chain substratum is topped by the pyroclastic and debris flow deposits of the Pigeon deposit (Appendix F). The horizons of the Pigeon deposit are oriented $145 \pm 05°/10$-30SW and $100 \pm 10°/20$-40SW, indicating that the rocks have flown from the NE and have emplaced in E-W striking valleys. The 170 and 095 striking fractures and veins of the Pigeon deposit are parallel and normal to the E-W striking substratum valleys. The E-W striking normal faults of the Pigeon deposit (slip < 2 m; Appendix J-table J-03) are located a few meters away from the valley walls. These structures originate from the destabilisation of the pyroclasts and blocks deposited over steep E-W striking valley walls. The Pigeon deposit contains also 140 striking fractures and $140 \pm 10°/70$SW-NE striking normal faults (n=10, slip < 1m; figure 19, Appendix J-table J-03), which are normal to the flow direction.
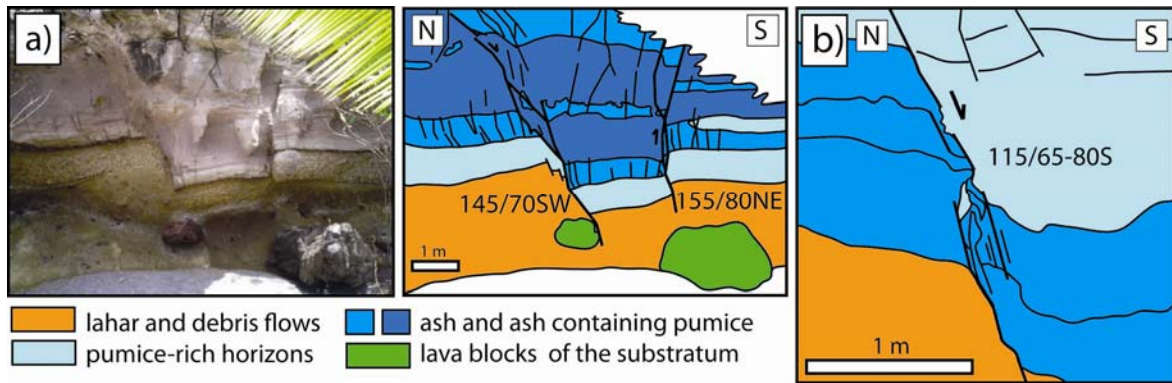
Figure 19: a-b) Normal faults of the Pigeon deposit (cf. Appendix F for location).

b) The SW Axial Chain area

North of Vieux-Habitants town, the fractures and veins measured in the lahars, debris flow deposits and lava flows strike 090 to 140 (Appendix J-table J-03). They correspond to randomly oriented structures measured along a N-S striking shore line. South of the town of Vieux-Habitants, over half of the fractures and veins measured strike 090 ± 20° (Appendix J-table J-03; figure 15-d, f).

Two 100/50NE oriented faults are found along the shore. The northernmost is located in the lahar deposit of Anse Duché Bay (e.g. Appendix G for location) and was possibly formed by the re-mobilisation and deposition of the mud and blocks. The second fault is located south of Petite Bay and separates a lahar with pumice capped by a lava flow, from colluvium in the hanging wall. This structure is a landslide scar filled with loose surface materials. It was not possible to determine in the field whether it corresponds to cliff erosion or to a recent earthquake.

3.3. The dykes of the Basse Terre Island

3.3.1. Introduction

The map of De Reynal (1966) is the only document which refers to dykes in the literature. In the area of what is today called the Axial Chain, De Reynal (1966) has drawn 9 dykes in the Vieux-Habitants River, mostly in the Morne Merwart area, which strike ENE to ESE and N-S. These dykes were not observed during this field study and might have been mistaken with lava flow levées. The other intrusions are located in an area that would be difficult to access even with a rope and a large machete. Another article by Wadge (1986) studies the dykes of the Lesser Antilles. Unfortunately, this article doesn't propose any dyke orientations for Guadeloupe. There are thus no reliable data on Basse Terre dykes in the literature. The only indications are indirect and concern the alignment of volcanic edifices to which most dykes are expected to be parallel.

3.3.2. Field dat

3.3.2.1. The recognition of dykes in the field:

It is not easy to identify a dyke in a rain forest environment mostly because of the limited extent of outcrops. The interface between the massive core of lava flows and their upper scoriaceaous breccia is often complex and is made of massive lava digitations that intrude into the upper breccia (figure 20-a). On a limited outcrop scale, such sheet-shaped digitations are easy to mistake for a dyke. They have irregular margins and are abundantly fractured parallel to their margins. Most Guadeloupean dykes, on the other hand, have straight borders and often develop cooling joints normal to their margins (figure 20-b, c). These simple criteria were used to distinguish dykes from lava flow structures.

3.3.2.2. Presentation of data:

Dykes are observed between 200 m and 500 m elevations. Few dykes are observed north of Piton Bouillante Peak, possibly because most of the visited rivers are filled with recent debris flows. The Losteau River contains two 090 striking dykes, the Jeanneton River contains two

small (20 cm thick) dykes striking 120 and 167/55NE and the Corossol River, in which lava flows are well exposed, contains a 070/75NW oriented intrusion (figure 20-d, e).
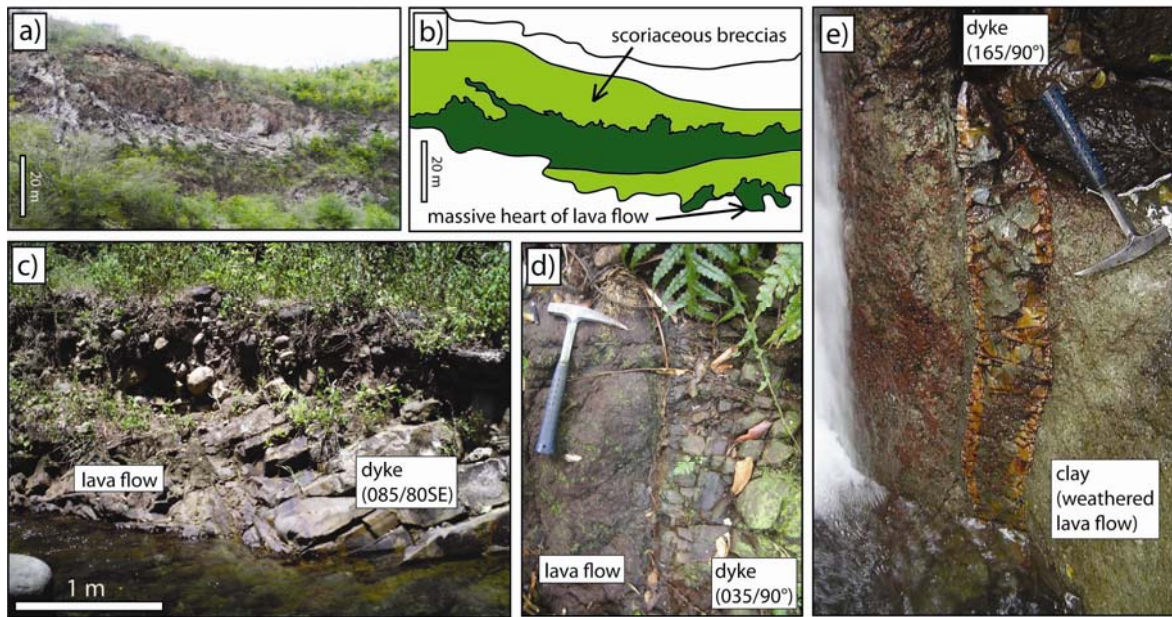
Figure 20: a-b) Pile of lava flows in the Beaugendre River (quarry, Marigot town); c) 2m thick dyke intruded in massive lava (Beaugendre River); d) edge of a dyke intruded in a scoriaceaous lava flow breccia (Dufour River, Beaugendre valley); e) 0.2 m thick dyke (Jeanneton stream, Petite Plaine River).
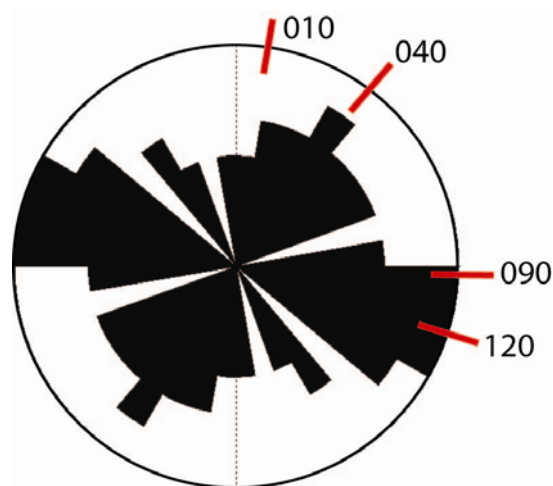
Figure 21: Rose diagram representing the strike of 46 dykes dipping 70° to 90° and measured in the Beaugendre valley.
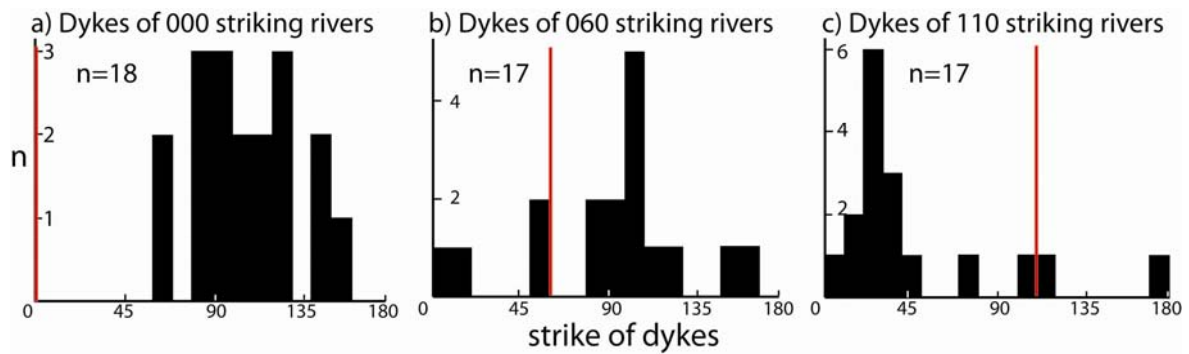
Figure 22: a-c) Histograms of the strike of dykes measured in 000, 060 and 110 striking rivers. There is a relationship between the strike of dykes and the strike of the river: the 110 striking rivers contain abundant 030 striking intrusions while 000 striking rivers contain E-W striking dykes. The red line corresponds to the mean orientation of the rivers.

The Vieux-Habitants River crosses at least four dykes. There are possibly more dyke outcrops, but it has not been possible to reach certain portions of the river due to canyons (e.g. Appendix G). Three 170-020 and a 110 striking dykes can be traced from the base to the top of 50-100 m high cliffs of scoriaceous breccia. These 3 to 5 m thick dykes are the thickest observed in Basse Terre.

The Beaugendre valley contains the largest amount of dykes seen in Guadeloupe. Forty-six intrusions that are 0.5 to 2m thick have been measured in this area. They strike 090 ± 05° (n=9), 120 ± 10° (n=16), 040 ± 10° (n=10) and 010 ± 10° (=5). The E-W to ESE-WNW and the NE-SW orientations predominate (figure 21).

Figure 22 shows a relationship between the strike of dykes and the orientation of the river in which they were measured. In other words, the mapping area is occupied by 010, 040, 090 and 120 striking dykes as mentioned earlier but the relative abundance of each of these dykes may entirely depend of the strike of the river in which they were measured. The field study provides information on the strike of dykes but the statistics made with these data must be interpreted with care.

From these data it can be seen that the northern and western parts of Beaugendre valley contain essentially E-W striking dykes. Further toward the east, NE-SW dykes are found, and further again, in the Beaugendre and Vieux-Habitants valleys, N-S striking intrusions dominate. These intrusions are radially distributed around a centre located in the vicinity of Morne-trois-Crêtes and Piton Bouillante peaks (e.g. figure 23).
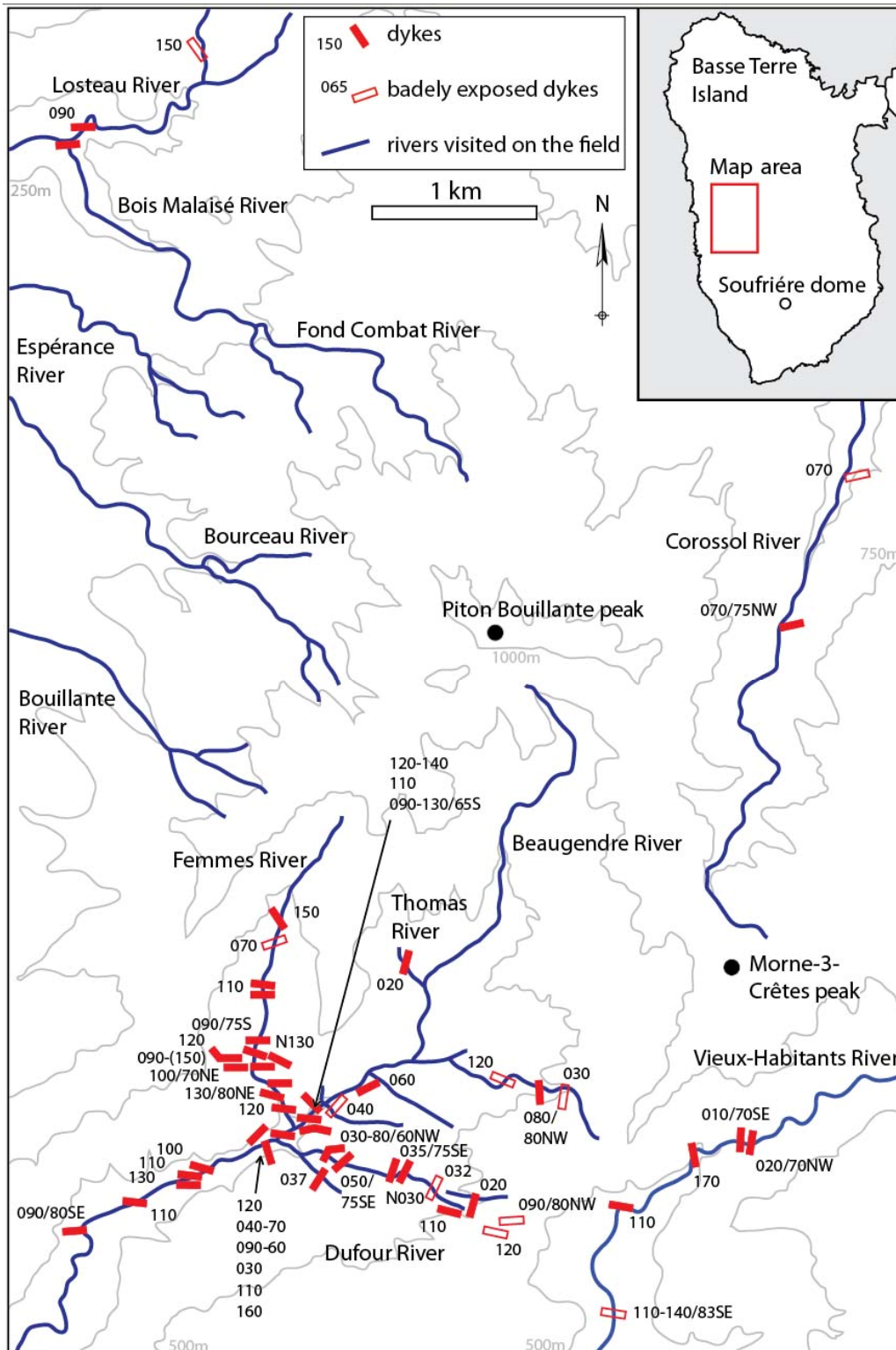
Figure 23: Dykes of the Beaugendre, Vieux-Habitants, Losteau and Corossol rivers. Filled red rectangles represent dyke intrusions. Unfilled red rectangles represent dyke intrusions which have not been identified with certainty due to the bad quality of outcrops. The topography is re-drawn from the IGN topographic map (1:25,000).

4. Discussion

4.1. Northern Chain Volcano

The northern part of Basse Terre Island is a NNW-SSE elongated mountain formed of the poorly exposed rocks of the Basal Complex and of the Northern Chain (figure 24-a). The Northern Chain is a single central volcano (e.g. age data of Samper 2007) made of the most fluid lava flows observed in Basse Terre (e.g. thin flows containing olivine). Most lava flows measured on this volcano have flowed to the west direction, although some have flowed to the NW (Deshaies area) and to the SW (Petite and Grande Plaine rivers). The lava has flown over the long N-S striking flanks of the elongated edifice and over its northern NW and southern SW facing flanks, respectively. The large amount of horizontal lava flows observed in Grande Plaine Valley may have been emplaced at the base of the Northern Chain volcano. The bulk of lava flows measured have flowed toward the west (e.g. NW or SW), even those measured east of the N-S crest (e.g. $2^{\text{éme}}$ Bras David River). This observation may indicate that the volcanic crest, or volcanic axis, was initially located east of the present-day mountain crest and has been eroded by the eastern rainfall. The volcanic crest could be regarded as an area used preferentially for the transport of magma. However, the lack of N-S dyke swarms and the dispersal of domes and other vents indicate that the magma was not exclusively channelled along the volcanic axis.

The small extent debris flows found in the rivers correspond to local destabilisation of valley walls. The products of the Northern Chain erosion have accumulated along the shore, on the coastal shelf of the island. These debris flow deposits have reworked pyroclasts, including pumice, which are evidence of violent eruptions. These eruptions may have, for the most part, occurred toward the end of the activity of the Chain and be linked with the formation of the domes. The reworked pyroclastic deposits located underneath a lava flow west of Mahaut town indicate that some effusive eruptions occurred after the violent explosive eruptions.

The Grande and Petite Plaine valleys have deeply incised into the edifice and may have formed by lateral collapse during or after the end of the Northern Chain activity (figure 24-b). There is no evidence to support this theory apart from the horse-shoe morphology of these deep valleys. Any debris avalanche deposits could have been transported away from the island through the Basse-Terre sub-marine valleys (e.g. bathymetry section). These collapses

may have occurred along weak horizons, such as the clay strata (e.g. weathered lava flows) observed in the lava pile as river outcrops.

The majority of the structures measured in the Northern Chain area correspond to lava flow cooling joints or fractures linked to the deposition of debris flows. The 160-000 striking fractures and veins measured in the vicinity of the Deshaies town are either related to sea erosion of a N-S striking shore line or are of tectonic origin.

4.2. The Malendure and Pigeon deposits

The Malendure and Pigeon deposits are an alternation of block and ash deposits (Malendure town), ash and pumice-rich fallouts, surges, pyroclastic flows and lahars. The Malendure and Pigeon deposits share many characteristics, such as the thick succession of alternating lahars and pyroclastic deposits and the abundance of pumice in both cases; and likely originate from the same eruptive event. These deposits were produced by Plinian eruptions, which formed an eruptive column (associated with fallout deposits) that eventually collapsed (pyroclastic flow and surge deposits) to form deposits that were rapidly mobilised by erosion (ash and pumice-rich lahars and debris flows). The formation of several successive eruptive columns explains the observed interbedding between the pyroclastic deposits and the lahars. After the explosive phase, dome growth occurred and the collapse of part of the dome produced the block and ash flows found in the Malendure town and further pyroclastic flow and fallout deposits. The rapid erosion of the pyroclasts shortly after their deposition produced lahars and debris flows such as those that capped the Malendure deposit.

The heterogeneity of the Pigeon deposit facies indicates that it has emplaced over a substratum with a complex structure and that the successive pyroclastic flows and lahars were channelled in different valleys. The 000 and 090 strikes of the Malendure and Pigeon deposits strata indicate that they have been channelised by E-W striking valleys. The most common orientation in the Pigeon deposit strata is however 145/10-30SW, indicating that it flowed mainly toward the SW. Thus the Malendure and the Pigeon deposits originate from an area located east and NE of their present-day location, respectively. This source area corresponds to the Les Mamelles domes. The available age data of the Pigeon deposit (e.g. Gadalia et al. 1988) indicates that it is about 0.5 Ma old. If the Les Mamelles domes are indeed contemporaneous of this deposit, then they are much younger than previously thought. In the

absence of an absolute age of the domes themselves, which are too hydrothermally altered to allow such a measurement, this interpretation remains possible. Note that according to this hypothesis, the Les Mamelles eruption is contemporaneous to the Icaque, Capesterre, Sans Toucher and Mt Caraïbe volcanoes (figure 24-d). The Basse Terre Island thus had an episode of intense volcanic activity about 0.5 Ma ago.

The Malendure and Pigeon deposits are an accumulation of loose and unconsolidated materials, which are likely to have abundantly broke at the time of their deposition to form fractures and faults (cf. sections 3.2.4. and 3.2.5). This property is illustrated by the abundance of fractures, veins and faults measured in these areas, such as the E-W and N-S striking structures of the Malendure deposit which are parallel to its flow direction and to the valleys in which it was channelled. The over 10 m of dip-slip observed along the 120/70NE oriented normal fault of Malendure point as well as the $140 \pm 10°$ striking thrust, normal faults, open fractures, veins and fractures measured in this deposit may neither be related to deposition processes nor to sea erosion and may have a tectonic origin. The 140 striking faults and fractures of the Pigeon deposit are likely to be related to its deposition. However, the abundance of 140 striking veins and fractures measured in the deposit and in its substratum may be related to the regional Montserrat-Bouillante fault. The movements along the regional fault have formed a wide fracture zone made of structures oriented NW-SE and possibly also oriented E-W, in the onshore rocks. An active hydrothermal field (e.g. the Bouillante geothermal field) has developed along the fault zone. This regional fault is not expressed as a thin plane of localised deformation in Basse Terre Island and corresponds to a broad fracture zone.

Note that this interpretation of the Pigeon and Malendure deposits is in contradiction with previous studies which link these rocks to 5 to 10 hydrovolcanic vents of the Bouillante Chain (cf. the work of Gadalia et al. 1988).

4.3. The Piton Bouillante volcano

4.3.1. The volcano

The Piton Bouillante Peak area is the northernmost part of the Axial Chain (figure 24-b). This conical edifice does not possess volcanic features identifiable with remote sensing data such

as lava flows, vents, dome, summit crater or else. Its NW flank is made of an alternation of lava flows and lahars to debris flow deposits (cf. Losteau and Bourceau rivers). The lahars to debris flow deposits likely originate from the fast erosion of the Northern Chain volcano, which had the vigorous relief of a recently extinguished volcano at the time of Piton Bouillante activity. The lava flows correspond to the constructional phase of the Piton Bouillante volcano which initiated 1.25 Ma ago (Samper 2007). The flows are thicker and more differentiated than the Northern Chain flows (e.g. no olivine phenocrysts observed in the Axial Chain area).

South of Bouillante town, the shore exhibits abundant lahars and debris flow deposits, which have reworked and are interbedded with pyroclastic deposits containing ash and pumice. These clastic deposits have been transported toward the SW. The lava flow(s) which capped them are oriented 165-000/10-30SW and have flowed toward the W. The lava flows have been emitted between 1 and 0.75 Ma according to the available age data (Briden 1978, Samper 2007, Blanc 1983). The reworked pyroclasts come from a violent eruption of the Piton Bouillante volcano or of the Northern Chain. The formation of the Pigeon deposit (see previous section) is the last event that occurred in the area, possibly after the end of the activity of the Piton Bouillante volcano.

The northern Axial Chain area does not contain many structures. The abundance of N-S striking structures measured in the Losteau and Bourceau rivers may be related to fault movement.

The A Sel Point welded scoria cone and the Pigeon Island vent have both been attributed to the Bouillante Chain by Gadalia et al. (1988). The Pigeon Island is the uppermost area of a rounded small-scale volcanic edifice, which may be similar to the many seamounts found along the Monsterrat-Bouillante regional fault (from bathymetry data). If it is likely that its feeding dykes have infiltrated the regional fault zone it is not possible to determine from field data either if the magma belongs to the Axial Chain volcano or to a different source. The A Sel Point vent may have a similar origin. It may also be a satellite vent of the Piton Bouillante volcano or it may be a rootless cone which has developed from a lava flow of the Axial Chain.

a) Building phase of the Piton Bouillante volcano, about 1 Ma ago:

N
aerial volcanoes
sub-marine volcanoes

4
5
S
6
2
7
undated vents
1) Montserrat-Bouillante transensional fault
3

b) Piton Bouillante volcano toward the end of its activity, undated:

6
8
Caraïbean sea
7

c) The Beaugendre and Vieux-Habitants valleys, undated:

6
8
10
9
7

d) Eruption of Les Mamelles, Mt Caraïbe and Capesterre volcanoes, about 0.5 Ma:

11
13
12

e) Eruption of the Grande Découverte volcano, after 0.3 Ma:

N
S
14
15
8
10
13
5
8
17
9
16
7
12
Caraïbean sea

| | lahars and debris flow deposits | | pyroclastic deposits | | lava flows |

Figure 24 (cf. opposite page)

52

4.3.2. The Piton Bouillante dykes

The majority of Guadeloupean dykes were observed in the Beaugendre valley, which has deeply incised into the Piton Bouillante volcano (e.g. next part), or on the other flanks of this volcano (e.g. Corossol and Vieux-Habitants rivers).

The strike of a dyke is determined by the local structures that it infiltrates (Mathieu et al. 2008), by local stresses generated by the topography and by regional stresses generated by regional fault movement. If a regional stress field exists, the dykes tend to orient according to it, normal to the least compressive stress, rather than according to the pre-existing fracturing (Krom et al. 1997). The Guadeloupean dykes strike 090, 120, 010 and 040. A portion of these intrusions may locally re-orient by infiltrating lava flow cooling joints and the extent of this process is difficult to evaluate due to the limited extent of outcrops.

The N-S striking dykes have the broadest distribution. The Vieux-Habitants River crosses the crest of Basse-Terre Island from east to west and contains only four dykes, indicating that there is neither a N-S dyke swarm nor a rift zone in Guadeloupe.

The dykes have roughly a radial distribution and their orientation may be controlled by the conical morphology of Piton Bouillante volcano (figure 23). The E-W striking dykes may also have formed in a N-S extensional stress field that corresponds to the regional Monsterrat-Bouillante fault stress field: the dykes are parallel to the main horizontal stress of the fault. The abundance of E-W striking dykes (figure 21) show that the regional fault has a strong influence on dyke propagation directions in Guadeloupe.

Figure 24: The construction of Basse Terre Island view from the west; the age data are from Samper (2007), Blanc (1983), Bouysse et al. (1985), Gadalia et al. (1988); 1) regional Monsterrat-Bouillante fault, 2) Directeur Volcano, 3) Vieux-Fort Volcano, 4) Basal Complex, 5) Northern Chain, 6) Piton Bouillante Volcano, 7) Pigeon vent, 8) Petite and Grande Plaine valleys, 9) Beaugendre valley, 10) Vieux-Habitants valley, 11 and 15) Les Mamelles eruption and domes, 12) Mt Caraïbe, 13) Icaque, Sans Toucher, Capesterre Volcanoes, 14) Grande Découverte Volcano, 16-17) Pigeon and Malendure deposits.

4.4. The southern part of the Axial Chain

The southern flank of the Piton Bouillante volcano is dissected by the two largest and deepest valleys of Basse Terre Island, which are called Beaugendre and Vieux-Habitants valleys (figure 24-c). They have deeply incised into the volcano and exposed its feeding system (e.g. dykes). Their morphology suggests that these huge horse-shoe shaped valleys may originate from a catastrophic event such as a caldera formation or a collapse event. These structures have re-used E-W striking pre-existing fracturing in the case of the Vieux-Habitants valley, as noted by Feuillet (2001). The large size of these structures and the absence of differentiated dykes render the caldera hypothesis doubtful. No field evidence, such as a debris avalanche deposit, has been found to support the collapse origin. Such a deposit of loose material would be rapidly eroded on the volcano flank and channelled by sub-marine valleys at the time of its deposition. Compared to the other valleys of the island, the Vieux-Habitants and Beaugendre valleys are too deep and too large to originate only from erosion. For these reasons I favour a collapse origin. The collapses may have been instantaneous or slow (e.g. creeping). Then, the Capesterre, Icaque and Sans Toucher volcanoes have built in the Vieux-Habitants valley, forming the youngest edifices of the Axial Chain. The Piton Bouillante and Sans Toucher volcano are roughly aligned with more recent volcanoes (e.g. Grande Découverte volcano) along a 140 striking line, which is called the volcanic axis. The Axial Chain lava flows dominantly strike 170/10-30SW, indicating the importance of either N-S striking eruptive fissures or N-S vent alignments.

Tens of meters of pyroclastic deposits and lahars to debris flows with pumice blocks have accumulated on the coastal shelf on the SW flank of the Axial Chain volcano. The pumice-rich pyroclastic deposits are abundant in Vieux-Habitants town and have been reworked south of the town. None of the clastic deposits are capped by lava flows indicating that they correspond to late violent eruptions of the Axial Chain. They may also be related to eruptions of the Grande Découverte volcano (figure 24-e), that has several documented violent eruptions: Danois rhyolitic pumice (0.244 Ma; Blanc 1983), Anse des Pères quartz-dacite (0.14 Ma), Montval quartz-dacite (0.108 Ma) and Pintade andesite pumice (0.042-0.046 Ma; Boudon et al. 1989, Bouysse et al 1985). The pumice found along the shore are indeed of andesitic (common occurrence), rhyolitic (e.g. Rocroy beach) and dacitic (e.g. north of Vieux-Habitants town) compositions. The lahars and debris flows that reworked and capped them

are from the erosion of the Axial Chain and Grande Découverte volcanoes. These deposits strike mostly N-S and have been transported toward the west.

The abundant 130-140 striking fractures, veins and the few faults of Beaugendre and Vieux-Habitants valleys are parallel to the volcanic axis and may be related to the Monsterrat-Bouillante regional fault. The 110 striking normal fault of Beaugendre valley and the 090 striking fault zone of Baillif River may be tensional structures related to the regional fault. The outcrops of lava flows, fallout and debris flow deposits contain abundant 080-100 striking fractures and veins, which may also be related to regional fault stresses. They are associated with a palaeo-hydrothermal field south of Vieux-Habitants town (e.g. Rocroy beach).

The pyroclastic deposits located along the shore have been attributed to the vents of the Bouillante Chain by previous studies (e.g. Gadalia et al. 1988). I disagree with this interpretation because the vents themselves, which were described as scoria cones and maar (e.g. circular depression underlain by a diatreme) can not be clearly identified in the topography. Also, the pumice-rich deposits found along the shore are highly differentiated (andesite to rhyolite) and are more likely to come from the central part of the volcano. The Bouillante Chain deposits were previously identified as hydrovolcanic deposits. The presence of water at the time of an eruption highly fragments the magma and quenches it, producing vesicle-free pyroclasts. Pumice are vesicle-rich pyroclasts, which can not be produced by such eruption. One of the lines of evidence upon which the Bouillante Chain has been distinguished from the Axial Chain is the diversity of its petrology (e.g. basalt to rhyolite) while the Axial Chain is mostly made of andesites. These rocks come actually from the most differentiated products of the Axial Chain, which were emitted toward the end of its activity and/or, they come from the Grande Découverte volcano. In conclusion, I suggest that the vent alignment of the Bouillante Chain does not exist.

4.5. The structures of Basse Terre Island

The rocks of Basse Terre Island are abundantly fractured and little faulted. Most of the structures are lava flow cooling joints or were acquired by a clastic deposit as it flowed, emplaced or was eroded (e.g. landslide scars and debris avalanche deposit structures for

example). A small part of these structures may be attributed to regional stresses and they strike: 160-000, 140 and 090-120.

The 160-000 direction corresponds to the strike of most lava flows measured in Basse Terre Island. The Northern Chain volcanic axis is oriented 170. The Grande Plaine River contains a 000 striking sinistral strike-slip fault and abundant 160-000 striking fractures and veins were measured in Deshaies town (Northern Chain) and in Losteau and Bourceau Rivers (northern Axial Chain). The thickest dykes of Basse Terre Island strike 160-010 (e.g. Vieux-Habitants River; Axial Chain). Finally, the sinistral strike-slip Ty fault strikes 170 (La Soufrière dome and Galion River; Grande Découverte volcano). The 160-000 striking structures are not abundant and are found in the whole island (figure 25). They may be related to the fracturing of the crust uplifted parallel to the subduction front and infiltrated by magma to form the Northern Chain.

The NW-SE direction is poorly represented by the data. The Malendure and Pigeon deposits (Bouillante town area) contain 130-150 striking fractures, veins and faults. The Beaugendre River cuts into 130-140 striking fractures, veins and faults, which are close to the Axial Chain 140 striking volcanic axis (figure 25). The 140 striking structures are restricted to the central part of the western shore, which corresponds to the area where the Montserrat-Bouillante sinistral transtensional fault intersects the shore; and to the Axial Chain volcanic axis area, which may have built above the regional transtensional fault.

The 090-120 striking structures are the most abundantly measured. A 120 striking dextral strike-slip fault (Grande Plaine River), a 120/70NE oriented normal fault (Malendure deposit, slip=10 m), a 110 striking normal fault (Beaugendre River) and a 090 fault zone (Baillif River) have been measured. Basse Terre Island dykes mostly strike 090. Abundant 080-100 striking fractures and veins were measured in the lahars and debris flow deposits south of Vieux-Habitants town. Finally, 090-110 striking faults, veins and fractures were abundantly measured in the Pigeon and Malendure deposits (figure 25). However, an important part of these last structures is likely linked to the emplacement of the deposits (cf. sections 3.2.4. and 3.2.5).

The Bouillante geothermal field is located at the intersection between 140 and 090 striking structures (Traineau et al. 1997). The source of the heat anomaly has been attributed to a magma chamber of the Bouillante Chain (e.g. Gadalia et al. 1988) but it is likely to correspond to the Piton Bouillante hypo-volcanic complex as envisaged by Sanjuan et al.

(1988). In this case, the fluids have to be transported from the heat source (Piton Bouillante core) toward the Bouillante geothermal field (Piton Bouillante flank) along fracture zones or fault planes. These fracture zones dip steeply, they strike 090-110 and have been intersected by several drill holes (Sanjuan et al. 2004, Lachassagne et al. 2009, Genter and Traineau 2004). At the surface, these structures are expressed as broad fractured areas. In the area around Bouillante town, some of the E-W striking valleys have possibly incised along the buried fracture zones. If we consider the Axial Chain area, many rivers strike 090-100, including the northern part of the Vieux-Habitants valley, which may have formed along pre-existing fractures (as suggested by Feuillet 2000). Another 120 striking fracture zone is buried beneath the Capesterre River (Baubron 1990).

The E-W direction corresponds to the orientation of the main regional horizontal stress (directions of the convergence of the tectonic plates). This stress field has a strong influence on the structure of Basse Terre volcanoes, which are heavily fractured in the E-W direction, especially in the southern half of the island.

There is no field evidence to support that the Bouillante-Capesterre normal fault (figure 25-Nb16) cuts into Basse Terre Island from west to east. This structure likely corresponds to a diffuse and heavily fractured area and not to a well delimited fault plane with a large dip-slip component. The volcanoes are likely to be heavily faulted at depth. Their outcropping part, on the other hand, is too rapidly affected by erosion and eruptions to develop fault scarps. The surface is fractured, possibly by the movement of the buried faults, but is not faulted.

The last structures which are worth noting in Basse Terre Island are its numerous collapse events. The collapse scars are located SW of the volcanic edifices: the Petite and Grande Plaine valleys occupy the SW flank of the Northern Chain volcano, the Beaugendre and Vieux-Habitants valleys occupy the SW flank of the Piton Bouillante volcano and the 3,100 BP and the 11,500 BP avalanches occupy the SW upper flank of the Grande Découverte volcano (e.g. Amic and Charmichaël craters, figure 25). A collapse event may have many origins, including regional strike-slip fault movements, which favour collapses 10°-20° from the fault plane according to Lagmay et al. (2000). According to the model of these authors, the collapses should affect the SE flanks of Guadeloupe volcanoes, which is not what is observed. The movement of the regional fault has sheared the volcanic edifices and formed faults and fractures that have been re-used by the collapse events. However, the regional fault movements have not triggered the collapses, if we follow the Lagmay et al. (2001) model. Other factors, such as the presence of weak horizons (e.g. weathered lava flows turned into

clay) in the lava pile and the subduction-related uplift in the vicinity of the volcano, may have favoured these collapse events. In the case of the Piton Bouillante volcano, the collapses have affected the only flank of the volcano that was un-buttressed by the Northern Chain or by the Outer Arc basement. The SW flank of Piton Bouillante was, at that time, facing out to sea (e.g. Le Friant 2001). In the case of the Northern Chain and Grande Découverte volcano, only their northern flanks were buttressed by older volcanic edifices at the time of their flank collapses. Another mechanism, which could not be solved from field data, is likely to be at the origin of the instability of the SW flanks of Guadeloupean volcanoes. This problem is addressed in Chapter III.
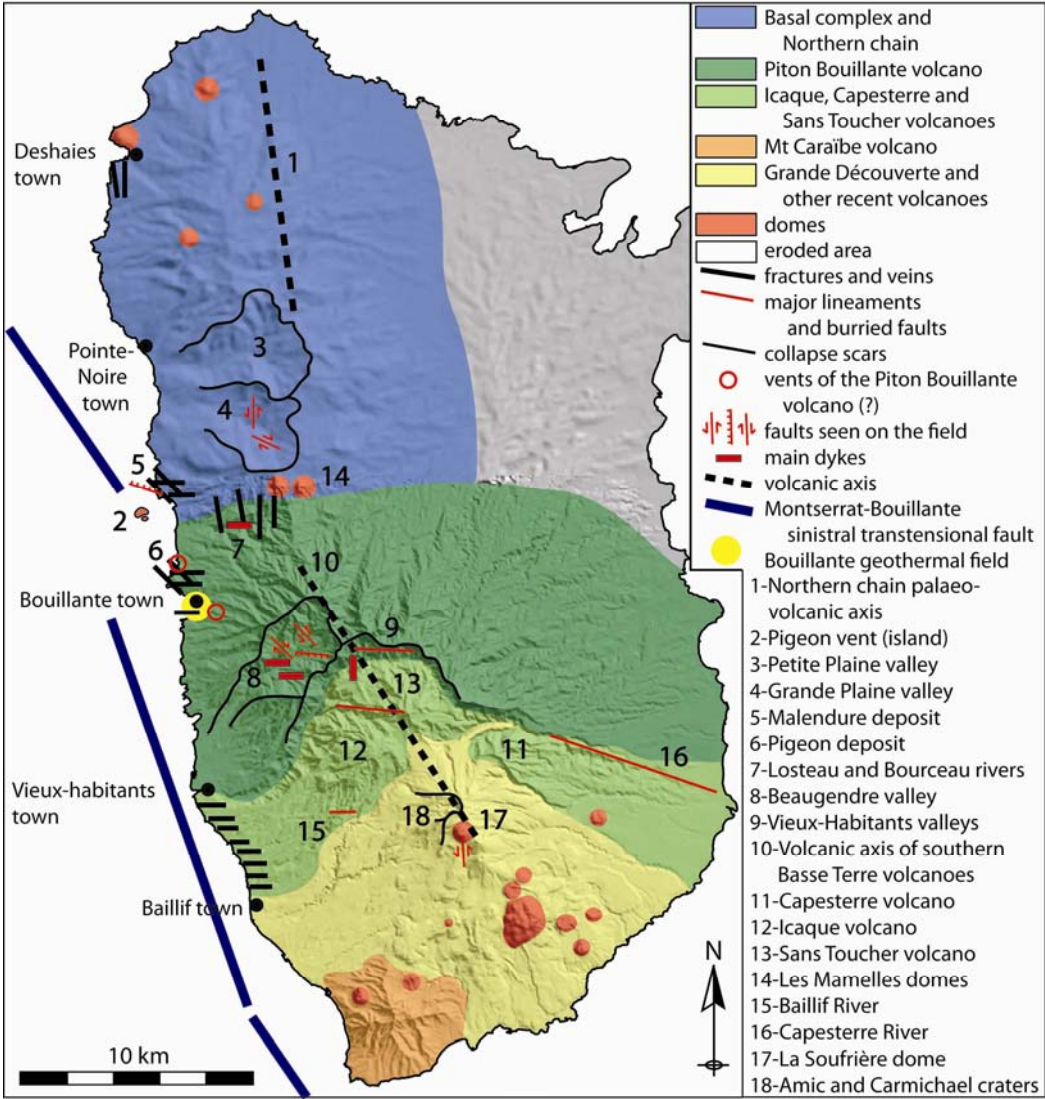
Figure 25: Map summarizing the main structures of Basse Terre Island.

4.6. Magma migration in Basse Terre Island

The alignment of the Northern Chain, Axial Chain and Grande Découverte volcanoes has been interpreted by many authors (e.g. Feuillet 2000 for example) as evidence for a progressive southward to south-eastward migration of the volcanic activity. This migration does not exist for individual Chains because they are central volcanoes whose eruptions occur at random locations within the area delimited by the edifice. The southward magma migration theory is not supported by several eruptions which seem to occur at random locations with respect to their age. For example, 0.5 Ma ago, five volcanic edifices have built north and south of older edifices. The Vieux-Fort seamount is contemporaneous with the Basal complex (northern Basse Terre) and has nevertheless built close to the active La Soufrière volcano (southern Basse Terre).

The volcanoes are aligned along regional structures: 1) the Northern Chain and Basal complex formed upon NNW-SSE striking structures parallel to the volcanic front; 2) the Pigeon, Directeur, Vieux-Fort, and other seamounts have built upon a NW to NNW striking portion of the offshore Montserrat-Bouillante regional transtensional fault; 3) The Axial Chain and Grande Découverte volcanoes have built upon another fault segment which is part of the NW striking Montserrat-Bouillante fault zone. The magma is probably transported by the crustal faults at depth. It was likely deviated by the load of older volcanic edifices as it rose to the surface (e.g. Kervyn et al. 2009) to build volcanoes south or north of these older edifices. This mechanism has formed volcanoes at random locations along the regional structures. The volcanoes are of any size depending on the volume of magma available in each rising batch.

5. Conclusion

Basse Terre Island is made of a juxtaposition of central volcanoes. The main volcanoes are the Northern Chain, which forms the northern half of the island, the Axial Chain and the recent volcanoes (Grande Découverte and subsequent activity). This study provides field data on Basse Terre volcanoes and proposes a model for the progressive formation of the island through a series of successive eruptions and collapse events. The Bouillante Chain is excluded

from this model and its existence is judged doubtful. The construction of the Grande Découverte volcano and other recent activity is excluded from this model because it has been studied in detail by many authors and is well understood. This model considers that the Northern Chain formed with 160 striking structures parallel to the subduction front, contemporaneously with many seamounts located along the Monsterrat-Bouillante transtensional fault. The Piton Bouillante volcano then grew south of the Northern Chain and has been dissected by two major sector collapses (e.g. Beaugendre and Vieux-Habitants valleys). About 0.5 Ma ago, intense volcanic activity formed three volcanic edifices inside the Vieux-Habitants valley, Les Mamelles domes north of Piton Bouillante volcano and Mt Caraïbe south of it. These volcanoes are aligned along a segment of the 140 striking Montserrat-Bouillante fault zone along which the magma is likely to have been transported. The Grande Découverte volcano has then built south of the Axial Chain volcanoes along this same 140 striking fault plane.

In the field, the 090-120 striking structures, which are the most represented in Basse Terre Island, are parallel to the main horizontal stress of the regional Montserrat-Bouillante fault upon which the southern part of the island is built. Note that the stress field related to this fault is a regional, plate-derived field. This stress field has a N-S orientated minimum principal stress that has controlled the major E-W dyke orientation and generated E-W fractures. This fracturing has been exploited by high-temperature circulation and has controlled collapses direction.

The model established with field data need to be confirmed to dedicated geochemical studies and age data. The structure of the Basse Terre volcanoes can not be fully grasped with surface data and needs geophysical studies such as gravity and magnetic that might be able to image the deep structures, especially the postulated 140 and 090-120 fault directions.

Chapter 3

-

The structure of Mt Cameroon volcano, West Africa

Chapter 3: The structure of Mt Cameroon volcano, West Africa

1. Introduction

Mt Cameroon is a ~4090 m high continental volcano sited on the 2000 km-long Cameroon Volcanic Line (CVL), an alignment of Paleocene to Recent intrusive complexes and central volcanoes (e.g. Déruelle et al. 1991). With a sub-aerial volume of ~1300 km^3, Mt Cameroon is one of the largest continental volcanoes and the most active volcano of West Africa. It has developed over a regional strike-slip fault and sits on a sedimentary basin that contains ductile layers upon which the volcano may have spread.

This chapter presents field observations collected on the Mt Cameroon summit area and across the topographic bulge at the SE base. The objective of this contribution is to propose an interpretation of Mt Cameroon's structure in the framework of its tectonic setting and to analyse the role of the sedimentary substratum on the volcano current morphology and instability features.

2. Geological setting

2.1. Geological setting

Mt Cameroon volcano sits on Pan-African mobile belt basement, which possesses a N-S trending foliation inherited from the main Pan-African compressive phase and has E-W, 030 to 050 trending foliations originating from the local re-orientation of the main foliation (McCurry 1971, Popoff 1988). It contains also late-orogenic dextral strike-slip faults grouped

as the Central African Shear Zone (CASZ), which strike 070 in the vicinity of the volcano (figure 01-a). This crystalline basement has been rifted prior the opening of the Equatorial Atlantic Ocean (105-100 Ma) and sedimentary basins bordered by NW-SE to N-S trending normal faults (e.g. Rio del Rey, Douala and Kribi/Campo basins) have formed in the studied area. The dextral strike-slip movements occurring along the re-activated CASZ have been transferred on the oceanic transform faults 100 Ma ago (Popoff 1988, Fairhead and Binks 1991, Déruelle et al. 2007).

The Cameroon Volcanic Line (CVL) is a 2000 km long alignment of alkaline intra-plate central volcanoes, monogenetic volcanic fields and batholiths (Wilson and Guiraud 1992, Déruelle et al. 2007). No age migration is observed along this volcanic alignment, which extends from Pagalu Island to Lake Chad (Burke and Wilson 1972; Fitton and Dunlop 1985). Most volcanoes are aligned along Pan-African and Mesozoic basement lineaments, which are oriented mostly 030, 050 to 070, 000 and 130 according to Moreau et al. (1987). Gravimetric and seismic refraction studies show that the crust below both the Adamawa plateau, located in the eastern part of the CVL (figure 01), and the oceanic islands of the CVL, has been uplifted during the Miocene (Fairhead and Okereke 1987, Meyers et al. 1998). Magma originates either from a "hot line" or from an active rift (e.g. Déruelle et al. 1991 for a detailed discussion on this matter). Those two models induce upwelling of the lithosphere below the CVL and the uplift observed at the surface.

2.2. Mt Cameroon volcano

Mt Cameroon is located at the SW edge of the onshore CVL. It is a 35×50 km long volcano elongated NE-SW parallel to a 040 striking summit rift zone (figure 01-b). The volcano formed at the intersection of 135 (Mesozoic sedimentary basin faults) and 050 (Pan-African structures) trending structures (Moreau et al. 1987).

The volcano is built upon 3 to 7 km of Cretaceous to Recent sedimentary rocks of the Rio del Rey basin (NW of the volcano) and Douala basin (SE of the volcano). The basins are bounded by 120 to 135 striking normal faults and cut by several 060 trending strike-slip faults (Benkhelil et al. 2002, Dumort 1968, Moreau et al. 1987).

The initial Mt Cameroon lava flows covered uplifted Miocene sediments (Hedberg 1968, Meyers et al. 1998, Dumort 1968). The volcano has grown by near-continuous activity from

10 Ma (Fitton 1983) or from 1-3 Ma (Marzoli et al. 2000, Hedberg 1968, Piper and Richardson 1972). The Limbe-Mabeta volcanic massif (Gèze 1943, Hedberg 1968) is located SW of Mt Cameroon (figure 01-b) and predates its growth. Mt Etinde (figure 01-b) is an independent nephelinitic volcanic edifice, which formed around 0.065 Ma (Nkoumbou et al. 1995), contemporaneously with Mt Cameroon.
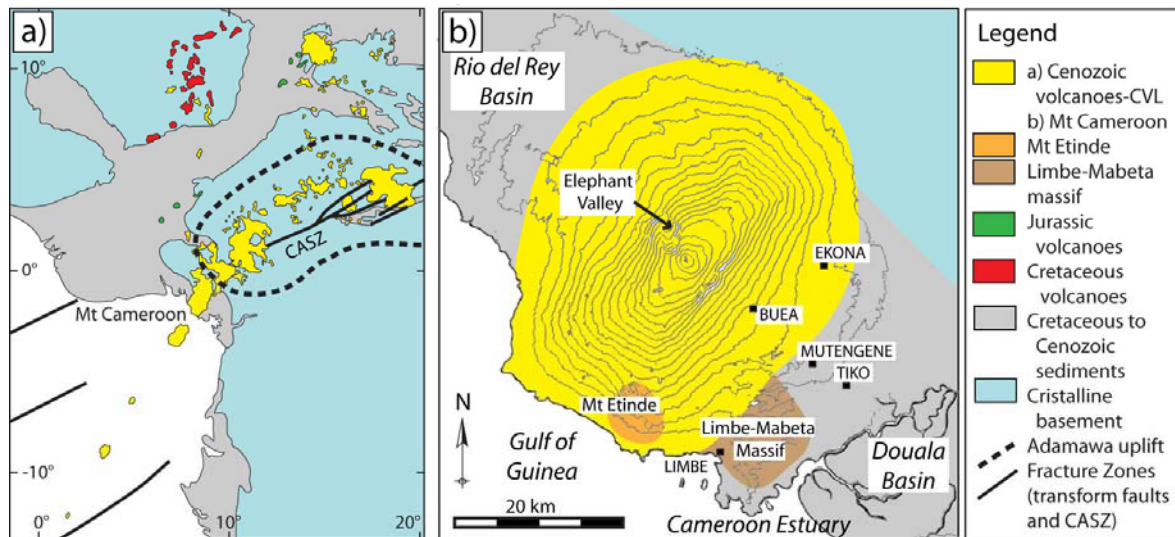
Figure 01: a) Mesozoic to Cenozoic volcanism in the vicinity of the CVL (after Dessauvagie 1974, Moreau et al. 1987, Popoff 1988, Meyers and Rosendahl 1991); b) Schematic geological map of Mt Cameroon. The interval between successive contour levels extracted from the SRTM is 200m.

Mt Cameroon is an unusually steep lava-dominated volcano that possesses a flat summit plateau, sharp break-in-slopes, a rift zone, a deep valley in the northern flank and topographic steps at its base (Gèze 1953, Déruelle et al. 1987). Based on this morphology and on the structural interpretation of the CVL as a series of horsts and grabens (Moreau et al. 1987), it has been proposed that Mt Cameroon was not a volcanic edifice *sensu stricto* but a volcanic horst covered by a thin succession of lava flows (Gèze 1943, Déruelle et al. 1987, Meyers et al. 1998). This study interprets these observations in a radically different way.

3. Remote sensing data

The following description of Mt Cameroon is based on the analysis of hill shade relief maps, slope maps and aspect maps extracted from the SRTM (Shuttle Radar Topographic Mission) 3 arc second (e.g. square pixels are 90 m over 90 m) DEM (Digital Elevation Model). The Mt Cameroon DEM has been downloaded from the USGS-a website.

3.1. Slope and summit area

Mt Cameroon has an elliptical shape in plan view, with 25° to 30° sloping flanks parallel to the long axis (e.g. long flanks or NW and SE flanks). The slope of the long flanks increases with elevation giving them a slightly concave profile (figure 02-b). The general continuity of these surfaces is altered in places by 3 to 4 subtle break-in-slopes on each long flank corresponding to small extent flatter areas (figure 02-a). The shortest flanks (NE and SW flanks; figure 02-c) have a gentler slope (10°-15°).
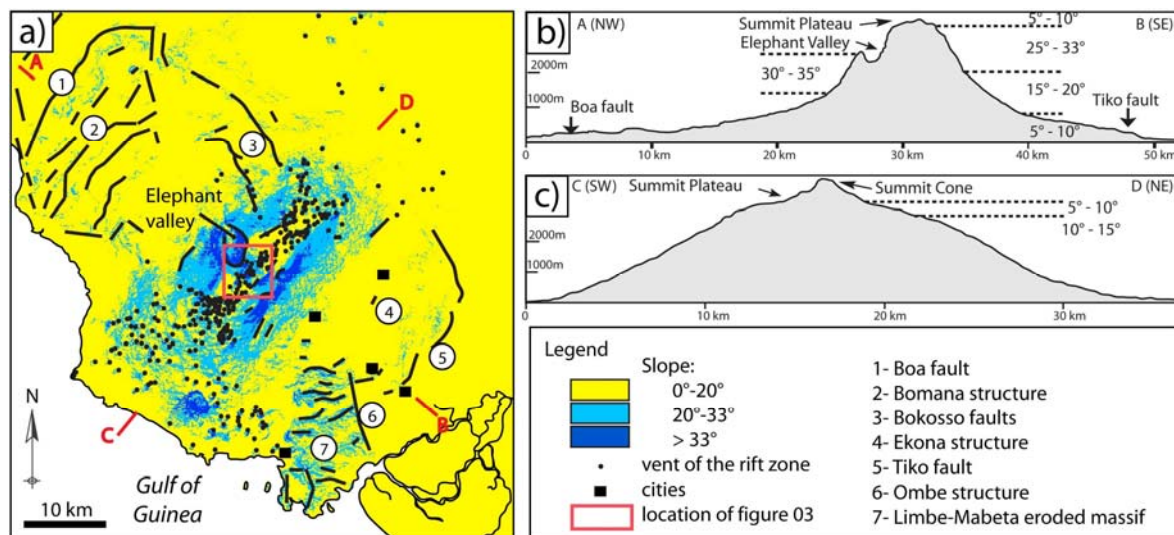
Figure 02: a) Simplified slope map of Mt Cameroon extracted from the SRTM that locates the lineaments and other faults described in the literature (e.g. Gèze 1953, Déruelle et al. 1987, Zogning 1988, Ateba and Ntepe 1997, Ubangoh et al. 1997, Suh et al. 2003, Ateba et al. 2009); b) and c) Cross-sections going through the summit of Mt Cameroon, normal to its long and short flanks, respectively.

The terrain suddenly becomes flatter at 2800-3000 m a.s.l. and forms a summit plateau that has the plan shape of an ellipse 12 x 5 km wide (figure 02-a). It is bordered by inward-facing topographic steps that are particularly well developed on the NE part of the plateau where some monogenetic vents had been erupted (figure 02-a). Field observations (this study) indicate that these steps are 10 m high cliffs cutting in the lava pile. No striations or other small-scale structures have been observed on these planes, so they may be a result of erosion. However, we suggest that these structures border a summit graben and have accommodated a downward movement of the summit of Mt Cameroon relative to its flanks.

The summit of Mt Cameroon is a composite cone, 3 km in diameter, rising at the centre of the summit plateau. This cone is made up of a cluster of pyroclastic cones and locally sourced lava flows. It rises from the summit plateau with a continuous gentle slope of 20°-25° except the SW flank, which is 33° over an area of limited extent close to the break-in-slope with the summit plateau (figure 02-c).

3.2. Rift zone

The spatial distribution of eruptive vents and fissures highlights a well-defined rift zone (figure 02-a) that is narrow (~2 km wide) in the summit area and oriented 040. Vent density is the highest at both extremities of the summit plateau. On the NE and SW flanks, monogenetic pyroclastic cones have a broader scatter and eruptive fissure orientations vary from 000 to 090. Vents are found in a broader zone and at lower elevation on the SW than on the NE flank. This vent distribution is consistent with the orientation of the principal horizontal stress of an elongated conical edifice (McGuire and Pullen 1989). The dykes intruded in the rift zone may represent a significant part of Mt Cameroon volume as suggested for elsewhere (Annen et al. 2001).

3.3. The Elephant Valley

The Elephant Valley cuts through the NW long flank of Mt Cameroon (figure 02). The head of the valley is located west of the summit cone and has a nearly E-W orientation before it curves to link the N-S striking and 3 km wide valley sides. Further toward the north, the

eastern flank shifts to a NW-SE direction narrowing the valley lower end that is 0.5 km wide at this location.

The uppermost parts of the valley walls are near-vertical and expose a pile of lava flows intruded by several dykes (field observations from this study, see next section). At lower elevations, the slopes of the valley sides are made up of loose material, eroded from the valley walls, at their angle of repose (~30°). Such collapses are responsible for the lobate morphology (small scale collapse scars) of portions of the walls. The east wall cuts the steep and slightly concave flank of the volcano. To the west of the valley, the flank is convex and steeper (30°-35°); it is bulged outward. This area is experiencing rapid erosion as highlighted by the dense river network cutting through it. The base of this peculiar area ends with a sharp break-in-slope that separates it from a shallower part of the flank.

The Elephant Valley has been interpreted to result from glacial erosion (Déruelle et al. 1987) or to be a radial rift caused by volcano spreading (Suh et al. 2003). The upper sub-vertical wall of the valley, the limited coverage by recent lava flows and the lack of an established drainage network however suggest that this valley is a relatively fresh feature that did not form only by erosion, but rather by a rapid collapse or tectonic process. Its linear outline (N-S and NW-SE) suggests that whatever process that formed it used pre-existing fracturing inherited from basement structures or developed in the edifice due to intrusion, spreading and/or landsliding.

Two less incised scars cut below the summit through the SE flank above Buea city. They correspond to significant and undated landslide events. In contrast, the rest of the steep flanks are noticeably free of any erosion features.

3.4. Boa, Tiko and Bokosso faults:

The volcano long flanks are surrounded at their base by topographically rough areas (figure 02-b, 03-b) that present a series of NE-SW ridges and valleys to the NW, parallel to the Mt Cameroon elongation, and topographic steps or terraces at the SE base, as noted by Gèze (1953). It is worth noting the asymmetry between the NW and SE bases: the succession of ridges and valleys affects a 27 km-wide area and extends 25 km from the base of the steep flanks to the NW. The SE topographic bulge is only 20 km wide and extends 15 km from the base of the steep flank. These two basal structures are offset to the NW relative to the Mt

Cameroon summit. These rough areas are delimited by sharp break-in-slopes that have been interpreted as major tectonic structures marking the edge of grabens and named Tiko and Boa faults (figure 02-a) to the NW and SE of Mt Cameroon, respectively (Gèze 1953). The breaks-in-slope upon which these faults are located could also be attributed partly to erosion by the river delta located in the Douala and Rio-del-Rey basins. The Tiko fault is not a simple linear structure but rather a series of lineaments with varying orientations, delineating a lobate structure. The river network that dissects the NW area as well as the delta erosion follows and accentuates its structure. The lobate morphology of these structures suggests that they are thrust faults. These faults strike parallel to the Mt Cameroon elongation and are located on both sides of the volcano, indicating that their formation is likely to be linked to the volcano.
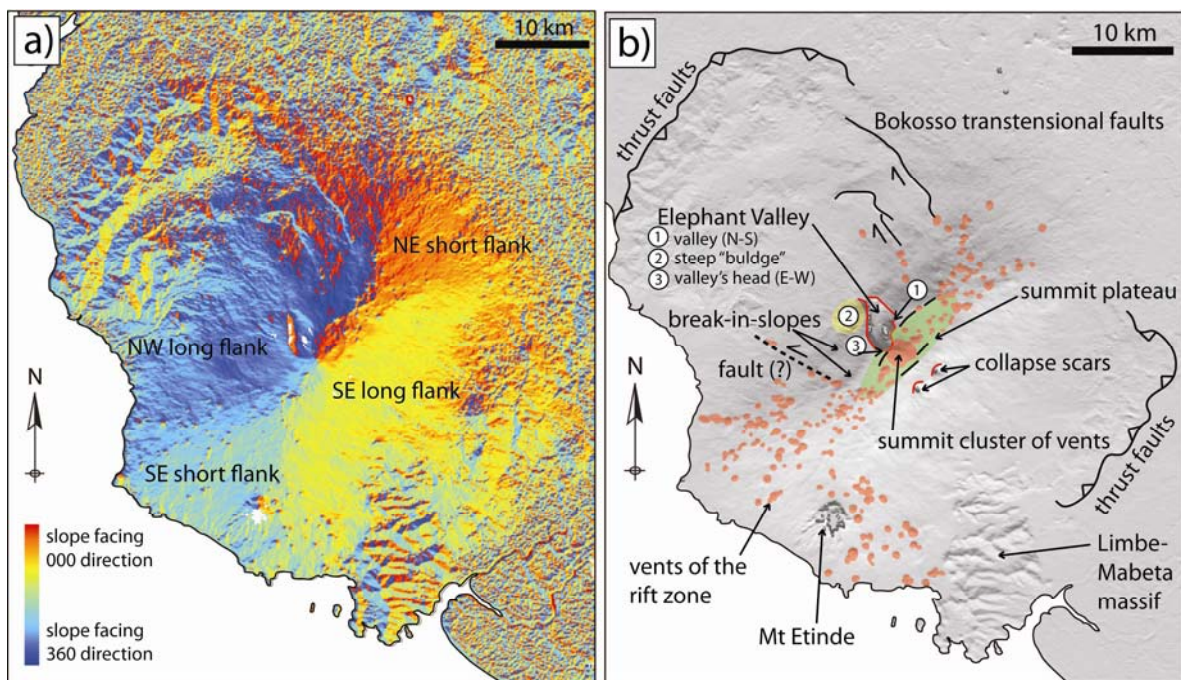
Figure 03: a) Aspect map of Mt Cameroon highlighting its long and short flanks; b) Hill shade map (sun elevation= 45°, azimuth= 180) and main structures spotted by this study. These documents are extracted from the SRTM.

The NE ridges are bounded by structures particularly well expressed in the NW flank of Mt Cameroon. Two NW-SE striking structures, identified as the Bokosso faults (figure 02-a, 03-

b), are seismically very active (Ubangoh et al. 1997). These 10-13 km long faults show up to 100 m of vertical displacement each with a downward motion in the SW part. Some of the pyroclastic vents strongly off-centred from the rift zone are located along the Bokosso faults (figure 02-a, 03-b). A similar but shorter vent alignment is observed on the other edge of the NW long flank. These vents may have been emplaced along a structure similar to the Bokosso faults. Based on their morphology (e.g. steep steps), these faults are interpreted as transtensional faults which accommodate the gravitational spreading of the volcano. They are similar to the Pernicana fault on Mt Etna, Italy (Borgia et al. 1992).

3.5. Other structures and concluding remark

Other structural features were inferred by previous studies, with limited field constraints, around Mt Cameroon, including the Bomana, Ombe, Limbe, Ekona faults and other escarpments at the base or along the summit plateau (Déruelle et al. 1987, Zogning 1988, Ateba and Ntepe 1997, Suh et al. 2003, Ateba et al. 2009; figure 02-a). All these faults were interpreted as regional tectonic structures. A last region that is worth noting is the Limbe-Mabeta eroded volcanic massif to the SSE of Mt Cameroon. It is characterized by a series of sub-parallel E-W oriented valleys bordered by the 170 striking Ombe structure on its eastern side (figure 02-a, 03-a, b).

4. Field data

A month of field study was carried at the summit and at the base of Mt Cameroon volcano. The aim of this field work is to unravel the structure and origin of the summit plateau and of the SE ridges (e.g. Tiko fault) observed on remote sensing data.

4.1. Summit area

4.1.1. Methodology

The area mapped around the summit is presented on figure 04, which integrates field and remote sensing observations. The analysis of satellite images does not allow the recognition of features smaller than ~10^4 m^2, thus special attention is paid to small scale features in the field. This includes the shape and location of craters and the distribution of eruptive fissures, open cracks and pit craters.

The 3 km in diameter summit cone is surrounded by two clusters of scoria cones, to the NNE and SSW (figure 04) that are aligned 040 to 045 along the rift zone. The structures measured in this area are located in a pile of basaltic lava flows (e.g. figure 04) interbedded with pyroclastic deposits. This disposition of rocks is observed in the whole summit area where 0.5 m to 2 m thick lava flows are interbedded with layers of scoria, lapilli and ash 0.2 m to 5 m thick.

Open cracks located in lava flows are difficult to discriminate from fractures linked to the emplacement and cooling of the lava. For this reason, open cracks are only measured in material with a smooth surface, such as scoria cones and scoria fallout that concentrates west of the summit cone. Field measurements are summarised in table 1. Key observations are highlighted below.

4.1.2. Dykes and open cracks

Few dykes are observed in the field, most being located in the Elephant Valley where their strike could not be determined with precision due to observation from great distance. A 0.5 m

thick dyke striking 055 is associated with an eruptive fissure east of the summit cones. Elsewhere, the strike of dykes is inferred from the orientation of eruptive fissures and the elongation and alignment of scoria cones craters and pit craters (figure 04, 05). Measured eruptive fissures were deep (2 to 15 m) and narrow (1 to 3 m wide) open fractures surrounded by spatter deposits. In the SW part of the map, some of these can be directly linked with the lava flow they fed (e.g. the 2000 eruption fissure). Several additional lineaments attributed, in part, to eruptive fissures, are mapped from remote sensing observation (figure 04). Several isolated or aligned pit craters (n=34) are observed in the summit cone and in the two clusters of cones that surround it. These circular, occasionally elliptical, depressions are less than 20 m wide. The small size of the pit craters may indicate that large magma bodies are rarely or never stored in the upper part of the volcano.

From these observations it can be concluded that most (70 %) of the dykes strike 040 to 060, which are the predominant directions, respectively, in the SW and in the central (summit area) to NE part of the map (figure 04). A limited proportion of dyke-related structures with other strikes are observed: 170, 030, 075 and 140. The 140 strike corresponds to two pit crater alignments in the summit area.

Table 1: Summary of field measurements made at the summit of the volcano. The "SW" area comprises the scoria cone cluster located SW of the summit cone, the western flank of the summit cone as well as the area located south of the Elephant Valley headwall. The "NE" area includes the cluster of cones located NE of the summit cone; * The most frequent strikes measured are in bold characters; ** Linear structures identified from remote sensing data.

Summit plateau area	SW of summit cone	NE of summit cone	summit cone
Crater elongation and/or alignment	**040-055***; 160-000; 070- 075	060; **000- 030**;110	**060**; 130-145
Eruptive fissures	**045**; 025; 070	050-060; 035; 080	none
Dykes	~ 060	055	none
Fumaroles alignment	none	000-030	060-070
Open fractures	**070-080**; **110**-100; 050-060	**050-060**; 010-030	040-060; 000-030; **110-090**; **130-140**
Lines **	**040**-060 and 020	**045**-050 and 032	none
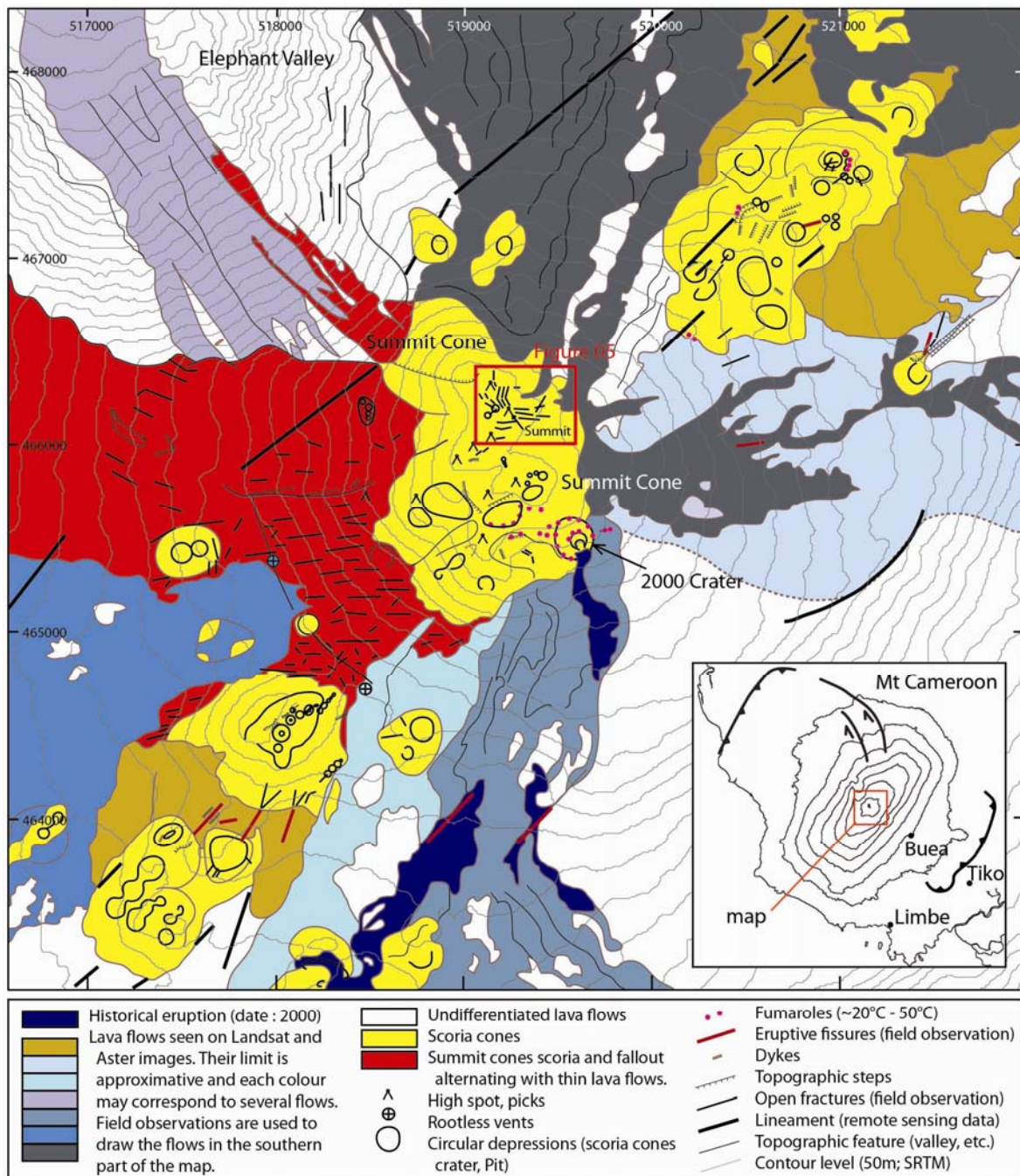
Figure 04: Map of the summit area that integrates field and remote sensing observations. The scoria cones and lava flow limits are drawn from Landsat and ASTER (Advanced Spaceborne Thermal Emission and Reflection Radiometer) images. To the south of the summit, the accuracy of lava flow boundaries is improved by using field observations. Scoria fallout are observed west of the summit cone from which they probably, for the most part, originate. This indicates prevailing winds from the E-NE (to be continued).

Open cracks are small structures, 0.2 to 3 m deep and 0.5 to 5 m wide. Two kilometres west of the summit cone, open fractures striking 110-100 are parallel to the Elephant Valley headwall. These extensional fractures can be attributed to either the formation of the valley or the instability of its steep flanks. Further toward the east, the fractures strike 070-080 as they affect the flank of the summit cone, following the curvature of the Elephant Valley headwall. In the whole mapping area, other open fractures are sub-parallel to the rift zone (050-060 striking open fractures). North-east of the summit cone, open fractures mostly strike 010 to 030, parallel to the eastern flank of the Elephant Valley.

4.1.3. Mt Cameroon summit peak

The summit cone is a cluster of pyroclastic vents intercalated with lava flows. Open fractures are concentrated on its western flank as well as in a restricted area located some tens of meters around the highest peak of Mt Cameroon. This highly fractured area (figure 05) is located at the NE edge of a 060 alignment of pyroclastic cones and contrasts with the unfractured constructs that form the rest of the summit cone. The open cracks surround a steep valley on average 100 m deep, 100 m wide and elongated E-W (figure 05, 06-a to c). This short valley has an elliptical shape in plan view. Its termination curves toward the north. Its northern flank cuts into a spatter deposit. The floor of the valley is occupied by a lava flow, the levées of which touch the valley wall; this flow was channelised by the valley.

The valley is surrounded by a dense network of open cracks and topographic steps 0.2 to 10 m high (figure 06-a to c). The longest of these steps are located within and are parallel to the valley walls. They form a stack of 2 m to 10 m high sub-vertical walls that alternate with sub-horizontal areas of smaller extent (figure 06-b). These steps affect loose tephra and do not extend into the spatter deposit. They accommodate the inward sliding of unstable scoria toward the valley floor.

Figure 04 (suite): This map is preliminary and each lava flow unit individualised may represent several successive flows, possibly of different ages. The boundary of most flows presented here has to be checked with detailed and dedicated field mapping. The bulk of open fractures, dykes, eruptive fissures and scoria cone craters mapped during this study are shown. The fumaroles reported on the map are ~20-50°C and are mostly located around the 2000 eruptive crater.
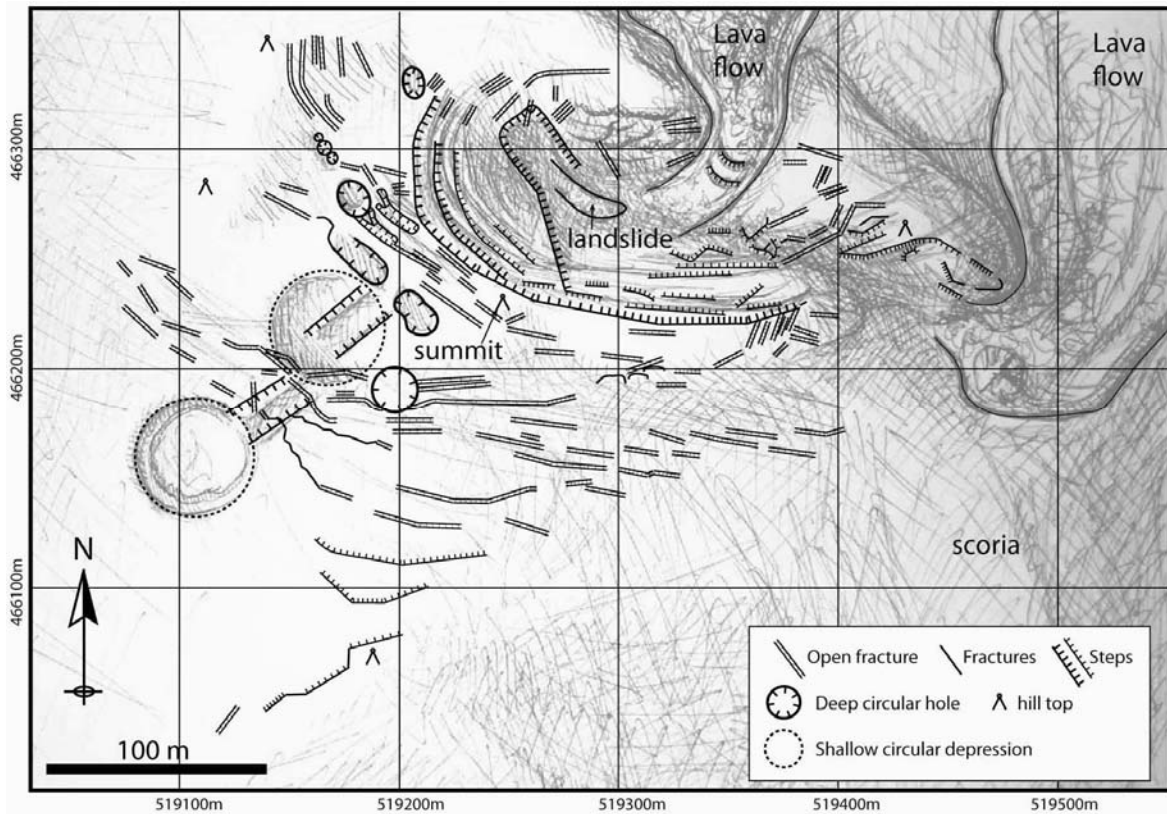
Figure 05: Map of the Summit Valley (NE edge of the 3 km in diameter summit cone) presenting the bulk of structures measured in the scoria cone deposits that surround the highest peak of Mt Cameroon (e.g. figure 04 for location). Detailed contour lines are not available for this area whose topography has been drawn by hand.

Some of the open cracks are parallel to the valley and their origin may be linked with the unstable steep valley flanks (figure 05, 06-b). Further away south and west of the Summit Valley, the largest concentration of cracks strikes 110-090. In the southern part of the map (figure 05) the open cracks are progressively replaced by topographic steps dipping outward relative to the steep local slope (figure 06-c). The pit craters are either elongated parallel to the nearest open fracture or are rounded holes located on the track of open fractures. Two larger shallow depressions that represent weakly expressed pit craters are aligned 045 (figure 05).

The measurements undertaken in this area show that the open fractures strike mainly 090-110 and 130-140. Other structures (open cracks and pit craters) are parallel to the rift zone (e.g.

040-060). The last direction, 000-030, is represented by a cluster of open fractures located NW of the valley.
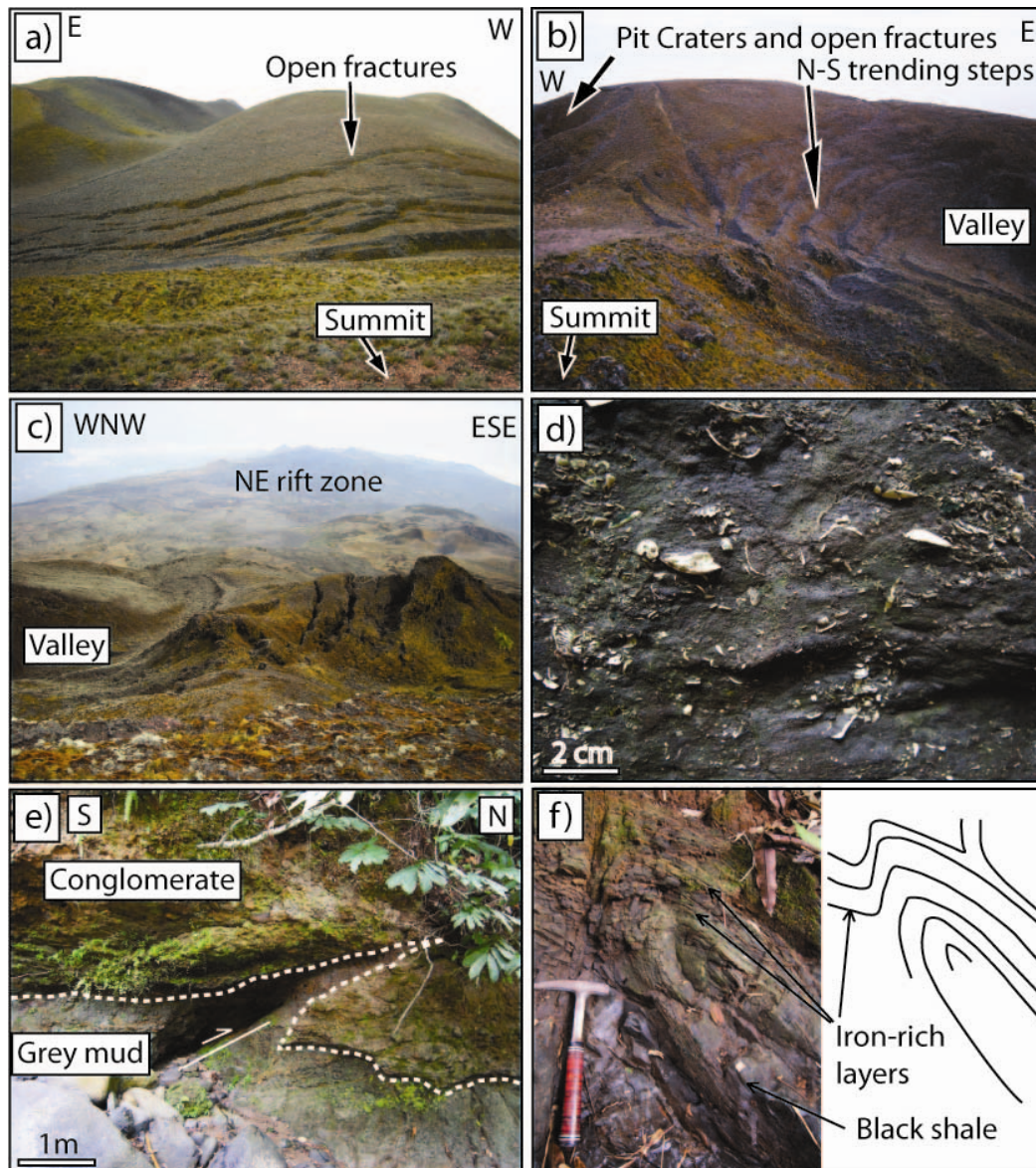
Figure 06: Pictures of the summit area (e.g. figure 05) and Douala basin sedimentary rocks; a) E-W striking open fractures located south of Mt Cameroon summit; b) N-S trending steps located west of the Summit Valley; c) Open fractures located east of the Summit Valley and view of the NE rift zone; d) Black shale containing broken white shells (Muodoni river); e) 080 trending thrust in grey mud and conglomerate (Issuassua river); f) Isoclinal fold in black shale (Tamben river). The hammer provides the scale.

In conclusion, the structures observed indicate that the elliptical Summit Valley has probably cut into the crater of a pyroclastic cone. The extensional structures curve west to east from 140 to 090 directions and may have accommodated the sliding of an unstable portion of the summit cone toward the NE along pre-existing fracture systems.
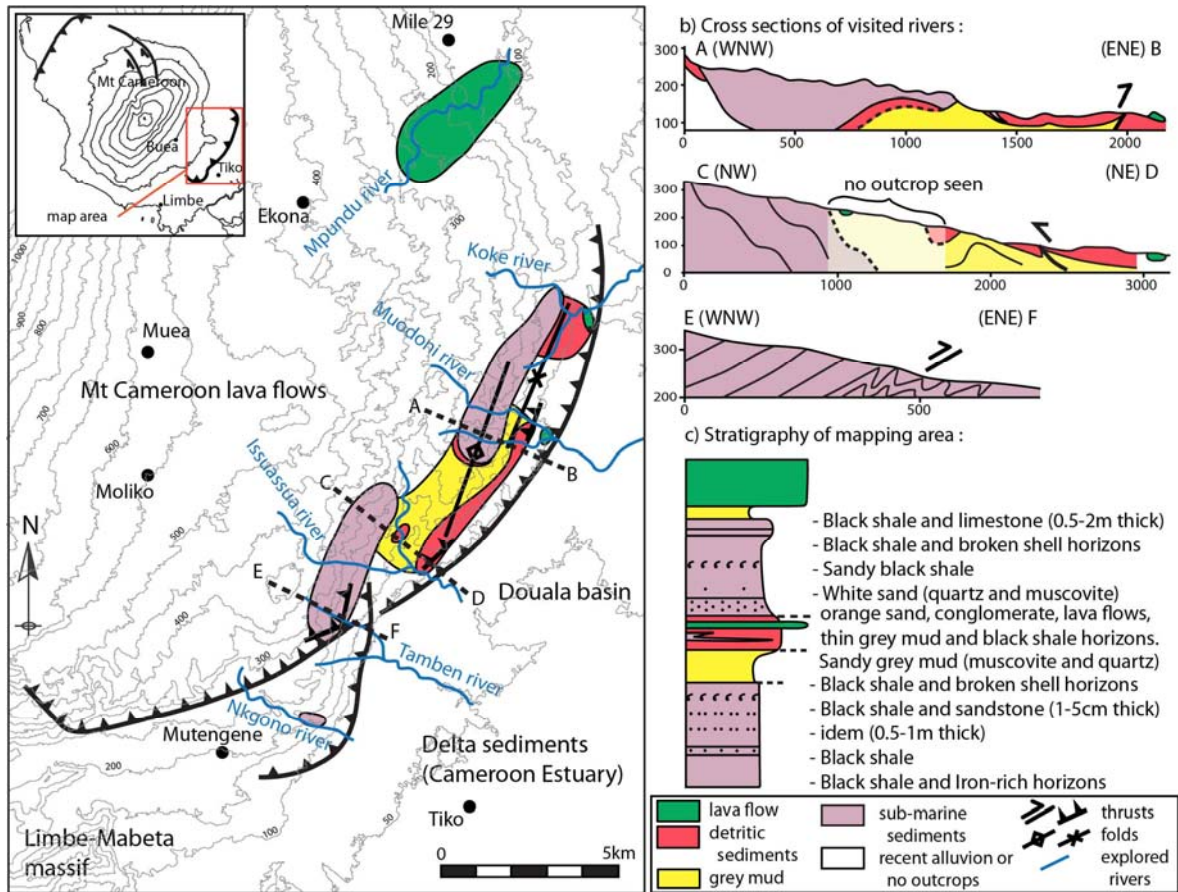
Figure 07: Summary of mapping completed at the base of the SE flank of Mt Cameroon. a) Geological map based on river outcrops; b) Profiles of Tamben, Issuassua and Muodoni Rivers. The sections show the folds and thrusts that affect the alternation of muddy and clastic weakly-indurated sediments of the Douala basin; c) Stratigraphy of the mapping area; this column is not scaled because sedimentary layer thicknesses have not been determined in the field.

4.2. Southern flank of the volcano

The second mapping area is located east of Buea City and north of Tiko Village (figure 07), at the base of the SE flank of Mt Cameroon. In this area, marine and river deposits from the Douala Basin are exposed below Mt Cameroon lava flows. More precisely, the area is located at the break-in-slope that borders the northern edge of deltaic sediments from the Cameroon estuary and that has previously been interpreted as an area affected by thrust faults (e.g. Tiko fault).

4.2.1. Lithology

In the map area, marine sediments are mud dominated. They consist of sand, sandstone, shelly limestone and black shale alternating with horizons of broken shells (figure 06-d). White sand containing grains of quartz and muscovite is also observed in the Muodoni and Koke rivers. The sand and broken shells suggest a palaeo-beach environment of deposition. Grey mud that contains quartz and muscovite grains and occasionally sand, is found in many places. The grey mud is either an independent sedimentary horizon or is weathered black shale. These sediments are similar to the Miocene to Pliocene strata described by Benkhelil et al. (2002) and Reyment (1954). According to these authors, deposition in this area started with the formation of dark micaceous clays containing sandy lenses and ended with the deposition of calcite sandstones, siltstones and wackestones containing molluscs, in a deltaic environment.

River deposits of the Douala basin consist of orange sand occasionally alternating with black shale and conglomerate. These discontinuous horizons are difficult to differentiate from present-day river deposits. They correspond to the Quaternary silty, clayey sand and weakly indurated sediments described by Benkhelil et al. (2002).

4.2.2. River outcrops

The sedimentary rocks are covered by Mt Cameroon lava flows that do not alternate with late Neogene-Quaternary sediments. The outcrops are scarce in the mapping area, being solely exposed in river. Key observations made in the field are summarised in table 2.

According to the stratigraphy established from field observations (figure 07-c), the rocks are more recent in the NE than in the SW. Also, a small portion of the rocks strike parallel to the sedimentary basin border faults and they dip toward the NE. These characteristics have been acquired at the time of the deposition of the sediments over basement blocks rotated by the normal and listric faults that border the Douala basin. This is a common morphology for passive margin sedimentary basins.

If we consider the measured sedimentary layer orientations, two main orientations are found to be dominant: 020/35NW and 060/20SE. Some folds and thrusts (figure 06-e, f) strike 020-030 and others strike 050-060. The mapping area is affected by two distinct deformation events with contrasting orientations. The orientation of these structures is close to, but does not match, the orientation of Mt Cameroon (e.g. 040).

Some of the sedimentary beds are oriented 060/10-50NW and 045/25-35NW. These strata form the flanks of ENE-WSW striking folds with steep NW-facing flanks. These folds are asymmetrical and verge toward the SE.

Some of the sedimentary horizons are oriented 020-025 and dip 20SE and 40-55NW (table 2, figure 08). These sediments form the flanks of symmetrical folds formed during a horizontal shortening. Most sedimentary layers dip toward the NW, suggesting that these sediments were tilted by thrust faults dipping toward the NW.

Table 2: Summary of measurements made in four rivers at the base of the southern flank of Mt Cameroon; * The most frequent strikes measured are in bold characters.

Rivers	Tamben	Issuassua	Muodoni	Koke
Black shale layering orientation	000-010; **020-030*** Dip: 15-50NW	**010-030**/35-45 SE 065-080/15-75 SE 110-125/16-40 SW	**020-030**; 040-060; 000-010 Dip: 10-50 SE-NW	140/20 NE
Sand and Conglome--rate horizon strike	none	020/50 NW 040-050/20-30 NW 070-090/05-15 SE	**020-030**; 065 Dip: 20-30 NW-SE	030; 050 Dip: 20 SE; 40 NW
Fractures	170; 140; 070	070; 000/70-80 W	**130**; 085	none
Thrust orientation	000-030; 045-060 Dip: 40 NW	070-090; 030-050 Dip: 70 NW; 30 SE	020, 40 NW	none
Fold strike	none	**010-030**; 050-070	**020-030**; 050-060	**030**; 050
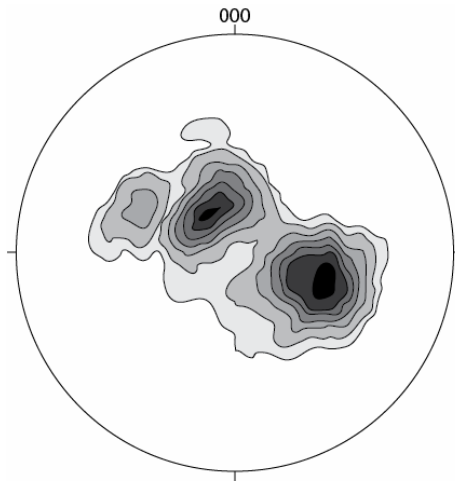
Figure 08: Lower hemisphere projection of the polar plane of sedimentary layers orientations measured at the base of Mt Cameroon south-eastern flank (n= 112 data)

5. Discussion

5.1. Mt Cameroon morphology

Déruelle et al. (1987) have noted that alkaline volcanoes tend not to have flank slopes as steep as Mt Cameroon's NW and SE flanks. These authors explained the steepness of the SE flanks by arguing that Mt Cameroon is a horst structure bounded by outward dipping normal faults corresponding to its steep flanks. Mt Cameroon would thus be made out of uplifted substratum covered by a thin layer of lava flows. If we follow the Déruelle et al. (1987) hypothesis, the Elephant Valley that deeply incised the volcano's NW flank should cut into basement rocks. I observed that the flanks of the valley are actually entirely made of lava flows. There is no field evidence to indicate that Mt Cameroon is anything else than a large volcano entirely made of accumulated lava flows and magma intrusions.

It is difficult to picture how Mt Cameroon developed its atypical present-day morphology; that is a large lava-dominated and elongated volcano with over 30° dipping slopes. Its long axis is parallel to the western CVL alignment and to regional lineaments: it is parallel to Pan-

African lineaments re-orientated by the CASZ or to other CASZ-related fractures. Mt Cameroon magma probably infiltrates a weak zone in the basement and has thus built an elongated volcano with a well defined rift zone. The flanks may have been initially shallow and may have been steepened by intrusions (dyke core complex and possibly shallow magma chamber) and subsequent landsliding. The Mt Cameroon base however lacks any convincing evidence of large debris avalanches. It is more reasonable to envisage that Mt Cameroon built originally with steep flanks. The volcanic products located on each side of the rift zone have accumulated with steeper flanks (as steep as 20° for shield volcanoes) than the products accumulated at the extremities of the rift zone as observed elsewhere by Rowland and Garbeil (2000). It is possible that dyke intrusions are much more common at Mt Cameroon than actual eruptions feeding lava flows. A low eruption to intrusion ratio would favour a thick dyke core complex that strongly pushes outward the volcano's upper flanks (figure 09), creating up to 30° steep slopes (Annen et al. 2001) and preventing the construction of a flatter shield volcano.

Once the volcano has reached a significant height and size, the spreading starts and produces extensive stresses normal to the dyke core complex, facilitating the passive intrusion of low buoyancy magma in this area (cf. Le Corvec and Walter 2009). Low buoyancy dykes are unlikely to reach the surface and this mechanism may explain the low eruption to intrusion ratio of Mt Cameroon. It is also possible that the forceful intrusion of dykes in the rift zone pushes the steep flanks of Mt Cameroon, facilitating the spreading.

5.2. Field data from the summit and the base of the volcano

The first part of the field study was dedicated to the summit plateau. The formation of this plateau may be linked to a large eruption that has involved the formation of a caldera even if such activity is rare on basaltic volcanoes; it may also be linked to a caldera-type subsidence process caused by deformation of hydrothermally-altered rocks (cf. analogue models by Merle and Lénat 2003, Merle et al. 2009) or to sagging caused by dense cumulates accumulated in the magma chamber as seen elsewhere by Walker (1988). However, no field evidence supports any of these theories. In this context and based on recently collected evidence, which indicate that Mt Cameroon is spreading over its weak substratum, a

progressive subsidence of the summit along inward–dipping normal faults is favoured. The field campaign failed to provide direct evidence of this subsidence.

The data collected around Mt Cameroon's summit confirm the presence of 070 and 100 trending structures (figure 04) that have been related to inflation-deflation movements around the summit by previous studies (Gèze 1953, Déruelle et al. 1987). In our field area, the open fractures with such a strike circled the head of the Elephant Valley. This valley cuts the steep northern flank of an active volcano almost to its summit. It is an unstable structure, the flanks of which are affected by extensional stresses responsible for the formation of superficial structures such as open cracks. At a smaller scale, similar instabilities surround the small valley located on the NE termination of the summit cone. These structures are impressive and worth noting. However, they are related to local instabilities and do not provide significant information on the general structure of Mt Cameroon, except that they show that the volcano is built of rocks that can become unstable on quite shallow slopes.

At the base of Mt Cameroon's SE steep flank, the substratum has a complex morphology. Several 050-060 striking asymmetrical folds measured at the base of the SE flank of Mt Cameroon are parallel to the western part of the Adamawa uplift that is elongated 055 and that affects the eastern part of the CVL. It is however possible that this uplift extends further and links with the offshore uplift studied by Meyers et al. (1998). In this case, the uplift also affects the Mt Cameroon area (Meyers et al. 1998) and is possibly responsible for the asymmetrical folds measured on the mapping area that have formed following the sliding of Douala basin sedimentary rocks along the flank of the domed area.

Symmetrical folds and thrusts striking 020-030 measured in the same area can be attributed to the spreading of Mt Cameroon over weak basin sediments. The weak sediments observed in rivers (black shale, grey mud, white sand) are at least tens of meters thick. These sediments are so weak that few thrusts develop in them. The deformation is mostly accommodated by folds. This situation is similar to the deformation style observed at Concepción, Nicaragua (Borgia and van Wyk de Vries 2003). These structures are not parallel to Mt Cameroon's elongation axis because the spreading of the volcano's southern flank is not uniform but has to re-orientate around the Limbe-Mabeta volcanic massif (e.g. figure 01-b). Spreading sediments are uplifted and pushed toward the ESE and the E rather than toward the SE. Close to the Limbe-Mabeta massif, spreading structures are more severely disturbed. They slide along the edge of the massif, producing E-W striking thrusts. These data show that the Tiko fault, as well as the symmetrical Boa and Bokosso faults are all linked to the spreading of the

volcano and are not related to regional movements as initially postulated by the authors that defined them (Déruelle et al. 1987, Zogning 1988, Ateba and Ntepe 1997, Suh et al. 2003, Ateba et al. 2009).

The deformed areas SE and NW of Mt Cameroon are surrounded by two large deltas that have buried sedimentary basin rocks under a thick succession of recent sediments. Consequently, it is impossible to determine the exact extent of the area affected by thrusts around Mt Cameroon. The deformation may either be limited to the highly deformed area observed on the SRTM or extend into the delta region where rapid sedimentation hides structures as soon as they develop.

5.3. Long flank instabilities

The Elephant Valley is the largest single structure that has deeply incised the volcano. It is a N-S striking valley whose western flank is bulged. It is suggested that a large coherent block of Mt Cameroon's flank has slid or is sliding toward the west, and has possibly rotated anticlockwise, to form the steep western bulge. Such landslide movement has produced a deep valley (Elephant Valley) in the volcano's flank. Such a scenario is similar, at a much larger scale, to the slump described at Casita, Nicaragua (van Wyk de Vries et al. 2000) and many volcanic landslides have one flank that opens preferentially to create a fractured graben feature that can be exploited by erosion (e.g. the examples of Merle et al. 2001). Such a sliding event is a slow phenomenon that is possibly associated with several rapid collapses responsible for debris avalanche generation. The fact that no morphology typical of debris avalanche deposits can be observed in the SRTM in this forest-covered area does not mean that they do not exist: very few field studies have been carried out at the NW base of Mt Cameroon due to its remoteness. Unravelling the origin of the Elephant scar will require dedicated field and palaeomagnetic studies.

Mt Cameroon's summit is sandwiched by the Elephant Valley to the NW and by two smaller collapse scars to the SE. The rest of the volcano's steep flanks do not exhibit collapse scars. The SE collapses may originate from the instability of the steep flanks. However, if the instabilities that affect Mt Cameroon's steep flanks were only due to the growth of slopes steeper than their angle of repose by eruption product accumulation, shallow collapses should affect all steep slopes (Acocella 2005). A possible explanation is that a phenomenon adds

instability in the vicinity of the summit, such as the pressure created by shallow magma accumulation immediately beneath the summit. Another magma chamber could be located at a deeper level, at the interface between Mt Cameroon lava pile and the underlying sedimentary rocks or in a weak sedimentary layer that is a location favourable for magma intrusions (cf. Roman-Berdiel et al. 1995, van Wyk de Vries and Matela 1998, Borgia and van Wyk de Vries 2003, figure 09). Such hypothesis needs to be checked with the help of geophysical tools.

Another type of instability affects the long and steep flanks, which have a step-like profile. This morphology corresponds to the sliding of the most superficial part of the steep flank over the spreading substratum. Such movements are accommodated by shallow outward dipping normal faults parallel to the volcano flank and involve several small blocks sliding the one on top of the other (figure 09). These are similar to the unstable areas observed on Mt Etna (Murray and Guest 1982) and Arenal volcanoes (Cecchi et al. 2004). This hypothesis is more satisfactory, in my point of view, than the horst theory that involves giant normal faults crossing the core of the volcano.

5.4. Spreading theory

The lateral flow of ductile sediment below a conical volcanic edifice induces horizontal extensional stresses in the edifice. As Mt Cameroon is elongated, the smallest principal stress ($\sigma3$) is normal to its elongation axis. This is illustrated by the fact that the longest flanks move more than the shortest flanks and have already spread and folded their basement whereas the shortest flanks have moved little, if at all. Such extensional stresses typically produce a graben at the summit of a conical volcanic edifice (Merle and Borgia 1996). The asymmetrical distribution of stresses over the elongated Mt Cameroon has formed a NE-SW elongated summit graben. This is evidenced by the km-long topographic step bounding the summit plateau interpreted as normal faults. The forceful intrusion of dykes along the rift zone is another mechanism that possibly contributes to the development of the summit graben (Le Corvec and Walter 2009).

Spreading also favours the activity of a well defined rift zone that is, like the summit graben, parallel to the volcano long axis. According to experiments made with cone-shaped volcanoes, spreading movements tend to reduce the steepness of slopes (Merle and Borgia

1996). Recent experiments (Le Corvec and Walter 2009) demonstrate that this mechanism affects spreading sand cones free of intrusions or in which the intrusion of analogue magma has been stopped. The intrusion of analogue magma along a rift zone, on the other hand, locks the spreading movement and pushes the flanks sideways without modifying the slope (Le Corvec and Walter 2009). During phases of intense magma activity, such as is possibly the case for present-day Mt Cameroon, the flanks are pushed sideways. They slide over the weak sedimentary basement and do not undergo the internal deformation and slope reduction commonly experienced by the flanks of spreading volcanoes.

The spreading hypothesis is also supported by geophysical data. The Mt Cameroon region is seismically active, even during non eruptive periods, and seismic observations with varying accuracy have been described from 1983 to 2000 (Fairhead 1985, Ambeh and Fairhead 1991, Tabod et al. 1992, Ateba and Ntepe 1997, Ubangoh et al. 1997, Ateba et al. 2009). Despite poor constraints on their location, individual earthquakes or seismic swarms concentrate at a shallow depth below Mt Cameroon's summit and below the SE and NW bases at crustal and sub-crustal depth. A cluster of seismic events is observed along the NW-SE trending Bokosso faults on Mt Cameroon northern flank. This seismic activity has so far been interpreted as movement along tectonic structures or magma generation and ascent from sub-crustal sources (Ateba and Ntepe 1997, Ubangoh et al. 1997, Ateba et al. 2009). Focal mechanisms of most earthquakes show nearly pure strike-slip movement without any consistent orientation of the compression and tension axes for the region (Ambeh et al. 1992, Tabod et al. 1992). Except for the significant depth calculated for some of these earthquakes, which can partly be attributed to the poor accuracy of epicentre location, seismic activity below the NW and SE flanks, including the Bokosso faults, is consistent with the spreading interpretation.

5.5. An asymmetric spreading?

The study of Mt Cameroon's SRTM show that thrusts are asymmetrically distributed around the volcano: the area affected by thrusts is larger in the NW than in the SE of the volcano. Also, the NW flank exhibits well developed strike-slip faults (Bokosso faults) that border the thrust faults and is affected by a large slump rotation, which has formed the Elephant Valley. Such evidence of significant movement does not exist on the SE flank.

Also, field measurement reveals that dykes and fractures formed by the active rift zone strike 040 and 060, SW and NE of the summit cone, respectively. This result describes a rift zone curved around the summit and convex toward the NW. This morphology may be due to the fact that the NW flank of Mt Cameroon has experienced more spreading than the SE one.
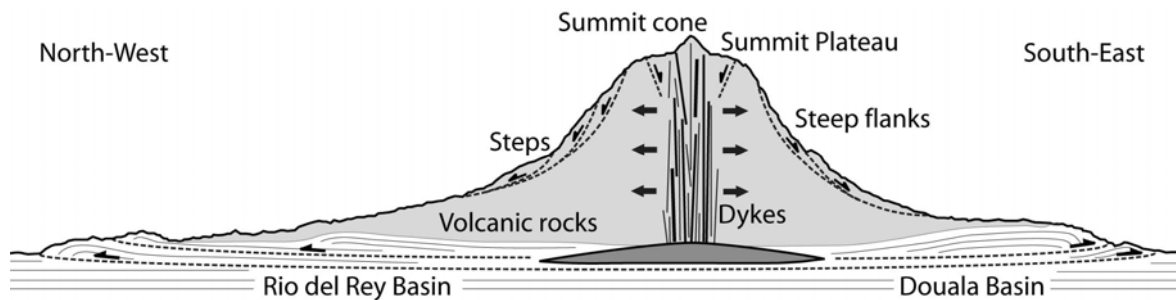
Figure 09: Hypothetical cross-section of Mt Cameroon (the sketch is not scaled)

Such an asymmetry is probably linked to the heterogeneity of the substratum that is probably made of a thicker and/or weaker sedimentary succession in the NW (Rio del Rey basin) than in the SE (Douala basin).

Note that the fastest spreading flank (NW) is associated with strike-slip and reverse faults and is slightly shallower than the SE flank (figure 09) that is not associated with strike-slip faults. The relationship between spreading-related structures and the slope of the spreading volcano has been investigated by analogue models (Delcamp et al. 2008).

6. Conclusion

The fluid basaltic magma of Mt Cameroon has infiltrated an inactive strike-slip fault zone. This mechanism has formed an elongated volcano with a well defined rift zone, which possesses the following characteristics.

This basalt-dominated elongated volcano is made of magma intrusions, lava flows and pyroclastic material rather than basement rocks as postulated by the horst theory. Its summit

is affected by a large amount of fracturing mostly related to local instabilities related to destabilisation movement around unstable steep valleys and to dyke intrusions.

The field data indicate the presence of basal thrusts and folds, which are related to the spreading of the volcano long flanks. The spreading is better expressed in the NW than in the SE of the volcano, possibly as a consequence of sedimentary basement heterogeneities. Several instabilities (large slump rotation, small volume collapses and shallow sliding) result from the spreading movement and from the pushing induced by the development of the dyke core complex.

The elongated morphology of Mt Cameroon promotes the spreading of the longest flanks perpendicular to the dyke core complex. This directed spreading facilitates the passive intrusion of dykes along the existing rift. Such mechanism occurs during phases of low magma activity and is driven by the volcano load and facilitated by the spreading of ductile sediments. During phases of more voluminous magma activity, the repeated forceful intrusions of dykes along the rift zone may push the steepest flanks of the volcano apart. The flanks then slide along the weak sedimentary basement. The slopes of these flanks are not modified during the process.

Mt Cameroon is an intriguing large and very active volcano that is experiencing spreading. A large part of the model developed in this article still remains to be validated by field and geophysical studies. Further field studies will be needed to identify or infer the existence of large volume debris avalanche deposits, to assess the morphology of the NW thrusts, to clarify the kinematic of the Bokosso faults and to unravel the structures that surround the summit graben. Geophysical tools may unravel the morphology of the intrusive system and more precisely determine the movement of the spreading-related faults. The instabilities of Mt Cameroon's long flank are a source of potential hazard that need to be systematically studied and continuously monitored using state-of-the-art integrated techniques in the future.

Chapter 4

-

The structure of Maderas volcano, Nicaragua
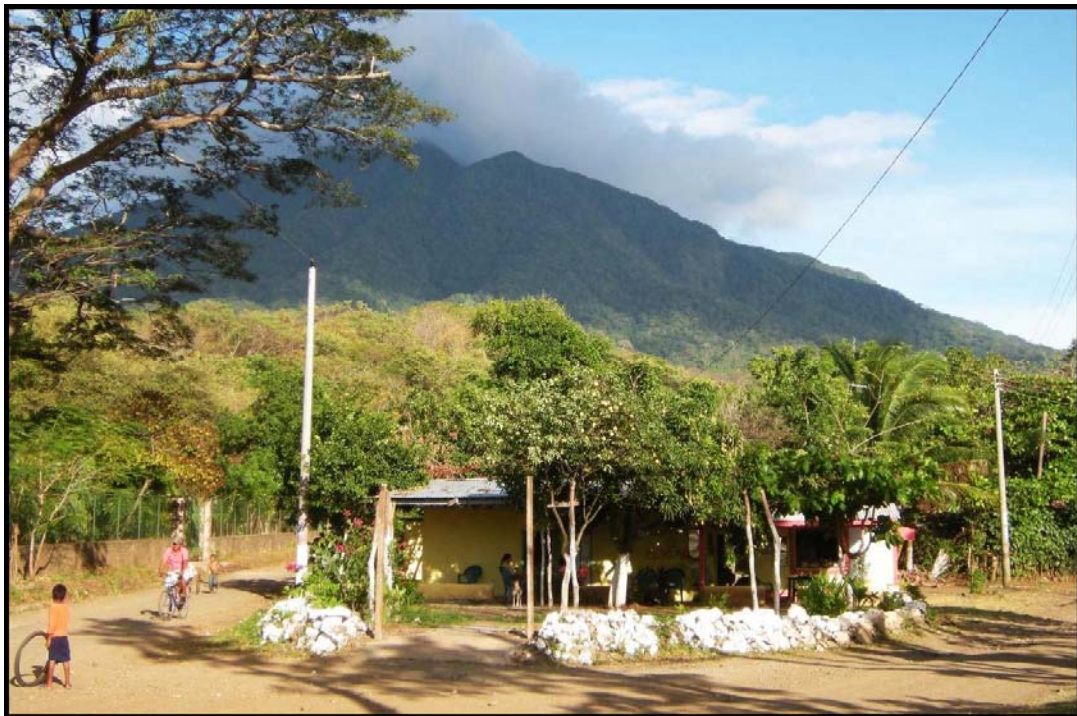
Chapter 4: The structure of Maderas volcano, Nicaragua

1. Introduction

Maderas is a case-study of a spreading volcano formed in an E-W directed extensional stress field with a diffuse dextral strike-slip component of movement (van Wyk de Vries and Merle 1996). The regional fault is hidden by the Nicaragua Lake. By comparison with the structures of western Nicaragua, van Wyk de Vries (1993) inferred that Maderas is located in a NW-SE striking dextral transtensional fault zone. The structure of the volcano has only been studied with aerial photography (van Wyk de Vries 1993). The aim of this chapter is to continue this pioneer work with additional remote sensing methods and fieldwork. Maderas is studied because its small volume facilitates the field investigation and because of the structure of its basement, which contains active transtensional faulting and ductile sedimentary layers.

2. Geological setting and Maderas geology

2.1. Geological setting

Maderas volcano is one of the 21 Quaternary arc volcanoes of Nicaragua (figure 01). These shield and strato-volcanoes are small edifices with individual volumes of about 30 km^3. From west to east, the country is structured as followed: a) Nicaraguan Trough (offshore) and

onshore associated uplift; b) Nicaraguan depression; c) Interior Highlands (figure 02). The Nicaraguan Trough formed following the subduction of the Cocos plate under the Caribbean plate. The Quaternary Central American volcanic front is located within the Nicaraguan Depression, which is a lowland originating from isostatic readjustments (van Wyk de Vries 1993) and bounded to the SW by a major uplift (Borgia and van Wyk de Vries 2003).

The subduction of a mid-oceanic ridge of the Cocos is responsible for uplift in the south of Nicaragua. The tectonics of the country is mostly linked to the rotation of the NW part of the Caribbean plate along its northern margin, which is bordered by the Montagua-Polochic fault zone (figure 01). This rotation is likely related to the 10° obliquity of the subduction quantified by GPS data (De Mets 2001; e.g. figure 01). The rotation of the plate has formed NW striking faults and folds, NE striking sinistral faults and N-S striking transtensional faults in the crust (Cruden 1991, Manton 1987). The neo-structures that affect Quaternary sediments and volcanic rocks strike NE (sinistral strike-slip faults), N-S (transtensional faults) and NW (normal faults; van Wyk de Vries 1993). Dextral strike-slip fault movements in western Nicaragua are documented by GPS measurements (De Mets 2001; figure 01). Thus, according to van Wyk de Vries (1993) and De Mets (2001) observations, the NW striking structures are dextral transtensional faults.
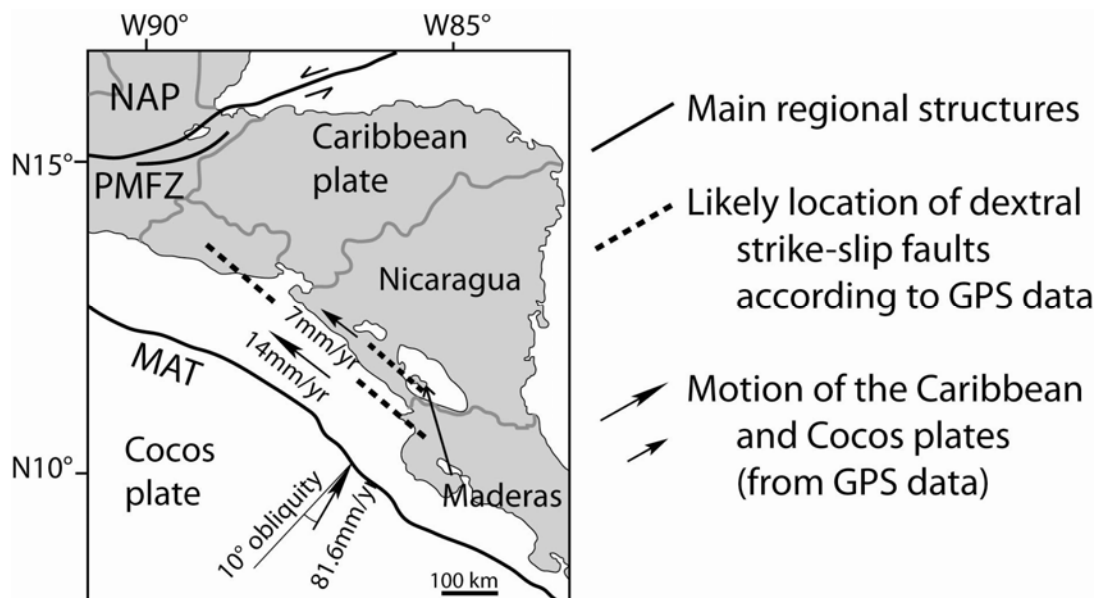
Figure 01: Regional setting of Nicaragua (after Cailleau et al. 2007; De Mets 2001; van Wyk de Vries 1993); the abbreviations stand for North American Plate (NAP), Polochic-Motagua fault zone (PMFZ) and Middle American Trench (MAT).

Nicaraguan volcanoes erupt basaltic (lava flows) to dacitic rocks (domes and pumice). Shield volcanoes are made of low-Al and MgO rich basalts, which were quickly transported through the crust along the fault zones upon which these volcanoes sit. The strato-volcanoes built away from fault zones and are thus made of a less primitive magma, which stays longer in the crust according to van Wyk de Vries (1993) and to Borgia and van Wyk de Vries (2003).
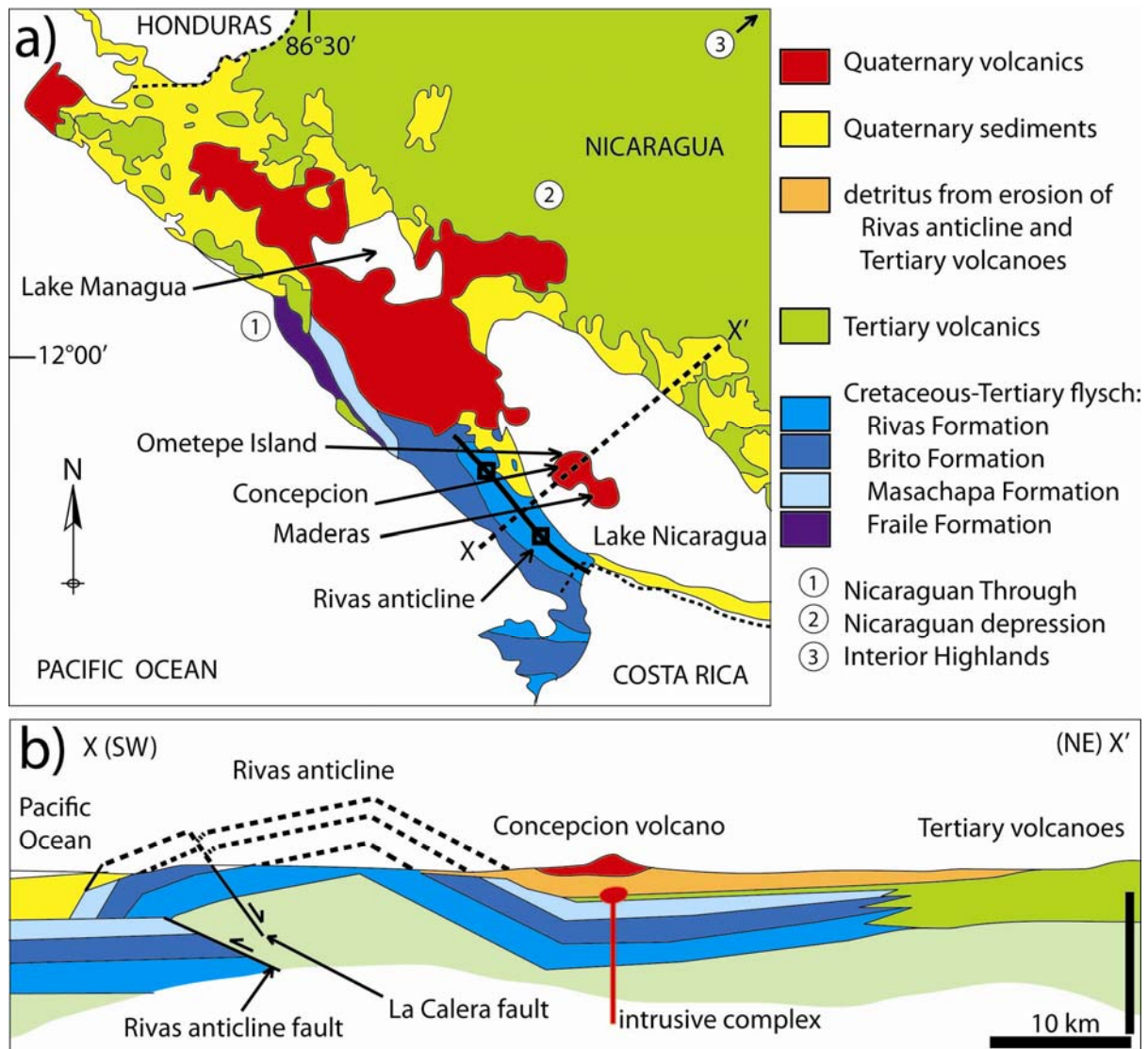
Figure 02: a) Geological map of part of Nicaragua (after Borgia and van Wyk de Vries 2003); b) Cross-section along Concepcion volcano that is similar beneath Maderas volcano (after Borgia and van Wyk de Vries 2003).

2.2. Maderas volcano

Maderas is a stratovolcano which, with Conception volcano, makes up the Ometepe Island in Lake Nicaragua (figure 02-a). This small volcano is 1345 m high, has a diameter of 11 km and has not erupted for at least 3000 years (Borgia et al. 2000). Ometepe Island volcanoes sit on a thick succession of folded Cretaceous to Tertiary marine sediments (e.g. Rivas Anticline, figure 02-a, b) and Quaternary Lake Nicaragua sediments originating from the erosion of the Rivas Anticline. These sediments consist of < 200 m organic-rich clays, sand and silts (van Wyk de Vries 1993). The volcanism in this area originates from a late Quaternary to Holocene SW jump of the volcanic front. Maderas formed an E-W directed extensional field associated with slight dextral transtensional motion. Once big enough, it started to spread over the weak Lake Nicaragua sediments (van Wyk de Vries 1993, Borgia and van Wyk de Vries 2003, Borgia et al. 2000). The Maderas volcano structure is a combination of gravitational spreading and regional stress-related structures according to van Wyk de Vries and Merle (1996). The stress field has formed a N-S graben at the volcano summit and has initiated slumping of its SW flank, which is evidenced by scarps located west of the summit according to van Wyk de Vries (1993) and Kerle et al. (2001).

Maderas volcano is covered with a dense rain forest, it is small in size and dormant. These three characteristics do not favour good quality outcrops and they are indeed rare, of limited extent and highly weathered. I obtained a limited amount of field data on the geology and structure of Maderas. These data are presented in the last part of this section. The structure of the volcano is also studied using remote sensing data, which are presented in the first part of this section.

3. Remote sensing

This section groups observations made from the ground (classed as field observations) with those from aerial photograph and satellite-based radar (SRTM).

3.1. SRTM

The SRTM (Shuttle Radar Topographic Mission) is a 3 arc second (e.g. square pixels are 90 m X 90 m) Digital Elevation Model (DEM). The Maderas SRTM has been downloaded from the USGS-a website. The SRTM is not ideal to study such a small volcano which is only represented by 120 pixels along an E-W striking line.

About four vents are visible on the SRTM and are located to the NE (Punta Gorda) and the northern lower flanks of the volcano (figure 03-a). The summit crater is also easy to spot. The upper flanks are dissected by many valleys. Two large lineaments striking 135 are located in this area: one cuts through the summit, the other is located 1.5 km east of the first (figure 03-a). The upper flanks are steep, while the summit area and the lower flanks are shallow (figure 03-b). The upper flanks located east and west of the summit are the steepest. The aspect map indicates that Maderas is a rounded volcano slightly elongated in an E-W direction (figure 03-c).
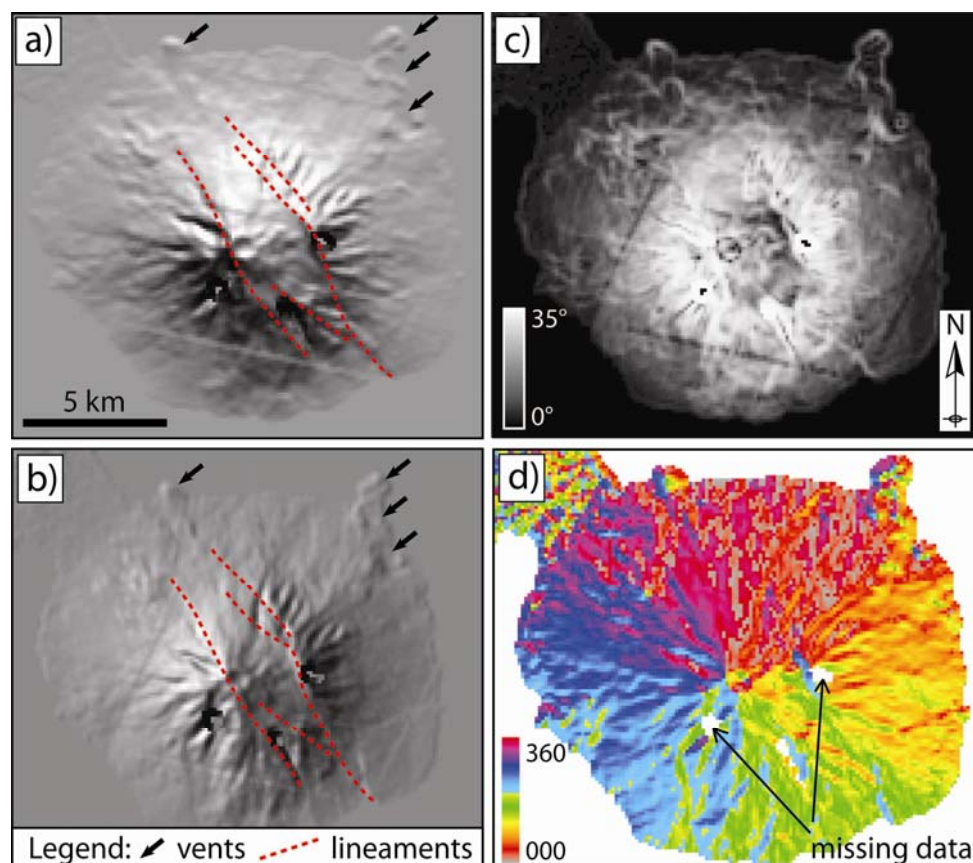
Figure 03: SRTM of Maderas volcano presented as (a) a shaded relief map (sun elevation= 45°, azimuth= 000); (b) a slope map and (c) an aspect map.

3.2. Field observations and aerial pictures

This section summarises the field observations made from the road and path which circles the base of Maderas volcano and from the paths that lead to its summit from Balgüe and Mérida towns. These observations confirm that the upper flanks are the steepest part of the volcano (e.g. grey areas of figure 04). The steepest slopes are observed in two areas located NE and W-SW of the summit. The western zone is the largest and encompasses the summit. The second zone has a smaller extent and is located 1.5 km east of the summit crater. An elliptical break-in-slope (e.g. figure 04) circles the summit and is elongated in the N-S to NW-SE direction. It is observed over the volcano flanks, which are not dissected by valleys and it separates a lower steep flank from an upper shallower flank.

The lineaments shown on figure 04-a correspond to high cliffs, steep valleys and linear canyons. They may all be related to faults and fractures even if no field evidence has been found to support this hypothesis (e.g. field data section). These lineaments are oriented 135, 090-110 and 170-180. The structures oriented 135 are well represented and they border the shallow summit corridor, which separates the two steepest areas of Maderas volcano. West of the summit, several valleys are oriented 090-110 and 170-180 striking cliffs are observed.
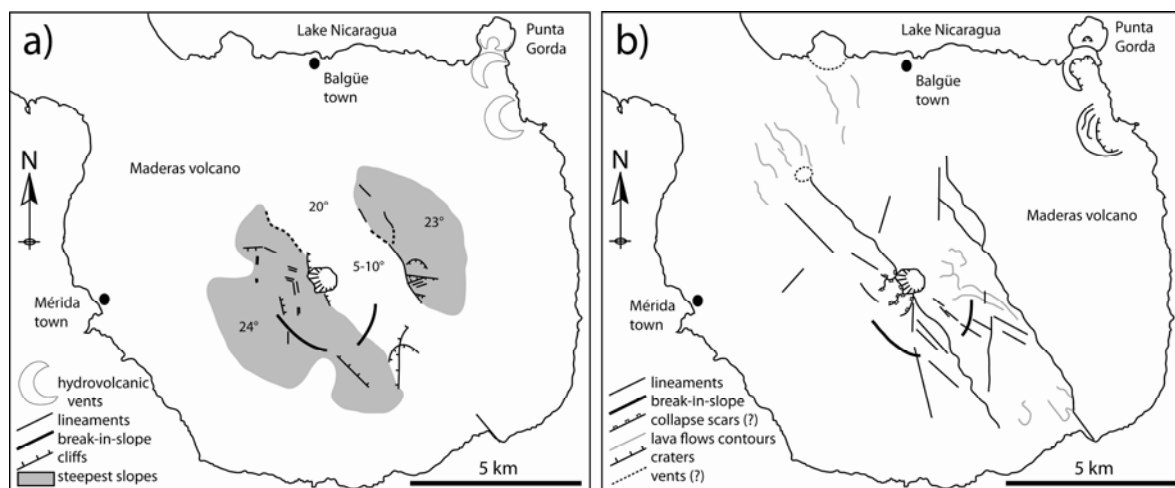
Figure 04: a) Field observations. The rivers are drawn from the topographic map of Ometepe Island. The angles shown on the map correspond to field estimates of the slopes of the Maderas flanks, where they are not dissected by valleys; b) structures and lineaments were observed on aerial photography.

The break-in-slope and the lineaments are also observed on the aerial photography (from INETER-Instituto Nicaragüense de Estudios Territoriales). The sun is directed toward the ENE in these photographs and thus, the N-S to NW-SE structures are emphasised. The lineaments identified on the aerial photograhps strike mostly 130-140 and border the upper part of the steepest flanks (figure 04-a, b). These 130-140 striking cliffs surround a flat-floored elongated area. This summit structure has the morphology of a graben. The 000 striking structures are poorly represented at the tip and inside this graben.

3.3. Combination of methods and digitalisation of a DEM

The SRTM and the field observations indicate that Maderas volcano has a 135 striking summit graben and steep upper flanks. The aerial photography provides more details on the location and morphology of the 135 striking structures. In order to make a more complete and detailed structural map of the volcano, I have digitalised the contour levels (interval= 20 m) of the topographic map of the volcano. These data are turned into a 1 arc second (resolution= 30 m) DEM using ENVI software (e.g. DEM_30m; figure 05). The DEM_30 m is presented by figure 05 (a to e). The lineaments interpreted from this document are compared with those obtained from the previously described sources and are presented on figure 06.

The structural map of Maderas established from remote sensing data (figure 06) shows that the most recent vents of the Maderas volcano are located N-NW of the volcano, while more ancient vents have probably been covered with lava flows and are invisible to remote sensing data. The DEM_30m reveals the presence of radial lineaments on the volcano lower flanks. These lineaments are organised in pairs of cliffs facing each other and intersecting at the base of the edifice. They are similar to the flower structures which develop on cones affected by gravitational spreading (e.g. Merle and Borgia 1996, Delcamp et al. 2008).

The 135 striking structures are well represented. The northern part of the eastern 135 striking cliff turns into a 000 striking cliff. Other 000 lineaments are observed north and south of the summit (figure 05, 06).
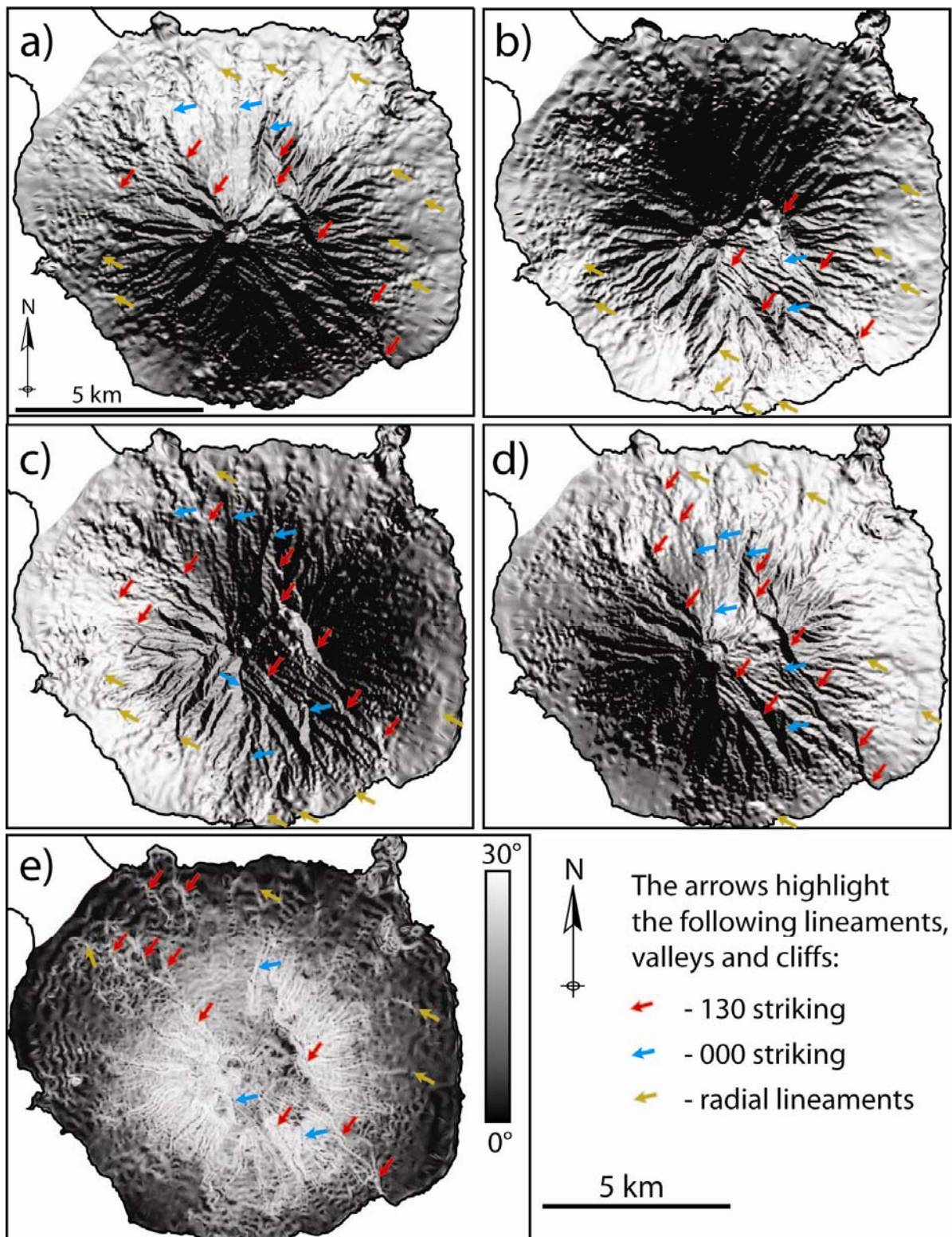
Figure 05: DEM_30m presented as (a-d) an hill shade map (sun elevation= 45°, azimuth= (a) 000, (b) 170, (c) 290, (d) 045) and as (e) a slope map.
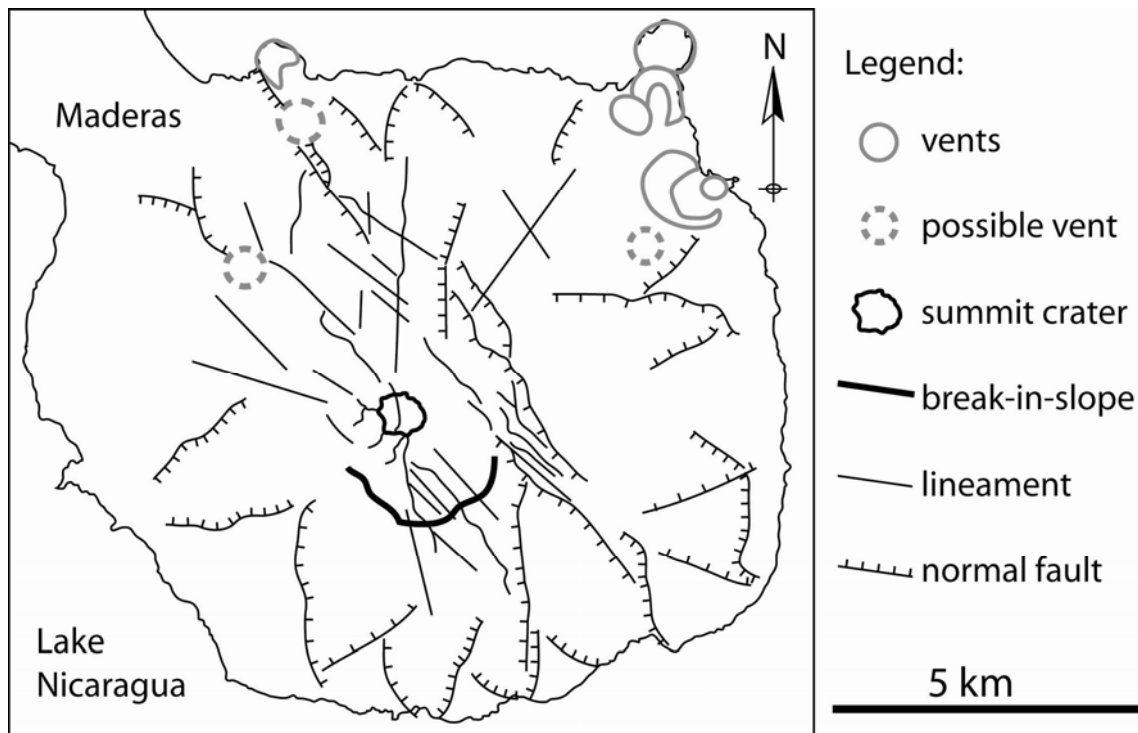
Figure 06: Structural map of Maderas volcano. Most lineaments are drawn from the DEM_30m.

4. Field data

4.1. Summit and base of the volcano

The small, extinct and rain forest covered Maderas volcano does not have a lot of well exposed outcrop. The summit area is a good example of the outcrop quality in this area. A layered and weathered 2 m thick outcrop of lapilli is located east of the summit (figure 07, 08-a). It may correspond to a weathered lapilli tephra with beds oriented 000/40W. The cliffs that surround the summit crater lake are covered with debris flow deposits. The remaining outcrops are too weathered to identify the lithologies.

The shore line did not provide many outcrops as Lake Nicaragua had an exceptionally high level at the time of this field study (it was the windy season). One outcrop of lava flow and its scoriaceous breccia and a debris flow deposit are exposed south of Mérida town. The lake

sediments that underlay Maderas volcano are exposed along the beach, north of Santa Cruz town (figure 07). They consist of unconsolidated sand (beach deposits), weak white clay and conglomerate horizons (lake deposits; figure 07-b).
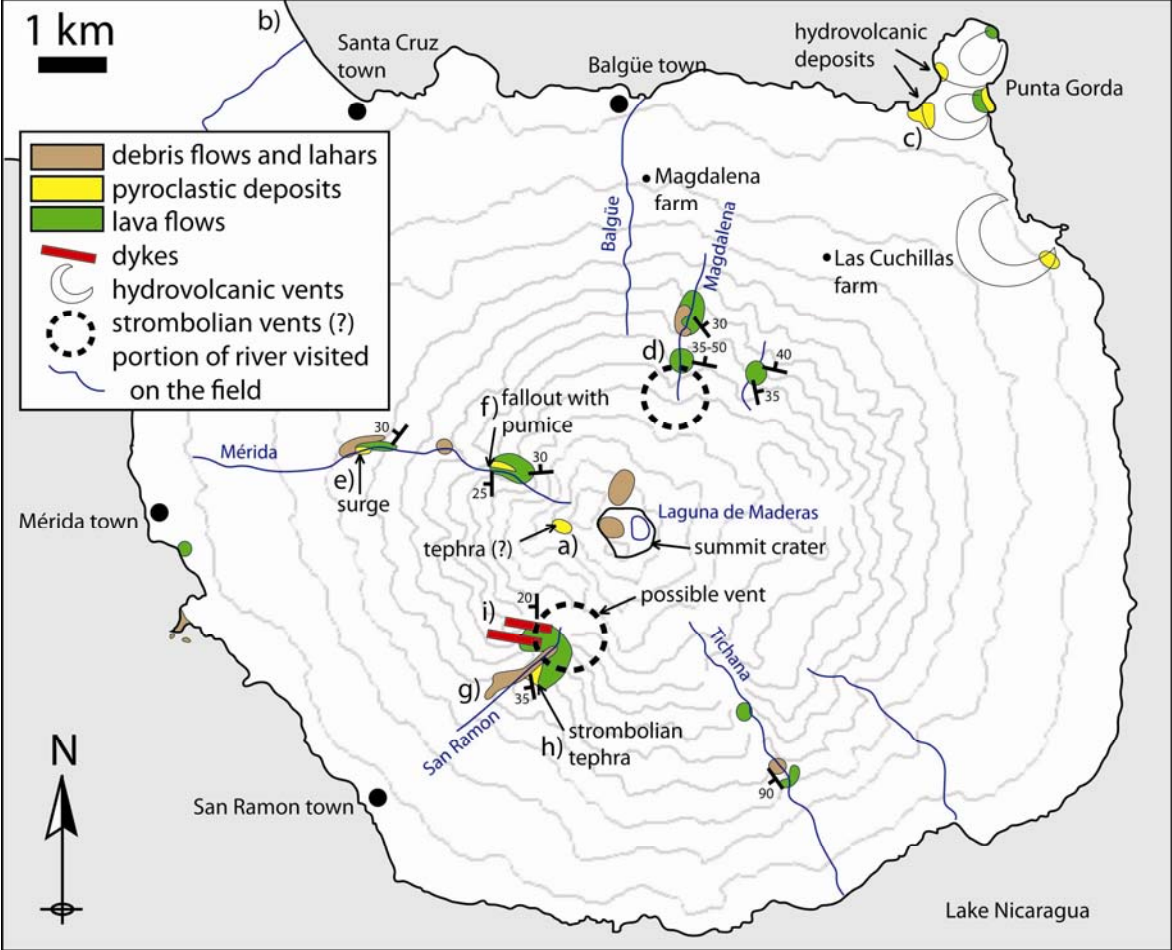
Figure 07: Map of outcrops found on Maderas volcano. The contour levels (100 m interval) are extracted from the SRTM; the a) to i) signs refer to figure 08 pictures.

The hydrovolcanic deposits erupted by the vents located NE of the volcano (e.g. Punta Gorda; figure 07) are exposed along the shore and along the road that circles the base of the edifice. These deposits are rare, thin (2 to 10 m high) and have a limited extent. They are laminar or can be locally undulated (figure 08-c) and are almost white possibly due to weathering. They consist of ash horizons with free feldspars and pyroxenes interbedded with lava lapilli horizons about 10 to 50 cm thick. Some lava blocks are found in these deposits, which are locally intercalated with lava flows.

4.2. Rivers

Five rivers have been visited north and east of the volcano of which three contained outcrops. A river located south of Las Cuchillas farm (northern flank; figure 07) cuts in a pile of lava flows with massive cores and outer scoriaceous breccias. Individual flows are over 10 m thick and are oriented about 160/30NE (n=4). Tichana River (SE flank) cuts into 5 to over 30 m thick lava flows flowing 150 SE according to an exposed lava flow border (n=1). Upstream a waterfall exposes a massive lava cut by 000/70W striking fractures (n=5). The Magdalena River (northern flank) cuts into a pile of lava flows and contains a recent debris flow deposit that is unconsolidated and located on top of river pebbles. Individual lava flows strike 040, 100 and 140 and dip 20-30 NE and NW (n=4). Upstream a 30 m high succession of waterfalls are made of alternating 0.5-1.5 m thick massive lava layers (n=5) and 2-3 m thick scoriaceous breccia layers oriented 100-110/35-50 NE (n=6; figure 08-d). These thin lava flows were likely erupted by a nearby strombolian vent (e.g. figure 07 for location).

The lower part of Mérida River (western flank of Maderas) contains several 5 to 15 m thick outcrops of lahars and debris flows and 3 to 20 m thick lava flows whose massive core and scoriaceous breccia are exposed. One of these flows is oriented 040/30 NW (n=1). The river contains also clastic deposits, such as a 2 m thick orange clastic deposit made of sandy horizons. There is also a lava lapilli deposit that is capped by a debris flow downstream in the Mérida River. A couple of meters upstream a similar 5 m thick outcrop is located below a lava flow. This clastic outcrop is baked and is made of ash with free feldspars, pyroxenes and white and lava lapilli horizons. The deposit horizon is undulated and contains holes, which correspond to eroded tree trunks. It has the structure of a pyroclastic surge deposit (figure 08-e).

A similar deposit capped by a lahar is found upstream on top of a 2 m thick pahoehoe lava flow oriented 160-020/20-30W (n=2). Further upstream the river becomes a canyon. A 20 m high cliff is made of a pile of lava flows with thick scoriaceous breccia. Individual flows are 5 to 10 m thick and strike 080/30NW (n=1). These lava flows are interbedded with baked river alluvium and with a discontinuous white horizon made of less than 10 cm thick horizons of pink ash with free feldspars and pyroxenes, lava and scoria lapilli and white to grey pumice lapilli. This white horizon is a weathered fallout deposit, which originates either from Maderas or from the nearby Concepcion volcano (figure 08-f, e.g. the Blanca pumice, Borgia and van Wyk de Vries 2003).
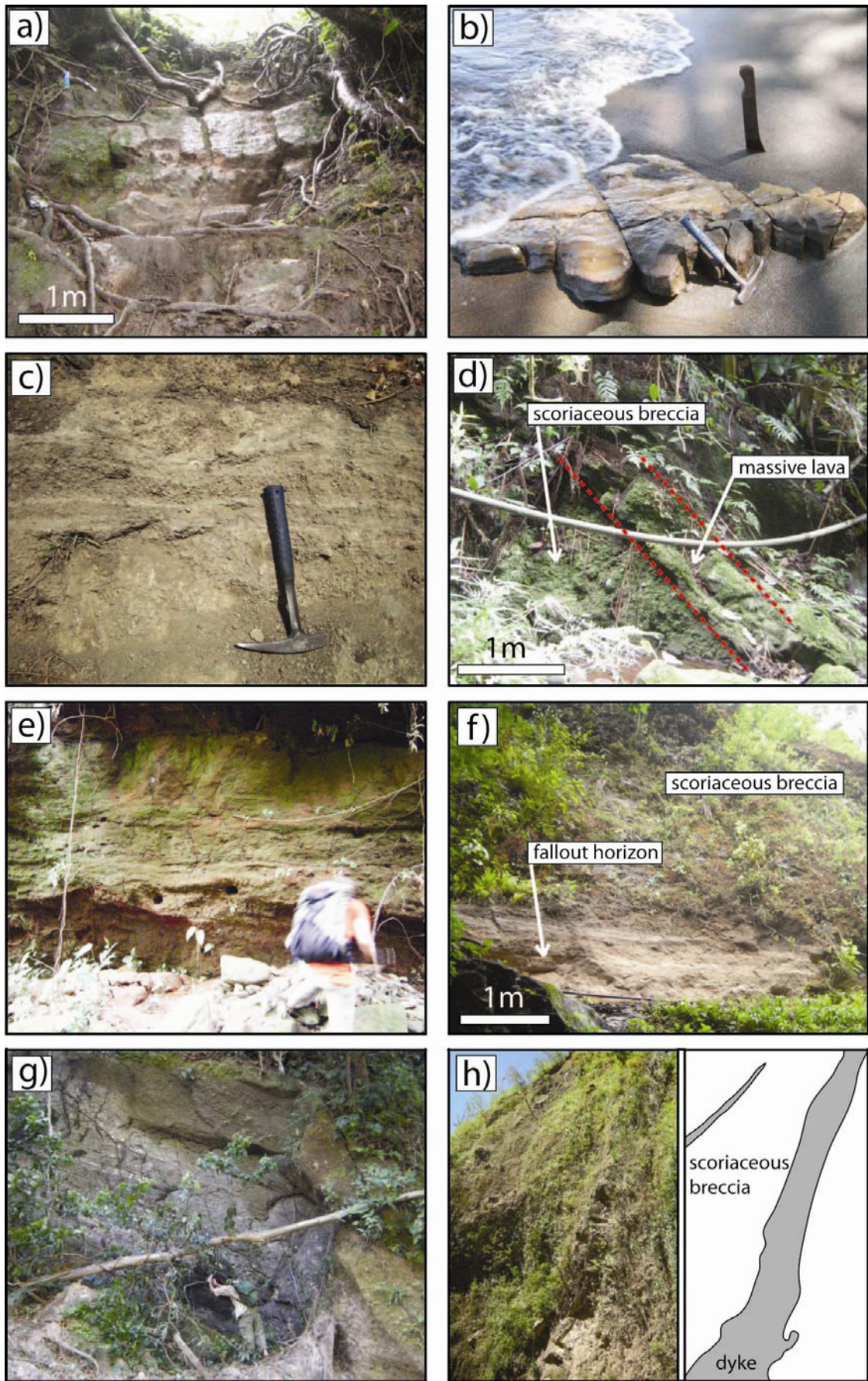
Figure 08 (cf. opposite page)

The San Ramon River (SE flank) contains 5 to 20 m thick recent lahar or debris flow deposits, which are not yet covered with vegetation. The valley walls are made of 10-15 m of thinly layered vesicle-rich lava lapilli to blocks capped by a pile of lava flows (figure 08-g). The basal horizons strike 160/35SW (n=2). This is a deposit probably related to a nearby scoria cone vent (figure 07). Further upstream a 40 m high cliff is made of scoria blocks and thin (1-1.5 m thick) massive lava horizons. This deposit is either a pile of blocky lava flows or an accumulation of coarse scoria cone ballistics. It is intruded by two 5 m thick dykes oriented 110/60SW and 115/65SW (figure 08-h). The 50 m high San Ramon waterfall is an alternation of 1-1.5 m thick massive lava and 5-10 m thick scoriaceous breccia, which are orientated 170-010/20W (n=5).

5. Discussion

Maderas is a small volume, extinct and rounded volcano. It possesses a flat summit bordered by 135 striking faults, its steepest upper flanks are located east and west of its summit and half-grabens have developed over its lower flanks (e.g. figure 09). The half-grabens accommodate the stretching of the lower flanks that is induced by the spreading of the volcano (e.g. Merle and Borgia 1996). The flat summit indicates that the spreading is affecting an extinct volcanic edifice. If Maderas was still active, summit eruptions would build a steep summit cone faster than the spreading movements could flatten it. When it was active, the spreading movements have favoured summit extension and the establishment of a central conduit, which is evidenced by the presence of a summit crater. The spreading may have formed thrusts and folds at the base of Maderas volcano, where they are likely to be

Figure 08: Pictures of a) weathered pyroclastic projection (west of summit crater); b) white clay horizon (Lake Nicaragua sediment); c) wavy hydrovolcanic deposit (Punta Gorda vents); d) thin lava flows (Magdalena River); e) pyroclastic surge deposit (Mérida River); f) white fallout deposit (Mérida River); g) recent lahars to debris flow deposit (San Ramon River); h) strombolian projection and fallout (San Ramon River); i) picture and sketch of San Ramon River dykes. These outcrops are located on figure 07.

hidden by Lake Nicaragua sediments. The shallow lower flanks of Maderas may also have favoured the formation of strike-slip faults at the expense of reverse faults (e.g. Delcamp et al. 2008).

The most recent vents have preserved their topographic expression and are located at the base of the volcano. They may have been fed by magma accumulated in weak horizons such as the Lake Nicaragua sediments or the basal reverse faults, which accommodate the spreading movements at the base of the volcano. The vents are hydrovolcanic at this lower elevation due to the interaction between the magma and the Lake Nicaragua water.

The field study also provides evidence of high energy eruptions, which are responsible for the surge and fallout deposits identified in the lava pile (e.g. Mérida River). The limited extent of field outcrops does not allow the mapping and the quantification of such phenomena.
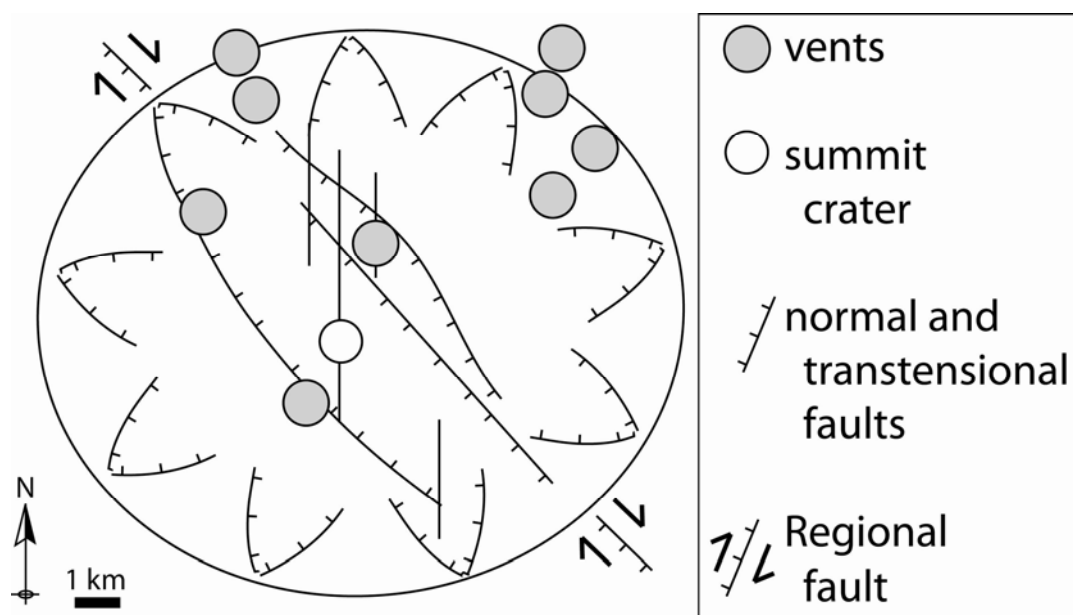
Figure 09: Structural sketch of Maderas volcano.

The last structures which are worth noting on Maderas volcano are its 135 summit graben and its 000 lineaments. Several eroded vents identified by the field study have developed along the 135 striking faults following the infiltration of magma along these structures. Also, the thickest lava flows found on the SSE flank of the volcano (e.g. Tichana River) may have been confined by the 135 striking cliffs. These two observations indicate that the 135 striking faults

formed before the end of the volcanic activity. The faults are fresh structures (e.g. steep cliffs) that are still active or were active until recently.

According to its regional setting, it is suggested that Maderas volcano has developed in a 135 striking dextral transtensional fault zone (c.f. the work of De Mets 2001 and van Wyk de Vries 1998). The 135 striking graben is parallel to the regional fault zone. The central vent is located on top of this fault zone that has facilitated the transport of magma in the crust (figure 09). The 000 lineaments, which cover the volcano, correspond to the fault zone tension structures emphasised by the spreading, which tends to favour extensional movements.

6. Conclusion

Maderas volcano is shaped by spreading and regional strike-slip movements. The spreading of the volcano over its ductile substratum has formed shallow slopes (5°-25°) that were likely steeper (about 30°) prior spreading. The radial spreading of the dormant volcano is also evidenced by a shallow dipping summit area. Half-grabens have developed on the volcano lower flanks and reverse or strike-slip faults may be hidden by Lake Nicaragua sediments at the base of the volcano.

Maderas has built in an active transtensional fault zone but has not become elongated parallel to it. The amount of eruptive vents is not sufficient to conclude that Maderas possesses a rift zone. These observations indicate that the viscous andesitic magma of Maderas has risen inside the regional active fault zone but has been unable to infiltrate in it to develop a rift zone, as observed elsewhere by Andrade (2009). This small volume has been formed by a limited supply of magma. The amount of magma available in this area is certainly linked to external geodynamic factors.

The 135 striking regional dextral transtensional fault has sheared the volcano. The deformation is accommodated by faults identified as lineaments on the remote sensing data. These lineaments have not been hidden by recent volcanic deposit because Maderas is a dormant or extinct volcano, and are thus exceptionally well preserved. The 135 striking graben is parallel to the regional fault plane. The 000 striking lineaments correspond to the tensional structures. The 000 and 135 lineaments possibly correspond to normal and transtensional faults. This interpretation is based on remote sensing data and lacks field evidences.

A large part of the model developed in this chapter has to be validated by additional studies. A field study of Maderas will not provide the required data in this outcrop-poor environment. Geophysical tools may unravel the morphology of the intrusive system and enable the quantification of fault movements. The instabilities of Maderas flanks are a source of potential hazard that need to be systematically studied. This volcano show so far that spreading and regional strike-slip movements can strongly modify the morphology of a volcano. The neighbourhood Concepcion volcano, which has also developed in the 135 striking regional dextral transtensional fault, may contain structures similar to the 135 and 000 striking faults of Maderas beneath its blanket of recent pyroclastic deposits.

Chapter 5

-

Analogue models
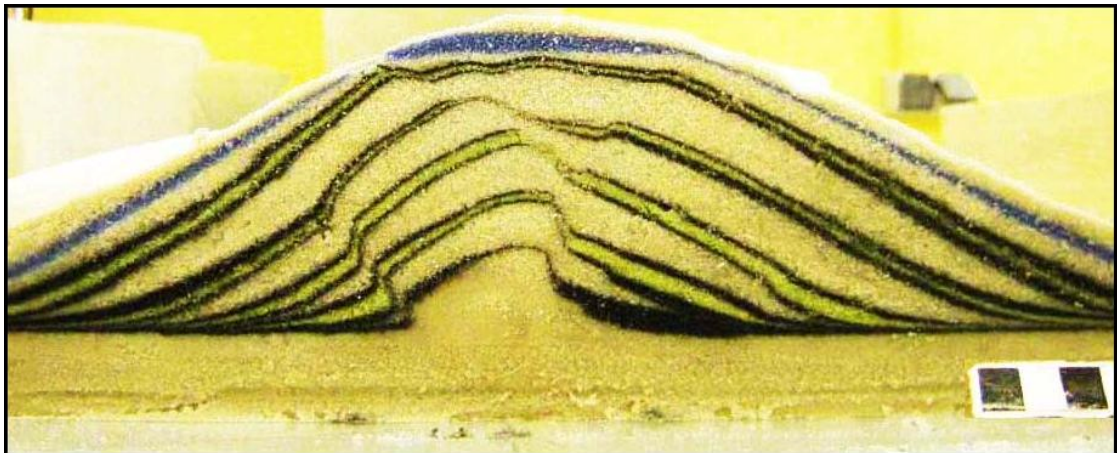
Chapter 5: Analogue Models

1. Introduction

Many volcanoes are associated with faults that facilitate the transport of magma in the crust. Active faults interact with the volcano as it grows or/and as it becomes eroded. Volcanoes are also deformed by local processes such as gravitational spreading, which have been observed worldwide (van Bemmelen 1949, Merle and Borgia 1996, Borgia et al. 2000). This chapter examines the structure of stable and spreading conical edifices interacting with faults that have a strike-slip component of movement.

Many volcanoes worldwide have formed upon strike-slip fault systems, which are found in every geodynamic context. The strike-slip component of a fault is either pure strike-slip movement or is associated with an orthogonal extensional (transtensional fault) or compressional (transpressional fault) component of movement. Transpressional and transtensional faults usually accommodate the internal deformation of a tectonic plate whose movement (e.g. regional or far-field displacement) is oblique to plate boundary (Dewey et al. 1998). It is difficult to study the structures associated with these faults in a volcanic context in the field. Strike-slip faults have an average slip of 1 mm to 1 cm per year (Dusquenoy et al. 1994, Bourne et al. 1998, Groppelli and Tibaldi 1999, Corpuz et al. 2004) and fault planes are rapidly hidden by volcanic output and fast erosion of the accumulated volcanic deposits. A volcanic edifice can be internally deformed by a strike-slip fault movement even if no structures are visible at the surface (Norini and Lagmay 2005) or may repair itself (dyke sealing fractures, etc.) between episodes of faulting (Belousov et al. 2005). The field approach is developed in the previous chapters, while this chapter concentrates on the use of analogue models in order to comprehend the interaction between edifices, spreading and strike-slip movements.

The fault kinematics and geometries considered here have been studied by previous authors. Sylvester (1988) designates the structures formed by strike-slip movements as: 1) Y shears are faults parallel to the principal displacement zone; 2) Riedel or R shears are synthetic faults

(same kinematics as Y) developing 15°-20° from Y; 3) conjugate Riedel or R' shears are antithetic faults developing 60°-75° from Y; 4) secondary antithetic or P shears develop 15°-20° from Y (figure 01). According to analogue experiments (e.g. flat-topped brittle substratum) R shears initially develop (Naylor et al. 1986) followed by P shears (Sylvester 1988). The Y shears dominate when a ductile layer is added to the brittle substratum (Naylor et al. 1986).
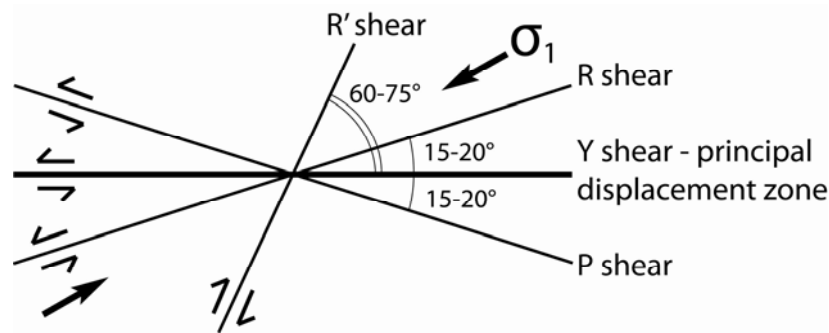
Figure 01: Sketch of the structures formed by sinistral strike-slip movements (after Sylvester 1988).

In theory, if a cone is added on top of a sheared flat substratum, its load will deflect the stress field (e.g. regional or far-field movement). A graben parallel to the regional sigma 1 and bordered by R and Y shears is expected to form at the summit of the cone (van Wyk de Vries and Merle 1998; figure 02-b). The graben extends and converts to reverse faults down the cone flanks to form a Sigmoid-I structure, which corresponds to an R shear according to Lagmay et al. (2000). The P shears developed around the summit and are named Sigmoid-II structures (Lagmay et al. 2000). They border a fast moving summit area (Andrade 2009; e.g. figure 02-b). In addition to these structures, folds are observed in the substratum, at the tip of Sigmoid-I fault (van Wyk de Vries and Merle 1998).

The Sigmoid-I and II designations are used by many authors who study the interaction between regional strike-slip movements and volcanoes (Lagmay et al. 2000, Norini et al. 2008, Andrade 2009). These structures form exclusively in cone-shaped edifices. Sigmoid-I is a curved transpressional fault over the cone flanks and border a graben at the cone summit. The curved Sigmoid-II structures develop on each side of the summit and accommodate extensional movements (figure 02-b).
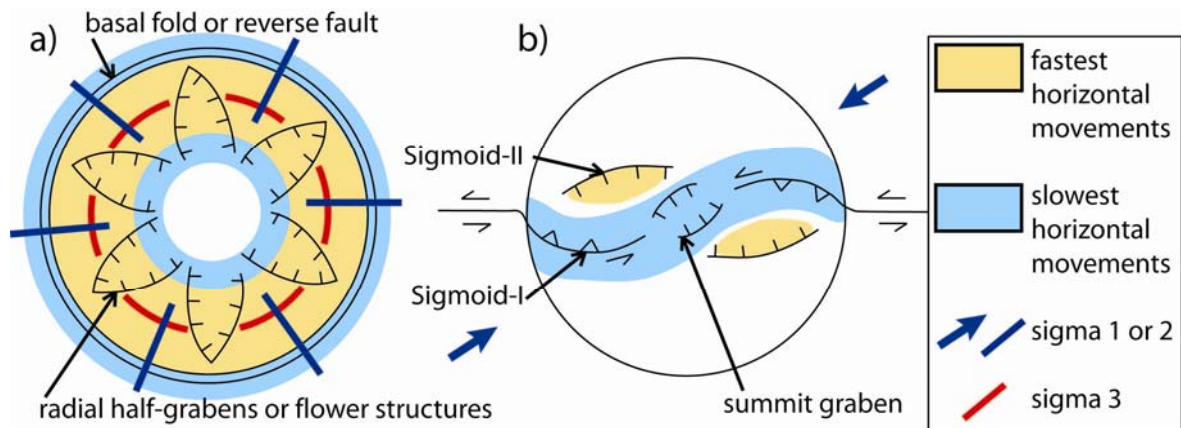
Figure 02: Sketch of the main structures formed in an experimental cone located (a) above a ductile substratum (after Merle and Borgia 1996) or (b) above a strike-slip fault (after Lagmay et al. 2000). The slowest and fastest horizontal movements are drawn after Delcamp et al. (2008) (a) and Andrade (2009) (b).

Cones interacting with transtensional and transpressional fault planes located 10° and 20° from their strike-slip component of movement have been modelled by Andrade (2009). When testing transpressional and transtensional faults the deformed area is almost parallel, respectively, to the R shear and to the strike-slip component of movement (Andrade 2009; figure 03). Concerning transtensional experiments, the summit graben is made of Y and R shears oriented 20° to 40° from the strike-slip component of movement. Further movement caused the summit to subside and the graben fractures to rotate to normal to Y (Norini et al. 2008; figure 03). In all the experiments, Sigmoid-II is a wide fracture zone in the mid-upper cone, which becomes part of the summit graben (transtension) and connects with sigmoid-I at the cone base (transtension, figure 03-a) or at the summit (transpression, figure 03-b). The summit graben subsides less and is narrower in transpressional experiments. If the strike-slip component of movement strikes 090, then the summit graben strikes 040-050 (sinistral transtension; figure 03-a) and 060-070 (sinistral transpression; figure 03-b) and corresponds to the maximum rotation.

The volcano spreading mechanism is also tested because it is a relevant processes which controls the slow-rate and long-term structural and magmatic evolution of a volcano (e.g. Borgia 1994). It concerns volcanoes of sufficient size, which are underlain by a substratum containing a low-viscosity layer. The excess load (volcano) drives outward spreading which forms concentric thrusts and folds or sub-radial strike-slip faults in the substratum around the

edifice (Merle and Borgia 1996). The volcano is in turn affected by concentric stretching and displays radial intersecting grabens and a fractured summit area (figure 02-a).

The fault planes tested in this chapter are located 20° and 40° from the strike-slip component of movement. The brittle substratum contains a ductile layer in half of the experiments. For each setup the strike of Sigmoid-I and II faults are measured and the component of movement of these faults is quantified. The results of analogue experiments are then compared to the structures of volcanoes located on top of active fault zone such as Guadeloupe (Lesser Antilles) and Maderas (Nicaragua) volcanoes.
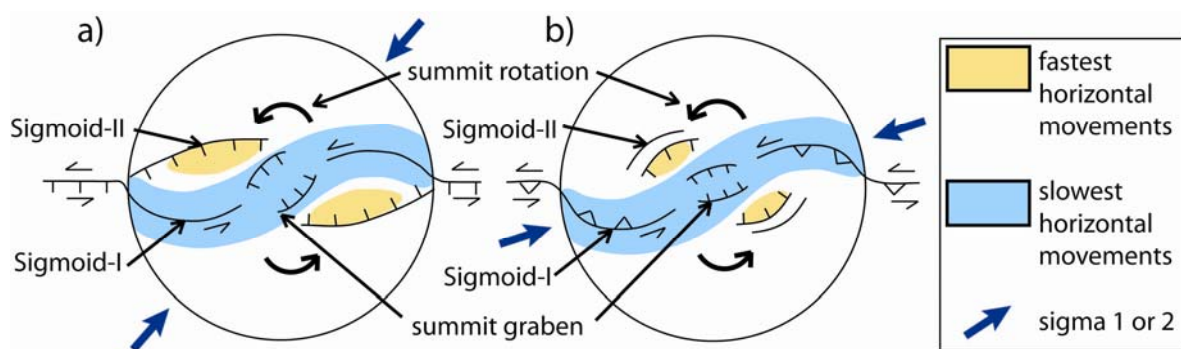
Figure 03: Sketch of the main structures formed in an experimental cone located above (a) a transtensional and (b) a transpressional fault (after Norini et al. 2008, Andrade 2009).

2. Experimental device, material and scaling

2.1. Material used

The substratum and the volcanic cone are modeled by a granular material. A first set of experiments is carried out with fine-grained ignimbrite powder and subsequent experiments are made with sand. These materials have slightly different densities, angles of internal

friction and cohesions (table 01). Sand is a Coulomb material that fails in shear and is suitable to model deformation of the upper crust (Hubbert 1937, Schellart 2000). It is the normal laboratory standard, but most experiments were carried out with ignimbrite powder, which allows the development of a greater amount of faults and the preservation of steep fault planes. This material is sieved Grande Nappe Ignimbrite, from Mont Dore volcano, France. It consists of glass and quartz grains less than 250 μm in diameter. The ignimbrite powder has an angle of internal friction of 38° and is more cohesive (100-230 Pa) than sand (0-10 Pa) because the smallest grains (about 1 μm in size) block the pore spaces in the powder. The sieved ignimbrite is similar to other granular materials as it fails in tension and, when confined, fails with shear band formation. Sand is used in subsequent experiments because it is easy to dye and can be, in contrast to ignimbrite, sliced at the end of experiments to provide insight into the internal structure of deformed experimental cones. The silicone is used to model a ductile substratum horizon.

2.2. Scaling

The scaling used here is similar to that employed in other analogue experimental work by Merle and Vendeville (1994), Donnadieu and Merle (1998) and Holohan et al. (2008). In our models 1 cm represents 1 km in nature giving a geometric scaling (e.g. ratio of model over nature length) of $H^* = 10^{-5}$ (table 01). The stress ratio, calculated from density, gravity, and length scales is $\sigma^* = \rho^*.g^*.H^* = 5 \cdot 10^{-6}$, meaning that models are about 10^6 times weaker than natural examples, and that viscosity and cohesion should be scaled accordingly. To scale viscosity and time we use the viscosity ratio (μ^*) and the stress ratio (σ^*) in: $t^* = \mu^*/ \sigma^*$. The time ratio (t^*) is 10^{-7} and the viscosity ratio (μ^*) is $5 \cdot 10^{-13}$. The natural viscosity of substrata is about 10^{16} Pa s, which corresponds to an unconsolidated claystone or other weak sediments (after Arnaud 2005). The fault velocity in the experiment is 4 cm.hr^{-1}. According to the geometric scaling (1 cm represents 1 km) and the time scaling (1 hour represents about 1000 yr), the experimental fault represents a natural fault with a slip velocity of 4 km per 1000 yr, that is 0.05 cm.yr^{-1}, which corresponds to a slow strike-slip fault (e.g. Dusquenoy et al. 1994, Groppelli and Tibaldi 1999, Corpuz et al. 2004).

Sand experiments are scaled with the same geometric scaling (H*) and stress ratio (σ*). These experiments are entirely brittle so time is not scaled.

Table 01: Parameters used to scale the ignimbrite powder experiments; *Ratio of model over nature variables; ** D_{CC} is negative by convention

Variable	Definition	MODEL	NATURE	Unit	Ratio *
Hc	height of the cone	$4.4\text{-}9\cdot10^{-2}$	$4.4\text{-}9\cdot10^{3}$	m	10^{-5}
$\varnothing_C$	cone diameter	0.18-0.33	$1.8\text{-}3.3\cdot10^{4}$	m	10^{-5}
Hh	total thickness of substratum	0.02	2000	m	10^{-5}
Hb	thickness of substratum located above the ductile layer	$0\text{-}7.5\cdot10^{-3}$	0- 750	m	10^{-5}
Hs	ductile layer thickness	$0\text{-}7.5\cdot10^{-3}$	0- 750	m	10^{-5}
β	cone slope	10°-30°	10°- 30°	/	1
Φ_I	angle of internal friction	35-40	30-40	/	~1
τ_I	cohesion of substratum	100	$2\cdot10^{7}$	Pa	$5\cdot10^{-6}$
g	gravitational acceleration	9.81	9.81	m s^{-2}	1
μ_S	ductile layer viscosity	10^{4}	$5\cdot10^{16}$	Pa s	$5\cdot10^{-13}$
t	time	65 min	1237 yr	/	10^{-7}
α	angle between the basal fault plane and the strike-slip component of movement	0°; 20°; 40°	0°; 20°; 40°	/	1
D_{EXC}	extensional component of movement of the basal fault plane	$1.8\text{-}3.5\cdot10^{-2}$	$1.8\text{-}3.5\cdot10^{3}$	m	10^{-5}
D_{CC}**	compressional component of movement of the basal fault plane	$-1.8\text{-}3.5\cdot10^{-2}$	$-1.8\text{-}3.5\cdot10^{3}$	m	10^{-5}
D_{SSC}	strike-slip component of movement of the basal fault plane	$4\cdot10^{-2}$	$4\cdot10^{3}$	m	10^{-5}

2.3. Experimental device

2.3.1. Model

The models comprise a faulted flat substratum overlain by a cone. The cone corresponds to the simplified shape of volcanoes. Hypovolcanic complexes and hydrothermal systems are not modelled. The flat substratum is the analogue of natural relief with the exception of slopping substrata, which are not modelled here. The fault movement is progressive and continuous throughout the experiment and earthquakes are not modelled.

The angle α corresponds to the angle that the experimental fault plane makes with the strike-slip component of movement. For convenience, the strike-slip component of movement is

oriented 090 and the extensional or compressional components of movement are oriented 000. The fault planes strike 090 (α=0°), 110 (α=20°) and 140 (α=40°). The movement is left-lateral and right-lateral when testing, respectively, transpressional and transtensional faults.

Many experiments (n=112) were conducted with ignimbrite powder and may be divided into three main sets, which are (1) transpressional, (2) transtensional and (3) strike-slip faults. The experiments conducted with transpressional and transtensional faults are subdivided into two subsets with 69% (α=20°) and 53% (α=40°) of strike-slip component of movement (D_{SSC}); the remaining component of movement is extension (D_{EXC}) or compression (D_{CC}) depending of the experiment. Each subset is again divided in two subsets for which the substratum may or may not contain a ductile layer.

The substratum has a constant thickness (Hh = 2 cm) and the models are faulted at a constant velocity (4 cm.hr^{-1}). The fault movement throughout the experiment is described by the amount of displacement parallel to the strike-slip component of movement (e.g. D_{SSC}). The cone height (4.4 to 9 cm), the cone slope (20° to 30°), the thickness of the ductile layer (0.2 to 0.75 cm) and of the brittle substratum on top of it (0 to 0.75 cm) are variables (cf. Appendix C). The intensity and velocity of the spreading depend on the cone height and slope (load) and on the thickness and depth of the ductile layer (Merle and Borgia 1996). The variables enable several spreading velocities to be tested in order to differentiate spreading related structures from regional fault related structures. The plot of figure 04 represents the cone steepness plotted against the ductile layer depth and thickness. It is used to differentiate "fast spreading" experiments for which the ratio Hb/Hs= 0 from "slow spreading" experiments for which Hb/Hs>0 (cf. table 01 for a definition of Hs and Hb).

2.3.2. Setup

Transtensional and transpressional faults have been previously modelled with different kind of experimental setups. Naylor et al. (1986) used two horizontal plates cut along a line parallel to the movement (strike-slip fault) to deform a sand box whose borders are compressed (transpression) or stretched (transtension). Wooller et al. (2003) used two independent plates which were able to move in the horizontal plane (strike-slip fault) and in the vertical plane to model extension or compression. It is difficult to determine the strike-slip component modelled when using the first setup. The second setup introduces a dip-slip

component of movement which is associated with asymmetrical deformation in the cone. The setup employed here is easier to handle and enables the amount of strike-slip movement to be varied precisely. It consists of two plates moving in the horizontal plane and whose border (fault plane) is oblique to the strike-slip component of movement. The fault plane forms an angle of 25° (transtensional experiments; Norini et al. 2008), 10° and 20° (transtensional and transpressional faults tests; Andrade 2009) and 20° and 40° (this study) with the strike-slip component of movement.
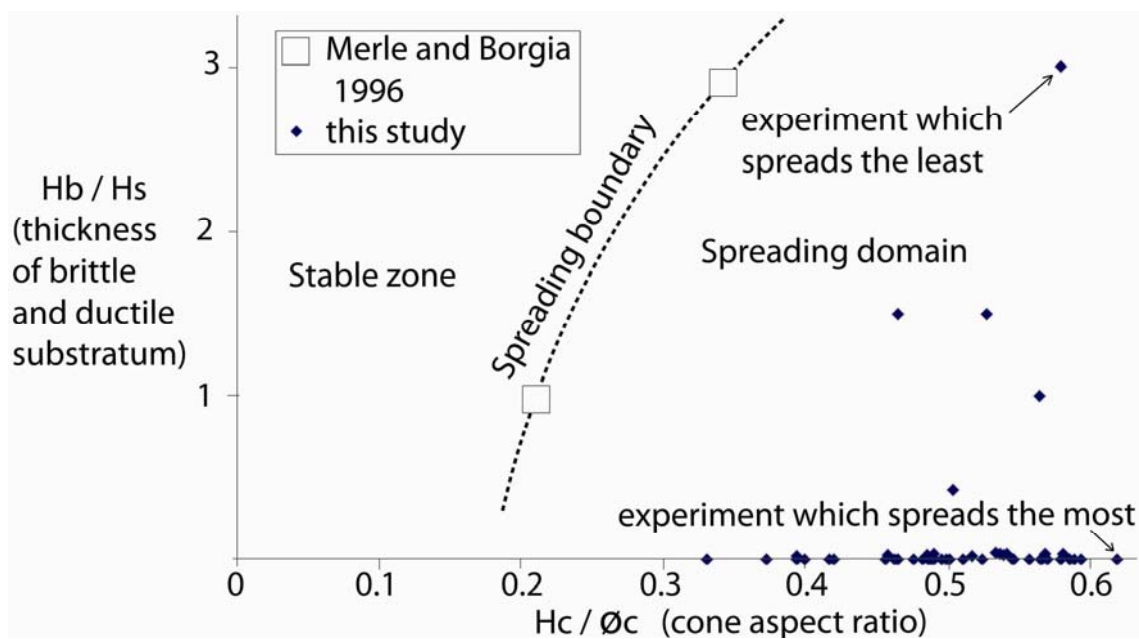
Figure 04: Plot of the experimental parameters of ductile substratum experiments; cf. table 01 for a definition of Hs and Hb (after Merle and Borgia 1996).

The models are made in a large box (69 cm and 94 cm in the N-S and E-W directions) to avoid border effects (figure 05). Two plastic plates cut along the 090 ($\alpha= 0°$), 110 ($\alpha= 20°$) or 140 ($\alpha= 40°$) directions are placed at the bottom of the box. Each plate is attached to a screw-jack connected to a motor, which is itself controlled by a computer. This system allows a continuous and constant displacement of plates at a velocity of 2 cm.hr^{-1} for each plate giving $D_{SSC} = 4$ cm.hr^{-1}. The transpressional and transtensional faults are modeled by moving the plastic plates toward or away the one from the other, respectively.

A 2 cm thick layer of ignimbrite powder which may contain a silicone layer is then placed in the box and the analogue cone is built on the middle of the box, on top of the contact between the plastic plates (figure 05). In subsequent experiments, an offset is introduced between the cone summit and the fault plane. A thin layer of ignimbrite powder is sieved on top of the experimental device to smooth the surface and black markers (grains of hematite) are dropped over it. The model is then deformed for 65 min. The surface deformation is recorded by vertical overhead photography. The pictures are taken every 2 min by time-lapse photography.
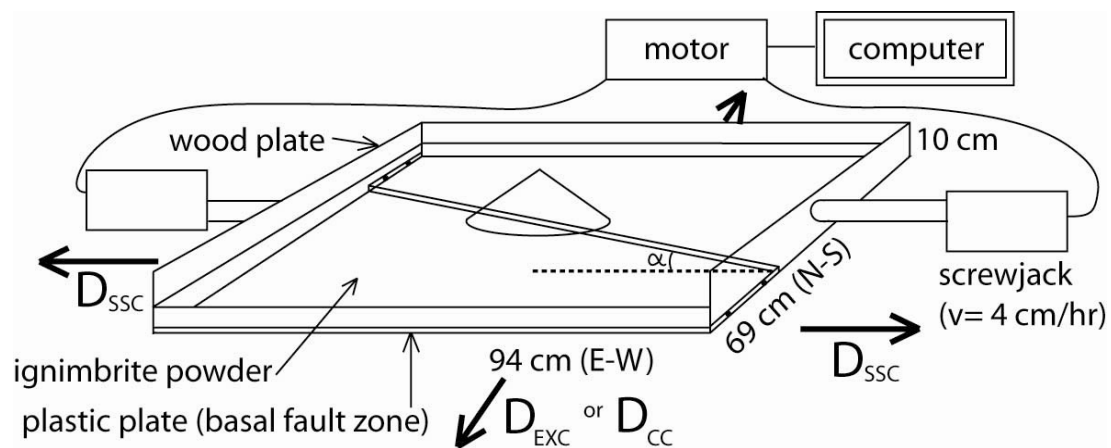
Figure 05: Experimental setup (see text for explanation)

The 11 sand experiments are similar to ignimbrite powder experiments except that ductile substratum is not used because it is not possible to cut an experiment that keeps spreading after the cessation of the plastic plate movements. The cone is made of several layers of dyed sand, which are used as reference horizons to quantify fault movements. At the end of the experiment the model is sprinkled with additional sand in order to preserve the structures that have developed at its surface. The model is then wet with soapy water and sliced in 10 to 15 cross-sections.

Cross-sections are used to quantify the dip-slip component of movement. To emphasise the faults and to simplify the observations the sand cones are larger ($Hc= 9$ cm) than the ignimbrite ones and the amount of strike-slip movement is equal (experiments F01 to F05) or twice greater than 4 cm (e.g. $D_{SSC}= 8$ cm; experiments F06 to F11). Three sets of experiment ($\alpha= 0°$, $20°$ and $40°$) were carried and cut normal to the fault plane, parallel to D_{EXC}- D_{CC} or parallel to D_{SSC}.

2.3.3. Analysis and dimensionless numbers

The cross-sections made from the sand experiments enable the fault dip and the amount of dip-slip movement to be quantified. The pictures of experiment surfaces are used to determine the kinematics of faults and to measure their strike (figure 06). A normal fault, for example, corresponds to a steep step in the granular material (figure 06-c). The horizontal displacements are quantified using Point Catcher code. This code works under Matlab software and was developed by M. James (Delcamp et al. 2008). It detects the black markers at the surface of the experiment and follows their displacement from one picture to another. The code produces several vector maps of the displacements which have occurred between successive shots. The amplitude of movement is represented by a contour map using Surfer software. The pictures of experiment surfaces and the displacement maps are presented by appendixes L to T.
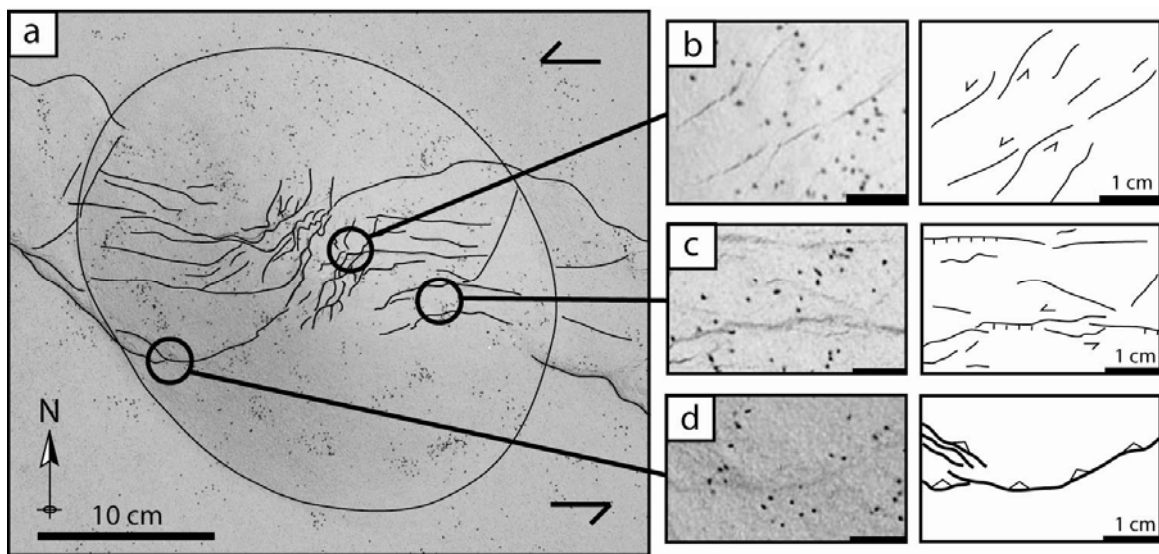
Figure 06: The kinematics of faults is deduced from the observation of the model surface. Experiment C12 (a) of this example contains sinistral strike-slip faults (b), transtensional faults (c) and transpressional faults (d).

The quantitative data obtained during the experiments are analysed with dimensionless numbers (table 02). The first number, $\Pi_{1\text{-FZ}}$, corresponds to the maximum thickness of the

fault zone in the cone normalised to the cone diameter. Then, the strike-slip (D_{SSC-C}) and the compressional (D_{CC-C}) or extensional (D_{EXC-C}) components of movement of each fault developing in the cone are measured. By convention, the compressional component of movement is expressed as a negative number. The $\Pi_{2-F\%}$ and $\Pi_{3-FC\%}$ numbers are a percentage of the D_{SSC}-D_{SSC-C} over D_{EXC}-D_{EXC-C} or D_{CC}-D_{CC-C}. The Π_{4-ECF} and Π_{5-SSF} numbers normalised the D_{SSC-C}, D_{EXC-C} or D_{CC-C} to the D_{SSC}, D_{EXC} or D_{CC} of the basal fault (table 02). The last number $\Pi_{6-offset}$ describes the cone offset (table 02).

Table 02: Dimensionless numbers

Π	Number	Description
Π_{1-FZ}	width fault zone / $\varnothing_C$	width of the fault zone normalised to the cone diameter (dimensionless fault width)
$\Pi_{2-F\%}$	(D_{EXC} or D_{CC} / D_{SSC})**.**100 (D_{SSC} / D_{EXC} or D_{CC})**.**100	Percentage of extension or compression versus the strike-slip component of movement; basal fault (dimensionless regional obliquity)
$\Pi_{3-FC\%}$	(D_{EXC-C} or D_{CC-C} / D_{SSC-C})**.**100 (D_{SSC-C} / D_{EXC-C} or D_{CC-C})**.**100	Idem for the faults developing in the cone (dimensionless edifice obliquity)
Π_{4-ECF}	|D_{EXC-C} or D_{CC-C} / D_{EXC} or D_{CC}|	Extensional or compressional components of movement of cone faults normalised to the basal fault components of movement (dimensionless cone to base normal ratio)
Π_{5-SSF}	D_{SSC-C} / D_{SSC}	Idem for the strike-slip component of movement (dimensionless cone to base strike-slip ratio)
$\Pi_{6-offset}$	offset / $\varnothing_C$	Distance between the basal fault zone and the cone summit normalised to the cone diameter

3. Results

3.1. Strike-slip faults

This section describes the structures formed in a cone sheared by a sinistral strike-slip fault. Note that structures related to dextral strike-slip fault movement are similar but rotated 90° from these presented in this section. The 8 strike-slip fault experiments have two variables, which are the cone slope (20° to 30°) and the rheology of the substratum (partially ductile or entirely brittle). The experimental basal fault has a sinistral sense of motion. Complementary description of these experiments is presented by appendixes L and M.

3.1.1. Brittle substratum experiments:

The results of brittle substratum experiments are presented in table 03, figure 07 and appendix L. In these experiments, the Sigmoid-I structure is a curved transpressional faults, which turn into a transtensional fault zone at the cone summit (table 03, figure 07-a). The strike-slip component of Sigmoid-I structure and of the basal fault zone are equal (e.g. $D_{SSC-C} = D_{SSC} = 2$ cm.hr^{-1}, appendix D). The direction of movement inverts along Sigmoid-I. This structure concentrates the slowest horizontal movements observed on deformation field maps (figure 07-b) and corresponds to the main fault zone. Sigmoid-II structures are transtensional faults. They border a graben which encompasses the summit and the fastest horizontal movements (2.4 cm.hr^{-1}) observed (figure 07-b). Along the Sigmoid-II structure, the vectors are directed in about the same direction, but the amplitude of those located closer to the summit is greater (figure 07-b). Sigmoid-II has thus a dextral sense of motion (table 03).

Table 03: Description of structures formed in cones located over brittle substratum; *slip of basal plastic plates in the E-W direction; **percentage of compressional and extensional movements accommodated by faults formed in the cone; ***The fault zone is 5 cm thick ($\Pi_{1-FZ} = 0.2$); TT and TP stand for transtensional and transpressional faults.

D_{SSC}* (mm)	Fault name	Strike	location	description	$\Pi_{3-FC\%}$** (%)
10-12	early structures	030-035	summit	Sinistral TT	/
> 15	Sigmoid-I	065-075	WSW and ENE cone flanks	Sinistral TP	$D_{CC-C} = 35$
> 15	Sigmoid-I	045-055	summit	Sinistral TT,graben	$D_{EXC-C} = 30$
> 15	Sigmoid-II	030-040	ESE and WSW of summit	Dextral TT, graben	$D_{EXC-C} = 25$
> 15	Fractures	035; 070; 105	E and W of Sigmoid-II; cone lower flanks	Tens of fractures	/
40	Fault Zone***	090; 060 (curved)	cone	slow horizontal movements	/
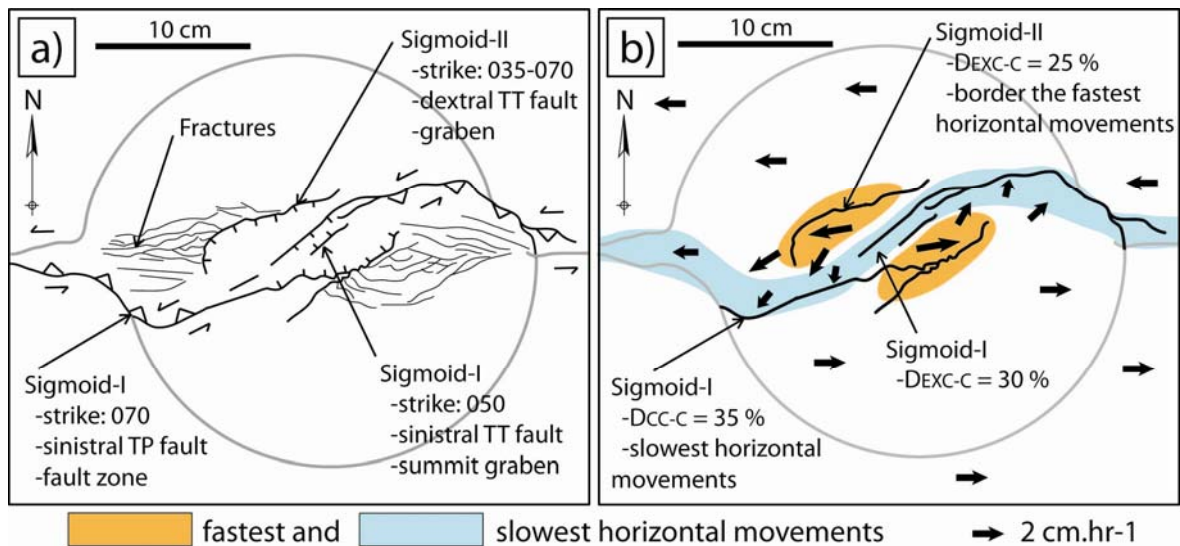
Figure 07: Strike-slip and brittle substratum experiments; a) sketch of sheared cone at the end of experiment E08; b) sketch map of amplitude and direction of horizontal movements; TT and TP stand for transtensional and transpressional faults.
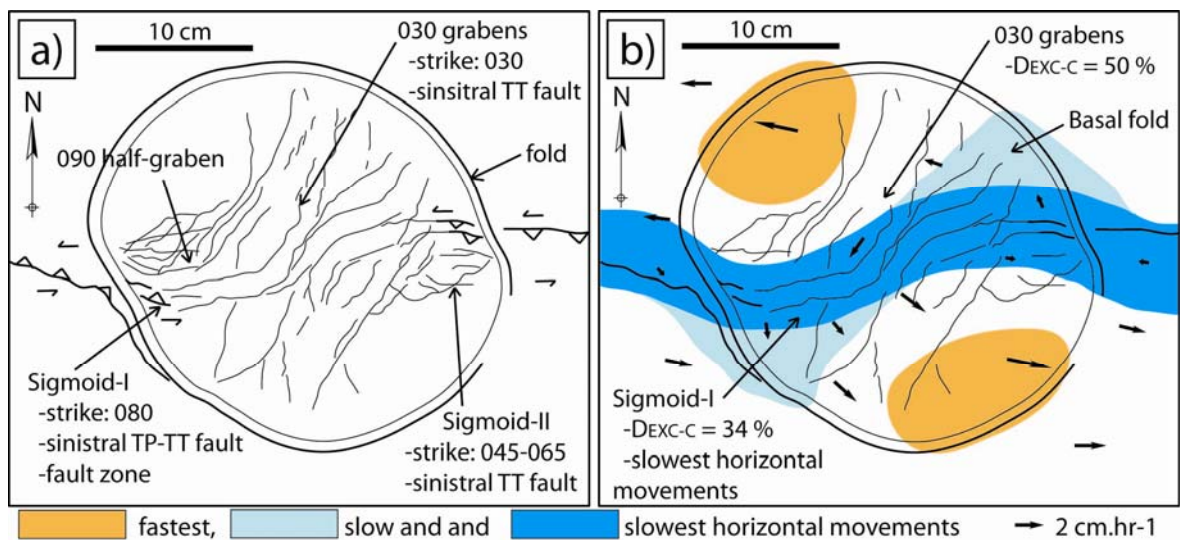
Figure 08: Strike-slip and ductile substratum experiments; a) sketch of sheared cone at the end of experiment E05; b) sketch map of amplitude and direction of horizontal movements; TT and TP stand for transtensional and transpressional faults.

3.1.2. Ductile substratum experiments:

The results of ductile substratum experiments are presented in table 04, figure 08 and appendix M. In these experiments, Sigmoid-I is a sinistral transtensional fault zone made of several parallel faults (figure 08-a). This structure is otherwise similar to the Sigmoid-I fault of brittle substratum experiments, as it mainly accommodates strike-slip motion and corresponds to the main fault zone (table 04). The slow horizontal movements which encompass Sigmoid-I structure extend at the NE and SW base of the cone, where Sigmoid-I accommodates compression (figure 08-b). The Sigmoid-II structure is similar to that of brittle substratum experiments and border, with Sigmoid-I, two shallow 090 striking half-grabens located E and W of the summit. Several additional shallow 030 elongated grabens (figure 08-a, table 04) are observed in the summit area. The fastest horizontal movements (2.6 $cm.hr^{-1}$) are observed over the NW and SE cone flanks, where the spreading movements and the basal plastic plate movements have the same direction and summed (figure 08-b).

**Table 04: Description of structures formed in cones located over ductile substratum**; *slip of basal plastic plate in the E-W direction; **percentage of compressional, extensional and strike-slip movements accommodated by faults formed in the cone; TT and TP stand for transtensional and transpressional faults.

D_{SSC}* (mm)	Fault name	Strike	location	description	$\Pi_{3\text{-}FC\%}$** (%)
5	Early structures	030-050	summit	Sinistral TT	/
> 5	030 elongated graben	020-030; 050-060	summit and flanks	Sinistral TT, graben	$D_{EXC\text{-}C}$ = 50
> 10	Sigmoid-I	-075-090 -100	-SE-NW flanks -Cone base	-Sinistral TT -Sinistral TP	$D_{EXC\text{-}C}$ = 34
> 10	Sigmoid-II	050-070	E and W of summit	Sinistral TT, graben	/
> 10	090 half-grabens	090	E and W cone flanks	Graben bordered by Sigmoid-I and II	/
40	Fault Zone	080; 060 (curved)	cone	slow horizontal movements	/

3.2. Transpressional faults

This section describes four experimental setups characterized by the following parameters: α is equal to 20° or 40° and the substratum is brittle or partially ductile. The 55 experiments presented here have other variables such as the cone slope (20° to 30°), the cone height (4 to 7 cm) and the thickness of the ductile substratum (0.2 to 0.75 cm). The experimental basal fault has a sinistral sense of motion. This section presents the observations made at the surface of the experiments and the displacement maps. A more detailed description of these experiments is presented by appendixes N, O and P.

3.2.1. Brittle substratum experiments

The results of brittle substratum experiments are presented in table 05 and figure 09. The Sigmoid-I structure of brittle transpressional experiments is similar to that of brittle strike-slip fault experiments: it is a curved transpressional structure, which accommodates most of the strike-slip movements and which is transtensional and border a shallow graben at the cone summit (table 05, figure 09-a). This summit graben is elongated 030 (α=20°) and 070 (α=40°). The Sigmoid-II structure, on the other hand, is made of several parallel sinistral transtensional faults, which accommodate a limited amount of slip and form progressively throughout the experiment (table 05, figure 09-a).

At the cone summit, the early formed faults rotate 5-10° anticlockwise throughout the experiment (table 05). Inside the straight area of slow horizontal movements, the slowest movements are rotated anticlockwise as they progressively encompass the Sigmoid-I structure (cf. figure 02 of appendix N). The fastest horizontal movements observed over the northern and southern cone flanks do not rotate and have the same amplitude than the basal plastic plate movements (e.g. $D_{SSC-C-max} = D_{SSC} = 2$ cm.hr^{-1}, figure 09-b).

The strike of faults and the thickness of the fault zone are the same for all the cone slopes (10° to 30) and sizes (height and diameter) tested. The amplitude of fault movements increases throughout the experiments while the relative amount of extension, compression and strike-slip movements accommodated by these faults ($\Pi_{3-FC\%}$ number) does not vary (cf. table 02 of appendix P).

Table 05: **Description of structures formed in brittle substratum experiments**; *slip of basal plastic plate in the E-W direction; **percentage of compressional, extensional and strike-slip movements accommodated by faults formed in the cone; ***The fault zone is 6.8-8 cm (Π_{1-FZ} = 0.25-0.32, α=20°) and 7.6-9 cm (Π_{1-FZ} = 0.28-0.35, α=40°) thick; TT and TP stand for transtensional and transpressional faults.

D_{SSC}* (mm)	Fault name	α	Strike	location	description	$\Pi_{3-FC\%}$** (%)
10-12	early structures	-20° -40°	-035-055 -070	summit	Sinistral TT	/
>10-12	Rotated early structures	-20° -40°	-035-040 -065-070	summit	Sinistral TT	/
> 12	Sigmoid-II (~ 10 faults)	-20° -40°	-100-115 -090-120	WNW and ESE cone flanks	Sinistral TT (curved)	-D_{EXC-C} = 17 -D_{EXC-C} = 47
25	Sigmoid-I (summit)	-20° -40°	-025-040 -070	Summit	Sinistral TT (curved)	-D_{EXC-C} = 25 -D_{EXC-C} = 30
25	Sigmoid-I (cone flanks)	-20° -40°	-095-105 -095-105	WSW and ENE cone flanks	Sinistral TP (curved)	-D_{EXC-C} = 35 -D_{EXC-C} = 50
40	Fault Zone***	-20° -40°	-073 -090	cone	Slow horizontal movements	/
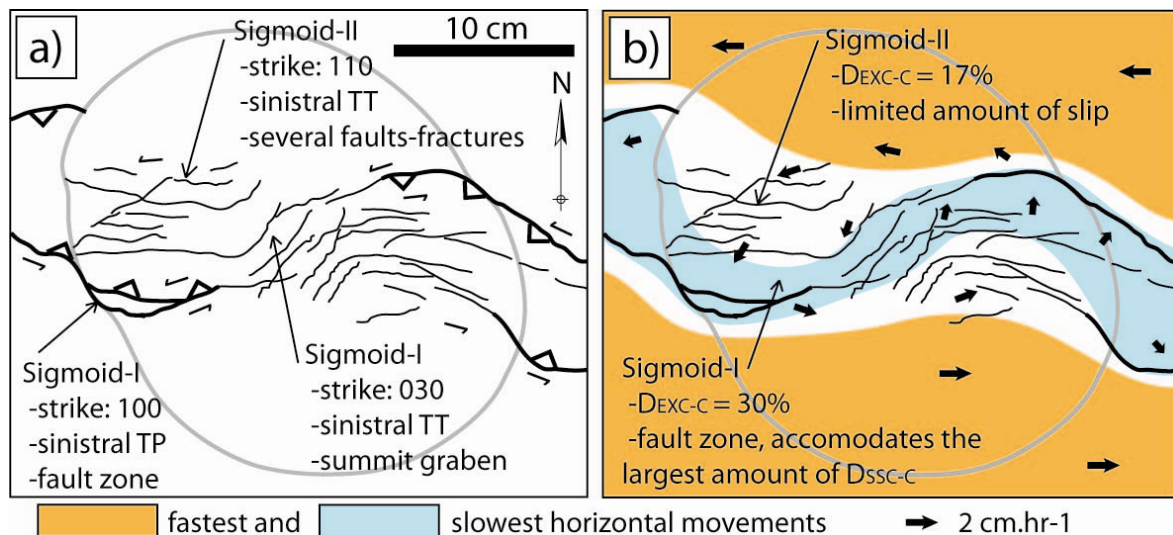
Figure 09: Transpressional and brittle substratum experiments (α=20°); a) sketch of sheared cone at the end of experiment C10; b) sketch map of amplitude and direction of horizontal movements; TT and TP stand for transtensional and transpressional faults.

3.2.2. Ductile substratum experiments

The results of ductile substratum experiments are presented in table 06 and figure 10. In the first minutes of experiment (D_{SSC} < 10 mm), the cone flanks moves fast, the summit moves slowly and the substratum velocity is negligible: the cone spreads. Then, spreading related half-grabens develop over the N and S lower cone flanks (cf. fast spreading experiments, figure 10-a).

Table 06: Description of structures formed in ductile substratum experiments; *slip of basal plastic plate in the E-W direction; **percentage of compressional, extensional and strike-slip movements accommodated by faults formed in the cone; TT and TP stand for transtensional and transpressional faults.

D_{SSC}* (mm)	Fault name	α	Strike	location	description	$\Pi_{3\text{-}FC\%}$** (%)
5-10	early structures	-20° -40°	-050-070 -040-060	summit	Sinistral and dextral TT	/
>10	One to 3 grabens	-20° -40°	-040-045 -060-070	Summit and NE-SW flanks	Sinistral and dextral TT	-D_{EXC-C} = 38 -D_{EXC-C} = 42
> 12-15	Sigmoid-I	-20° -40°	-090-100 -100-120	WSW and ENE cone flanks	Sinistral TT (curved)	/
25	Sigmoid-II	-20° -40°	-110-125 -115-125	WNW and ESE cone flanks	Sinistral TT (curved)	/
25	half-grabens	20° 40°	100	E and W cone flanks	Graben bordered by Sigmoid-I and II	-D_{EXC-C} = 28 -D_{EXC-C} = 42
40	Fault Zone	-20° -40°	-073 -090	cone	slow horizontal movements	/

For D_{SSC} > 10 mm, a 070 striking linear area of slow horizontal movement develops in the cone. Inside this area, the slowest movements rotate anticlockwise to progressively encompass the Sigmoid-I structure (cf. figure 02 of appendix O).

The Sigmoid-I and II transtensional faults border 2 shallow half-grabens, elongated in the 100 direction and located E and W of the summit (figure 10-a). The movements invert along these grabens, which accommodate mainly strike-slip movements (table 06, figure 10-b).

In the meantime, the structures formed at the cone summit from D_{SSC} > 10 mm progressively multiply and elongate to form 1 to 3 overlapping shallow grabens elongated 040 (α=20°) and

060-070 (α=40°; figure 10-a). The fastest horizontal movements are located on each side of these grabens, over the cone NW and SE flanks (figure 10-b).

The amplitude of fault movement increases throughout the experiments and is larger for fast spreading experiments. The relative amount of extension, compression and strike-slip movements accommodated by the faults ($\Pi_{3\text{-FC\%}}$ number) and the geometry of faults did not vary when the spreading velocity varies (cf. tables of appendix H).
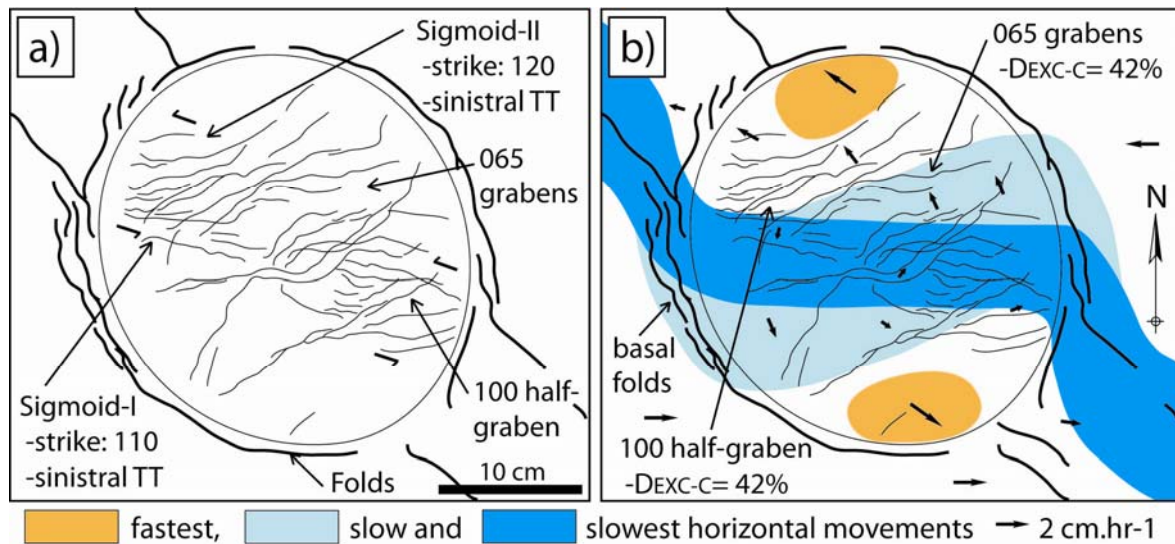
Figure 10: Transpressional and ductile substratum experiments (α=40°); a) sketch of sheared cone at the end of experiment D12; b) sketch map of amplitude and direction of horizontal movements; TT stands for transtensional fault.

3.3. Transtensional faults

This section describes four different experimental setups characterized by the following parameters: α= 20° or 40° and the substratum is brittle or partially ductile. The 25 experiments have other variables such as the cone slope (20° to 30°), the cone height (4 to 7 cm) and the thickness of the ductile substratum (0.2 to 0.75 cm). The experimental basal fault has a dextral sense of motion. This section presents the observations made at the surface of the experiments and the displacement maps. Complementary description of these experiments is presented in appendixes Q, R and S.

3.3.1. Brittle substratum experiments

The results of brittle substratum experiments are presented in table 07 and figure 11. The Sigmoid-I and II structures form in the early stages of the experiments, when $D_{SSC} > 10$ mm (tables 07). These curved transtensional structures accommodate all the fault movements is the cone. They border a deep graben, which corresponds to the cone fault zone (figure 11-a). At the cone summit, a graben elongated 145 ($\alpha= 20°$) and 160 ($\alpha= 40°$) develops inside the fault zone. Several half-grabens bordered by curved N-S striking normal faults develop E and W of the summit and are connected to Sigmoid-I and II on each sides of the fault zone (figure 11-a).

Sigmoid-I accommodates mostly strike-slip movements ($D_{SSF-C} = 80\%$) as well as a limited amount of compression at the cone base (table 07, figure 11-b). The fastest horizontal movements are observed inside the fault zone and are accommodated by the antithetic Sigmoid-II structure (figure 11-b). The matter is rotated clockwise inside the fault zone.

The thickness of the fault zone, the faults strike and the amplitude and direction of movements are the same for all the size and cone shape tested.

Table 07: Description of structures formed in brittle substratum experiments; *slip of basal plastic plate in the E-W direction; **percentage of compressional, extensional and strike-slip movements accommodated by faults formed in the cone; ***The fault zone is 7-7.7 cm ($\Pi_{1-FZ} = 0.27$, $\alpha=20°$) and 7.5-11 cm ($\Pi_{1-FZ} = 0.29-0.41$, $\alpha=40°$) thick; TT and TP stand for transtensional and transpressional faults.

D_{SSC}* (mm)	Fault name	α	Strike	location	description	$\Pi_{3-FC\%}$** (%)
>10	Sigmoid-I (summit)	-20° -40°	-145 -160	summit	Dextral TT	-D_{EXC-C} = 25 -D_{EXC-C} = 26
>10	Sigmoid-I (cone flanks)	-20° -40°	-100 -120	WNW and ESE cone flanks	Dextral TT	-D_{EXC-C} = 19 -D_{EXC-C} = 20
>10	Sigmoid-II	-20° -40°	-110 -130	WSW and ENE cone flanks	Sinistral TT (curved)	-D_{EXC-C} = 75 -D_{EXC-C} = 70
>10	Fault Zone***	-20° -40°	-122 -135	Bordered by Sigmoid-I and II	Slow horizontal movements	/
>15	Half-grabens	20° 40°	140-170-030	Inside fault zone	Curved normal faults	/
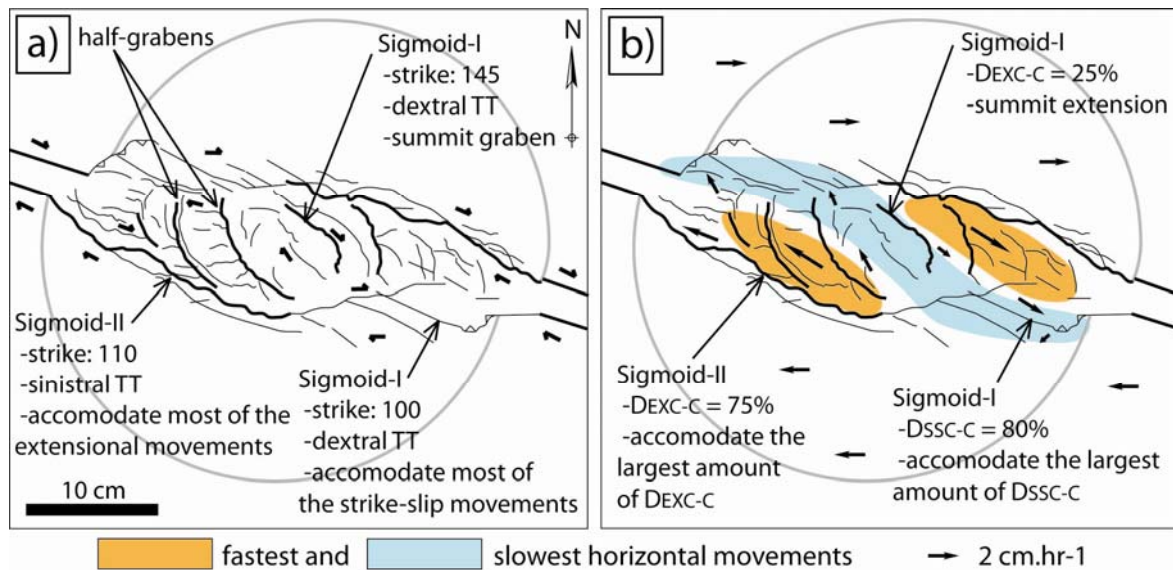
Figure 11: Transtensional and brittle substratum experiments (α=20°); a) sketch of sheared cone at the end of experiment C23; b) sketch map of amplitude and direction of horizontal movements; TT stands for transtensional fault.

3.3.2. Ductile substratum experiments

The results of ductile substratum experiments are presented in table 08 and figure 12. In these experiments, Sigmoid-I and II structures are similar to those of brittle substratum experiments: the Sigmoid structures border a deep graben, which corresponds to the fault zone (figure 12-a). The Sigmoid-I structure is made of 3 to 5 parallel faults, which form throughout the experiment and progressively enlarges the fault zone. The cone summit subsides in a 160 (α= 20°) and 170 (α= 40°) elongated graben (figure 12-a, table 08). The N-S striking half-grabens formed inside the fault zone are progressively disconnected from Sigmoid-I structure as the fault zone enlarges (figure 12-a). The half-grabens of the N and S cone flanks and the fold formed at the cone base are spreading related structures (figure 12-a).

The slowest horizontal movements encompass Sigmoid-I structure. The fastest horizontal movements encompass Sigmoid-II and the NE and SW cone flanks, where the direction of the basal plastic plates and spreading related movements is identical (figure 12-b). The percentage of extension and compression accommodated by Sigmoid-I and II is similar to those measured in brittle substratum experiments, but the amount of slip accommodated by ductile substratum experiments faults is larger (table 08).

Table 08: **Description of structures formed in ductile substratum experiments**; *slip of basal plastic plate in the E-W direction; **percentage of compressional, extensional and strike-slip movements accommodated by faults formed in the cone; ***The fault zone is 7-7.5 cm (Π_{1-FZ} = 0.29, α=20°) and 9 cm (Π_{1-FZ} = 0.36, α=40°) thick; TT and TP stand for transtensional and transpressional faults.

D_{SSC}* (mm)	Fault name	α	Strike	location	description	$\Pi_{3-FC\%}$** (%)
5-10	early structures	20° 40°	170-020	E and W of summit	Curved normal faults	/
12	Sigmoid-I (summit)	-20° -40°	-160 -170	summit	6 to 10 curved dextral TT faults	-D_{EXC-C} = 50 -D_{EXC-C} = 59
12	Sigmoid-I (cone flanks)	-20° -40°	-100-110 -120	WNW and ESE cone flanks	Dextral TT (curved)	-D_{EXC-C} = 30 -D_{EXC-C} = 33
12	Sigmoid-II	-20° -40°	-100 -130	WSW and ENE cone flanks	Dextral TT (curved)	-D_{EXC-C} = 71 -D_{EXC-C} = 68
12	Fault Zone***	-20° -40°	-120 -135	Bordered by Sigmoid-I and II	Slow horizontal movements	/
12	Half-grabens	-20° -40°	150-000- 050	Inside fault zone	Curved normal faults	/
12-18	Spreading related grabens	20° 40°	several	N and S lower cone flanks	Normal and TT faults	/

Figure 12: Transtensional and ductile substratum experiments (α=20°); a) sketch of sheared cone at the end of experiment C35; b) sketch map of amplitude and direction of horizontal movements; TT stands for transtensional fault.
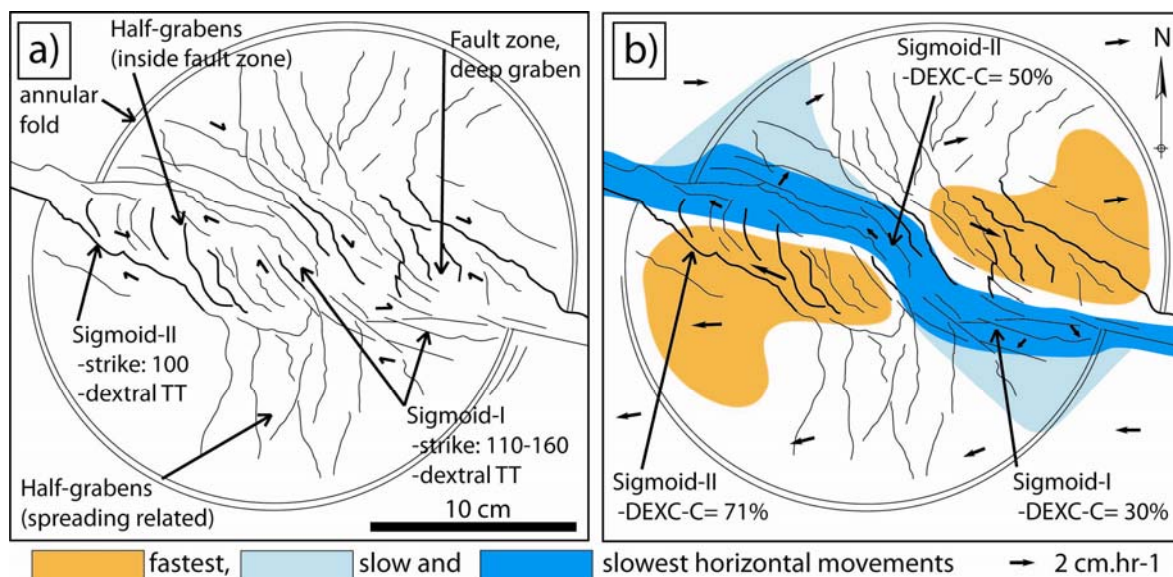
3.4. Cross-sections of transpressional and transtensional experiments

The 6 experiments presented in this section are transpressional and transtensional brittle substratum experiments. These sand cones were cross-cut normal to the fault plane and parallel to D_{EXC} and D_{SSC}. The experimental parameters are the following: $\alpha=20°$, Hc= 8-9 cm and D_{SSC}= 4cm and 8cm at the end of the experiment.

3.4.1. Cross-sections of transpressional and brittle substratum experiments

The cross-sections of transpressional experiments reveal that the Sigmoid-I and II structures dip 50° toward the core of the cone. Sigmoid-I faults accommodate about 1 cm of reverse dip-slip motion (table 09).

The cross-sections show that the material is asymmetrically uplifted in the cone (figure 13-a). The Sigmoid-I faults border the base of the extruded material, which is topped by several Sigmoid-II faults characterized by a small amount of dip-slip and a limited vertical extent (table 09; figure 13-b, c, d). Sigmoid-II faults develop at the back of the uplift to accommodate the depression left behind the extruded material.

The uplifted material has been mapped using the profiles (figure 13-a). This uplift has limited amplitude in the substratum where it is parallel to the basal fault zone. In the cone, it is set at about 10°-20° anticlockwise from the basal fault zone and develops at the back of the transpressional part of Sigmoid-I faults. Ideally, this uplift would be symmetrical at the summit of the cone and topped by a graben. However, it is observed that the material is extruded preferentially N or S of the summit graben, depending of the experiment (figure 13-c). This unstable structure introduces asymmetry in the cone.

The F10 experiment cross-sections show that the material is uplifted toward the inside of the cone (figure 13-f). The reconstructions made out of the profiles show that the material is moved in the WNW-ESE to NW-SE direction, toward the cone summit area (e.g. figure 13-a).

Table 09: Dip angle and amount of dip-slip motion of faults estimated from the measure of the apparent dip and dip-slip of faults on 000, 020 and 090 oriented profiles.

	Sigmoid-I			Sigmoid-II	Half grabens
	substratum	cone upper flanks	cone summit	cone	fault zone
Transpressional and brittle substratum experiments (n=3)					
dip angle	10-15°	50°	45-55°	50-62°	/
dip-slip (cm)	0.1-0.3	0.6-1.3	1-1.5	0.2-0.5	/
Transtensional and brittle substratum experiments (n=3)					
dip angle	/	65°-75°	60°	50-65°	65-75°
dip-slip (cm)	/	0.5-1	0.2-0.6	1.6-2	0.5-0.8
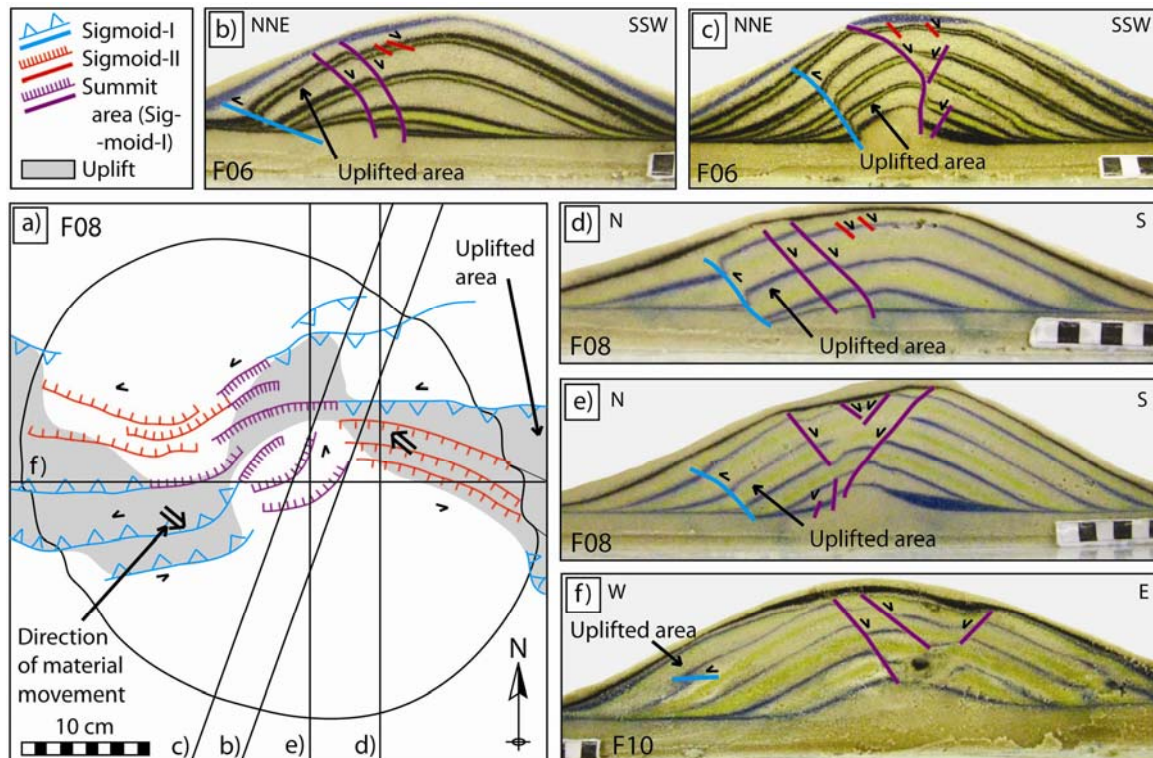
Figure 13: Sketch and pictures of cross-cut sand experiments; a) structural map of experiment F08; b-c) experiment F06 cut normal to the basal fault plane; d-e) experiment F08 cut along N-S profiles; f) experiment F10 cut along E-W profiles.

3.4.2. Cross-Sections of transtensional and brittle substratum experiments:

The cross-sections of transtensional and brittle substratum experiments are presented by figure 14. The profiles indicate that the Sigmoid-I fault dip 60-70° toward the cone core and accommodates a limited amount of dip-slip motion (figure 14-b; table 09). The spacing between the dyed horizons varies on each side of Sigmoid-I, indicating that this fault accommodates a large amount of strike-slip displacement (figure 14-b, c, d).
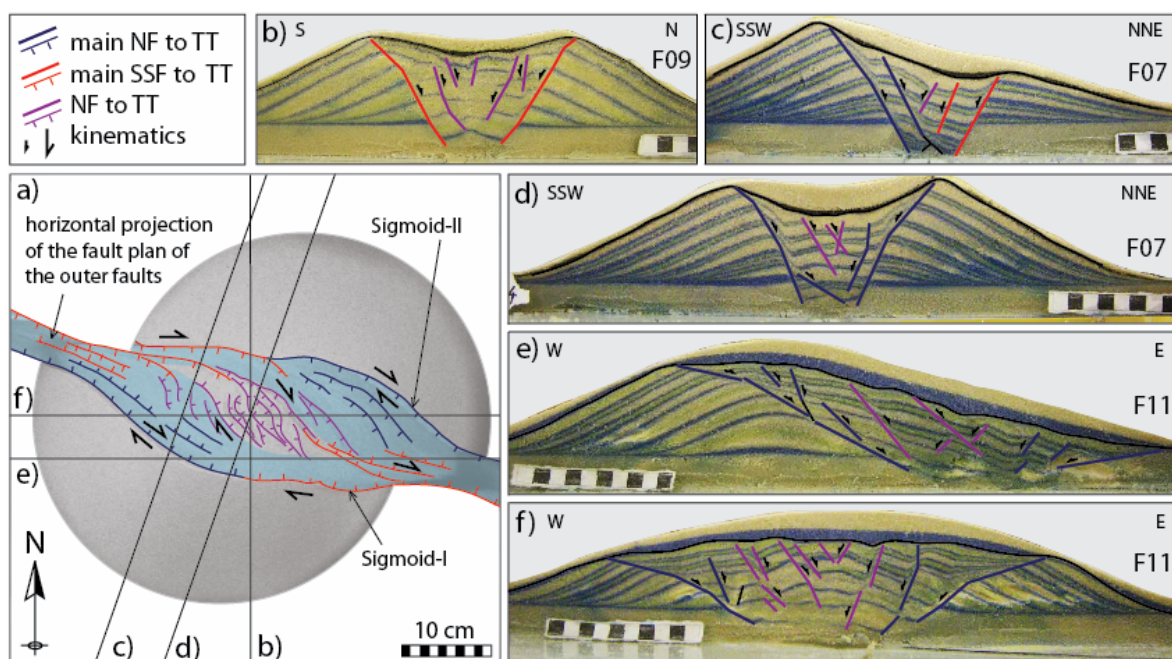
Figure 14: Sketch and pictures of sand experiments; a) structural map of experiment F11; b) N-S profile of experiment F09; c-d) experiment F07 cut along lines perpendicular to the basal fault plane; e-f) E-W profiles of experiment F11. TT, SSF and NF stand respectively, for transtensional, strike-slip and normal faults.

Sigmoid-II is a broad 60° dipping fault zone made of two parallel and closely spaced normal faults. The large dip-slip component of this structure equals the thickness of the substratum. Identical values of dip and dip-slip are measured in each experiment, whatever the amount of horizontal slip applied to the sand cone (e.g. D_{SSC-C}= 4 or 8 cm at the end of the experiment).

The normal dip-slip movements are mostly accommodated by Sigmoid-II, by the half-grabens located inside the fault zone delimited by Sigmoid-I and II faults and, to a lesser extend, by Sigmoid-I structure.

The faults planes have been projected on the horizontal plane (e.g. the blue area of figure 14-a). The fault plane of Sigmoid-II structure is shallower and has thus a broader horizontal extent than the Sigmoid-I one. Sigmoid-I and II fault planes border a subsiding area in which the cone base is in contact with the experimental plastic box (figure 14-b-f).

The apparent dip of dyed horizons is measured on each 000 and 020 orientated profiles and mapped. Outside the fault zone, the apparent dip of un-deformed horizons is shallow on the flanks and steeper at the summit (3° to 28° measured, figure 14-b-f). The horizons located inside the fault zone are 5° to 15° steeper than the surrounding un-deformed horizons (figure 14-d, c, d) and they have likely been rotated. According to the general movement of faults (dextral) this rotation, which is confined to the fault zone area, is likely to be clockwise.

3.5. An offset between the fault and the cone summit: "Offset" experiments

3.5.1. Introduction

In this section, the cone is shifted from the fault zone. The offset corresponds to the distance between the basal fault zone and the cone summit over an horizontal line perpendicular to the fault zone. The offset is 1 and 5 cm (e.g. $\Pi_{6\text{-offset}}= 0.04\text{-}0.2$). The bulk of setups described in previous sections are reproduced here and a total of 24 experiments have been preformed for this section.

The experiments of this section are described in terms of their differences with the experiments described previously. The cone is divided in two parts by the fault zone: a) part A, which is the largest area and comprises the cone summit (southern part of the cone); b) part B, which is smaller (northern part of the cone). The faults bordering part A and part B are called, respectively, part A-Sigmoid-I and II and part B-Sigmoid-I and II.

3.5.2. Strike-slip, transpressional and transtensional experiments

A cone located above a brittle substratum sheared by a strike-slip fault has poorly developed part A-Sigmoid-I faults (figure 15-a). Part-A-Sigmoid-II, in contrast, is elongated from the summit to the base of the cone and is associated with a large dip-slip component of movement. On the part B side, the Sigmoid-I transpressional fault is well developed and extends toward the cone base. Part B-Sigmoid-II is poorly developed and consists of en-echelon normal faults with a limited extend. The fault zone is wider where it is delimited by part A-Sigmoid-II and part B-Sigmoid-I.

The cones located in the vicinity of 20°-transpressional faults develop similar structures (figure 15-b). Part-A Sigmoid-II fault consists of several parallel transtensional faults dipping out from the fault zone and bordered by a transtensional fault dipping toward the fault zone and restricted to the summit area. Part B-Sigmoid-I consists of several transpressional faults extending from the fault zone to the cone base. The remaining structures are poorly developed or missing (e.g. part B-Sigmoid-II). The same cone sheared by a 40°-transpressional fault develops only a part A-Sigmoid-II fault and a summit graben. A reverse fault develops at the base of the part B, especially on the side where Part B-Sigmoid-I is expected to develop.

In the 20° and 40°-transtensional experiments, the widest portion of the fault zone is bordered by a part B-Sigmoid-I fault, which is transpressional at the cone base, and by part A-Sigmoid-II fault, which has a large dip-slip component of movement (figure 15-c). This part of the fault zone contains several half-grabens delimited by normal faults, which are perpendicular to the fault zone and dip toward the cone summit. On the other side of the cone, part B-Sigmoid-II is located in the lower cone flank and part A-Sigmoid-I is transpressional over a limited area (1-2 cm long) at the base of the cone. These faults border a thinner fault zone which contains strike-slip faults corresponding to the curved part of the Sigmoid-I structure. Note that this curved portion of Sigmoid-I is located over the cone upper flank, while it is located at the cone summit in previous experiments (e.g. previous sections).

For the bulk of brittle substratum experiments, the fastest horizontal movements are located inside the fault zone and are bordered by part A-Sigmoid-II fault (cf. figure of appendix L). On the opposite side, along part B-Sigmoid-II fault, fast horizontal movements are not observed. Sigmoid-I is always a transpressional fault with a large strike-slip component of

movement (cf. table of appendix L). The part A-Sigmoid-II and part B-Sigmoid-I faults accommodate the largest amount of movement, which are greater when $\Pi_{6\text{-offset}}$ increases.

Similar structures are observed when a ductile substratum is added to the experimental setup. Part B-Sigmoid-I faults are better expressed and develop over the cone lower flank, which is bordered, in the substratum, by a reverse fault. Part A-Sigmoid-II faults border radial grabens (strike-slip and transtensional experiments; figure 15-d) or are missing (transpressional experiments; figure 15-e).

The strike of the faults are measured for brittle experiments deformed by strike-slip movement, 20°-transtensional and 20°-transpressional faults (n=186). These values are identical, within a 10° error, to the strike of faults described in previous sections.
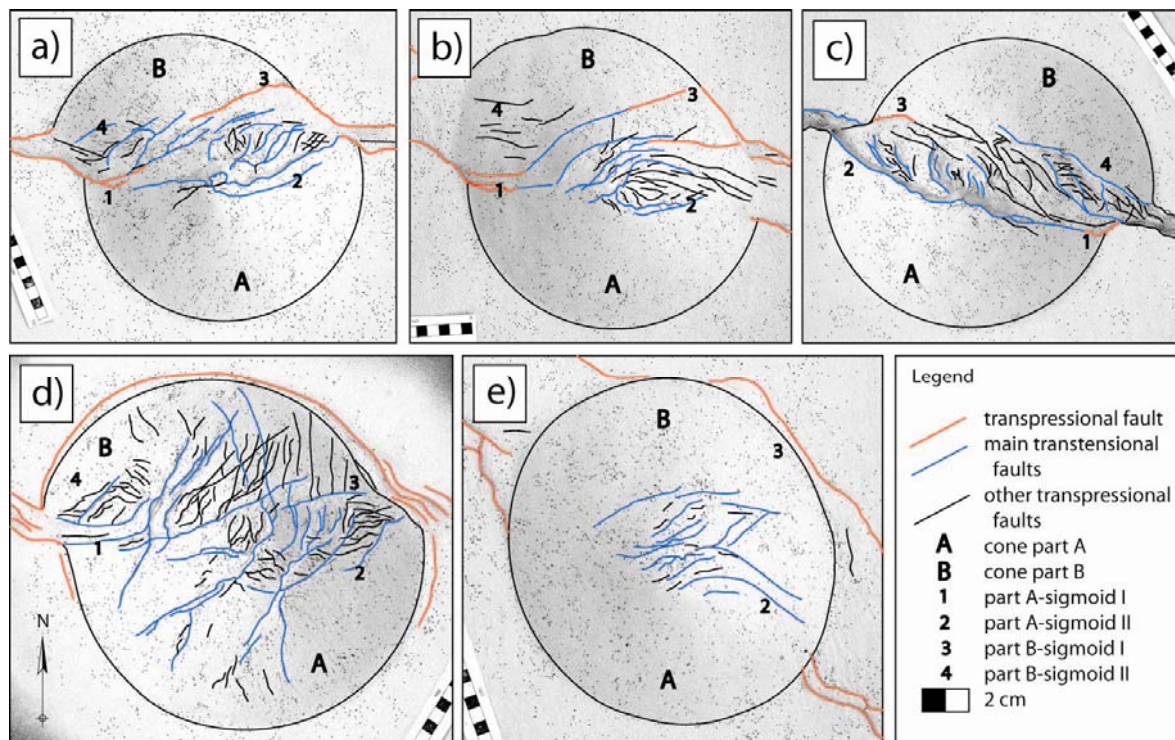
Figure 15: Pictures made at the end of the experiments; a) E10 (sinistral strike-slip fault, $\Pi_{6\text{-offset}}$= 0.13); b) C42 (sinistral transpressional fault, a=20°, $\Pi_{6\text{-offset}}$= 0.19); c) C49 (dextral transtensional fault, a=20°, $\Pi_{6\text{-offset}}$= 0.06); d) E11 (sinistral strike-slip fault, ductile substratum, $\Pi_{6\text{-offset}}$= 0.11); e) D22 (sinistral transpressional fault, ductile substratum, a=40°, $\Pi_{6\text{-offset}}$= 0.15).

4. Discussion

4.1. Analogue models

4.1.1. Fault geometry

One of the most important results concerns the location, kinematics and strike of faults that have developed in the cones. The synthetic Sigmoid-I fault, which is observed in strike-slip experiments, is transpressional along most of its length and transtensional at the cone summit (figure 16), where it borders the summit subsidence. Sigmoid-I fault is an area of slow horizontal movements (cf. displacement maps of appendix D to L) for two reasons: 1) it accommodates a large amount of vertical movements and 2) it is a major strike-slip fault along which movements are reversed and are equal to zero along the fault plane.

The profiles obtained from transpressional experiments indicate that most movement is organised around an uplift which is parallel to the basal fault zone in the early stage of the experiment. The uplifted area then rotates anticlockwise. Once the deformation is sufficient, the synthetic transpressional Sigmoid-I faults develop at the front of the extruded material. Note that these faults are steep because they accommodate strike-slip movements in addition to reverse movements. Sigmoid-II synthetic transtensional faults parallel to Sigmoid-I develop at the back of the extruded matter to accommodate the extension linked to the material movement. These faults have a limited slip, are a back-product of the uplift development and do not border a summit extension. The summit transtensional faults, or the central part of Sigmoid-I, do not rotate and accommodate summit subsidence. Note that strike-slip experiments are similar to transtensional experiments and that the movements may also be organised around an uplifted area. The main difference is that, in strike-slip experiments, the Sigmoid-II faults are well developed transtensional faults, which border a subsiding area around the Sigmoid-I summit graben.

In transtensional experiments, Sigmoid-I faults (steep dip and limited dip-slip) and Sigmoid-II faults (shallow dip and large dip-slip) border a deep graben, which is parallel to the basal fault zone (figure 16). The graben or fault zone is narrow at the cone base and wider at the summit. It develops under the influence of the N-S directed D_{EXC} extensional field. The numerous half

grabens, which strike 000 and develop around the larger summit graben, developed in an E-W directed extensional field.

A rotation of the early formed summit fractures is occasionally observed but the main active cone faults did not rotate. The displacement maps indicate that the material is rotated clockwise (dextral basal fault) or anti-clockwise (sinistral basal fault) in the cone. This rotation affects also the uplifted material of transpressional, and possibly of strike-slip, experiments. Sigmoid-I and II faults did not rotate but accommodate the material rotation.
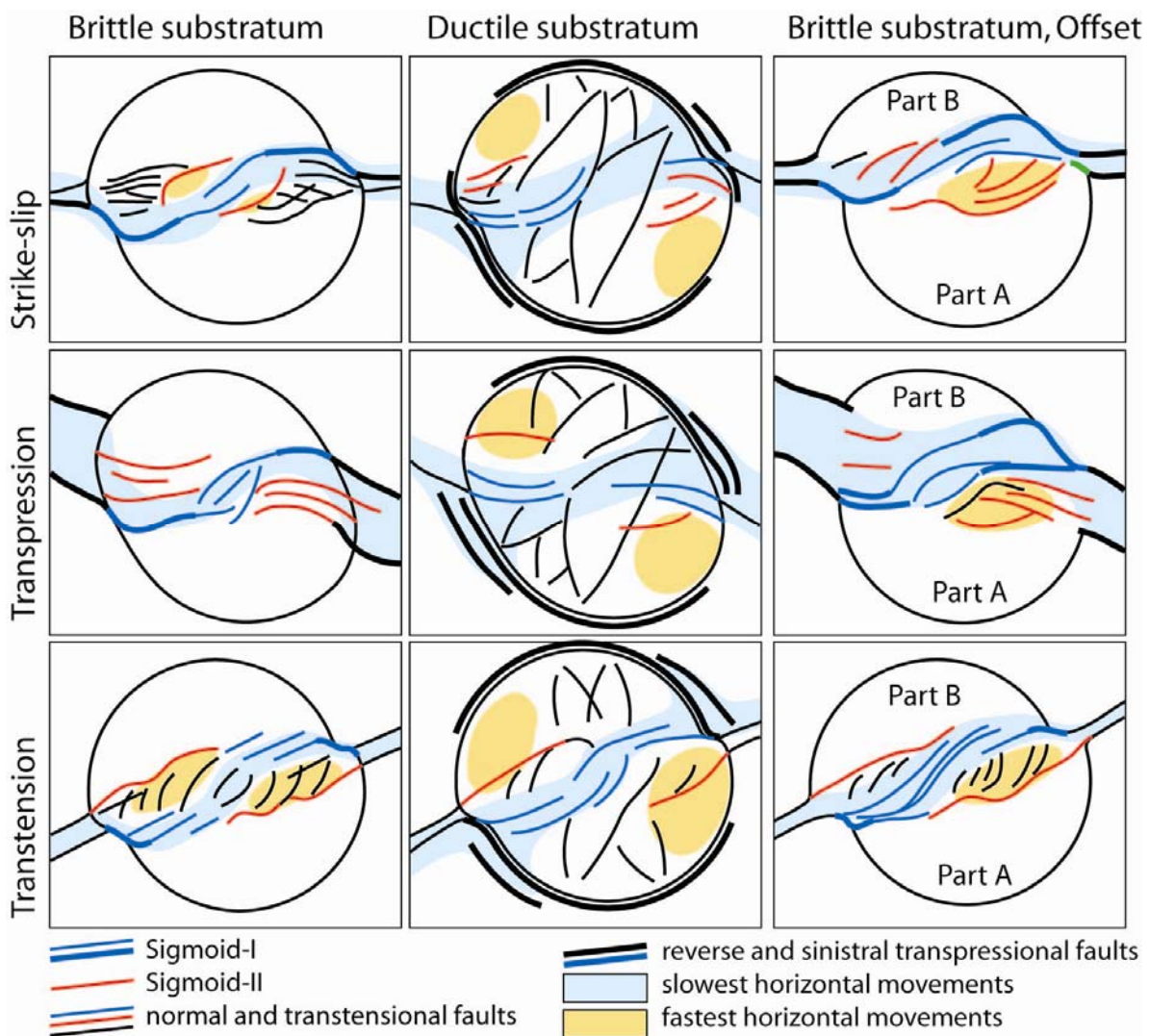
Figure 16: Main structures developing in cones located in the vicinity of sinistral strike-slip, transpressional and transtensional fault zones.

The experiments have in common a well developed Sigmoid-I fault whose central part delimits a summit graben. Sigmoid-II is either absent (transpressional experiments), restricted to the cone upper flanks (strike-slip experiments) or well developed (transtensional experiments). Sigmoid-II accommodates extension and connects with Sigmoid-I fault at the base of the cone (transtensional experiments) or at mid-slope (strike-slip experiments). The material either subsides (transtensional experiments) or is uplifted in the cone above the basal fault zone (transpressional and strike-slip experiments). Fast summit extension is only observed in the strike-slip and transtensional experiments.

4.1.2. Fault orientation

The strike of Sigmoid-I, II and summit faults in the bulk of the experiments are determined by the basal fault geometry (kinematics and angle of basal plates). Sigmoid-I and II faults develop 10° to 20° from the basal fault zone. They may develop in P shears (Sigmoid-II) and R shears (Sigmoid-I) associated with this fault zone but they do not systematically have the same kinematics as the P and R shears as defined by Sylvester (1988). Indeed, P and R shears are synthetic faults, while Sigmoid-II is antithetic in strike-slip and transtensional experiments. Sigmoid-I and II do not correspond to P and R shears. They are slightly oblique (10°-20°) to the basal fault zone because they adapt to the geometry of the cone in which they develop.

The bulk of measurements made at the cone summit, including the central part of Sigmoid-I, the other summit grabens and their elongation directions, indicate that the summit systematically undergoes a fast subsidence, especially in the strike-slip and transtensional experiments. The strike of the summit graben depends of the basal fault geometry. In brittle experiments, the summit structures develop with an angle of 40° (strike-slip experiments), 60° (transpressional experiments) and 30° (transtensional experiments) from the basal fault zone (figure 17). These structures correspond to tension features, similar to strike-slip fault tension faults, which develop with a greater angle from the basal fault zone as its compressional component of movement increases.
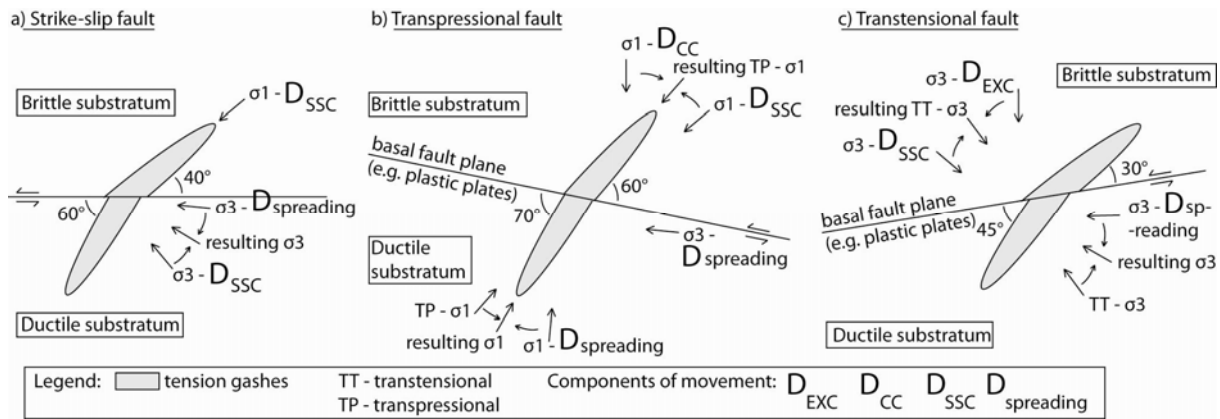
Figure 17: Orientation of tension features (e.g. grabens located at the cone summit) in sinistral (a) strike-slip, (b) transpressional and (c) transtensional experiments. For brittle substratum experiments, the summit graben develops in the stress field of the D_{SSC} that is rotated by the additional D_{EXC} or D_{CC}. The resulting stress field corresponds to that of transtensional or transpressional faults and is itself rotated by the gravitational spreading movements when a ductile substratum is added to the experiment.

4.1.3. Ductile substratum experiments

In the ductile substratum experiments, the material is transported in a direction that is imposed by the fault movement. The spreading is expressed by radial extension in the cone where the material is transported from the summit area (extension) toward the cone base (compression). The spreading increases the amplitude of fault movements, especially in the cone lower flank area. The maximum velocity is obtained in the cone lower flanks where the spreading and fault movements have the same direction and are summed.

The strike of Sigmoid-I and II faults depends of the basal fault geometry and is unchanged by spreading movements. The spreading increases the extensional component of the faults and may change their kinematics. For example, Sigmoid-I in the strike-slip and transpressional experiments is transpressional above a brittle substratum and is transtensional in ductile substratum experiments. The fault zone is turned into a graben for all fault geometries but

large-scale subsidence of this graben is restricted to transtensional experiments. Several long and shallow grabens, which are not observed in previous experiments, develop at the summit.

Folds and reverse faults develop in the substratum, at the base of the volcano. These structures are better developed at the base of Sigmoid-I, where the spreading and the fault movements are going in opposite directions, and are little expressed at the base of the fastest moving area.

Compared with brittle experiments, the summit structures of cones located above a ductile substratum develop with a greater angle from the basal fault zone: 60° (strike-slip fault), 70° (transpressional fault) and 45° (transtensional fault; figure 17). The summit grabens are rotated 10° to 20° from the brittle substratum grabens because they tend to be orthogonal to the area of fastest extension (e.g. the lower flank area located E and W of the fault zone).

4.1.4. An offset between the cone summit and the fault zone: "offset" experiments

On the largest half-cone (part A) delimited by the fault zone in the "offset" experiments, Sigmoid-I is poorly developed and Sigmoid-II has a large extensional component of movement. On the opposite side (part B), Sigmoid-II is reduced to absent and Sigmoid-I is a broad fault zone which extends over a large area from the cone flank to the cone base. Thus, the extension increases along part A faults and compression dominates along part B faults. Part A-Sigmoid-II and part B-Sigmoid-I delimit the broadest fault zone. These observations lead to the conclusion that the smaller part B flank is extruded. This flank slides along part A-Sigmoid-II fault and toward part B-Sigmoid-I faults. Note that this result is similar to those obtained with analogue models of cones and reverse faults interactions (Tibaldi 2008, Merle et al. 2001, Branquet and van Wyk de Vries 2001). However, the northern part B flank is extruded symmetrically by a reverse fault while, in Offset experiments, part B flank moves faster where it contains part A-Sigmoid-I and part B-Sigmoid-II.

4.1.5. Dimensionless numbers

The dimensionless numbers have been calculated for each experiment and this section focuses on the analysis of these numbers. This analysis provides data on the kinematics of Sigmoid-I and II faults.

The analysis of dimensionless numbers indicates that when the extensional component of the basal fault increases (D_{CC} to D_{EXC}, e.g. $\Pi_{2-F\%}$), Sigmoid-I fault accommodates a largest amount of extension ($\Pi_{3-FC\%}$ increases; figure 18-a). Sigmoid-I has usually the same kinematics as the basal fault plane, with the exception of the Sigmoid-I developing in strike-slip experiments (figure 18-a). Sigmoid-I is the continuation of the basal fault plane inside the cone. The fault is always transtensional, and accommodates a same amount of extension for all experiments, when a ductile substratum is added to the experimental device (figure 18-a).

The summit graben, or central part of Sigmoid-I, accommodates the same amount of extension for all the brittle substratum experiments. The addition of a ductile substratum to the experimental device increases its D_{EXC-C} relatively to its D_{SSC-C} (e.g. $\Pi_{3-FC\%}$, figure 18-b). The kinematics of this fault is independent of that of the basal fault because this structure similar to the tension structures of strike-slip faults (D_{SSC}). It is little influenced by the compressional and extensional components of movement (D_{CCC} and D_{EXC}), which only modify its strike (see previous section).

Sigmoid-II is not a well developed fault in transpressional and strike-slip fault experiments for which it accommodates mostly strike-slip movements (big D_{SSC-C} and small D_{EXC-C}, e.g. figure 18-c). The D_{EXC-C} of Sigmoid-II is larger in transtensional experiments because it borders the graben that develops above the basal fault plane.

In the cone, the strike-slip component of movement is mostly accommodated by Sigmoid-I and, to a lesser extent, by the summit graben (figure 18-d). The extensional and compressional components of movement are also mostly accommodated by these structures (figure 18-e). The transtensional experiments are an exception as the extension is also accommodated by the Sigmoid-II fault (figure 18-e). This observation indicates that Sigmoid-I, which includes the summit graben for brittle experiments, is the fault which accommodates most of the movement. It may be regarded as a curved Y-shear. Sigmoid-II is a by-product of the uplift that develops in transpressional and strike-slip experiments. This fault only accommodates an important amount of dip-slip in transtensional experiments because it

borders the graben that develops above the basal fault plane. The addition of a ductile layer did not significantly modify the distribution of movement.
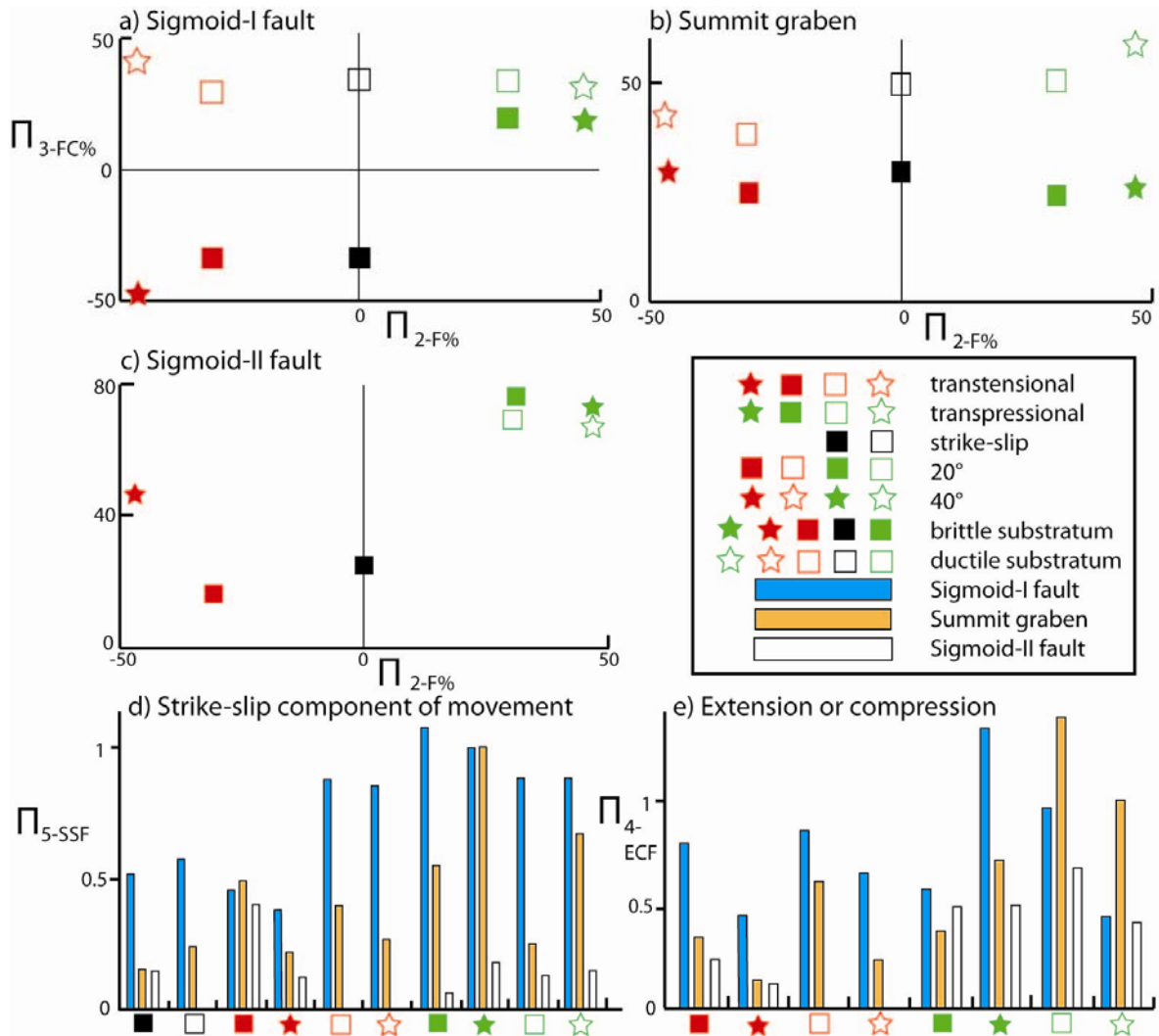
Figure 18: a-c) Plot of $\Pi_{2\text{-F\%}}$ versus $\Pi_{3\text{-FC\%}}$ for Sigmoid-I and II and for the summit graben; $\Pi_{2\text{-F\%}}$ is the percentage of D_{EXC} and D_{CC} over D_{SSC}; $\Pi_{3\text{-FC\%}}$ is the percentage of $D_{EXC\text{-}C}$ and $D_{CC\text{-}C}$ for each fault; the compression ($D_{CC\text{-}C}$, D_{CC}) is negative; d-e) Plot of the strike-slip, extensional and compressional components of movement of measured faults ($\Pi_{5\text{-SSF}}$) showing that most movements are accommodated by Sigmoid-I and, to a lesser extent, by the summit graben.

4.2. Implications for natural examples

4.2.1. Implications for the transport of magma

The regional stress field has a strong influence on the growth of a volcano because it controls the orientation of dyke injections. It has long been recognised that dykes and vent alignments are parallel to the greatest principal stress (Nakamura 1977). The cone loading effects on the regional fault is at the origin of the formation of a summit graben (e.g. van Wyk de Vries and Merle 1998). The summit graben is observed for the bulk of the experiments and it is elongated parallel to the main horizontal stress. This structure favours parallel dyke injections and the establishment of a central conduit (figure 19). The summit extension favours more magma influx, which produces more load that favours further summit extension, and so on (after van Wyk de Vries and Merle 1998).

In transtensional experiments, a deep graben forms above the basal fault zone. The deep graben is expected to favour dyke injections parallel to it and to promote the formation of a rift zone (fluid magma) or of an alignment of volcanic edifices (for more viscous magma or at a larger scale). In strike-slip experiments, Sigmoid-II faults border the subsiding upper flank and summit area to which eruptions are expected to be restricted. Eruptions may be restricted to the summit graben area over regional transpressional faults. Finally, the bulk of cone faults are susceptible to be infiltrated by minor magma injections oblique to the main stress axes.

The addition of a ductile substratum increases the extensional component of the faults. The magma is expected to behave as described previously. A greater volume of magma, with lower buoyancy, may be injected in a spreading context. The dyke injections may push the flanks, increasing the amplitude of spreading movements which favour further dyke injections, and so on.

4.2.2. Predicting collapse events

Major collapse events, or avalanches, have been recognised on many volcanoes worldwide after the phenomenon that was witnessed in 1980, during Mt St Helens eruption (Moore and Rice 1984). Avalanches are catastrophic events which affect active or inactive edifices and which may have many origins. One of these origins can be dyke dilatation, which favours

flank failure parallel to the maximum horizontal stress according to Moriya (1980). The orientation of this stress in experiments indicates that the failure is likely to occur parallel to the summit graben (figure 19). The failure may also be parallel to the deep graben bordered by Sigmoid-I and II faults in transtensional experiments if a dyke core complex forms in it.
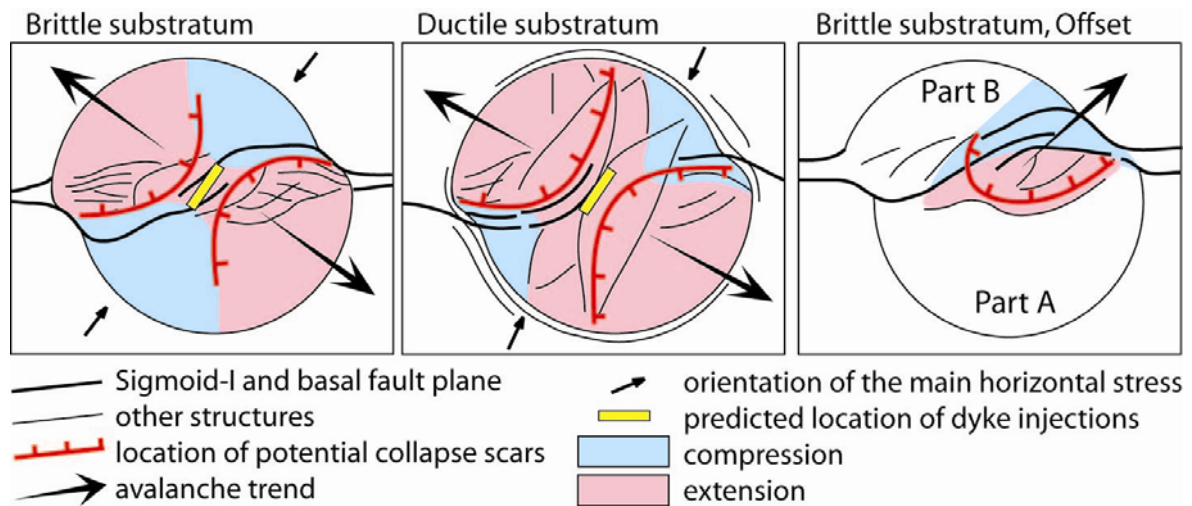
Figure 19: Sketches summarizing the likely location of dykes and collapse scars in a cone developing in the vicinity of a sinistral strike-slip fault zone. The location of these structures is similar for transtensional and transpressional experiments.

According to Lagmay et al. (2000), collapse events are likely to develop in a volcano within 10°-20° of the regional strike-slip fault plane. This collapse should be bordered by a Sigmoid-II fault and develop toward Sigmoid-I fault. However, the main structure of strike-slip and transpressional experiments is Sigmoid-I. It crosses the whole cone from bottom to top and from E to W, while Sigmoid-II is absent or restricted to the summit area. A Sigmoid-I fault is the most likely to border an avalanche. If we consider an E-W striking basal fault plane with a sinistral motion, the NE and SW cone flanks are in compression and the NW and SE flanks are in extension, according to the orientation of the main horizontal stress. This is highlighted by the ductile substratum experiments for which folds develop at the base of the NE and SW flanks and for which the fastest moving flanks are the NW and SE flanks (figure 19). The flanks that are in compression are likely to be internally deformed and may be affected by superficial collapses. However, a large collapse event is more likely to be parallel to the

summit graph, to be border by Sigmoid-I fault and to affect the flanks which are in extension. Thus, the largest events may be directed toward the SE and NW (figure 19).

The cones behave in a different way when there is an offset between the fault zone and the cone summit. In this case, the small cone flank (part B) is extruded and slides along the well developed part A-Sigmoid-II fault. This sliding is analogue of sector collapses in nature. It affects exclusively the NE flank (figure 19).

4.2.3. Ore geology

This study models the location of faults in a volcanic cone and has thus an application to ore geology. The faults are parallel to the basal fault zone (brittle substratum) or scattered (ductile substratum). Epithermal fluids are likely to circulate along these structures. Sigmoid-I is the best developed fault. It is a steeply dipping structure that cuts through the core of the edifice to its base. It is the most likely to connect with the hypovolcanic complex. The majority of hydrothermal fluids are expected to be transported by Sigmoid-I and this fault should concentrate most of the epithermal breccias and other ore deposits. This hypothesis needs to be checked in the field.

4.2.4. Comparison with natural examples

4.2.4.1. Maderas volcano, Nicaragua:

Maderas is a small, dormant volcanic cone with a circular base. It sits on a 135 striking dextral transtensional fault and it spreads over its weak substratum. A 135 elongated graben has developed in the volcano, parallel to the regional fault (figure 20-a). This graben corresponds to the subsiding structure bordered by Sigmoid-I and II that forms in transtensional experiments. This extensional structure facilitates the rise of magma toward the surface as evidenced by the five vents and the summit crater that are located in it. The volcano possesses also several 000-striking lineaments whose kinematics could not be determined on the field. These structures correspond to the shallow graben of the analogue models that develops parallel to the main horizontal stress. This shallow graben forms 45° from the basal fault plane in transtensional and ductile substratum experiments. The 000 striking lineaments

of Maderas form also 45° from the regional fault and are thus likely to be normal faults. The location of these structures (e.g. rotated clockwise from the regional fault) confirms that the regional fault has a dextral sense of motion.

The percentage of extensional component of the regional dextral transtensional fault of Maderas could be approximated if these percentages were known over the 135-striking transtensional faults of Maderas volcano. This information can not be obtained from the rare and weathered outcrops of the area but could be deduced from a geodetic study (e.g. GPS).

4.2.4.2. Guadeloupe volcanoes, Lesser Antilles:

Guadeloupe Island is an assemblage of composite volcanoes. This section focuses on the southern part of the island (e.g. the Axial Chain and Grande Découverte volcanoes), which sits upon a 145-striking sinistral transtensional fault (figure 21-a). The volcanoes do not possess a graben parallel to the regional fault. This structure may be hidden by a large magma output. The magma is also too viscous to enable the formation of a well defined rift zone. The volcanoes are however aligned parallel to the regional fault zone.

The volcanoes possess abundant 090-120 striking fractures, faults and dykes. Guadeloupe volcanoes are also characterised by repeated sector collapses. This section focuses on the Piton Bouillante volcano, which is a circular edifice that possesses many 090-120 striking exposed dykes and two large sector collapse scars called the Beaugendre and Vieux-Habitants valleys. The 090-120 striking dykes are parallel to the regional maximum horizontal stress and develop 55° to 25° from the regional fault plane. This value falls into the orientation of the maximum horizontal stress of transtensional experiments. The uncertainty on the value did not enable the distinction between ductile and brittle substratum experiments. However, there is no clear evidence to indicate that Guadeloupe volcanoes are spreading. It is reasonable to assume that they are comparable to brittle substratum experiments.

Note that the Guadeloupean dykes are not parallel to the basal fault zone as would have been expected from transtensional experiments (see previous section) because they are observed high in the volcano. There, they are parallel to the summit graben in the models and to the main horizontal stress. The buried dykes located beneath the flanks of Piton Bouillante may be striking 145, parallel to the deep graben of the models.
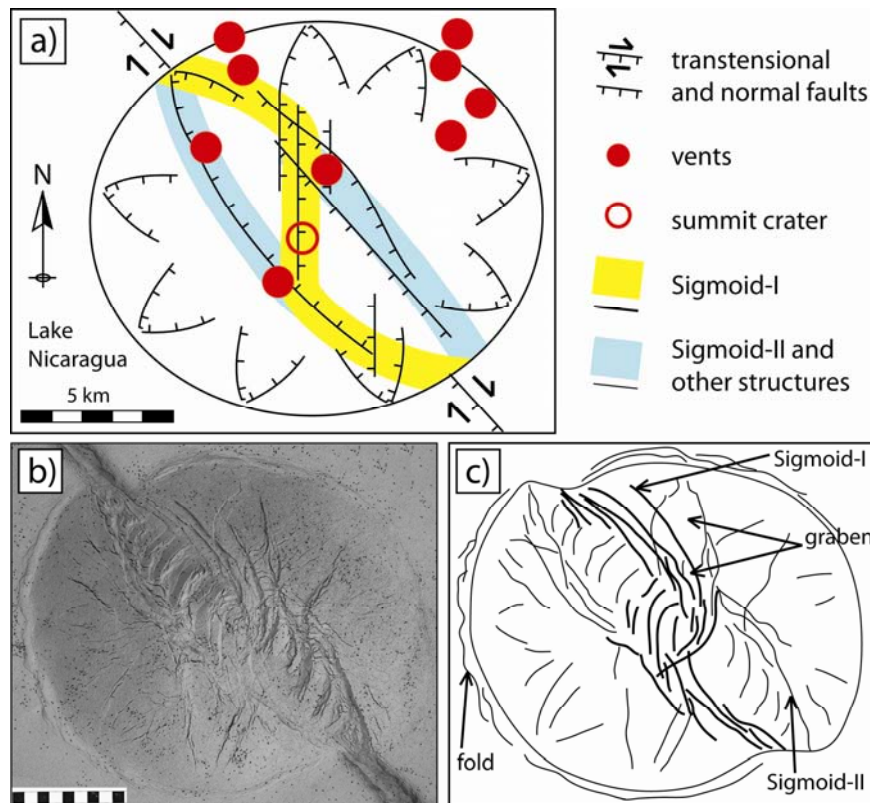
Figure 20: a) Structural sketch of Maderas volcano, Nicaragua; b-c) Picture and sketch of experiments C19 (transtensional fault, α= 20°, ductile substratum).

The collapse scars (Beaugendre and Vieux-Habitants valleys) cut into the southern, SW and western flanks of the volcano (figure 21-a). By comparison with the analogue experiments, the unstable area is delimited by a Sigmoid-I fault (S-SSE of Piton Bouillante peak), by the summit graben of the models on the north (Piton Bouillante peak area) and it comprises one of the cone flanks, which would be in extension according to the models (SW flank). The avalanche orientation then corresponds to that predicted by analogue models. It must be kept in mind that these structures may have many other origins. For example, they affect the only flank which was not buttressed by other volcanoes and was, at the time of the avalanche events, facing the sea (e.g. Le Friant 2001). The regional fault movement is a factor among others, which has fractured the edifices and placed the SW flank in extension.

Finally, the hydrothermal fluids of the Bouillante geothermal system are located in an area that corresponds to the location of Sigmoid-I fault. These fluids may have been transported by a Sigmoid-I fault which strikes 160 to about E-W in the summit area.

Note that, as volcanoes were building south of Piton Bouillante volcano, the Sigmoid-I fault has likely been shifted toward the south (figure 21-a). According to the models, the present-day area which is in extension and susceptible to be affected by collapses, is the SW part of Grande Découverte volcano. This area has indeed experienced two recent avalanches, 3,100 and 11,500 years ago (Boudon 1987).
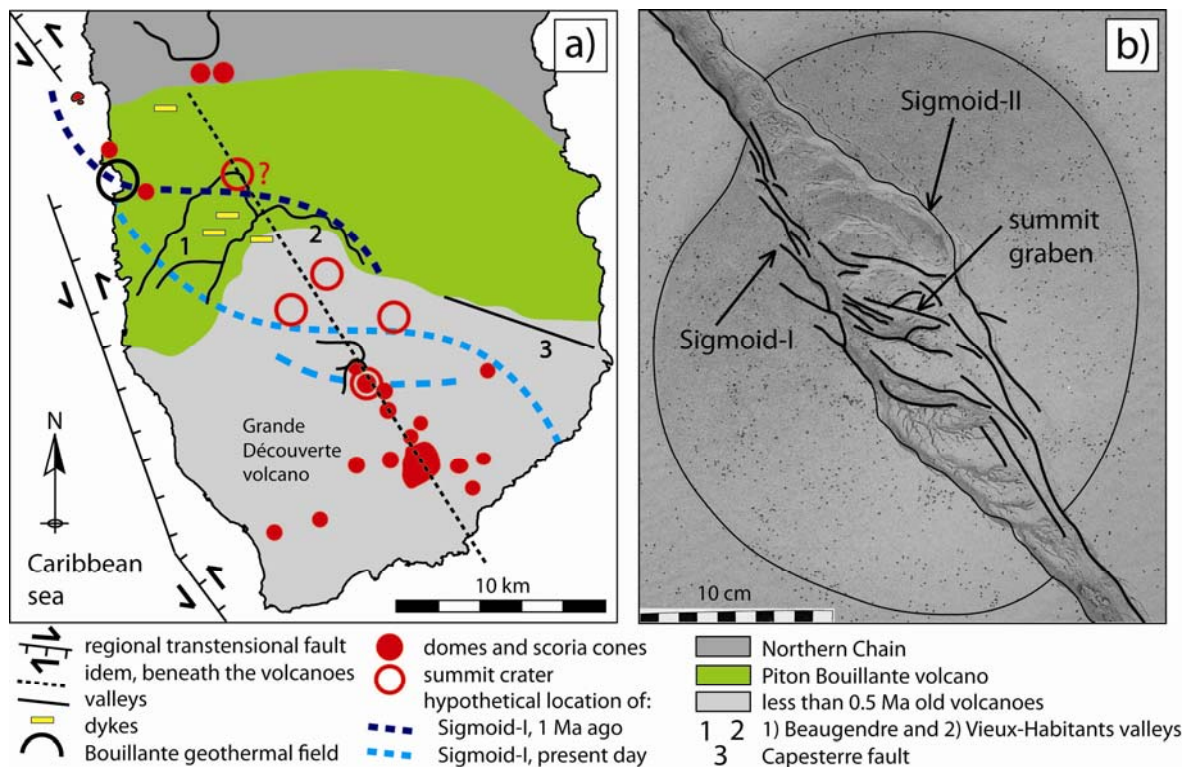
Figure 21: c) Structural sketch of the southern part of Basse Terre Island, Guadeloupe, Lesser Antilles. The regional faults represented on this figure correspond to individual fault planes, which are part of a 50 km wide sinistral transtensional fault zone; d) Picture of experiment C33 (transtensional fault, α= 20°, brittle substratum).

5. Conclusion

Analogue experiments made with deformed cones of granular material have been used to determine the location, kinematics, strike and slip of faults that develop in a cone located above strike-slip, transtensional and transpressional regional faults. The cone responds to the basal fault movement by developing a complex set of faults. One of these faults is named Sigmoid-I. It is synthetic (e.g. same sense of motion) and has the same kinematics (e.g. strike-slip, transtensional or transpressional) to the basal fault with the exception of its central part (summit graben) and with the exception of strike-slip experiments. This major structure accommodates most of the movement. The second fault is named Sigmoid-II and accommodates more movement as the extensional component of the basal fault increases. Sigmoid-II is well developed only for transtensional experiments. The movements inside the cone are organised around an uplifted area (strike-slip and transpressional experiments) or a subsiding area (transtensional experiments). The elongation direction of the summit graben is used to determine the orientation of the main horizontal stress, to which it is parallel. The addition of a ductile substratum modifies the kinematics of Sigmoid-I and forms broad shallow grabens parallel to the main horizontal stress and to the basal fault zone.

The analogue models may be used to identify the preferential area for dyke injection (summit), the fracture zone likely to transport the hydrothermal fluid and to concentrate the deposition of ore minerals (Sigmoid-I fault) and the unstable flanks (e.g. NW and SE flanks for E-W striking faults with a sinistral motion). The models were used to understand the location of the faults, dyke injections, geothermal fields and collapse scars of Maderas and Piton Bouillante (Guadeloupe) volcanoes. These models may be used to better understand the structure of many other volcanoes which have developed in the vicinity of a fault that possesses a strike-slip component of movement.

Chapter 6

-

Conclusions

Chapter 6: Conclusions

1. General conclusions

A multi-disciplinary approach was used to (1) unravel the structure of Guadeloupe, Mt Cameroon and Maderas volcanoes and (2) to understand the interaction between these volcanoes and regional strike-slip fault movements.

1.1. Basse Terre Island, Lesser Antilles

This study provides structural and lithological data on Basse Terre volcanoes and proposes a model for the progressive formation of the island through the formation of discrete volcanic centres, which degrade with erosion and collapse. The Bouillante Chain is excluded from this model and its existence is judged doubtful. My model considers that the Northern Chain has been built on 160° striking structures parallel to the subduction front, contemporaneously with many small-volume seamounts located along the Montserrat-Bouillante transtensional fault system. The Piton Bouillante volcano was then emplaced south of the Northern Chain and was dissected by the Beaugendre and Vieux-Habitants valleys, which were formed either by major sector collapses or/and erosion. About 0.5 Ma ago, intense volcanic activity constructed three volcanic edifices inside the Vieux-Habitants valley, Les Mamelles domes north of Piton Bouillante volcano and Mt Caraïbe south of it. These volcanoes are aligned along a 140° striking fault segment of the 50 km wide Montserrat-Bouillante fault zone along which the magma is likely to have been transported. The Grande Découverte volcano was then built south of the Axial chain volcanoes upon the same 140° striking fault segment.

In the field, the 090°-120° striking structures are the most abundantly measured in Basse Terre Island. These structures are approximately parallel to the offshore Marie-Gallante graben and to the main horizontal stress of the regional plate motion and of the Montserrat-

Bouillante fault, upon which the southern part of the island is built. This regional stress field has a N-S orientated minimum principal stress that has controlled the major E-W dyke orientation and generated E-W fractures. This fracturing has been exploited by hydrothermal fluid circulation and has controlled collapse directions.

My model has been established with field data and confirms the onshore occurrence of 090°-120° striking structures, which were postulated by offshore geophysical data (mostly bathymetry).

1.2. Mt Cameroon volcano, western Africa

The study of Mt Cameroon reveals that the volcano is spreading on its weak substratum. The study provides field data obtained at the SE base of the volcano to support this model and to determine the characteristics of the spreading. The elongated morphology of Mt Cameroon promotes the fast spreading of its long flanks, the immobility of its short flanks and the formation of an elongated summit plateau. The NW long flank spreads faster than the SE one, possibly as a consequence of substratum heterogeneities. Indeed, the sedimentary horizons may be thicker or weaker under the SE flank of Mt Cameroon. The gravitational spreading has formed thrusts in the substratum sediments, which are linked to the edifice by transtensional faults. The observed steepness of the long flanks is possibly related to the pushing generated by dyke injections in the fault zone, which is in extension due to spreading movements. Eventually, the flank instabilities are a consequence of the spreading movement of the flanks.

The field and remote sensing analysis also demonstrate that Mt Cameroon is not a horst capped by a thin layer of lava flows as proposed by Gèze (1943), Déruelle et al. (1987) and Meyers et al. (1998) but rather a large volume volcano entirely made of lava.

1.3. Maderas volcano, Nicaragua

The small-volume Maderas volcano has an interesting morphology, which has been shaped by spreading and regional fault movements. The spreading has diminished the steepness of the volcano flanks and has formed a shallow summit area. This dormant volcano has not recently

re-built a steep summit area as the neighbourhood Concepcion volcano did. The half-grabens located over the lower flanks of the volcano accommodate the radial extension of the spreading edifice.

In addition to these structures, Maderas volcano possesses a NW-SE graben and N-S striking lineaments, which are parallel, respectively, to the fault plane and to the tension features of the regional dextral transtensional fault.

The field study failed to provide structural data to complete the remote sensing observations. The field data however indicate that most of the eruptive vents of Maderas are located along the NW-SE graben. The study of lava flow thicknesses reveals that the NW-SE graben has possibly formed while the volcano was still active.

1.4. Analogue models

Based on the analogue modelling, the following theories have been established. A cone located in the vicinity of a fault with a strike-slip motion develops a curved structure named Sigmoid-I fault. Sigmoid-I is a transpressional or transtensional fault, which accommodates most of the strike-slip movements in the cone. It forms an angle of 10°-20° with the basal fault plane and curves at the summit of the cone where it defines a summit graben. Sigmoid-II is a major transtensional structure, which is observed in strike-slip experiments and is well developed in transtensional experiments. The addition of a ductile substratum to the experimental device modifies the kinematics of Sigmoid-I, forms additional shallow grabens parallel to the summit graben and forms radial half-grabens over the lower flanks of the cone. The models are used to predict the orientation of dyke injections and the likely location of sector collapses in nature.

Sigmoid-I and II are well developed on the extinct Maderas volcano and their locations were used to confirm the strike and kinematics of the regional fault upon which it sits. The Guadeloupe volcanoes are aligned parallel to a regional sinistral transtensional fault. Their dykes, faults, fractures and geothermal fields may be aligned along a Sigmoid-I structure. This structure is not visible at the surface and has possibly been hidden by eruptions and obscured by erosion. Also, the location of dykes and sector collapses in Guadeloupe matches these predicted by analogue models.

1.5. Contribution of the study

This study contributes to extend our knowledge of the interaction between volcanic cones and regional strike-slip fault movements through three natural examples. In Guadeloupe, the regional transtensional fault is responsible for the alignment of the Axial Chain and Grande Découverte volcanoes. The regional fault movement has fractured these volcanoes along the NW-SE and E-W directions. These structures have channelled magma and hydrothermal fluids and have facilitated large sector collapses.

The regional inactive strike-slip fault over which Mt Cameroon has built has channelled the magma in the crust. The regional fault has favoured the formation of a rift zone which has promoted the formation of a large-volume elongated volcano. The fault has indirectly favoured the fast spreading of Mt Cameroon long flanks.

The regional transtensional fault of Nicaragua has channelled a magma that was too viscous to form a dyke swarm and a rift zone. Instead, the magma has risen vertically and has formed the Maderas volcanic cone. The active fault has then fractured the edifice along the NW-SE and N-S directions. The NW-SE graben has confined the lava flows and eruptive vents have formed along this structure.

The analogue models have provided quantitative data on the Sigmoid-I and II structures. Sigmoid-I accommodates most of the fault movements in the cone. This structure is the most likely to be exploited by magma and hydrothermal fluid circulation. The Sigmoid-I structure is expected to be covered with eruptive vents and to be paralleled by landslide scars at the surface of the volcano and to concentrate ore minerals at depth. The Sigmoid-I fault planes of active volcanoes are expected to be covered with recent volcanic output and to be hidden to surface geology exploration.

Finally, this study has proved that the combination of remote sensing and field analyses provide relevant data. It also demonstrates the potential of field studies carried in rain forest environment, provided that the study is carried along the shore line and in river beds. It shows that such volcanoes can be faithful sources of field data as long as the rivers are active enough.

Guadeloupe provides most of the data because the abundant rivers have deeply incised in the edifice. The rivers of Mt Cameroon have mostly incised into the substratum of the volcano,

where the best outcrops were found. The poor quality of Maderas outcrops is a consequence of its small size and of a lack of water in the river beds.

2. Further work

Our knowledge of the interaction between volcanic cones and strike-slip faults will beneficiate from detailed studies of the regional faults and of the geology of the volcanoes.

It is essential to better document the kinematic of regional faults in order to comprehend the deformations that a nearby volcanic edifice has and will experienced. The access to the past and present location, geometry, kinematics and slip velocity of the regional fault may lead to better grasp its impact on a volcano. The Monsterrat-Bouillante transtensional fault of the Lesser Antilles has beneficiated from several dedicated bathymetric studies. Its past motion and the location of individual fault segments are currently being documented. The seismic activity of this fault system is monitored, which gives an access to its present day motion. A synthesis of the existing seismic and bathymetry, which are currently own by several laboratories, may provide relevant informations on the fault system.

The CASZ fault, which has channelled Mt Cameroon magma, is inactive. A dedicated field study, aiming at mapping the exact location of this structure, may help to understand its interaction with the volcano. Unravel the kinematics of this structure has only an interest for the comprehension of the Pan-African orogeny and is not essential to our understanding of Mt Cameroon volcano.

The NW-SE striking transtensional fault of Lake Nicaragua is hidden by Quaternary lake sediments and water. Onshore, the NW-SE striking fault systems are covered with Quaternary volcanic rocks. A remote sensing analysis of western Nicaragua may reveal the location of recently formed fault planes. The study of buried fault systems will necessitate the use of geophysical tools, such as seismic tomography. The NW-SE fault system of western Nicaragua affects a pile of Cretaceous to Quaternary sedimentary layers. The offset of horizons by the fault system may be imaged to provide data on the location and dip-slip components of faults.

The structures of the volcanoes can not be fully grasped without a study of their geology, building history and feeding system. The documentation of magma and hydrothermal fluids

movements inside the edifice may contribute to locate the structures that have channelled these fluids. The past and present movements of fluids can be accessed with geological maps and geophysical tools, respectively.

The geological map of Basse Terre Island has been drawn in 1966 and is outdated. For example, the debris flows and avalanches, which are abundant in Basse Terre Island, were unknown phenomena in the 60s and have been mapped as hyalotuff deposits. In 1988, a new map of the southern extremity and active part of the island (Grande Découverte volcano) has improved our knowledge of this area. The mapping needs to be extended to the northern part of the island by using and completing the field data presented by this thesis and by inspecting the eastern flanks of the volcanoes. The pursuit of the field study of this thesis may lead to un-discovered outcrops.

The geological map of Mt Cameroon probably exists but is own by private companies. The publication of this map will be of a great help to all the future structural, geochemical and geophysical studies that will be carried on the volcano.

The Maderas volcano possesses rare and weathered outcrops. Based on the observations made during this project, it does not seem possible to produce a geological map of this volcano. Unrevealing its structure will necessitate the use of geophysical and remote sensing tools.

Additional geophysical and geochemical analyses need to be combined to field mapping in order to produce the geological maps. Such studies have been carried out in Guadeloupe and have provided essential data on the migration of the volcanic activity and on the location of buried fracture zones. The Capesterre fault, for example, has been detected by the geochemical analysis of the weathered surface of the volcano. The pursuit of these efforts and the extension of these tools to the two other volcanoes will lead to new discover.

The interest of geological maps is to document the vent alignments, dykes and variations in the eruption sites throughout the history of the volcano. These observations will provide insights into the movement of the magma inside the volcano. This information may be used to determine the location of the buried structures which have been infiltrated by the magma. The mapping of sector collapses may too beneficiate to our comprehension of the structure of these volcanoes.

The study of the present day location of magma may help to locate the structures actively exploited by magma infiltration and to better characterise the orientation of the least principal stress. The active Grande Découverte volcano of Guadeloupe is well monitored. The

monitoring of Mt Cameroon may be improved, not only to provide insight into the structure of this volcano, but also to anticipate the eruption sites and related hazards of this very active volcano.

The Analogue models have demonstrated their capacity to provide informations on the kinematics of Sigmoid-I and II structures. These models can be improved by varying the component of extension and compression associated with the regional faults, in order to model a larger range of fault geometries. The natural examples may be more realistically modelled by adding ductile layers (analogues of hydrothermally altered volcanic cores and low strength layers located in the lava pile) and golden syrup injections (analogue of plumbing system and/or individual dyke injections) to the sand cones. Many other parameters of the experimental device may be modified in order to more closely represent individual volcanic examples.

Finally, the quantitative data on the interaction between strike-slip faults and volcanic cones provided by this study need to be compared to a greater amount of natural examples. Only then can the models proposed by this thesis be fully validated.

Acknowledgements

Bibliography

Acocella V (2005) Modes of sector collapse of volcanic cones: Insights from analogue experiments. Journal of Geophysical Research 110, doi:10.1029/2004JB003166

Ambeh WB, Fairhead JD (1991) Regular deep seismicity beneath Mt Cameroon volcano: lack of evidence for tidal triggering. Geophysical Journal International 106:287-291

Ambeh WB, Fairhead JD, Stuart W (1992) Seismotectonics of the Mount Cameroon volcanic region, West Africa. In: Gasparini P. et al. (eds), Volcanic seismology, IAVCEI Proceedings of Volcanology, Springer, Berlin, pp 45-61

Andrade D (2009) The Influence of active tectonics on the structural development and flank collapse of ecuadorean arc volcanoes. PhD Thesis, Blaise-Pascal university, Clermont-Ferrand, France

Annen C, Lénat J-F, Provost A (2001) The long-term growth of volcanic edifices: Numerical modelling of dyke intrusion and lava-flow emplacement. Journal of Volcanology and Geothermal Research 105:263-289

Arnaud N (2005) Les Processus de démantèlement des volcans, cas d'un volcan bouclier en milieu océanique: Le Piton des Neiges (île de La Réunion) = Disassembly processes of volcanoes, case study of an oceanic shield volcano: the Piton des Neiges (Réunion Island). PhD Thesis, La Réunion university, France

Ateba B, Ntepe N (1997) Post-eruptive seismic activity of Mount Cameroon (Cameroon), West Africa: a statistical analysis. Journal of Volcanological and Geothermal Research 79:25-45

Ateba B, Dorbath C, Dorbath L, Ntepe N, Frogneux M, Aka FT, Hell JV, Delmond JC, Manguelle D (2009) Eruptive and earthquake activities related to the 2000 eruption of Mount Cameroon volcano (West Africa). Journal of Volcanological and Geothermal Research 179:206-216

Baubron JC (1990) Prospection géochimique par analyse des gaz des sols en vue de la localisation d'une fracture majeure sous recouvrement. Faille Montserrat-Marie Galante: secteur de Marie-Galante et Capesterre-Belle-Eau, Basse-Terre (Guadeloupe) = Geochemical prospection by gas analysis of a major burried fracture: the Montserrat-Marie Gallante fault. BRGM report R-31069

Benkhelil J, Giresse P, Poumot C, Ngueutchoua G (2002) Lithostratigraphic, geophysical and morpho-tectonic studies of the South Cameroon shelf. Marine and Petroleum Geology 19(4):499-517

Belousov A, Walter TR, Troll VR (2005) Large-scale failures on domes and stratocones situated on caldera ring faults: sand-box modeling of natural examples from Kamchatka, Russia. Bulletin of Volcanology 67(5):457–468

Blanc F (1983) Corrélations chronologiques et géochimiques des formations volcaniques du sud de la Basse-Terre de Guadeloupe (Petites Antilles), Début du cycle récent = Chronological and geochemical correlations of recent Basse-Terre volcanism, Guadeloupe (Lesser Antilles). PhD Thesis, Grenoble university, 171 p.

Borgia A, Ferrari L, Pasquare G (1992) Importance of gravitational spreading in the tectonic and volcanic evolution of Mount Etna. Nature 357:231-235

Borgia A (1994) Dynamic basis of volcanic spreading. Journal of Geophysical Research, 99(B9):17791-17804

Borgia A, Delaney PT, Denlinger RP (2000) Spreading Volcanoes. Annual Review of Earth and Planetary Sciences 28:539-570, doi:10.1146/annurev.earth.28.1.539

Borgia A, van Wyk de Vries B (2003) The volcano-tectonic evolution of Concepcion, Nicaragua. Bulletin of Volcanology 65(4):248-266

Bouchot V, Sanjuan B, Traineau H, Guillou-Frottier L, Thinon I, Baltassat JM, Fabriol H, Bourgeois B, Lasne E (2010) Assessment of the Bouillante geothermal field (Guadeloupe, French West Indies): toward a conceptual model of the high temperature geothermal system. World Geothermal Congress 2010, Bali, Indonesia

Boudon (1987) Mécanismes éruptifs et mode de mise en place des dépôts d'éruptions explosives dirigées, Exemples de la Soufrière (Guadeloupe) et de la Montagne Pelée (Martinique) = Eruptive mechanisms and emplacement of lateral eruption deposits, case study of La Soufrière (Guadeloupe) and Montagne Peléé (Martinique). PhD Thesis, Paris VII university, 382 p.

Boudon G, Dagain J, Semet M, Westercamp D (1988) Carte géologique au 1/20000e du Massif volcanique de la Soufrière = Géological map of Soufrière volcano. BRGM-CNRS-DRM-IPGP, BRGM (Ed.), Orléans

Boudon G, Semet MP, Vincent PM (1989) The evolution of la Grande Découverte (La Soufrière) volcano, Guadeloupe. FWI IAVCEI Proceedings in Volcanology, J Latter (Ed.), Volcano Hazards: Assessment and Monitoring 1: 86-109

Boudon G, Semet MP, Vincent PM (1992) Les éruptions à écroulement de flanc sur le volcan de la Grande Découverte (la Soufrière) de Guadeloupe: Implications sur le risque volcanique = Sector collapse eruptions, implication for Risks and Grande Découverte volcano (la Soufrière), Guadeloupe. Bulletin de la Société Géologique de France 163 (2):159-167

Boudon G, Komorowski JC, Semet M, Le Friant A, Deplus C (1999) Frequent volcanic flank-collapses in the Lesser Antilles arc: origin and hazards. EOS Transactions, American Geophysical Union 80(46): F1142

Bourne SJ, England PC, Parsons B (1998) The motion of crustal blocks driven by flow of the lower lithosphere and implications for slip rates of continental strike-slip faults. Nature, 391:655-659

Bouysse P, Westercamp D, Andreieff P, Baubron JC, Scolari G (1985) Le volcanisme sous-marin Néogéne récent au large des côtes Caraïbes des Antilles françaises. Relations avec le volcanisme à terre et évolution du front volcanique = Neogene submarine volcanism of french Lesser Antilles : relationship with onshore eruptions and volcanic axis evolution. Géologie de la France 1:101-11

Bouysse P, Westercamp D (1990) Subduction of Atlantic aseismic ridges and Late Cenozoic evolution of the Lesser Antilles island arc. Tectonophysics 175:349-390

Bouysse P, Westercamp D, Andreieff (1990) The Lesser Antilles arc. In: Moore JC, Mascle A, et al. (Eds), Proceedings of the Ocean Drilling Program, Scientific Results 110:29-44

Branquet Y, van Wyk de Vries B (2001) Effets de la charge des édifices volcaniques sur la propagation de structures régionales compressives : exemples naturels et modèles expérimentaux = Effects of volcanic loading on regional compressive structures: new insights from natural examples and analogue modelling. Comptes Rendus de l'Académie des Sciences-Series II A-Earth and Planetary Science Letter, 333(8):455-461, doi:10.1016/S1251-8050(01)01660-3

Briden JC, Rex DC, Fallar AM, Tomblin JF (1979) K-Ar geochronology and paleomagnetism of volcanic rocks from the Lesser Antilles island arc. Philosophical Transaction of the Royal Society of London 291(A):485-528

Burke K, Wilson JT (1972) Is African plate stationary? Nature 239(5372):387-390

Cailleau B, La Femina PC, Dixon TH (2007) Stress accumulation between volcanoes: an explanation for intra-arc earthquakes in Nicaragua? Geophysical Journal International, 169:1132-1138, doi: 10.1111/j.1365-246X.2007.03353.x

Carlut J, Quidelleur X, Courtillot V, Boudon G (2000) Paleomagnetic directions and K/Ar dating of 0 to 1 Ma old lava flows from La Guadeloupe Island (French West Indies): implications for time averaged field models. Journal of Geophysical Research 105(B1):835-849

Cecchi E, van Wyk de Vries B, Lavest JM (2004) Flank spreading and collapse of weak-cored volcanoes. Bulletin of Volcanology 67(1):72-91

Chabellard JG, Philip H, Gaulon R (1986) Déformations et régimes de contraintes actuel et récent dans l'arc des Petites Antilles entre Martinique et Antigua = Strain and recent stress of the Lesser Antilles Arc between Martinique and Antigua. Compte Rendue de l'Académie des Sciences de Paris 303(II-1):81-86

Corpuz EG, Laguerta E, Alanis P, Marilla J, Lendio M, Gabinete E, Bacolcol T (2004) Volcanic and crustal motions from GPS and ground deformation measurements at Mayon volcano, Philippines. Florence, Italy, International Union of Geophysical Sciences, 32nd International Geological Congress

Cruden DM (1991) A simple definition of a landslide. Bulletin of Engineering Geology and the Environment, 43(1):1435-9537

Dagain J (1981) La mise en place du massif volcanique Madeleine-Soufrière, Basse-Terre de Guadeloupe, Antilles = Formation of Madeleine-Soufrière, Basse-Terre of Guadeloupe. PhD thesis, Paris sud-Orsay university, 156 p.

Davidson J, De Silva S (2000) Composite volcanoes. In: Sigurdsson H (ed.), Encyclopedia of volcanoes, Academic Press, New York, pp 663–681

Delcamp A, van Wyk de Vries B, James MR (2008) The influence of edifice slope and substrata on volcano spreading. Journal of Volcanology and Geothermal Research 177:925–943

DeMets C, Jansma PE, Mattioli GS, Dixon TH, Farina F, Bilham R, Calais E, Mann P (2000) GPS geodetic constraints on Caribbean-North America plate motion. Geophysical Research Letters 27(3):437-440

DeMets (2001) A new estimate for present-day Cocos-Caribbean plate motion: implications for slip along the Central American volcanic arc. Geophysical Research Letters, doi: 0094-8276/01/1999GL000000$05.00

Déruelle B, Nni J, Kambou R (1987) Mount Cameroon: an active volcano of the Cameroon Line. Journal of African Earth Sciences 6(2):197-214

Déruelle B, Ngounouno I, Demaiffe D (2007) The "Cameroon hot line": An unique example of active alkaline intraplate structure in both oceanic and continental lithosphere. Compte Rendu de Geosciences 339:589-600

Déruelle B, Moreau C, Nkoumbou C, Kambou R, Lissom J, Njongfang E, Ghogomu RT, Nono A (1991) The Cameroon Line: A review. In: Kampunzu AB, Lubala RT (eds) Magmatism in extensional structural settings, The Phanerozoic African plate. Springer-Verlag, Berlin, pp 274-327

Dessauvagie TFJ (1974) The Geological Map of Nigeria. The Nigerian Mining, Geological and Metallurgical Society, scale 1:1,000,000

De Reynal de Saint-Michel A (1966) Carte géologique de la France et notice explicative, département de la Guadeloupe, Basse-Terre et les Saintes = Geological map of France and notice, Guadeloupe area, Basse-Terre and Saintes. Ministère de l'industrie de Paris, scale 1:50,000

Dewey JF, Holdsworth RE, Strachan RA (1998) Transpression and transtension zones. Geological Society, London, Special Publications 135:1-14, doi: 10.1144/GSL.SP. 1998.135.01.01

Dickinson WR, Seely DR (1979) Structure and Stratigraphy of Forearc Regions. American Association of Petroleum Geologists Bulletin 63:2–31

Donnadieu F, Merle O (1998) Experiments on the indentation process during cryptodome intrusions: New insights into Mount St. Helens deformation. Geology 26(1):79-82, doi: 10.1130/0091-7613(1998)026

Dumort JC (1968) Geological map and notice of Douala Ouest. In: Direction des Mines, Géologie, Cameroun, scale 1:500,000

Dusquenoy T, Barrier E, Kasser M, Aurelio M, Gaulon R, Punongbayan R, Rangin C, French-Filipino Cooperation Team (1994) Detection of creep along the Philippine fault: first results of geodetic measurements on Leyts Island, central Philippines, Geophysical Research Letters 21:975-978

Fairhead JD (1985) Preliminary study of the seismicity associated with the Cameroon volcanic province during the volcanic eruption of Mount Cameroon in 1982. Journal of African Earth Sciences 3:297-301

Fairhead JD, Binks RM (1991) Differential opening of the Central and South-Atlantic oceans and the opening of the West African rift system. Tectonophysics 187:191-203

Fairhead JD, Okereke CS (1987) A regional gravity study of the West African rift system in Nigeria and Cameroon and its tectonic interpretation. Tectonophysics 143(1-3):141-159, doi:10.1016/0040-1951(87)90084-9

Fabriol H (2001) Champ géothermique de Bouillante : synthèse des études géophysiques = Bouillante geothermal field: synthesis of geophysical studies. BRGM report no. RP-50259-FR, BRGM, Orléans, France

Feuillet N (2000) Sismotectonique des Petites Antilles, liaison entre activité sismique et volcanique = Sismotectonics of Lesser Antilles, relationship between seismic activity and volcanissm. PhD thesis, Paris 7 René Diderot university, 283 p.

Feuillet N, Manighetti I, Tapponnier P (2002) Arc parallel extension and localization of volcanic complexes in Guadeloupe, Lesser Antilles. Journal of Geophysical Research 107(B12):2331, doi: 10.1029/2001JB000308

Fitch TJ (1972) Plate convergence, transcurrent faults, and internal deformation adjacent to Southwest Asia and the Western Pacific. Journal of Geophysical Research, 77:4432–4460

Fitton JG (1983) Active versus passive continental rifting - Evidence from the West-African rift system. Tectonophysics 94(1-4):473-481

Fitton JG, Dunlop HM (1985) The Cameroon Line, West-Africa, and its bearing on the origin of oceanic and continental alkali basalt. Earth Planetary Science Letter 72(1):23-38

Francis P, Wells A (1988) LANDSAT Thematic Mapper observations of debris avalanche deposits in the Central Andes. Bulletin of Volcanology 50:258-278

Freeth SJ, Kay RLF (1987) The lake Nyos gas disaster. Nature 325:104-105

Gadalia A (1985) Cadre structural de l'activité hydrothermale des zones d'exploration de Bouillante et de Moscou (Guadeloupe) = Structure of geothermal area of Bouillante

and Moscou (Guadeloupe). BRGM report, 85-SGN-080-GTH, BRGM Orléans, France

Gadalia A, Gstatler N, Westercamp D (1988) La chaîne volcanique de Bouillante, Basse-Terre de Guadeloupe (Petites Antilles): identité pétrographique, volcanologique et géodynamique = the Bouillante Chain, Basse-Terre, Guadeloupe (Lesser Antilles): petrology, volcanology and geodynamic. Géologie de la France, 2-3:101-130

Garrabé F, Andreieff P, Bouysse P, Rodet J (1988) Carte géologique de Grande-Terre: département de la Guadeloupe = Geological map of Grande-Terre, Guadeloupe. BRGM Orléans (ed.), scale 1:50,000

Genter A, Traineau H (2004) Synthèse méthodologique sur l'exploration géothermique haute énergie dans les DOM: approche géologique = Methodological synthesis on high energy geothermal exploration in French overseas regions: geological approach. GHEDOM project, BRGM report BRGM/RP-53130-FR, BRGM, Orléans, France

Gèze B (1943) Géographie physique et géologie du Cameroon occidental = Pysical geography and geology of western Cameroon. Mémoire du Museum National d'Histoire 17:1-272

Gèze B (1953) Les volcans du Cameroun occidental = Western Cameroon volcanoes. Bulletin de Volcanology 13:63-92

GLCF website - http://glcf.umiacs.umd.edu/index.shtml

Groppelli G, Tibaldi A (1999) Control of rock reology on deformation style and slip-rate along the active Pernicana Fault, Mt Etna, Italy. Tectonophysics 305:521–537

Guisseau D, Patrier Mas P, Beaufort D, Girard JP, Inoue A, Sanjuan B, Petit S, Lens A, Genter A (2007) Significance of the depth-related transition montmorillonite-beidellite in the Bouillante geothermal field (Guadeloupe, Lesser Antilles). American Mineralogist 92(11-12):1800-1813

Hedberg JD (1968) A geological analysis of the Cameroon trend. PhD Thesis, Princeton University

Holohan EP, van Wyk de Vries B, Troll VR (2008) Analogue models of caldera collapse in strike-slip tectonic regimes. Bulletin Volcanology 70:773–796, doi: 10.1007/ s00445-007-0166-x

Hubbert MK (1937) Theory of scale models as applied to the study of geologic structures. Geological Society of America Bulletin 48(10):1459-1519

Jarrad RD (1986) Terrane motion by strike-slip faulting of forearcslivers, Geology 14(9):780–787

Jordan T (1975) The present-day motions of the Caribbean plate. Journal of Geophysical Research 80:4433-4439

Julien P, Bonneton JR (1984) Etude néotectonique de la Soufrière de Guadeloupe = Neotectonic study of La Soufrière of Guadeloupe. Compte Rendu de l'Académie des Sciences Paris 298(2):907-909

Kerle N, van Wyk de Vries B (2001) The 1998 debris avalanche at Casita volcano, Nicaragua-investigation of structural deformation as the cause of slope instability using remote sensing. Journal of Volcanology and Geothermal Research 105(1-2):49-63, doi:10.1016/S0377-0273(00)00244-4

Kervyn M, Ernst GGJ, van Wyk de Vries B, Mathieu L, Jacobs P (2009) Volcano load control on dyke propagation and vent distribution: Insights from analogue modelling. Journal of Geophysical Research 114:B03401, doi:10.1029/2008JB 005653

Komorowski JC, Boudon G, Semet M, Villemant B, Hammouya G (2002) La Soufriére de Guadeloupe: une histoire d'effondrements sectoriels récurrents et de fluides hydrothermaux acides: Quo vadimus? = La Soufrière of Guadeloupe: repetitive sectorial collapses and acide hydrothermal fluids : Quo vadimus? Réunion des Sciences de la Terre, Nantes: 9-12

Komorowski JC, Boudon G, Semet M, Beauducel F, Anténor-Habazac C, Bazin S, Hammouya G (2005) Guadeloupe. In: JM Lindsay, REA Robertson, JB Shepherd & S Ali (Eds), Volcanic Atlas of the Lesser Antilles, Seismic Research Unit, The University of the West Indies, Trinidad and Tobago, WI:65-102

Krom AHM, Bakker A, Koers RWJ (1997) Modelling hydrogen-induced cracking in steel using a coupled diffusion stress finite element analysis. The International Journal of Pressure Vessels and Piping 72(2):139-147(9)

Lachassagne P, Marechal JC, Sanjuan B (2009) Hydrogeological model of a high-energy geothermal field (Bouillante area, Guadeloupe, French West Indies). Hydrogeology Journal 17:1589–1606

Lagmay AMF, van Wyk de Vries B, Kerle N, Pyle DM (2000) Volcano instability induced by strike-slip faulting. Bulletin of Volcanology 62:331-346, doi: 10.1007/s00445 0000103

Le Mouel JL, Pozzi JP, Rossignol JC, Feuillard M (1979) Levé aéromagnétique de l'archipel de la Guadeloupe, Description et implications tectoniques = Airborn Magnetic study of Guadeloupe archipelago, description and tectonic implications. Annales de Géophysique 31:531–548

Le Friant A (2001) Les Déstabilisations de flanc des volcans actifs de l'arc des Petites Antilles : origines et conséquences = Sector collapses of Lesser Antilles Arc : origin and consequences. PhD thesis, Paris 7 René Diderot university

Le Corvec N, Walter TR (2009) Volcano spreading and fault interaction influenced by rift zone intrusions: Insights from analogue experiments analyzed with digital image correlation technique. Journal of Volcanology and Geothermal Research 183(3-4):170-182, doi: 110.1016/j.jvolgeores.2009.1002.1006

Lopez S, Bouchot V, Lakhssassi M, Calcagno P, Grappe B (2010) Modelling of Bouillante geothermal field (Guadeloupe, French Lesser Antilles). Proceedings, 35th workshop on geothermal reservoir engineering, Stanford University, Stanford, California, SGP-TR-1988

Manton WI (1987) Tectonic interpretation of the morphology of Honduras. Tectonics 6:633-651

Marzoli A, Piccirillo EM, Renne PR, Bellieni G, Iacumin M, Nyobe JB, Tongwa AT (2000) The Cameroon line revisited: Petrogenesis of continental basaltic magmas from lithospheric and asthenospheric mantle sources. Journal of Petrology 41:87-109

Mathieu L, van Wyk de Vries B, Holohan EP, Troll VR (2008) Dykes, cups, saucers and sills: Analogue experiments on magma intrusion into brittle rocks. Earth and Planetary Science Letters 271(1-4):1-13, doi:10.1016/j.epsl.2008.02.020

Maury RC, Westbrook GK, Baker PE, Bouysse P, Westercamp D (1990) Geology of the Lesser Antilles. In: Dengo G and Case JE (eds.), The Caribbean region, The Geology of North America, Geological Society of America H(5):141-166

McCurry P (1971) Pan-African orogeny in Northern Nigeria. Geological Society of America Bulletin 82(11):3251-3262

McGuire WJ, Pullen AD (1989) Location and orientation of eruptive fissures and feederdykes at Mount Etna; influence of gravitational and regional tectonic stress regimes. Journal of Volcanology and Geothermal Research 38(3-4):325-344, doi:10.1016/0377-0273(89)90046-2

Merle O, Borgia A (1996) Scaled experiments of volcanic spreading. Journal of Geophysical Research 101(B6):13805-13817

Merle O, Lénat JF (2003) Hybrid collapse mechanism at Piton de la Fournaise volcano, Reunion Island, Indian Ocean. Journal Geophysical Research 108(B3):2166, doi:2110.1029/ 2002JB002014

Merle O, Vendeville B (1994) Experimental modelling of thin-skinned shortening around magmatic intrusions. Bulletin of Volcanology 57(1):33-43, doi:10.1007/BF0029 8705

Merle O, Vidal N, de Vries BV (2001) Experiments on vertical basement fault reactivation below volcanoes. Journal of Geophysical Research 106(B2):2153-2162

Merle O, Barde-Cabusson S, van Wyk de Vries B (2009) Hydrothermal calderas. Bulletin of Volcanology 72(2):131-147, doi:10.1007/s00445-009-0314-6

Meyers JB, Rosendahl BR (1991) Seismic-reflection character of the Cameroon Volcanic Line - Evidence for uplifted oceanic-crust. Geology 19(11):1072-1076

Meyers JB, Rosendahl BR, Harrison CGA, Ding ZD (1998) Deep-imaging seismic and gravity results from the offshore cameroon volcanic line, and speculation of African hotlines. Tectonophysics 284(1-2):31-63

Moore JG, Rice CJ (1984) Chronology and character of the may 18, 1980, explosive eruptions of Mount St Helens. In: Explosvie volcanism: inceptions, evolution and hazards, National academy press (ed.), chapter 10, pp. 133

Moreau C, Regnoult JM, Deruelle B, Robineau B (1987) A new tectonic model for the Cameroon Line, Central-Africa. Tectonophysics 141(4):317-334

Moriya I (1980) Bandaian eruption and landforms associated with it. Collection of articles in memory of retirement of Prof. K. Hishimura, Tohoku University 66:214–219

Murray JB, Guest JE (1982) Vertical ground deformation on Mount Etna, 1975-1980. Geological Society of America Bulletin 93(11):1160-1175, doi: 1110.1130/0016-7606

Nakamura K (1977) Volcanoes as possible indicators of tectonic stress orientation-principle and proposal. Journal of Volcanology and Geothermal Research 2(1):1-16, doi:10.1016/0377-0273(77)90012-9

Naylor MA, Mandl G, Sijpesteijn CHK (1986) Fault geometries in basement-induced wrench faulting under different initial stress states. Journal of Structural Geology, 8:737-752

Nkoumbou C, Déruelle B, Velde D (1995) Petrology of Mt Etinde nephlinite series. Journal of Petrology 36:373-395

Norini G, Lagmay AMF (2005) Deformed symmetrical volcanoes. Geology, 33(7):605-608, doi: 10.1130/G21565.1

Norini G, Capra L, Groppelli G, Lagmay AMF (2008) Quaternary sector collapses of Nevado de Toluca volcano (Mexico) governed by regional tectonics and volcanic evolution. Geosphere 4(5):854-871, doi: 10.1130/GES00165.1

Piper JDA, Richardson A (1972) Palaeomagnetism of Gulf of Guinea Volcanic Province, West-Africa. Geophysical Journal of the Royal Astronomical Society 29(2):147-171

Popoff M (1988) From Gondwana to the South-Atlantic - Connections between the Benue Through and the basins of northeastern Brazil from the Precambrian to the opening of the Gulf of Guinea in the early Cretaceous. Journal of African Earth Sciences 7:409-431

Poussineau S (2005) Dynamique des magmas andésitiques: approche expérimentale et pétrostructurale; application à la Soufrière de Guadeloupe et à la Montagne Pelée = Andesitic magma dynamic : experimental and petrostructural study applied to the Soufrière of Guadeloupe and to the Montagne Peléé. PhD thesis, Orléans university, 295 p.

Reyment RA (1954) The stratigraphy of the Southern Cameroon. Geologiska Foreningens Handling Board 76:661-683

Roest WR, Collette BJ (1986) The Fifteen Twenty Fracture Zone and the North American–South American plate boundary. Journal of the Geological Society 143(5):833-843, doi:10.1144/gsjgs.143.5.0833

Roman-Berdiel T, Gapais D, Brun JP (1995) Analogue models of laccolith formation. Journal of Structural Geology 17(9):1337-1346

Rowland SK, Garbeil H (2000) The slopes of oceanic basalt volcanoes. In: Mouginis-Mark PJ, Crisp J, Fink J (eds.) Remote sensing of active volcanism, pp 223-247

Samper A (2007) Etude géochronologique, aspects géomorphologiques et géochimiques du volcanisme de l'île de Basse Terre (Guadeloupe), et datation des structures d'effondrement de flanc majeures de l'Arc des Petites Antilles = Geochronological, geomorphological and geochemical study of Basse Terre Island volcanoes ; and dating of collapse structures of the Lesser Antilles Arc. PhD thesis, Paris Sud-Paris XI university

Sanjuan B, Le Nindre YM, Menjoz A, Sbai A, Brach M, Lasne E (2004) Travaux de recherche liés au développement du champ géothermique de Bouillante (Guadeloupe) = Research on the Bouillante geothermal field. Report n° BRGM/RP-53136-FR, BRGM, Orleans, France

Sanjuan B, Traineau H (2008) French West Indies: Development of the Bouillante geothermal field in Guadeloupe. IGA News 73:5-9

Schellart WP (2000) Shear test results for cohesion and friction coefficients for different granular materials: scaling implications for their usage in analogue modelling. Tectonophysics 324(1-2):1-16

Schmid R (1981) Descriptive nomenclature and classification of pyroclastic deposits and fragments. Geologische Rundschau 70(2):794-799

Suh CE, Sparks RSJ, Fitton JG, Ayonghe SN, Annen C, Nana R, Luckman A (2003) The 1999 and 2000 eruptions of Mount Cameroon: Eruption behaviour and petrochemistry of lava. Bulletin of Volcanology 65:267-281

Sylvester AG (1988) Strike-slip faults. Geological Society of America Bulletin 100(11): 1666-1703, doi: 10.1130/0016-7606(1988)

Tabod CT, Fairhead JD, Stuart GW, Ateba B, Ntepe N (1992) Seismicity of the Cameroon Volcanic Line, 1982-1990. Tectonophysics 212:303-320

Thinon I, Bitri A, Guennoc P, Truffert C (2004) Levés sismique et magnétiques du plateau occidental de l'île de Basse-Terre, Guadeloupe (campagne GEOBERYX03), Apport à la compréhension du contexte structural du champ de Bouillante = Sismic and Magnetic of western Basse-Terre (campaign GEOBERYX03), Implications for the structure of Bouillante geothermal field. BRGM/RP-53152-FR, BRGM report, Orleans, France

Thinon I, Guennoc P, Bitri A, Truffert C (2010) Study of the Bouillante Bay (West Basse-Terre Island shelf): contribution of geophysical surveys to the understanding of the structural context of Guadeloupe (French West Indies - Lesser Antilles). Bulletin de la Société géologique de France,181(1):51-65

Thinon I, Guennoc P, Bitri A, Truffert C (2010) Study of the Bouillante Bay (west Basse-Terre Island shelf): contribution of geophysical surveys to the understanding of the structural context of Guadeloupe (French West Indies-Lesser Antilles). Bulletin de la société géologique de France 181(1):51-65

Tibaldi A (2008) Contractional tectonics and magma paths in volcanoes. Journal of Volcanology and Geothermal Research 176:291-301

Traineau H, Sanjuan B, Beaufort D, Brach M, Castaing C, Correia H, Genter A, Herbrich B (1997) The Bouillante geothermal field (F.W.I) revisited: new data on the fracture geothermal reservoir in light of a future simulation experiment in a low productive well. Proceeding 22nd Workshop on Geothermal Reservoir Engineering, Stanford University, SGP-TR-155

Ubangoh RU, Ateba B, Ayonghe SN, Ekodeck GE (1997) Earthquake swarms of Mt Cameroon, West Africa. Journal of African Earth Sciences 24(4):413-424

USGS-a website - http://seamless.usgs.gov/

USGS-b website - https://lpdaac.usgs.gov/

Van Bemmelen RW (1949) The Geology of Indonesia: General Geology of Indonesia and Adjacent Archipelagos. Gov. Print. Off., The Hague, Netherlands

van Wyk de Vries B (1993) Tectonics and Magma Evolution of Nicaraguan Volcanic Systems. PhD thesis, Open University, 328 p.

van Wyk de Vries B, Merle O (1996) The effect of volcanic constructs on rift fault patterns. Geology 24(7):643-646

van Wyk de Vries B, Merle O (1998) Extension induced by volcanic loading in regional strike-slip zones. Geology 26:983-986

van Wyk de Vries B, Matela R (1998) Styles of volcano-induced deformation: Numerical models of substratum flexure, spreading and extrusion. Journal of Volcanology and Geothermal Research 81:1-18

van Wyk de Vries B, Kerle N, Petley D (2000) Sector collapse forming at Casita volcano, Nicaragua. Geology 28(2):167-170

Viruete JE, Contreras F, Stein G, Urien P, Joubert M, Ullrich T, Mortensen J, Perez-Estaun A (2006) Transpression and strain partitioning in the Caribbean Island-arc : Fabric development, kinematics and Ar-Ar ages of syntectonic emplacement of the Loma de Cabrera batholith, Dominican Republic. Journal of structural geology 28(8): 1496-1519

Wadge G (1986) The dykes and structural setting of the volcanic front in the Lesser Antilles island arc. Bulletin of Volcanology 48:349-372

Walker GPL (1988) Three Hawaiian calderas: an origin through loading by shallow intrusions. Journal of Geophysical Research 93:714,773-714,784

Weber JC, Dixon TH, DeMets C, Ambeh W, Jansma P, Mattioli G, Saleh J, Sella G, Bilham R, Pérez O (2001) GPS estimate of relative motion between the Caribbean and South American plates, and geologic implications for Trinidad and Venezuela. Geology 29(1):75–78

Westercamp D (1980) Une méthode d'évaluation et de zonation des risques volcaniques à la Soufriére de Guadeloupe, Antilles Françaises = Evaluation of volcanic Risks in Guadeloupe, La Soufrière volcano, Lesser Antilles. Bulletin of Volcanology 43:431-452

Westercamp D, Tazieff H (1980) Martinique-Guadeloupe-Saint-Martin-La Désirade. In: Guides Géologiques Régionaux. Masson (ed.), Paris, 135 p.

Wilson M, Guiraud R (1992) Magmatism and rifting in Western and Central Africa, from late Jurassic to recent times. Tectonophysics 213:203-225

Wooller LK, Murray J, Rymer H, van Wyk de Vries B (2003) Volcano Instability and Collapse from Basement Faulting. in EGS - AGU - EUG Joint Assembly, pp. 00304

Zogning A (1988) Le Mont Cameroun, un volcan actif: contribution à l'étude de géographie physique appliquée = Mt Cameroon, an actif volcano : contribution to the applied physical geography. PhD Thesis, University of Yaoundé.

Appendix A: glossary

-**Accretionnary lapilli**: Accretionnary lapilli develop in an eruption column or cloud by accretion of concentric moist ash layers around a nucleus, which is usually a lithic. The water necessary for their formation comes either from the atmosphere or from the erupted material (e.g. hydrovolcanic eruptions).

-**Andesite**: Calcalcaline rocks are named basalts ($SiO_2 < 53$ %), andesites (53 % $< SiO_2 < 62$ %), dacite (62 % $< SiO_2 < 68$ %) and rhyolites ($SiO_2 > 68$ %). The rocks erupted by Basse Terre and Maderas volcanoes are dominantly andesites and contain phenocrysts of pyroxene and feldspar.

-**Block and ash flow**: Block and ash flows are pyroclastic flows originating from the partial destruction of a growing dome. They are low energy flows channelised in valley ("Merapi type") or high energy surge and directed blasts ("Pelée type").

-**Debris flows and lahars**: A debris flow is a dense flow, which remobilises pyroclastic deposits during or shortly after their deposition, or can be due to slow erosion. The instability of mobilised rocks and their high water content are the main triggering processes of these flows, which usually occur during the rain season. The gravity controls the movement of the flow, which is channelised by a valley. It deposits its largest elements (debris flow deposit) and evolves into a lahar (figure A-01-a) and stream flow deposit.

A debris flow deposit is made of angular to slightly rounded blocks, decimetric to metric in size, embedded in a limited to absent thin matrix (figure A-01-b). A lahar deposit contains smaller blocks, an abundant thin muddy matrix and is capped by a thin (about 5-10 cm thick) muddy horizon. The sorting is absent to poor. The blocks have usually various compositions.

A debris avalanche corresponds to a large sector collapse triggered by an eruption ("St Helens type") or not ("Bezimianny type"). The deposits got a much larger extent than those of debris flows or lahars (e.g. 11,500 BP and 3,100 BP events in Guadeloupe).

-**Dyke**: A dyke is a small-scale sub-vertical magma intrusion. Its thickness is small when compared to its length and height. Flat to dipping intrusions are called sills or cone-sheets. Thicker intrusions may be called plugs, necks, chimney or crypto-dome depending of their morphology and origin.
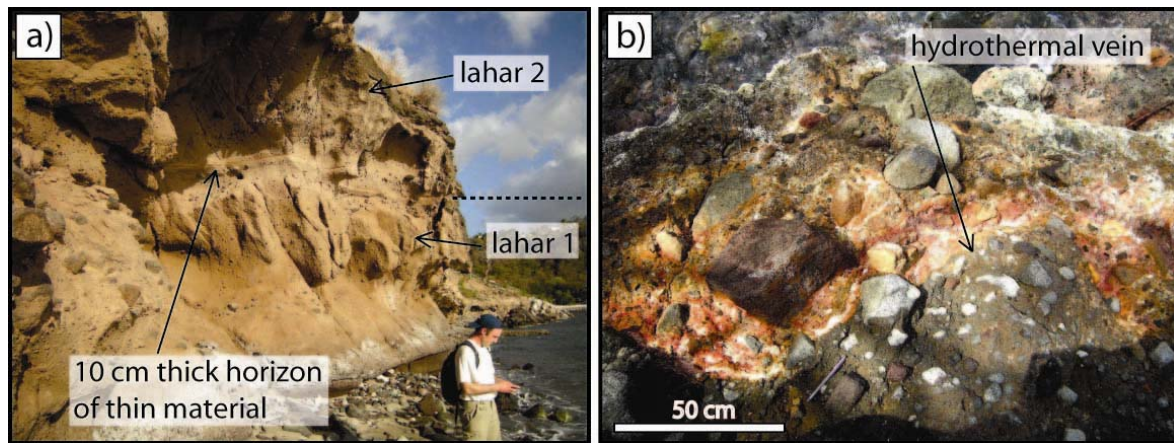
Figure A-01: a) Picture of two successive lahars (Petite bay, Guadeloupe); b) Debris flow altered by hydrothermal circulation (Rocroy beach, Guadeloupe).

-Eruptive regime – continuous: This regime forms a vertical column, which is fed for several hours to days (Plinian eruption) and produces fallout deposits. At the end or during the eruption, the column collapses and produces pyroclastic flows, which emplace on top of fallout deposits. The column usually collapses several times and forms pyrocalstic deposits interbedded with fallout deposits. The deposits contain ash and vesiculated pyroclasts (pumice and scoria).

-Eruptive regime – instantaneous: This regime corresponds to a single explosion, which produces a vertical column (called Vulcanian type if the volume of emitted material is large). The column collapses immediately. The deposit contains ash and juvenile pyroclasts more or less vesiculated. Bombs and xenoliths are usually abundant.

-Eruptive regime – intermittent: This regime corresponds to successive explosions projecting pyroclasts vertically. Hydrovolcanic eruptions are intermittent and may produce a huge variety of deposits: pyroclastic flows, fallout, basal surges (column collapses, e.g. Surtseyan dynamism) and proximal projections of hyalotuffs and cauliflower bombs (e.g. maar for example).

-Fallout: A fallout is a pyroclastic deposit formed by the setting of material projected in the air by a volcanic eruption. Fallout deposits are also called tephra deposits. An accumulation of scoria, bombs, lapilli and ash produced by a stromblian dynamics (e.g. scoria cone) and an accumulation of welded scoria (Hawaiian dynamics) are proximal deposits. Further from the vent, the size of pyroclasts decreases and layering develops. Distal fallout blankets the relief,

the pyroclasts are well sorted and the thickness of the deposit decreases exponentially as the distance from the vent increases. Such deposits are usually cold and correspond to the deposition of plume dispersed pyroclasts such as pumice, ash and accretionnary lapilli.

-**Grain size:** According to Fisher 1961-1966 (e.g. Schmid 1981) a pyroclast smaller than 2 mm is called ash. A lapilli is 2 to 64 mm sized and bigger grains are called bombs or blocks. A similar classification is used for sedimentary deposits for which the clasts are named, from the fine to coarser: clay, sand and blocks.

-**Hydrovolcanism:** Hydrovolcanic eruptions are volcanic eruptions in which superficial or ground water is involved and increases the fragmentation of the magma. A large amount of water (e.g. sub-marine eruption) prevents explosions and fragments the outer surface of lava flows (e.g. pillow lava) to from hyaloclasts. A smaller amount of superficial water, which may come form a lake, a river, shallow sea or from ground water (e.g. phreatomagmatic eruptions) increases the violence of the eruption and produces hyalotuff deposits. A hyalotuff is a fragmented magma deposit with glassy (quenched) pyroclasts.

-**Lava flows**: Basse Terre Island lava flows have a massive heart 1 m to tens of meters thick surrounded by a coarse breccia, which corresponds to the solidified outer part of the flow brecciated by the movement of the inner un-solidified lava (figure A-02-a). This breccia may be absent (pahoehoe, fluid flows rare in Guadeloupe), thinner than the massive heart ("aa" flows for example) to much thicker than the massive part ("aa" flows, blocky flows which are infrequent in Guadeloupe). Lava flows may be chanalised by their levées, which are accumulations of brecciated lava located on each side of the flow or restricted in valleys.

The massive heart has either a uniform texture or is layered (flow bending texture) and its outer margin is vesiculated. The breccia is made of vesiculated red lava blocks with an angular outer margin (scoria). Many Guadeloupean outcrops correspond to weathered flows, which may consist of slightly altered lava with a red taint or to intensely weathered flows turned into white clay. These latter flows do not contain recognisable phenocrysts but may have conserved their structures such as their cooling joints.

Cooling joints form in a flow as it cools. They rarely have a well defined polygonal shape (columns) in Guadeloupe and are usually rare, randomly orientated and irregularly spaced fractures. The closely spaced parallel fractures develop in most lava flows parallel to their margin: they are horizontal fractures at the base and at the top of a flow and are sub-vertical at its margins.

-Pyroclast: A pyroclast is a particle or a block which has been fragmented by an explosive eruption. It corresponds either to erupted magma (juvenile material such as ash, pumice, scoria, etc.) or to an older substratum fragmented by an eruption (accessory such as cooled lava flow, domes, etc. or accidental such as crystalline basement, sedimentary horizon).
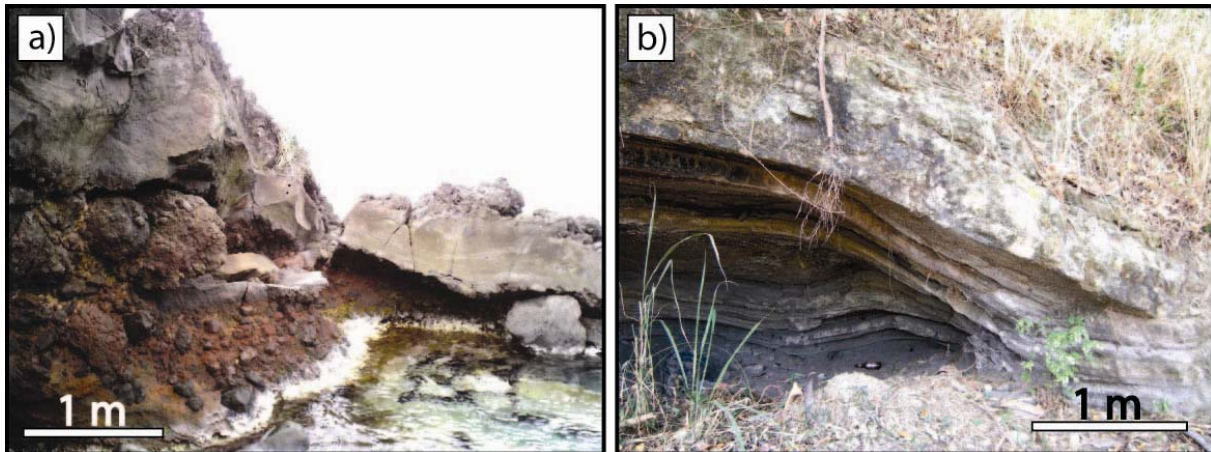
Figure A-02: a) Lava flow with its scoriaceous red breccia (bottom) and its massive heart (Grande bay, Guadeloupe); b) Surge deposit (Courbaril town, Guadeloupe).

-Pyroclastic deposit: It is a primary deposit formed by an eruption. Once such a deposit is modified by a sedimentary process it is called a reworked pyroclastic deposit, if it has been little transported and a debris flow, a lahar or other if the reworking process has been more intense. Pyroclastic deposits may originate form the auto-breccification of the surface of a dome or of sub-aerial (e.g. lava flow breccia) or sub-marine lava flows (hyaloclastites developing around pillow lava). They may also have been ejected in an intermittent, continuous or lateral way by a more violent volcanic eruption.

-Pyroclastic flow: Pyroclastic flows are chanalised by valleys, are poorly to un-sorted and form at high temperature (welded and oxidized deposits containing charcoal). The thickness of the deposits vary greatly and in an irregular way. A flow is made of a basal dense and concentrated horizon flowing in a laminar regime and is capped by a turbulent ash cloud ("ash cloud surge") which develops from the basal horizon. The deposit consists in a lower unit containing mostly blocks (sometimes of a large size) and few thin particles. It is poorly to well sorted and may overlie a thin basal bed. The upper ashy unit is a surge and/or fallout deposit.

-Pyroclastic surge: A surge is a high energy, turbulent and little concentrated flow. It blankets the relief but is thicker in depressions. Its thickness is irregular and a basal erosion may develop (channels are observed). It deposits when the energy decreases and it has a wavy structure similar to the cross-bedding of sedimentary deposits (figure A-02-b). A basal bed containing rocks pulled up from the substratum may be individualised. It develops on top of a pyroclastic flow ("ash cloud surge"), in front of a pyroclastic flow ("ground surge"), from the collapse of an eruptive column or from a hydrovolcanic eruption.

-Rift zone: long-lived volcanic feature characterized by a vent alignment at the surface and intense dyke emplacement along fractures at depth.

-Scoria cone: A scoria cone is a conical accumulation of scoria (vesiculated lava blocks) and thin lava flows (strombolian activity). It is called a monogenic edifice (built by a single eruption) and an adventive vent (part of a composite volcano).

-Rootless vent: Unroofed vents develop on top of a lava flow which comes in contact with water (sea water for example). These scoria cones are not feed by a dyke injection (rootless). They originate from the vaporisation of water heated by the lava.

-Veins: In Guadeloupe, the deposits contain white veins (fractures filled with zeolith minerals) corresponding to superficial fluid circulation. For example, some of the lava flows contains zeolith and quartz minerals located in veins, in vesicles and around blocks and which have formed following the circulation of hot water in an uncooled lava flow. A large variety of minerals (calcite, quartz, sulphurs, feldspars) develop within veins or in a diffuse manner in part of the rock in a geothermal field (e.g. Bouillante bay, Malendure Point, Rocroy beach, La Soufrière and Les Mamelles domes; figure A-01-b).

Appendix B: map of the Northern Chain, Guadeloupe
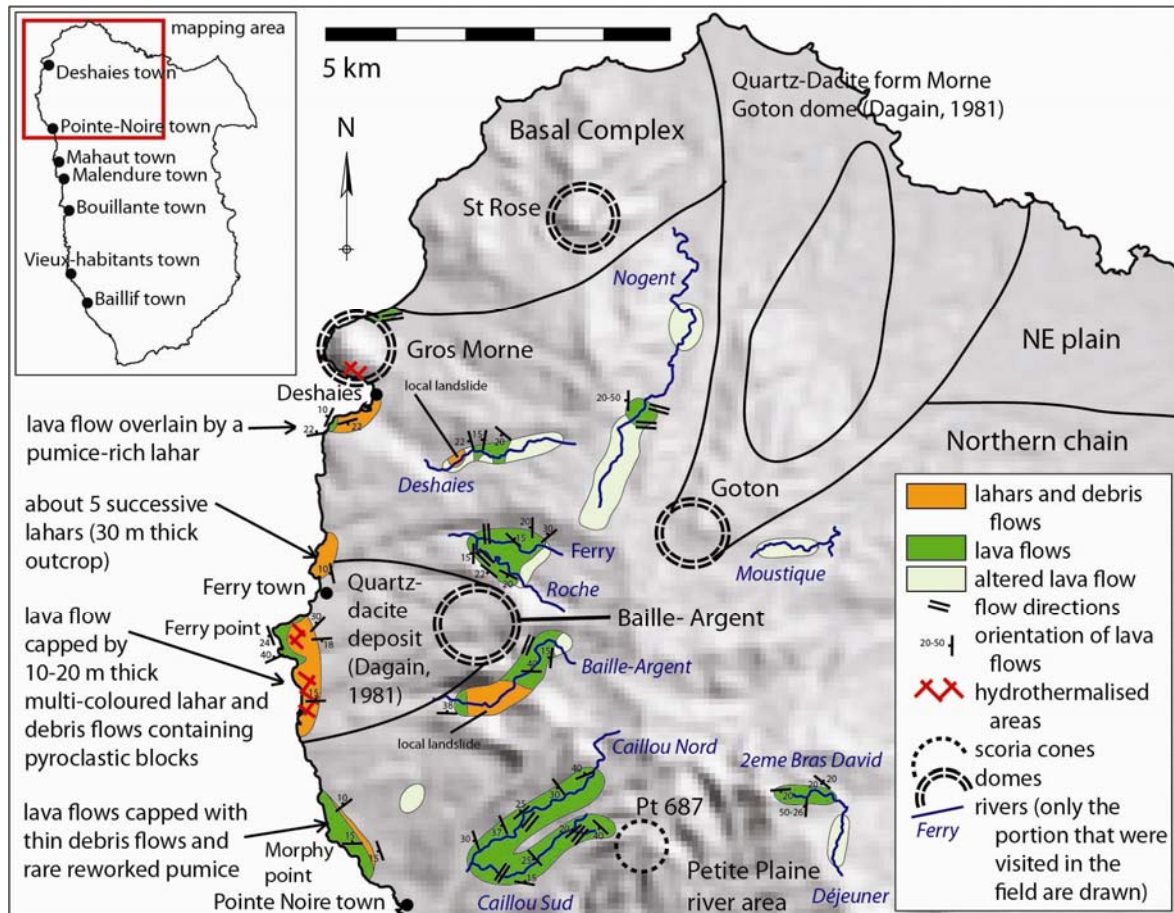
Figure B-01: Map presenting the geology of northern Basse Terre Island and the area visited during this study (rivers and shore line). The domes and their associated deposits, the Basal Complex and the Northern Chain geological units are drawn after Dagain (1981). The topography is a hill shade map of the SRTM (sun elevation= 45°, azimuth= 045).

Explanatory notes:

-Weathered lava flows: white clay rocks, which are usually observed upstream where the river is not large enough to deeply incise the weathered substratum to expose fresh rocks. A 2 m thick weathered lava flow capped by fresh flows is observed downstream in the Deshaies valley.

-**Fresh lava flows:** massive andesite lava and scoriaceous breccias, which are found in the Baille-Argent River (one outcrop) and in Cailloux Nord and Sud Rivers. The lava flows are 15 to 20 m thick (Grande Ferry canyon and Baille-Argent River), 30 m thick (one outcrop exposed by a waterfall in 2$^{\text{éme}}$ Bras David River) and 5 to 20 m thick (Caillou rivers).

-**Lahars and debris flows:** In the rivers, these deposits have a limited extend and are made of lava blocks embedded in a non-abundant orange matrix. The Deshaies River 30 m-thick debris flow contains some centimetre-long lava blocks embedded in a white clay matrix.

A 20 m-thick lahar with pumice and lava blocks at its base is found in Deshaies town. The Ferry town lava flows are covered by multi-coloured deposits (Ferry point) containing occasionally blocks of pyroclastic deposits (south of Ferry point) and which are 30 m thick (Ferry town) to 2-5 m thick (Morphy point).

Appendix C: map of the southern Northern Chain, Guadeloupe
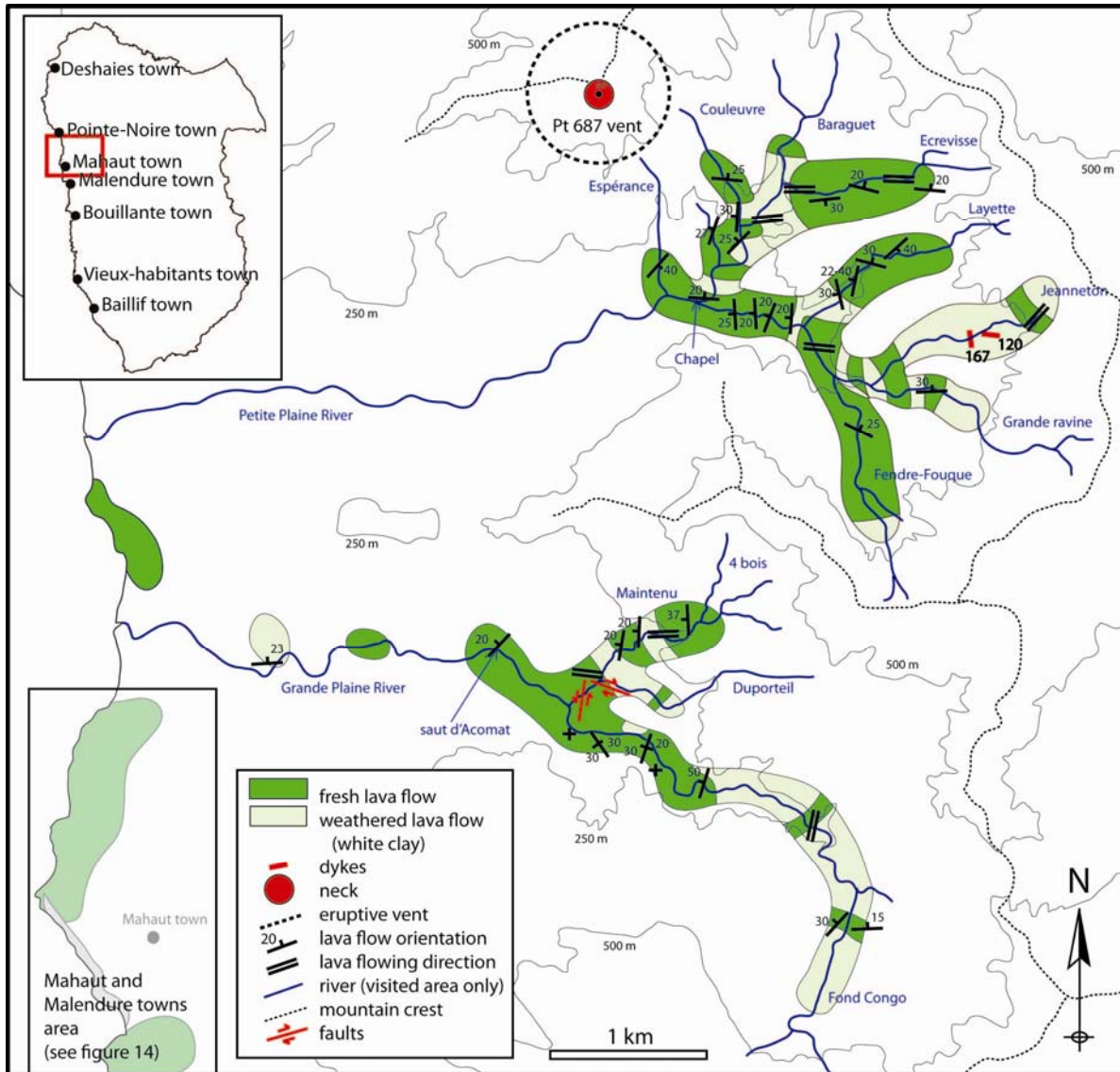
Figure C-01: Map of the geological units observed in Petite and Grande Plaine rivers. The contour levels (every 250m) are from the IGN map (1:25,000).

Explanatory notes:

-Weathered lava flows: white clay rocks, which are usually observed upstream. A 7 m thick weathered lava flow capped by fresh flows is observed downstream in the Petite Plaine valley.

-Fresh lava flows: massive andesite lava flows.

-Dykes: The Jeanneton River contains two 20 cm thick dykes, which strike 120 and 167/55NE.

-P^{t}687 vent: The P^{t}687 peak located north of Esperance River (Petite Plaine valley), is a cylindrical peak of massive lava exhibiting a vertical columnar jointing that has been observed from a distance of 1 km. It likely corresponds to the neck of the eruptive vent observed in 1966 by De Reynal. The 5 to 8 m thick "aa" lava flows located upstream in the Caillou Sud River may have been emitted by the P^{t}687 vent.

Appendix D: map of the Mahaut town area, Guadeloupe
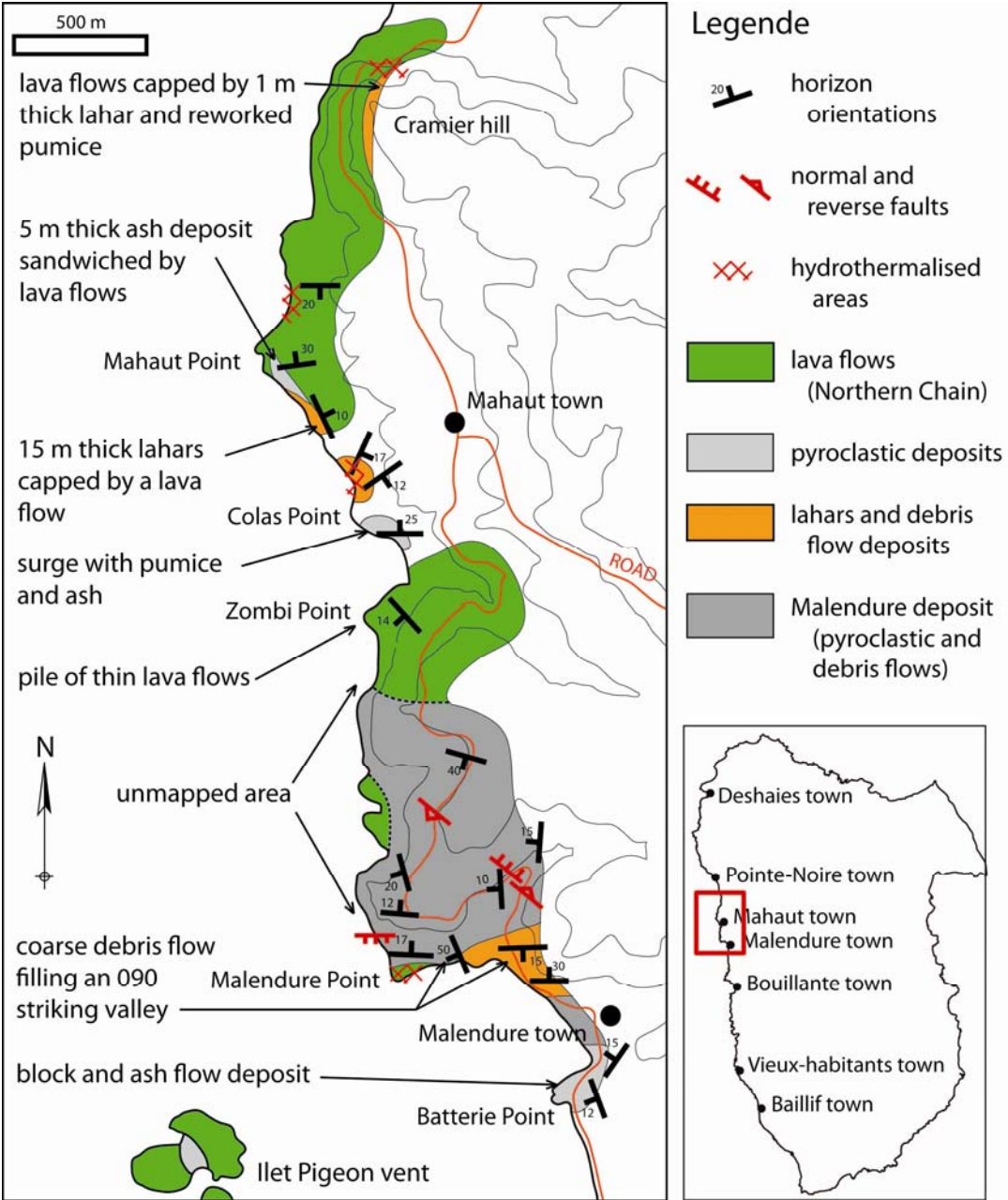
Figure D-01: Geological map of the shore line between Malendure and Mahaut towns. The topography (every 50 m) is redrawn from the IGN map (1:25,000).

Explanatory notes:

-lava flows: < 5 m thick massive lava outcrops capped by colluviums, reworked pumice (Cramier hill) and by the Malendure deposit. The alternation of 1-2 m thick scoriaceous breccias and massive lava horizons with olivine, pyroxene and feldspar phenocrysts of Zombi point has been emitted by a nearby vent or corresponds to the front of a lava field.

-Ilet Pigeon vent: The two small Pigeon islands are located 1 km offshore and west of Malendure Point. This conical edifice (from bathymetry data) is made of lava with phenocrysts of feldspar and pyroxene.

-pyroclastic deposits: These deposits are layered ash deposits (fallout) and lahars sandwiched by lava flows (Mahaut Point). A surge deposit is located at Colas point. A 5 m thick deposit containing horizons of ash, pumice and rare lithics (Appendix H-f) caps the lava of the Ilet Pigeon vent. This deposit has a sub-horizontal layering which moulds the substratum. I interpret these rocks as a fallout deposit, which is possibly part of the Malendure deposit (see next section).

-Malendure deposit:

1) Basal pyroclastic flow deposit: 10 m thick, locally wavy ash-rich deposit containing horizons of lava lapilli and pumice (Malendure Point). One of the pumice horizons is observed to erode the lowermost ash horizon.

2) fallout: The base of this 5 m thick fallout deposit contains a discontinuous pumice horizon, has locally a wavy structures and is interpreted as an ash cloud surge deposit (Malendure point).

3) debris flow: 10 m and 20 m thick deposits made of cm to m long lava blocks and clay. In the northern part of the Malendure Bay, coarse debris flows, locally varicoloured and channelled by 090 striking valleys, are found. These late deposits erode and cap the Malendure deposit.

4) block and ash flow: 20 m thick deposit made of lava blocks of homogeneous composition (e.g. lava with pyroxene and feldspar phenocrysts) and which contain 0.8-1 m thick pumice and pink ash horizons (Malendure town).

The Malendure point deposit is made, from base to top, of horizons (1), (3), (2) and (3) (cf. Appendix H-e).

Appendix E: map of the Bouillante area, Guadeloupe
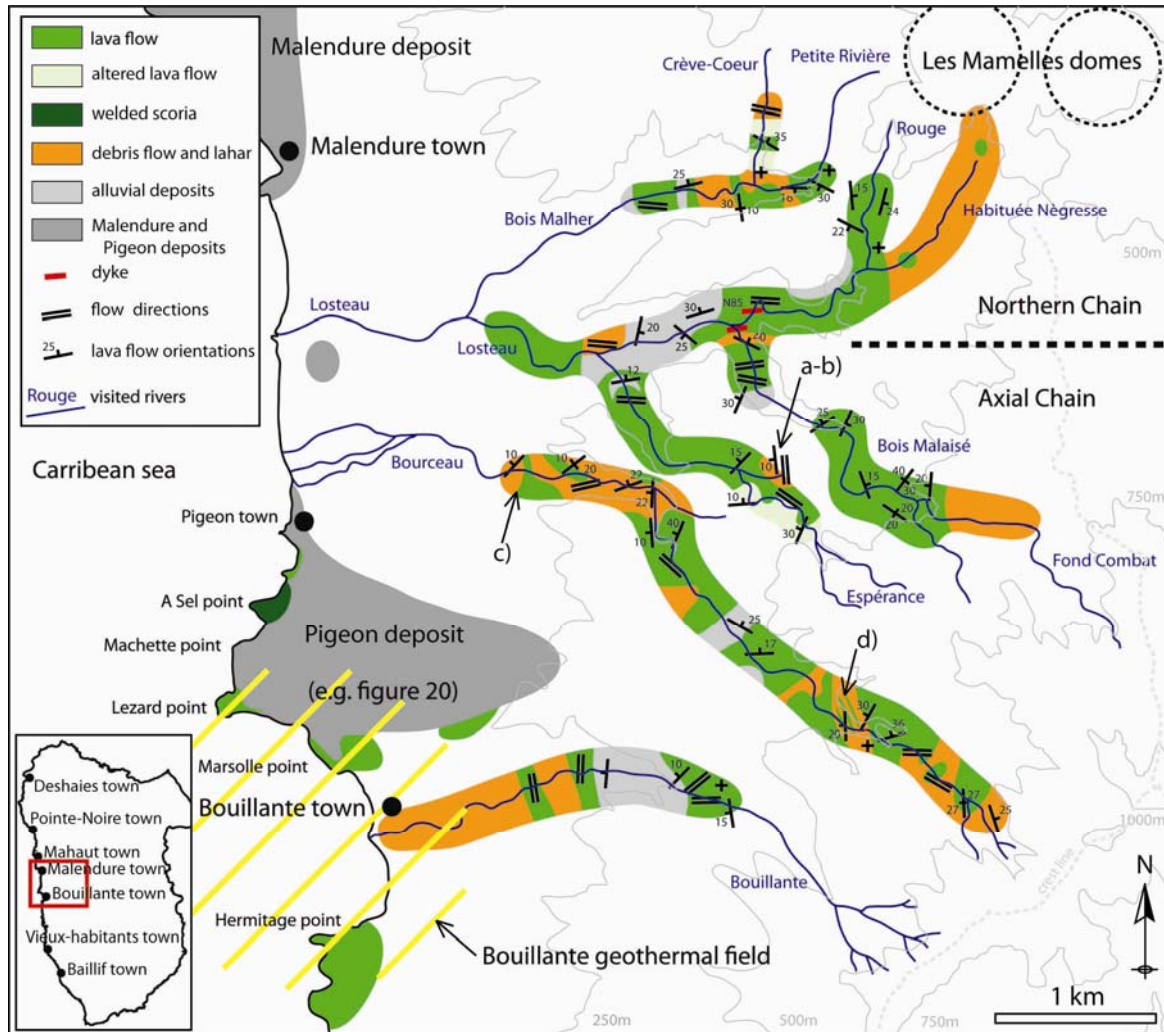
Figure E-01: Geological map of the Bouillante area. Topography redrawn from the IGN map (1:25,000). The a) to d) signs locate the pictures of figure 11.

Explanatory notes:

-lava flows: massive and scoriaceous lava, which are ~ 10 m (Bois Malher and Crève-Coeur rivers), at least 30 m to 5-10 m downstream (Rouge River), 5-20 m (Bois Malaisé River) and 1.5-2 m (Bourceau River) thick.

-alluvium: Up to 20 m thick alluvial deposits made of cross-bedded muddy sand horizons are located above the lava flows of Losteau River. This river is flowing over a flat land where it is able to deposit the sediments it carries. A 1 m and a 2 m thick backed sandy mud horizons and an at least 10 m thick alluvium deposit are sandwiched (Losteau and Espérance rivers) and topped (Bouillante River) by lava flows.

-debris flows: The Habituée Négresse River debris flows, and the 5 m-thick outcrop of varicoloured clay containing blocks of weathered and fresh lava found at the junction between the Espérance and Losteau rivers, may originate from the erosion of the nearby Les Mamelles domes. The outcrops of Fond Combat River are covered by an at least 7 m thick landslide deposit made of cross-cutting filled channels and in which sharp contacts between a pink and a grey clay matrix are observed. The downstream part of Bouillante River contains a coarse debris flow capped by a 50 m thick pile of lahars, which have reworked a pyroclastic deposit.

-debris flows and lava flows alternation: The 60 m high waterfall encountered upstream in Espérance River provides a section into a 30 m-thick debris flow deposit located on top of a 7 m thick scoriaceous lava flow breccias. The top of the debris flow is eroded by a valley confined lava flow. The Bourceau River cuts in an alternation of debris flows, alluvial deposits and lava flows. Upstream Bourceau River, a cliff exhibits 3 to 7 m thick debris flows interbedded with 1.5 to 15 m-thick lava flows and downstream, the debris flows alternate with at least three 5 to 20 m thick lava flows and a 30 m-thick layered lahar (alternation of blocky horizons embedded in a muddy sand matrix) is found below a 20 m thick lava flows.

-dykes: A 3 m and a 1.5 m thick dykes striking 085 and containing olivine, pyroxene and feldspar phenocrysts are found at the junction between the Losteau and Bois Malaisé rivers. The dykes are surrounded by 090 striking fault zones

Appendix F: map of the Bouillante town area, Guadeloupe
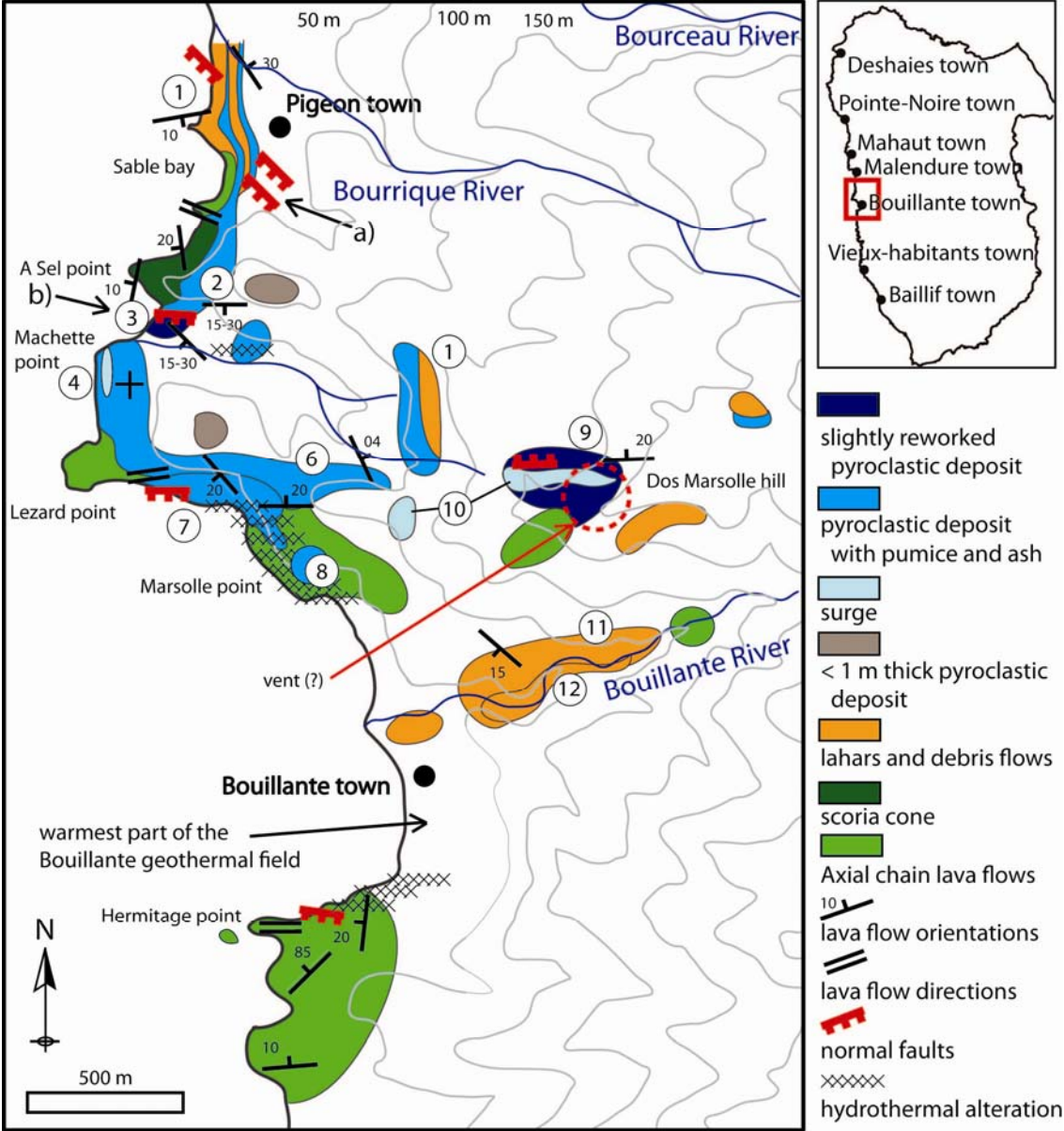
Figure F-01: Geological map of the Pigeon deposit. The topography is redrawn from the IGN map (1:25,000); The geological units numbered from 1 to 12 are described in the table F-01; The letters a) to b) locate the pictures of figure 19.

Explanatory notes:

-lava flows: North of the Bouillante Bay, the lava flows contain many open fractures filled with clastic sediments (lava blocks embedded in a yellow matrix). Hydrothermally altered lava containing feldspar and pyroxene phenocrysts are found at Marsolle and Hermitage points. The outer margin of a thick lava flow is found at Lézard point. The block flow of Dos Marsolle hill contains bombs and may be located a few meters away from its eruptive vent. The 1.12 Ma old Lézard Point and the 0.97 Ma old Marsolle Point (Fabriol 2001) lava flows belong to the Axial Chain.

-A Sel Point vent: It is a 50 m height cliff made of layered and welded red scoria (e.g. spatter deposit) which is dated at 0.84 Ma (Gadalia et al 1988).

-Pigeon deposit: The Pigeon deposit is made of an alternation of coarse (debris flows) and thin (pyroclastic flows) deposits. The deposit has been partially altered by the circulation of hydrothermal fluids (e.g. in the Marsolle to Lezard points area). Additional descriptions of the Pigeon deposits are presented by table F-01 and map and by Appendix H-g.

a) North of A Sel point: The lava flows of the basement do not crop out beneath the northernmost Pigeon outcrops (Bourceau River delta area), which contain thicker and coarser debris flow horizons. The contact between the horizons is irregular.

b) A Sel point: The scoria cone is moulded by a 50 m thick layered pyroclastic flow deposit, which is separated from a coarse deposit by a fault zone. This coarse deposit is either a pyroclastic flow or a lahar which has remobilised proximal projections. A few meters south of this area (Machette point), an ash cloud surge deposit dominated by thin flat to coarse wavy horizons is observed. East of this area, paths cut into thinly layered ash while the hill tops are covered with a less than 1 m thick layer of ash and pumice.

c) Lezard point: A 50 m thick pumice-rich pyroclastic flow deposit has been channelled by an E-W striking valley according to the orientation of its horizons.

d) Dos Marsolle hill: A pyroclastic deposit containing in place (e.g. coarse dark ash surge horizons) and reworked (e.g. pumice and lava block-rich layers) horizons is observed. This deposit was likely deposited on a steep E-W striking slope on which it was immediately destabilised.

e) more recent fallout: Some of the pyroclastic deposits observed may be related to recent eruptive events (e.g. the fresh 2 m thick pumice horizon found on top of hydrothermalised lava flows in Marsolle point; table 4-Nb8) but most of the deposits described here are likely related to the same eruptive event and are regrouped under the Pigeon deposit designation.

Table F-01: Horizons of the Pigeon deposit; *thickness of outcrops

Nb	description	composition	high*	structure
1	lahars and pyroclastic flows or fallout	lahars (lava blocks in abundant yellow muddy matrix, 3-5 m thick) interbedded with thin deposit (ash dominated, some horizons of white pumice, 0.5-4 m thick)	20 m	wavy horizons, large-scaled
2	pyroclastic flow	lava blocks (base only) and abundant ash and pumice horizons	50 m	flat layering
3	pyroclastic flow or lahars	layers with abundant to absent yellow muddy matrix, Andesite pumice (cm-dm sized), lava blocks (cm-m sized), possibly bombs	5-15 m	cross-bedding
4	ash cloud surge	thin pink ash; wavy coarse ash (0.8 m thick)	10 m	flat layering
5	pyroclastic flow or lahars	pumice, lava blocks (cm-m sized) and yellow matrix	0.5-1 m	flat layering
6	fallout	ash with accretionary lapilli, some pumice	1-10 m	flat layering
7	pyroclastic flow	1 m thick ash horizon (base only), pumice dominated deposit with lava blocks	50 m	flat layering
8	fallout	white pumice	2 m	flat layering
9	reworked pyroclastic deposit	reworked pyroclastic deposit with pumice, lava blocks and rare ash matrix	5 to 20 m	flat layering to cross-bedding
10	pyroclastic flow	coarse black ash and lapilli blocks	1-3 m	wavy
11	lahars	lava and pumice blocks in abundant thin matrix; several thin horizons (10 cm thick)	50 m	flat layering to cross-bedding
12	debris flow	blocks (cm-m sized) in rare matrix	1-20 m	none

Appendix G: map of the SW Axial Chain, Guadeloupe
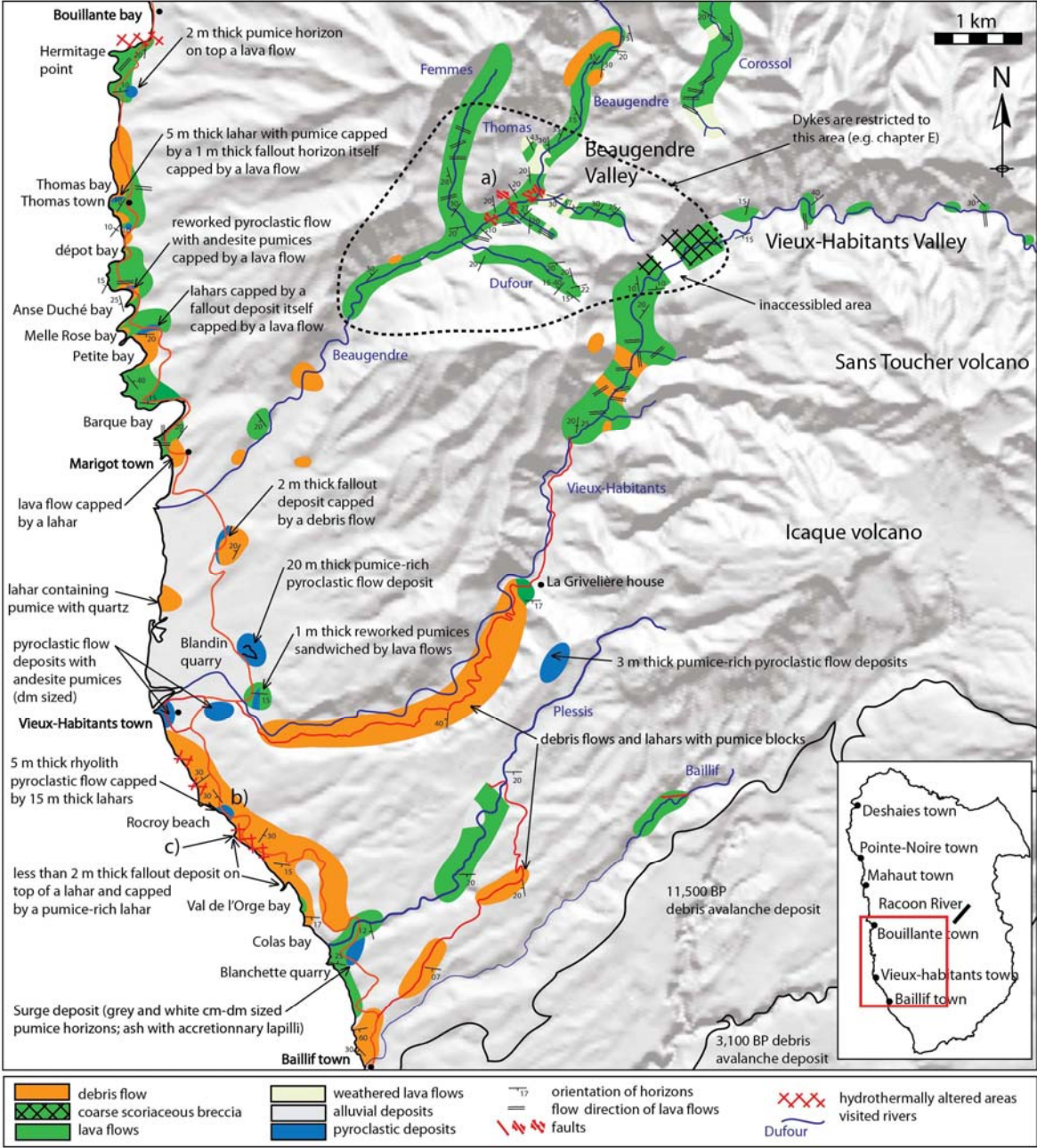
Figure G-01: Geological map of the SW part of the Axial Chain. The topography is a hill shade map of the IGN-25m-DEM (lighting azimuth = 0°, elevation = 45°). Letters a) to d) locate the pictures in figure 14.

Explanatory notes:

-lava flows: massive and scoriaceous breccias outcrops. The individual flows are 20-30 m thick and 5-10 m thick upstream of Dufour and Beaugendre rivers. A 600 m long (in the E-W direction) and 100 m high cliff made exclusively of vesiculated lava blocks (cm to dm sized) of homogeneous composition (e.g. small feldspar and pyroxene phenocrysts) is observed in the Vieux-Habitants River. This cliff contains the bulk of dykes identified in this river and is either a thick lava flow breccias (e.g. block lava flow or levée) or a scoria cone.

-alluvium: Three alluvial deposits are sandwiched by lava flows (Beaugendre valley). A 10 m thick cross-bedded sand is overlain by a 30 m thick lava flow (Vieux-Habitants River) and a 3 m thick red sand deposit is topped by a lava flow (Plessis River).

-debris flows: These deposits topped the lava flows. They are of small extent (Vieux-Habitants River), 50-100 m thick (upstream Beaugendre River) or form most of 100 m high waterfalls (Racoon River). The debris flows rework pumice downstream Beaugendre River. They contain lava and pumice blocks embedded in a non-abundant matrix and some lenses of layered pumice-rich pyroclastic deposits along the road south of Vieux-Habitants and Plessis Rivers.

-pyroclastic deposits:

1) Between Bouillante and Marigot towns: 5 to 10 m-thick outcrops of lahars and debris flows are observed. These deposits have a flat layering, which turns locally into large-scale cross-bedding for valley-confined deposits (e.g. Thomas Bay). The lahars are variably rich in pyroclastic blocks (usually pumice). Some ash and pumice horizons less than 2 m thick are found between successive lahars (e.g. Dépot and Anse Duché bays). Undisturbed fallout deposits are also found on top of the lahar horizons (e.g. Petite Bay; Thomas Bay). These deposits are capped by at least one lava flow. Small extent white pumice accumulations are found in two locations on top of lava flow (e.g. Hermitage point and Thomas town).

2) Vieux-Habitants town: The pumice-rich pyroclastic flow of Blandin quarry contains ash with accretionary lapilli and andesite pumice (cm to dm sized) horizons. Large andesite pumice fragments (e.g. dm sized) are also found in the town. These deposits have been

reworked by lahars and debris flows north of the town. A 1 m-thick reworked pyroclastic horizon sandwiched by two lava flows is found north of the town, beneath the Vieux-Habitants pyroclastic deposits.

3) South of Vieux-Habitants town: The lava flows are capped by up to 50 m thick lahars and debris flow deposits. Pyroclastic deposits less than 5 m thick are found underneath or between successive lahars (Rocroy beach). Lahars are either free of pyroclastic blocks or contain abundant pumice (cm-dm sized) blocks. The pumice clasts are usually andesite but rhyolitic pumice with amphibole and quartz phenocrysts are also found (Rocroy beach). Thus, south of the town of Vieux-Habitants, the lava flows are at the base of the stratigraphic column, are capped by pyroclastic deposits (Rocroy beach and Colas Bay) and several lahars, which have reworked pyroclastic deposits, capped them.

Appendix H: stratigraphic columns, Basse Terre Island
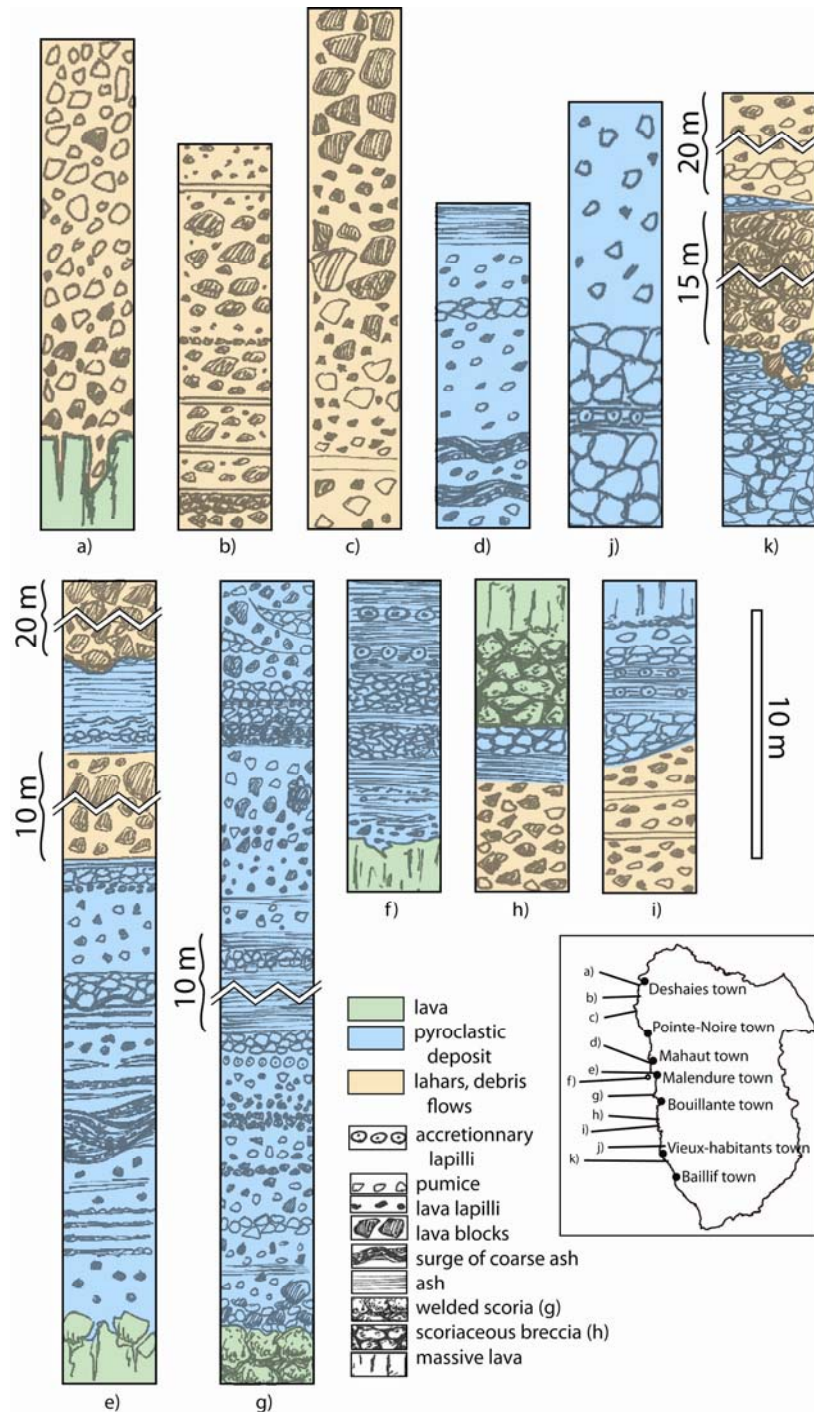
Legend: a) lahar of Deshaies point; b) lahars of Paul Thomas beach; c) Lahars of Petite Bay; d) pyroclastic flow of Colas point; e) Malendure point and deposit; f) fallout, Ilet Pigeon Island; g) pyroclastic flows, A Sel point; h) clastic deposits capped by a lava flow, Joubert point; i) idem, Petite Bay; j) pyroclastic flows, Blandin quarry; k) pyroclastic flow and lahars, Rocroy beach.

Appendix I: orientation of horizons, Basse Terre Island

Table I-01: Lava flow orientations, flow directions and thickness. *mean thickness of flows

location	Orientation of lava flows	n	Flow directions	n	High*(m)
Northern Chain					
Deshaies River	165-025/10-22W	6	105	1	/
Ferry River	175-005/15-30SW; 030-050/25NW	11	090-110; 130	12	15-20
Baille-Argent River	020/30NW	3	095	2	15-20
Caillou Rivers	140-150/12-40SW	8	050	9	5-20
2$^{\text{éme}}$ Bras David River	000-015/30NW	5	085	2	30
Petite Plaine valley	165-015/20-30W	30	080-110	23	/
Grande Plaine valley	045/20-40NW-SE; flat	3	065-085; 015	18	/
Ferry town	025/10NW	1	070-085	6	5
Bouillante area-northern Axial Chain					
Bois Malher, Rouge, Petite Rivière, Créve-Cœur, Losteau and Hab. Négresse rivers	Horizontal 150-020/10-30W 150-020/10-30E	8 6	075-115	10	10-30
Bois Malaisé, Fond Combat and Espérance rivers	005/15-30 NW 030 ± 05°/30 NW-SE	6 11	135 ± 10°	10	5-20
Bourceau and Bouillante rivers	055-077/10-60S 055-077/10-60N 175-025/20W	4 12	135 ± 10° 085-105	6 11	1.5-2
Lezard point	/	/	085	3	<20
Southern Axial Chain					
Beaugendre valley	170-005/10-30 SW; 130-155/15 NE-SW	8 14	100 040	8 11	5-30
Vieux-Habitants valley	175-005/10-25 SW	9	085-095 030-050	11 11	20-30
Corossol	175/20 NE 130-150/10-40NE-SW	5 9	075-105 035-055	11 5	20-30
Racoon	/	/	055-065	12	/
N of Vieux-Habitants town	/	/	065-105	26	/
S of Vieux-Habitants town	175/10 SW	1	105	1	/

Table I-02: Horizons orientation. *VH stands for Vieux-Habitants town

location	Deposits	Orientation of horizons	n
Malendure deposit	Pyroclastic and debris flows	170/08-50W	19
		035 ± 10°/20E-W and 100 ± 10°/20N-S	21
Bourceau River	Debris flows	055/10-20N	4
Pigeon deposit	Pyroclastic and debris flows	145 ± 05°/10-30SW	
		100 ± 10°/20-40SW	
Plessis River	alluvium	165-015/25 W	2
North of VH*	Debris flow and lahars	145/25 NE	7
		030/15 NW	8
South of VH*	Debris flow and lahars	Various strikes (090 ± 05°, 010-030, 150) and dips (10-60°)	20

Appendix J: orientation of structures measured in Basse Terre and Cameroon
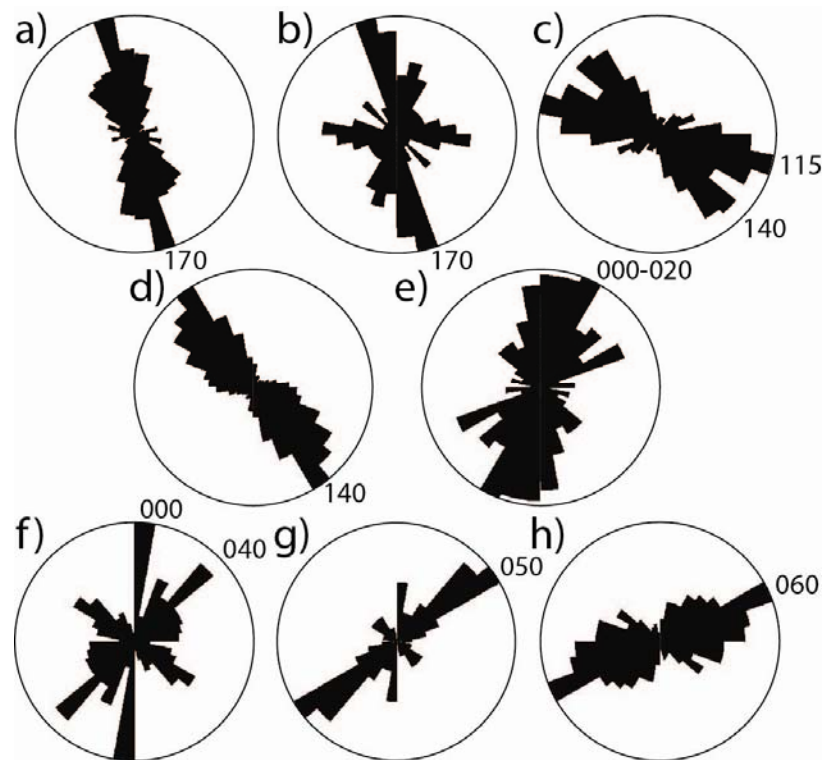
Figure J-01: Lower hemisphere projection rose diagrams. The diagrams display the strike of the vertical structures measured in Guadeloupe: a) fractures and veins measured in debris flows located shore line north of Pointe Noire town (n= 529); b) fractures measured in lava flows in the Petite and Grande Plaine valleys (n= 59); c) fractures and veins measured in the lava flows of the Malendure area (n=324); d) fractures and veins measured in the Malendure deposit (n= 1380); e) fractures and veins measured in the debris flows of Bourceau River (n= 223); and measured in Cameroon: f) fractures and veins measured in the rivers at the SE base of the volcano (n=274); g-h) dykes, eruptive fissure and crater alignments (g, n= 42) and fractures and open cracks (n= 652) measured at the summit of Mt Cameroon volcano.

Table J-01: Structures measured in river outcrops, in Basse Terre Island.*The structures were measured in fresh lava flows (except when a different rock type is given); ** Total amount of structures measured in each area; *** The abbreviations stand for fractures (F), fault zones (FZ), veins (V), quartz (Qz) and strike-slip fault (SSF); ****faults which have not been identified with certitude and may have been mistaken with lava flow cooling joints.

Location	Orientation of structures		Type of structure		n**
Northern Chain					
2$^{\text{éme}}$ Bras David River	170-010 and 080-100*		F***		100
Petite and Grande Plaine Rivers	170-010 and 080-100		F		114
	000 and 100		Qz V		
Deshaies River	125/60SW (in debris flow)		F (related to debris flow formation)		10
Grande Plaine valley	en-echelon Qz V		175 sinistral SSF		1
	120/62SW plane with horizontal striae; 010 sinistral SSF (Qz V); 120 (F)		related to lava flow formation or tectonic origin?		20
SW Axial Chain					
Beaugendre valley	random		F, FZ		1228
	125 ± 10° (n=39)		V		169
	110/72 SW (fault plane) and 055-080 (quartz veins)		sinistral transtensional fault		1
	145 (C) and 130 (F); 125 (fault)		dextral strike-slip faults		2
	140/60 SW (5 m thick C)		normal fault (?)****		1
	145		fault (?)		1
Vieux-Habitants valley	024 ± 10° (n=170)		F, FZ		770
	025 ± 05° (n=16); 135 ± 05° (n=25); 090 ± 10° (n=33)		V		137
Baillif	070-090 (50 m thick C)		fault (?)		1
	000-025 (n=52); 070-095 (n=101).		F, FZ		253
NW Axial Chain					
Losteau River	000 ± 10° (n=45), 035 ± 10° (n=38), 100 ± 15° (n=42)		F		193
	random (in weathered lava flows)		F		100
Crève-coeur river	145 and 165-000		Qz V		5
NW Axial Chain area	175 ± 10° (n=15), 035 ± 10° (n=20), 070-120 (n=52)		FZ		116
	170-020		FZ,V		240
	000 ± 15° (29% of data)		F		647
Bois Malaisé river	080-100, 120-130/40N-S (F, n=30)		fault (?)		1
Grande Découverte volcano					
Upstream Galion River	170 ± 10° (n=83), 060 ± 05° (n=67) (F and V located in lava flows)		175 sinistral SSF (Ty fault?)		453
Noire River	045 ± 05°		5 m thick fault zone (Carmichael crater?)		1
Rivers located west of La Soufrière dome	050 ± 05° (n=157)		related to DAD formation		1296
	170 ± 05° (n=185) (fractures located in DAD)		tectonic origin?		

Table J-02: Structures measured in coastal outcrops of the Northern Chain.*The abbreviations stand for fracture (F), fault zones (FZ), veins (V) and open fractures filled with colluvions (OF); **total amount of structures measured in each area

Outcrop location	lithology	Structure Orientation (strike only)	type	n**
north of Pointe Noire town	debris flows and lahars	160-000; 130-140; 080-110 (n=303; n=120; n=63)	F, FZ, V*	548
	lava flows	160-015; 130-150 (n=65; n=36)	F, FZ	139
Pointe Noire to Mahault towns	lava flows	085-110	F	3
		random	Qz, zeotith V	422
Pigeon Island	pyroclastic	010/65SE (slip < 1m)	normal faults	5
south of Mahault town	Malendure deposit	140 ± 10° (n=491)	zeolith V	1000
		140 ± 10°; 110 ± 10°; 000 ± 10° (n=143; n=151; n=58)	F	477
		110 (slip= 0.5-10 m); 000 (slip= 1 m); 140 ± 05° (slip= 1.2-3 m)	normal faults	7
		140 (slip < 0.1 m)	reverse faults	2
Malendure town	block and ash deposit	105 ± 05°; 145 ± 05° (n=12; n=11)	OF	26
		100; 145 (n=50; n=60)	F, V	184

Table J-03: Structures measured in coastal outcrops of the Axial Chain*The abbreviations stand for fractures (F), fault zones (C), veins (V) and normal faults (NF); **total amount of structures measured in each area

Outcrop location	lithology	Structure orientation	type	n**
Bouillante geothermal field area				
Hermitage point	Lava flows	080 ± 15° (n=42)	V*	94
		random	F	55
		110; 110/60SW-NE	NF?	1
	Hydrothermally altered lava flows	120 ± 05° (n=9)	F	22
		random	V	80
Marsolle point	Hydrothermally altered lava flows	105-145 (n=205)	V	370
		075 ± 10°; 140 ± 05° (n=13, n=18)	F,FZ	67
A Sel point	Red welded scoria	120 ± 15° (n=186)	F, V	317
north of A Sel point	Pigeon deposit	140 ± 10°; 170 ± 05° (n=302, 121)	F, V	658
		140 ± 10°/70SW; 140 ± 10°/70NE (slip= 0.2-1 m)	NF	10
south of A Sel point	Pigeon deposit	095 ± 15° (n=59)	F, V	134
		110/60SW (slip < 1 m); 110/75S 090/72S (slip= 2m)	NF	3
SW Axial Chain area				
North of Vieux-Habitants town	debris flows	120 ± 20° (n= 398)	F, V	750
	Lava flows	090 to 140	F,V	670
South of Vieux-Habitants town	Debris flows, lahars	090 ± 20° (n= 994) 090 ± 20° (dip=50-70°; n= 331)	F, V	2500
Anse Duché bay	lahars	100/50NE	NF	1
Petite bay	Lahars, lava flow	100/50NE	NF	1

Appendix K: experimental parameters

Experiment	α (°)	kinematics	silicone ?	Hs*	Hb*	Hc*	øC*	β (°)	offset*
E01	0	SSF**	Yes	0.5	/	7	26	27	/
E03	0	SSF	Yes	0.4	/	6	26	25	/
E05	0	SSF	Yes	0.2	/	6	25	25	/
E07	0	SSF	Yes	0.25	/	7	26	29	/
E09	0	SSF	Yes	0.2	/	7	26	27	/
E11	0	SSF	Yes	0.25	/	7	26	28	2.8
E12	0	SSF	Yes	0.6	/	7	27	29	3.3
E02	0	SSF	No	/	/	6	27	25	/
E04	0	SSF	No	/	/	7	25	31	1.2
E06	0	SSF	No	/	/	7	25	29	/
E08	0	SSF	No	/	/	8	27	30	/
E10	0	SSF	No	/	/	8	25	32	3.2
G01	0	SSF	No	/	/	/	/	/	/
C03	20	TP**	No			6	28	22	/
C06	20	TP	No	/	/	8	26	30	0.6
C10	20	TP	No	/	/	7	26	28	/
C12	20	TP	No	/	/	7	24	28	0.4
C16	20	TP	No	/	/	6	26	26	/
C18	20	TP	No	/	/	6	26	25	/
C20	20	TP	No	/	/	8	26	30	/
C26	20	TP	No	/	/	6	27	24	/
C30	20	TP	No	/	/	4	19	25	/
C34	20	TP	No	/	/	5	28	20	/
C36	20	TP	No	/	/	5	29	20	/
C40	20	TP	No	/	/	7	26	29	2.7
C42	20	TP	No	/	/	7	26	28	5
C44	20	TP	No	/	/	7	26	29	3.2
C46	20	TP	No	/	/	6	26	23	3.8
C50	20	TP	No	/	/	6	26	26	1.6
C52	20	TP	No	/	/	9	31	30	/
C56	20	TP	No	/	/	5	32	18	/
C58	20	TP	No	/	/	9	31	29	1.2
G04	20	TP	No	/	/	/	/	/	/
C08	20	TP	Yes	0.3	/	7	24	31	/
C14	20	TP	Yes	0.25	/	7	25	28	/
C22	20	TP	Yes	0.25	/	8	24	32	/
C24	20	TP	Yes	0.3	/	8	27	30	/
C28	20	TP	Yes	0.3	/	7	26	28	/
C32	20	TP	Yes	0.4	/	6	26	23	/
C38	20	TP	Yes	0.3	/	5	27	19	/
C48	20	TP	Yes	0.6	0.4	8	26	30	/
C54	20	TP	Yes	0.5	0.5	7	26	29	/
C60	20	TP	Yes	0.4	0.6	6	26	25	4
D06	40	TP	No	/	/	7	25	29	/
D10	40	TP	No	/	/	6	27	23	/
D14	40	TP	No	/	/	7	26	27	/
D18	40	TP	No	/	/	6	26	26	2
D22	40	TP	No	/	/	6	26	26	4
D30	40	TP	No	/	/	7	26	29	/
G02	40	TP	No	/	/	/	/	/	/
D02	40	TP	Yes	0.4	/	7	27	28	/
D04	40	TP	Yes	0.5	/	7	26	26	/
D08	40	TP	Yes	0.3	/	7	26	29	/

D12	40	TP	Yes	0.25	/	6	27	25	/
D16	40	TP	Yes	0.25	/	8	26	30	2.8
D20	40	TP	Yes	0.4	/	6	26	26	3
D24	40	TP	Yes	0.5	0.5	7	26	29	/
D26	40	TP	Yes	0.4	0.6	7	26	28	1.2
D28	40	TP	Yes	0.5	/	6	26	23	/
C01	20	TT**	No	/	/	/	/	/	/
C02	20	TT	No	/	/	6	25	23	/
C07	20	TT	No	/	/	8	26	30	/
C09	20	TT	No	/	/	7	26	29	/
C13	20	TT	No	/	/	6	26	25	/
C15	20	TT	No	/	/	7	25	29	/
C21	20	TT	No	/	/	6	25	26	/
C23	20	TT	No	/	/	8	26	30	/
C27	20	TT	No	/	/	6	26	23	/
C29	20	TT	No	/	/	5	18	29	0.4
C33	20	TT	No	/	/	7	28	26	/
C37	20	TT	No	/	/	6	28	21	/
C39	20	TT	No	/	/	7	28	25	1.5
C43	20	TT	No	/	/	7	26	27	3
C47	20	TT	No	/	/	7	27	27	5.5
C49	20	TT	No	/	/	7	26	27	1.6
C53	20	TT	No	/	/	9	31	30	/
C55	20	TT	No	/	/	7	33	23	/
C59	20	TT	No	/	/	8	31	26	/
G05	20	TT	No	/	/	/	/	/	/
C04	20	TT	Yes	0.45	/	5	28	21	/
C05	20	TT	Yes	0.5	/	7	27	28	/
C11	20	TT	Yes	0.3	/	6	25	27	0.4
C17	20	TT	Yes	0.25	/	6	25	27	/
C19	20	TT	Yes	0.2	/	8	27	29	/
C25	20	TT	Yes	0.3	/	7	25	30	/
C31	20	TT	Yes	0.3	/	7	27	26	/
C35	20	TT	Yes	0.35	/	5	27	21	/
C41	20	TT	Yes	0.25	/	7	26	27	/
C45	20	TT	Yes	0.75	0.25	7	27	27	1
C51	20	TT	Yes	0.35	0.65	7	27	26	/
C57	20	TT	Yes	0.5	0.5	7	25	30	7.8
D05	40	TT	No	/	/	6	26	25	/
D09	40	TT	No	/	/	6	26	23	/
D13	40	TT	No	/	/	6	27	24	/
D17	40	TT	No	/	/	6	29	22	1.8
D21	40	TT	No	/	/	7	26	28	3.2
D29	40	TT	No	/	/	7	27	28	/
G03	40	TT	No	/	/	/	/	/	/
D01	40	TT	Yes	0.3	/	7	26	30	1.2
D03	40	TT	Yes	0.4	/	6	26	26	/
D07	40	TT	Yes	0.5	/	7	27	27	/
D11	40	TT	Yes	0.35	/	6	27	25	/
D15	40	TT	Yes	0.3	/	7	26	28	2.5
D19	40	TT	Yes	0.3	/	7	26	28	2.5
D23	40	TT	Yes	0.25	0.75	7	25	30	/
D25	40	TT	Yes	0.7	0.3	7	26	27	/
D27	40	TT	Yes	0.4	/	7	26	28	0.8

*in centimetre; **strike-slip (SSF), transpressional (TP) and transtensional (TT) faults.

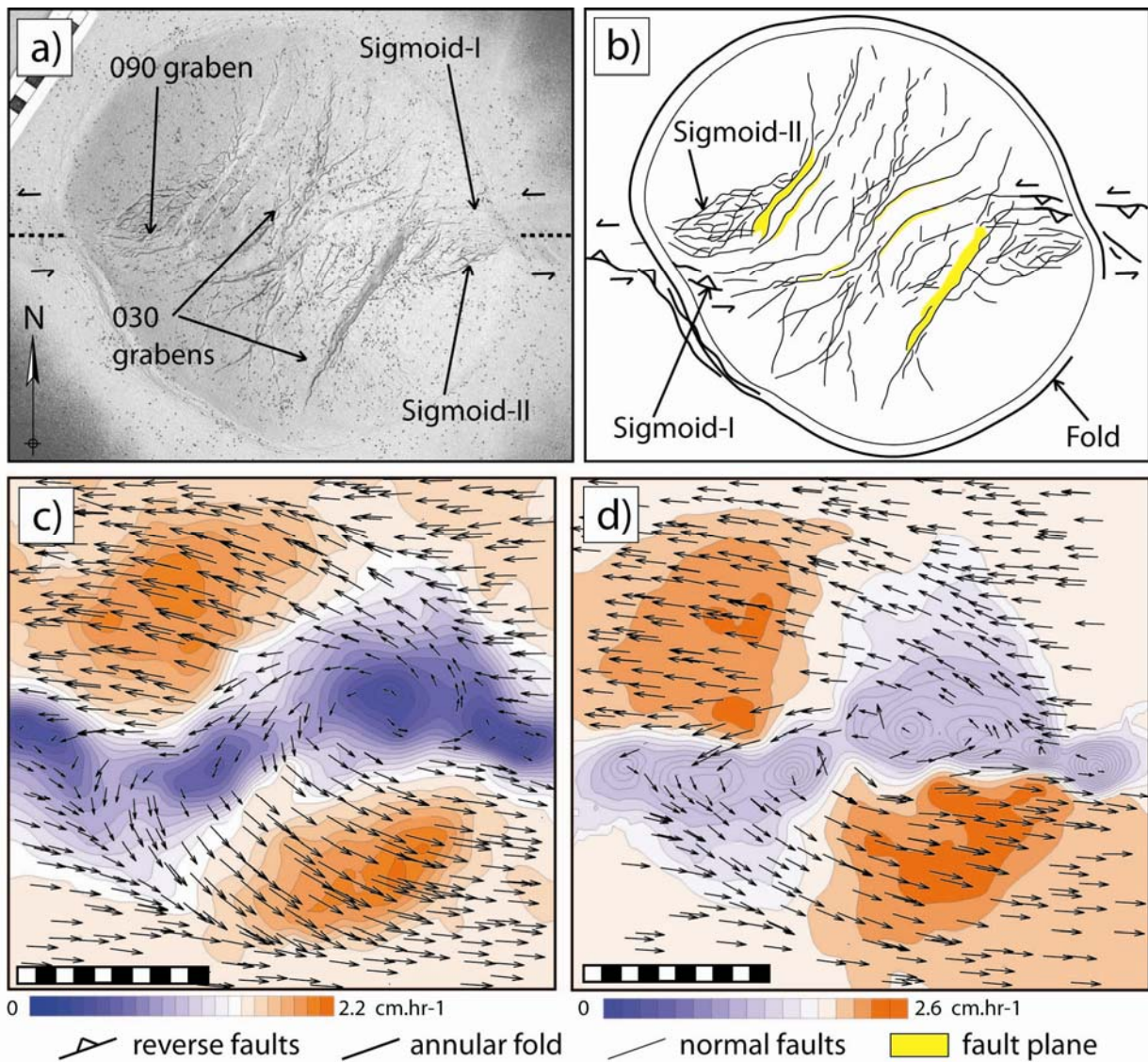# Appendix L: Strike-slip fault experiments (brittle substratum)
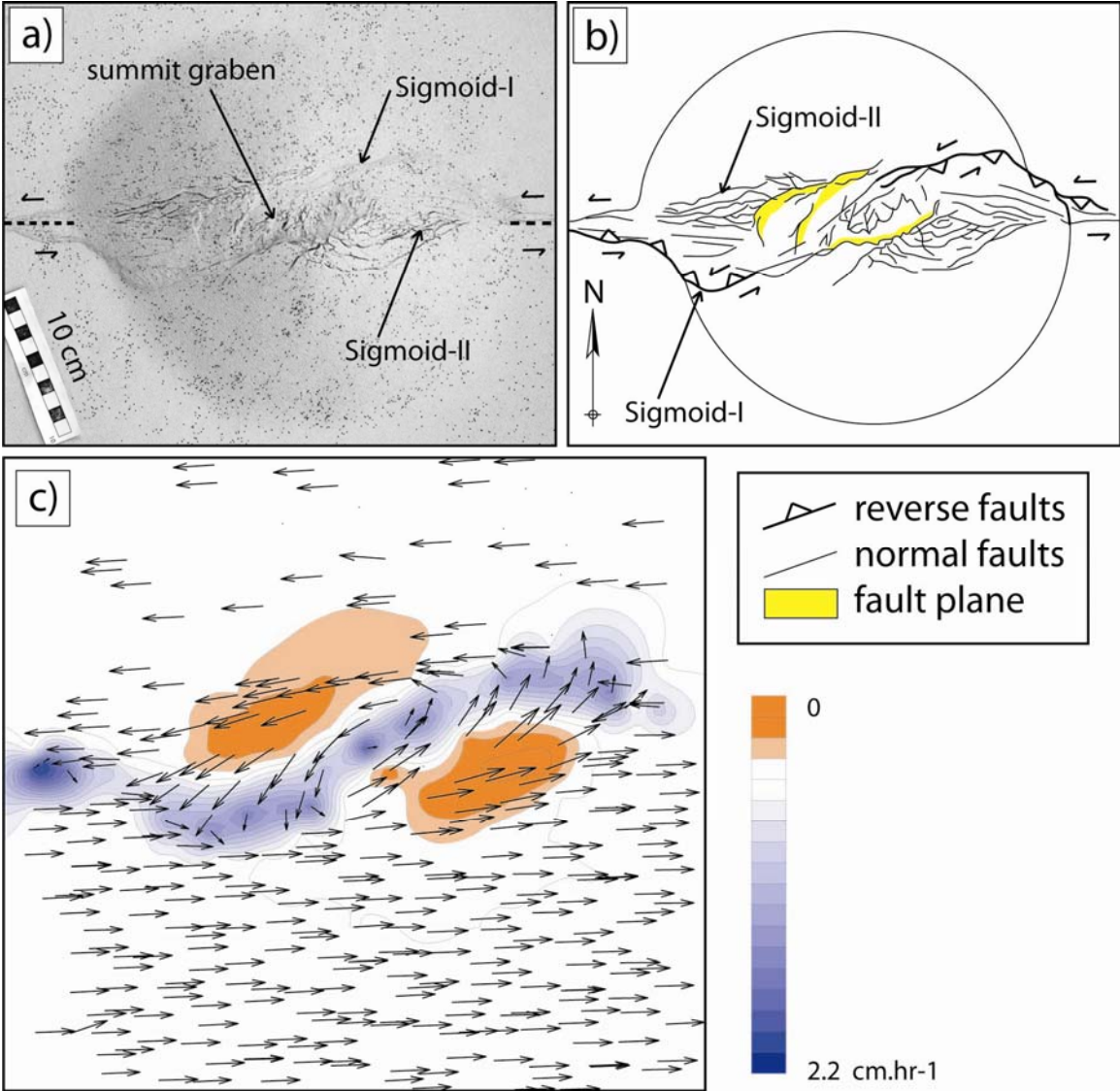
Figure L-01: a-b) Picture and sketch of experiment E08; c) Map of the amplitude and direction of horizontal movements for D_{SSC}= 15-18 mm (experiment E06).

Table L-01: Faults strike and slip; *The best represented strikes are in bold character; **Orientation of fastest vectors; *** Fault zone or slow moving area as observed on maps of horizontal displacements.

A. Fault analysis		Strike of faults	n
1) Sigmoid-I		045-055 (summit graben); **065-075***; 105 (cone base)	43
2) Sigmoid-II	**summit graben**	**030-040;** 060-085	24
	cone flanks	035-050; 060-**070**-080; 095-**105**	64
B. Deformation fields		**Slip of faults (cm)**	Π_3(%)
1) Sigmoid-I at **the cone flanks**	D_{CC-C}	1-1.2	35
	D_{SSC-C}	2	65
2) Sigmoid-II at **the summit**	D_{EXC-C}	1.2-1.4	25
	D_{SSC-C}	4	75
3) Sigmoid-I at the cone summit	D_{EXC-C}	0.2	30
	D_{SSC-C}	0.6	70
	velocity	2.4 cm.hr^{-1}	/
	Strike**	065-070	/
4) Fault zone**	**Strike**	060 and 090	/

# Appendix M: Strike-slip fault experiments (ductile substratum)

Figure M-01: a-b) Picture and sketch of experiment E05; c-d) Maps of the amplitude and direction of horizontal movements for D_{SSC}= 7-11 mm (c), D_{SSC}= 30-40 mm (d). The experiments (c) E03 ("slow spreading") and (d) E07 ("fast spreading") are presented.

Table M-01: Faults strike and slip; *The best represented strikes are in bold character; **Orientation of fastest vectors; *** Fault zone or slow moving area as observed on maps of horizontal displacements.

A. Fault analysis		Strike of faults	n
1) Sigmoid-I		**075-090***; 100 (cone base)	71
2) Sigmoid-II	cone flanks	040-050; 060-070	71
3) 030 elongated graben		020-**030**; 050-060	114
B. Deformation fields		Slip of faults (cm)	Π_3(%)
1) Sigmoid-I at the cone flanks	D_{EXC-C}	1-1.4	34
	D_{SSC-C}	2.2-2.5	66
2) 030 striking grabens (summit area)	D_{EXC-C}	0.8-1	50
	D_{SSC-C}	0.8-1	50
	velocity	2.2-2.6 cm.hr^{-1}	/
	Strike**	090	/
3) Fault zone***	Strike	060 and 080	/

Appendix N: Transpressional experiments (brittle substratum)
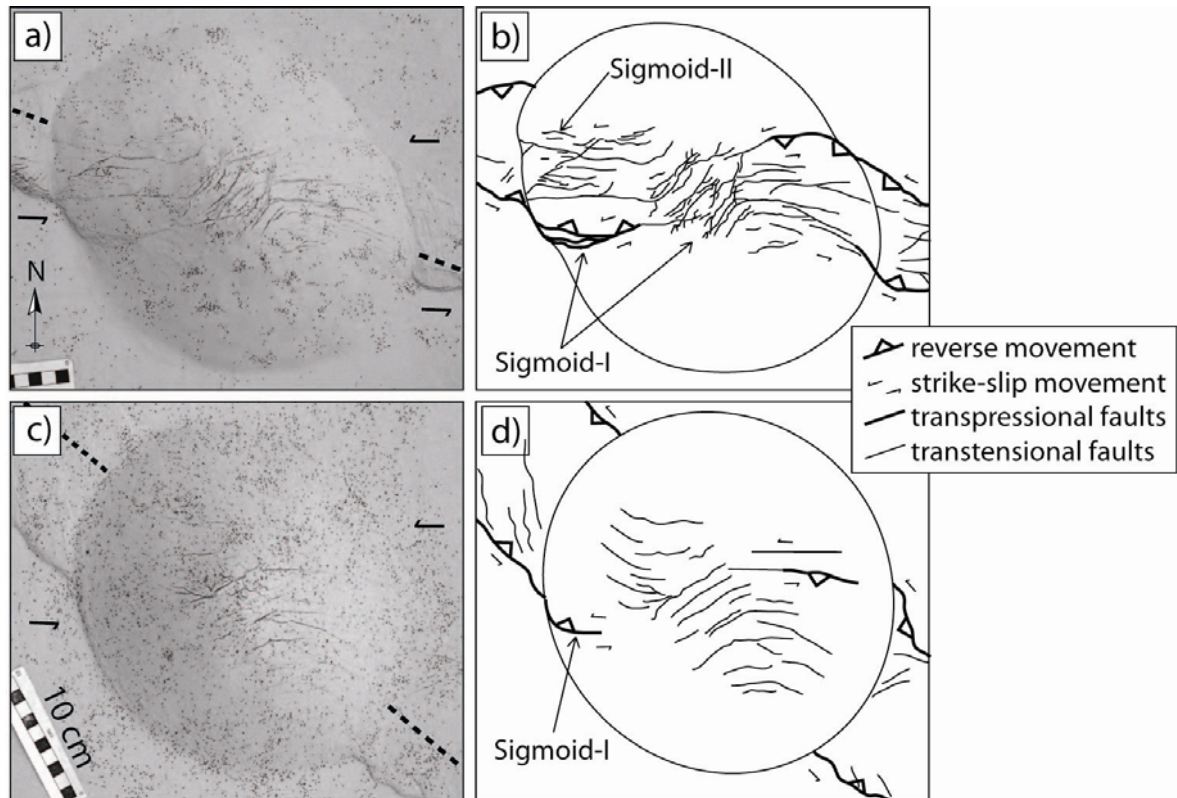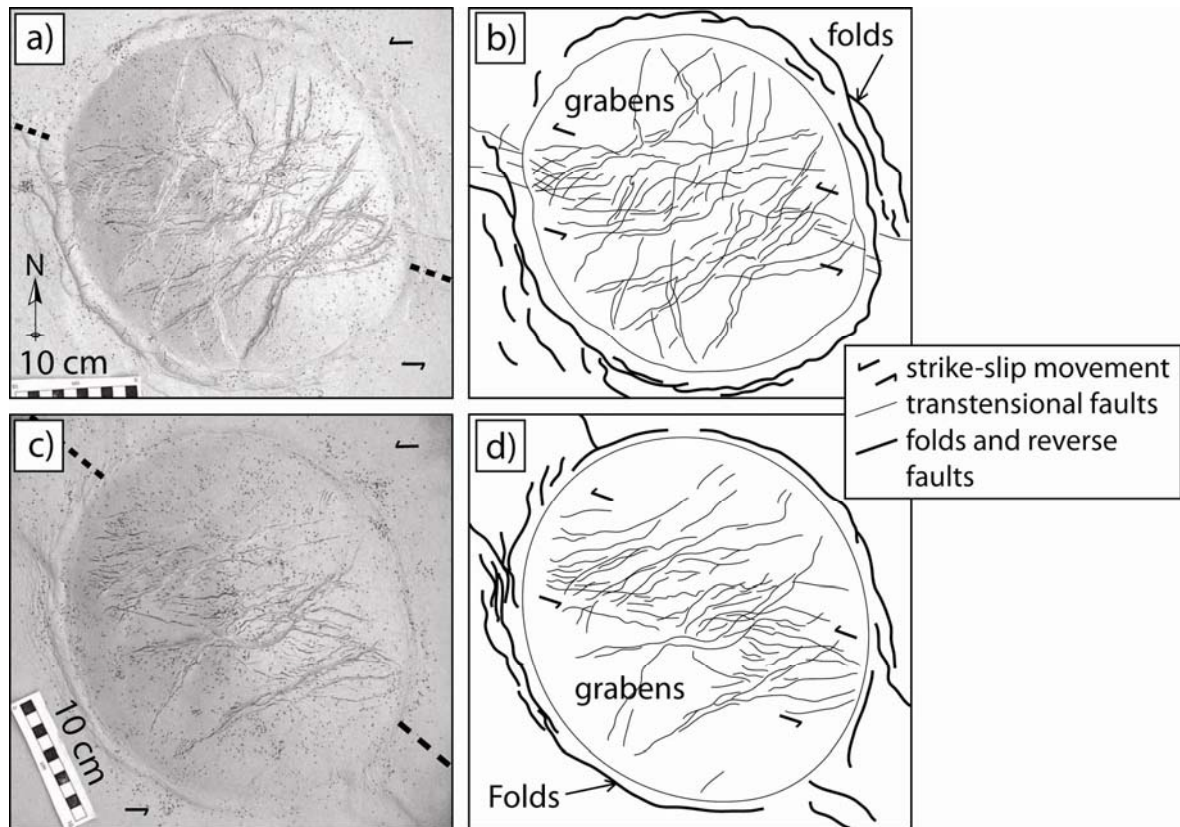

Figure N-01: Picture and sketch of brittle substratum (a-b) experiment C10 (α=20°) and (c-d) experiment D30 (α=40°).
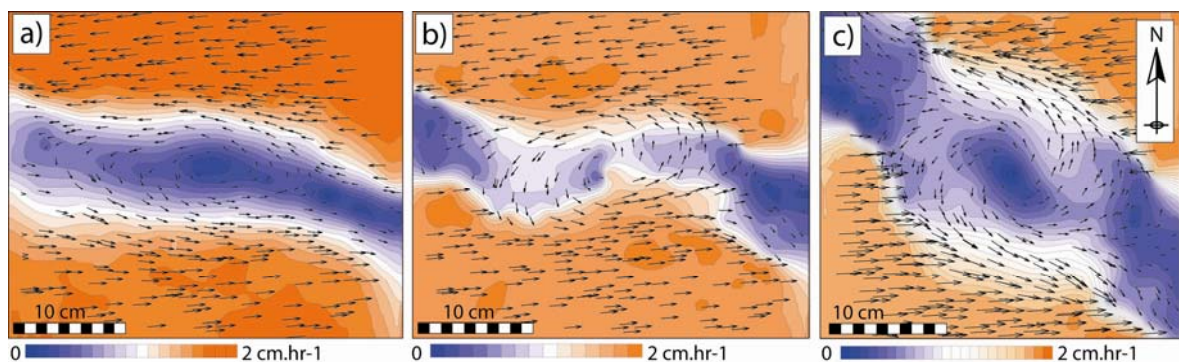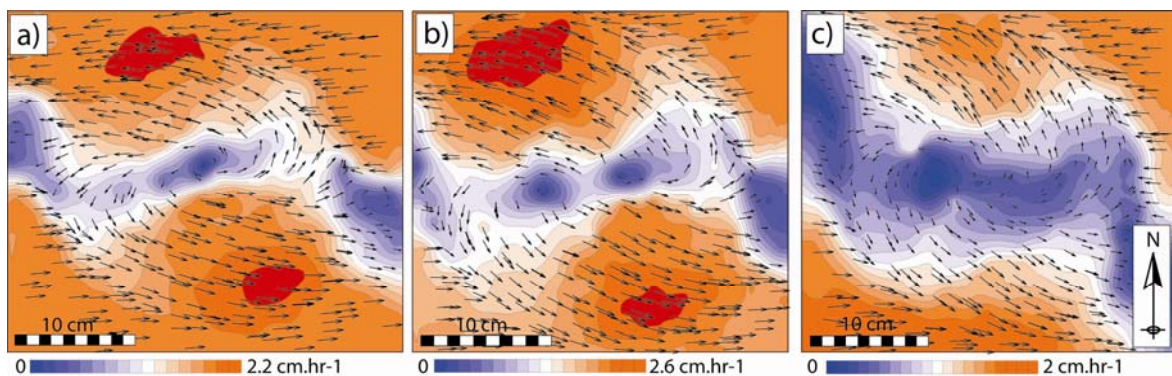

Figure N-02: Maps of the horizontal movements of the experiment surface for D_{SSC}= 7-11 mm (a), D_{SSC}= 26-30 mm (b), D_{SSC}= 33-37 mm (c); The experiments (a-b) C16 (brittle substratum, α=20°), (c) D30 (brittle substratum, α=40°) are presented.

Appendix O: Transpressional experiments (ductile substratum)

Figure O-01: Picture and sketch of ductile substratum (a-b) experiment C54 (α=20°; "fast spreading") and (c-d) experiment D12 (α=40°; "slow spreading").

Figure O-02: Maps of the horizontal movements of the experiment surface for D_{SSC}= 18-22 mm; The experiments (a) C14 ("slow spreading", α=20°), (b) C38 ("fast spreading", α=20°) and (c) D12 ("slow spreading", α=40°) are presented.

Appendix P: Transpressional experiments (numerical data)

Table P-01: **Strike of faults**; a) Sigmoid-I fault over the cone flank; b) Sigmoid-I at the cone summit (brittle substratum) or summit grabens (ductile substratum); c) Sigmoid-II fault; d) First structures which develop when D_{SSC}= 5-7 mm; e) Elongation direction of the summit grabens; *The best represented and most significant strikes are in bold character

α	a)Sigmoid-I	n	b) Summit	n	c) Sigmoid-II	n	d) t1	n	e) t	n
A. Brittle substratum (8 and 4 experiments)										
20°	095-105	18	025-040	31	095-**100**-**115***	61	**035-045**-055	26	030	8
40°	095-105	6	065-**070**-078	24	**090**-107-**120**	55	070	12	070	4
B. Ductile substratum (9 and 5 experiments)										
20°	070 **090-100**	41	020-030 **050-060-070**	108	110-125	30	050 065-**070**-075	22	040-045	9
40°	095-100 115-120	46	040-050 **060-070**	46	115-125	9	040-060	12	060-070	5

Table P-02: Fault slip measured when D_{SSC}= 10 mm (t1) and D_{SSC}= 40 mm (t2); *Fault zone corresponds to the slowest horizontal movements.

|		α=20°			α=40°		
		t1 (cm)	t2 (cm)	Π_3	t1 (cm)	t2 (cm)	Π_3
A. Brittle substratum experiments							
a) Sigmoid-I fault (cone flank)	D_{CC-C}	0.4-0.6	1.4	35	1	1.2-1.7	50
	D_{SSC-C}	1-1.3	1.7-2	65	1-1.4	1.3-1.7	50
b) Sigmoid-I fault (summit)	D_{EXC-C}	0.2-0.4	0.5-0.7	25	0.3-0.5	0.3-0.5	30
	D_{SSC-C}	1	2	75	0.8-1	0.8-1	70
c) Sigmoid-II fault	D_{EXC-C}	0.1-0.3	0.3-0.5	17	0.4-0.5	0.4-0.5	47
	D_{SSC-C}	1-1.3	1.4-1.7	83	0.5	0.5	53
d) Fault zone*	Strike	093	073	/	110	090	/
B. Ductile substratum experiments							
a) 100 striking grabens	D_{EXC-C} Slow	0.8	1.1	27	1.3	2.2	42
	Fast	0.9	1.8	29	/	/	/
	D_{SSC-C} Slow	2	3.2	73	1.8	3.4	58
	Fast	2.5	3.7	71	/	/	/
b) 040 to 070 striking grabens	D_{EXC-C} Slow	0.45	1	40	0.8-0.9	0.8-0.9	42
	Fast	0.8	1.2	36	/	/	/
	D_{SSC-C} Slow	0.7	1.2	60	1.1-1.2	1.1-1.2	58
	Fast	1.4	2	64	/	/	/
c) Fault zone*	Strike	070	074	/	065	065	/

Appendix Q: Transtensional experiments (brittle substratum)
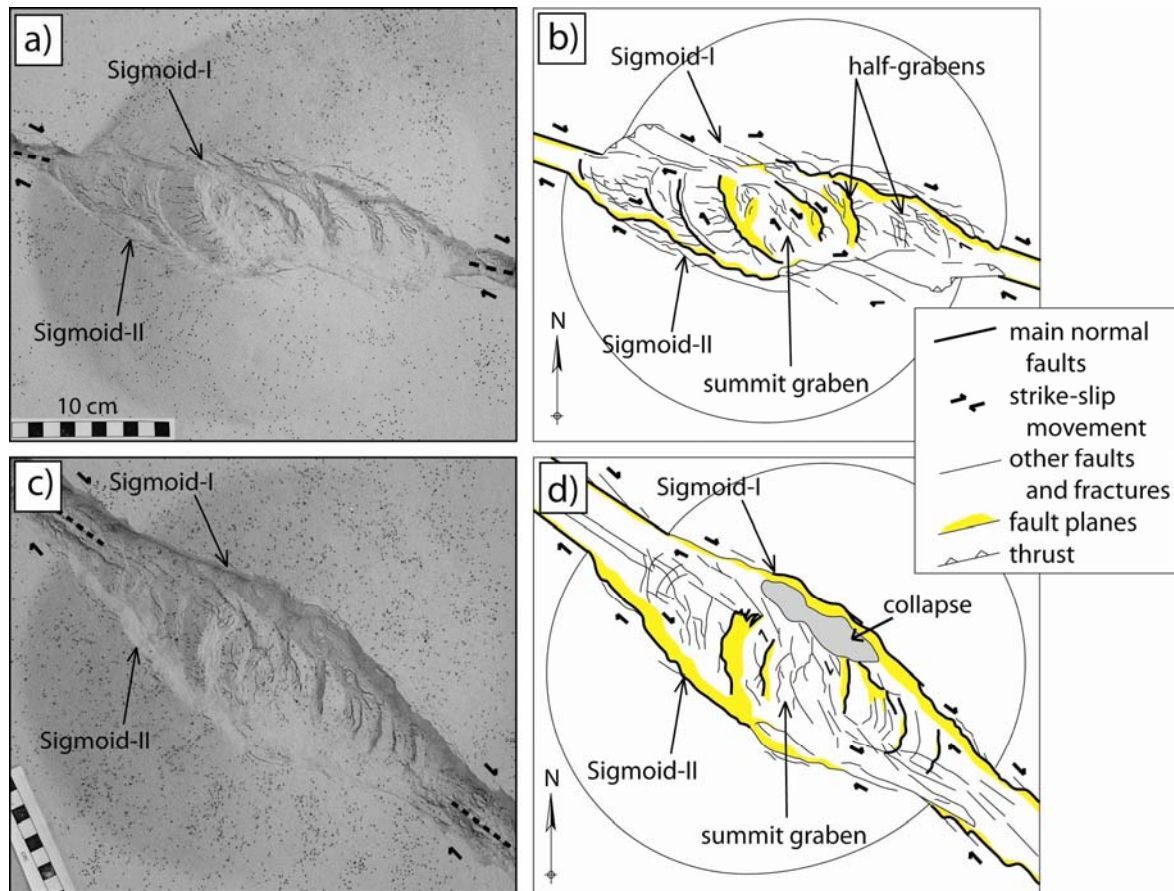
Figure Q-01: Picture and sketch of brittle substratum (a-b) experiment C23 (α=20°) and (c-d) experiment D29 (α=40°).
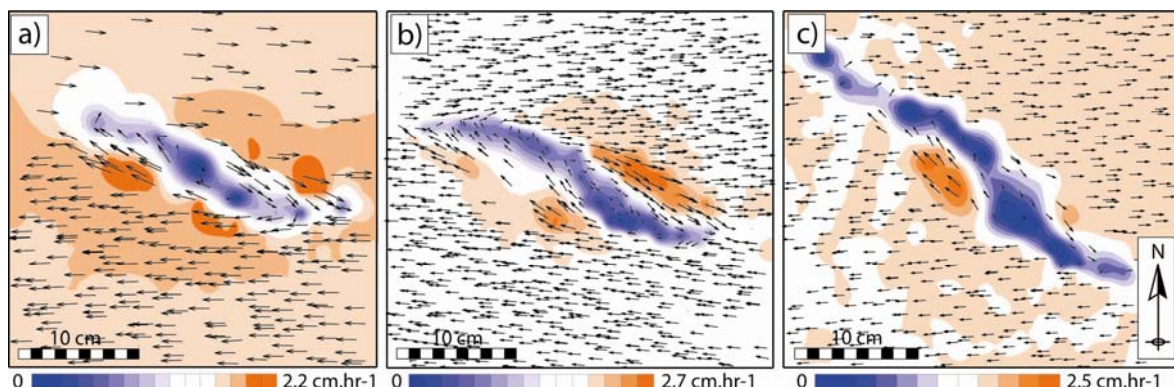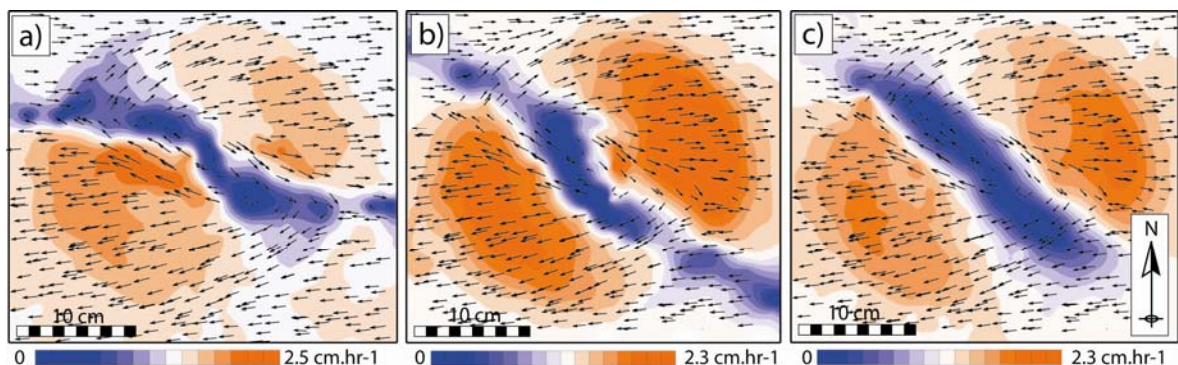

Figure Q-02: Maps of horizontal movements made for D_{SSC}= 18-22 mm (a), D_{SSC}= 12-14 mm (b), D_{SSC}= 28-32 mm (c). The experiments (a) C15 (brittle substratum, α=20°), (b) C53 (brittle substratum, α=20°), (c) D05 (brittle substratum, α=40°) are presented.

Appendix R: Transstensional experiments (ductile substratum)
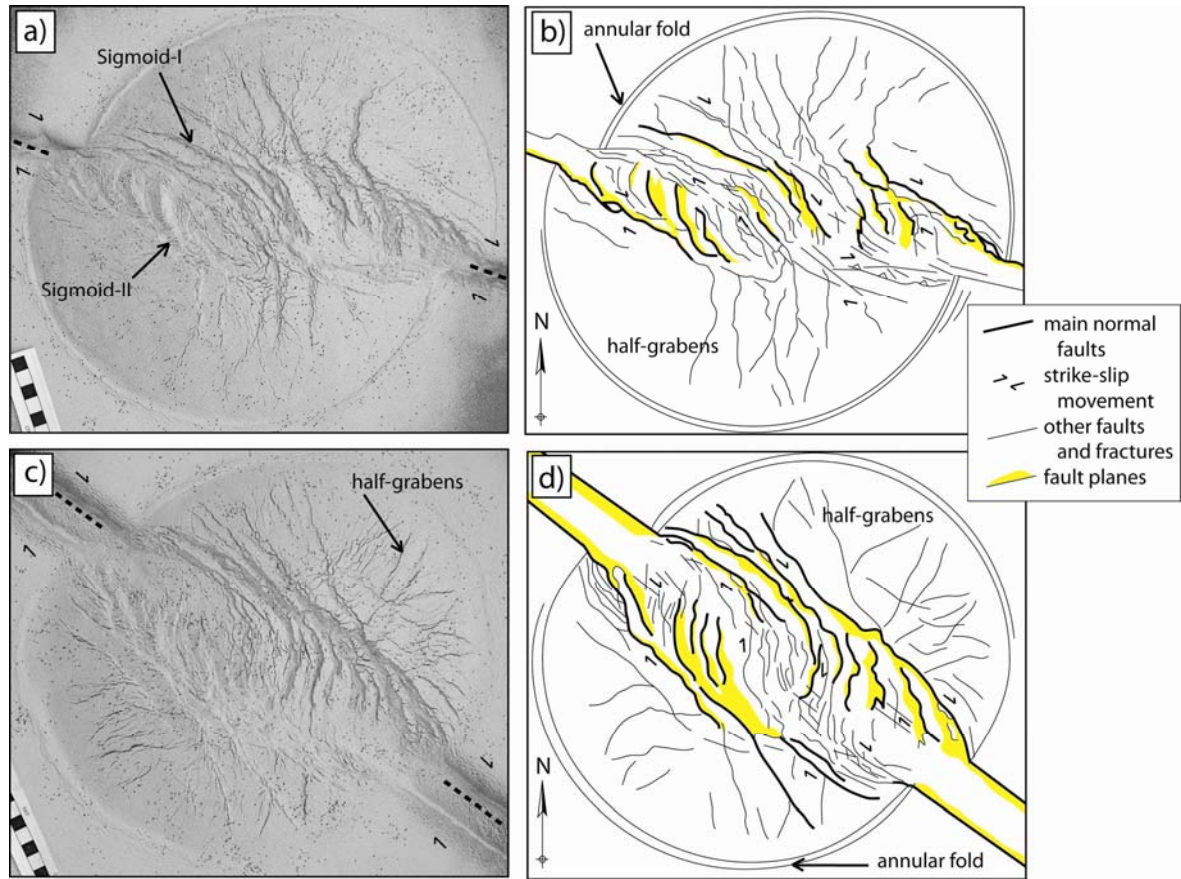
Figure R-01: Picture and sketch of ductile substratum (a-b) experiment C35 (α=20°) and (c-d) experiment D07 (α=40°).

Figure R-02: Maps of horizontal movements made for D_{SSC}= 15-17 mm (a), D_{SSC}= 8-10 mm (b) and D_{SSC}=23-25 (c). The experiments (a) C19 ("fast spreading", α=20°) and (b-c) D07 ("fast spreading", α=20°) are presented.

Appendix S: Transtensional experiments (numerical data)

Table S-01: **Strike of faults**; a) Sigmoid-I fault in the cone flank area; b) Sigmoid-I at the cone summit; c) Sigmoid-II fault; d) Structures located inside the fault zone; e) Elongation direction of summit graben; *The best represented and most significant strikes are in bold character

α	a) Sigmoid-I	n	b) Summit	n	c) Sigmoid-II	n	d) Fault zone	n	e)	n
1. Brittle substratum (8 and 4 experiments)										
20°	090-100 + **120**-140	139	170-005 + 140-150	117	110-**120**-140	125	140-**170**-025	128	145	8
40°	115-125 + 130-140	76	175-010 + 140-160	45	120-140 + 150	53	170-**005**-030	41	160	4
2. Ductile substratum (8 and 5 experiments)										
20°	100-110 + N120-130	250	none	none	100-110 + 120-130	145	150-**170**-010-050	334	160	8
40°	**120**-130 + 145	112	none	none	120-**130** + 160	82	**020** + 175	120	170	5

Table S-02: **Fault slip**; Fault zone (d) or area delimited by Sigmoid-I and II faults or slow area as observed on maps of horizontal displacement; *Velocity stands for the maximum amplitude of movement measured inside the fault zone and Strike stands for the direction of the fastest vectors.

		Brittle substratum				Ductile substratum			
		α=20°		α=40°		α=20°		α=40°	
		slip(cm)	Π_3	slip(cm)	Π_3	slip (cm)	Π_3	slip (cm)	Π_3
a) Sigmoid-I faults (cone flank)	D_{EXC-C}	1	19	1	20	1.5-2	33	1.5	30
	D_{SSC-C}	4-4.5	81	4	80	3.5	67	3.3-3.7	70
	Strike	100	/	122	/	095-100	/	125	/
b) Sigmoid-I faults (summit)	D_{EXC-C}	0.5-1	25	2-3	26	3	50	3.5	59
	D_{SSC-C}	2.2	75	3-5	74	3	50	2.3-3	41
	Strike	135	/	160	/	135	/	160	/
c) Sigmoid-II faults	D_{EXC-C}	0.9	75	1.5-2	70	1.2	71	1.4	68
	D_{SSC-C}	0.1-0.5	25	0.5-1	30	0.3-0.7	29	0.3-1	32
	Strike*	120	/	140	/	120-125	/	145	/
d) Fault zone	**Velocity**	2.2-2.7 cm		2-3 cm		2.5 cm		2-2.3 cm	
	Strike	122	/	135	/	120-125	/	135	/
	D_{EXC-C}	1	19	1	20	1.5-2	33	1.5	30

Appendix T: Experiments; Offset introduced between the cone summit and the basal fault zone
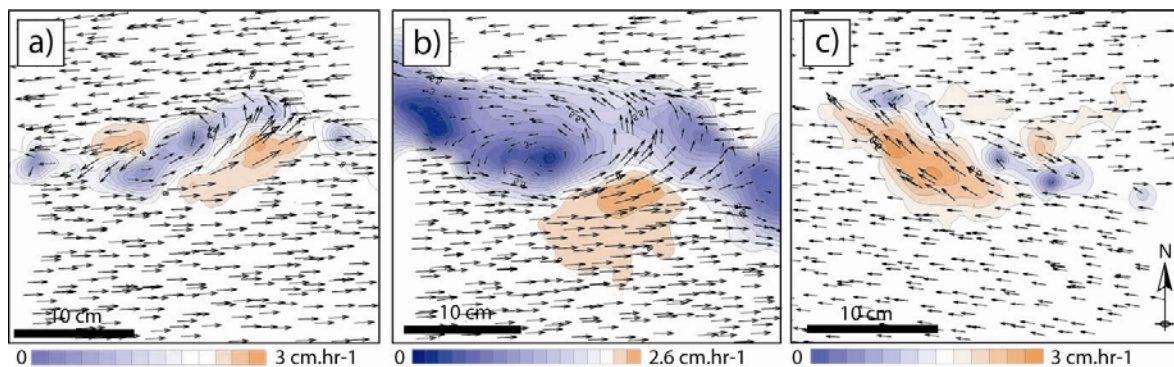
Figure T-01: Maps of the horizontal movements of the surface of brittle substratum experiments for D_{SSC}= 18-20 mm; (a) E10 (sinistral strike-slip fault, α=0°, Π_6= 0.13), (b) C42 (sinistral transpressional fault, α=20°, Π_6= 0.19) and (c) C47 (dextral transtensional fault, α=20°, Π_6= 0.2). The Part B of the cone is located in the upper part of the figures (e.g. northern flank of the cone).

Table T-01: Fault slip and strike; the experiments C46 and C42 (sinistral transpressional faults, ɑ=20°) and C47 (dextral transtensional fault, ɑ=20°) are presented; *v stands for the maximum horizontal velocity measured (in cm.hr^{-1}).

Experiment	D	Sigmoid-I slip (cm)		Sigmoid-II slip (cm)		Summit area
		Part A	Part B	Part A	Part B	
E10 (Π_6= 0.13)	D_{SSC-C}	0.6	1.2	0.6	0.2	3.2
	D_{CC-C}	1.2	1.6	/	/	/
	D_{EXC-C}	/	/	1.4 (v=3)*	0.4	/
	strike	100	125	/	/	053
C46 (Π_6= 0.14)	D_{SSC-C}	1.6	3.2	0.2	0.6	2
	D_{CC-C}	0.4	1.2	/	/	/
	D_{EXC-C}	/	/	0.6 (v=2.4)*	/	0.6
	strike	110	110	/	/	075
C42 (Π_6= 0.19)	D_{SSC-C}	1.8	3	0.4	0.8	2.6
	D_{CC-C}	0.8	1.4	/	/	/
	D_{EXC-C}	/	/	0.8 (v=2.6)*	/	1
	strike	110	120	/	/	070
C47 (Π_6= 0.2)	D_{SSC-C}	3.6	4	1.2	0.6	4.6
	D_{CC-C}	/	1.6	/	/	/
	D_{EXC-C}	/	/	1.4 (v=3)*	1.2	/
	strike	095	095	/	/	115